Università degli Studi di Ferrara

UCA Universidad de Cádiz

INTERNATIONAL DOCTORAL COURSE IN
"EARTH AND MARINE SCIENCES (EMAS)"

CYCLE XXXIII

COORDINATOR Prof. COLTORTI MASSIMO

CARNIAN PLUVIAL EPISODE IN IRAN (TURAN PLATE AND IRAN PLATE) AND WESTERN TETHYS DOMAIN

Scientific/Disciplinary Sector (SDS) GEO/02

Candidate
Dott. Mina Mazaherijohari

Supervisor
Prof. Piero Gianolla

Co-Supervisor
Dr. Guido Roghi

Years 2017/2021

This thesis is dedicated to my family.

For their endless love, support and encouragement

Acknowledgments

Undertaking this PhD has been a truly life-changing experience for me and it would not have been possible to do without the support and guidance that I received from many people. First of all, I would like to express my sincere gratitude to my supervisor Piero Gianolla not only for his careful support, but also for his consistent support throughout this project, without your wise guidance and constant feedback this project would have not been the same! From the bottom of my heart I would like to say big thank you to my family for all the unconditional support in these intense academic years. I would also like to say a special thank you to Guido Roghi, Evelyn kustatscher, Jacopo dal Corso, Tamsin Mather, Chu Doliang, Marcello Caggiati, and Joost Frieling for the thoughtful comments and recommendations on this dissertation. Colleagues from Ferrara, Oxford, and Leeds universities are thanked for their collaboration and help during geochemical analyses (Total Organic Carbon (TOC) measurements and Mercury concentrations). They are Gianluca Bianchini, Valentina Brombin, Renzo Tassinari, Chiara Marchina, and Gian Marco Salani from University of Ferrara; Tamsin Mather, Hugh Jenkyns, Joost Frieling, and Stephen Wyatt from University of Oxford; Jacopo Dal Corso from University of Leeds. I gratefully acknowledge the cooperation of colleagues from the University of Tehran and Geological Survey of Iran, Mashhad branch, particularly Ebrahim Ghasemi-Nejad, Jafar Taheri, Abradat Maafi, and Maryam Hosseiniyoon for the assistance in part of fieldwork. Mine Engineer Hajiyan (from the company of Maadan Khavar) is also acknowledged for providing hospitality at the Aghdarband Coal mine during our fieldwork in Iran. My thanks also go out to the support I received from the collaborative work I undertook with the Padova University for palynological sample preparations.

I am also very grateful to all those at the IUSS office, especially Mrs. Daniela Siri and friends who were always so helpful and provided me with their assistance throughout PhD academic years.

Table of contents

Abstract

During the Carnian age (early Late Triassic), a global climate change took place later termed the Carnian Pluvial Episode (CPE) and dated through biostratigraphic calibration from the Julian 2 to the Tuvalian 2 intervals. The CPE was an interval of climatic change towards more humid conditions. Multiple negative carbon isotope excursions (NCIE) suggest the injection of large amount of ^{13}C-depleted CO_2 into the Carnian ocean-atmosphere system that could have been induced by volcanic gas emissions related to Wrangellia Large Igneous Province (LIP) volcanism, or other coeval volcanic events. A detailed fieldwork, together with paleobotanical, palynological, stratigraphical, and sedimentological study was performed on the upper Triassic successions of Turan Plate (NE Iran) and Iran Plate (Central Iran) to peruse the signals of CPE in these regions.The Middle-Upper Triassic Aghdarband Basin (NE Iran), consists of marine, marginal marine and continental succession deposited along the southern margin of Eurasia (Turan Plate) in a highly mobile tectonic context. The core of the Aghdarband Syncline consists of a sequence of fine siliciclastic sediments with a distinct continental interval forming the Miankuhi Formation. The continental interval of Miankuhi Fm. rests on an unconformity surface separating it from the underlying Sina Formation. The paleobotanical assessments of the upper Triassic successions the Aghdarband Basin resulted in the identification of a plant fossil assemblage coming from the basal continental facies of the Miankuhi Formation dominated by roots and vegetative organs of *Neocalamites iranensis* n. sp., with few seeds and plant fossils of undefined botanical affinity. Well-preserved terrestrial palynomorphs from the studied interval confirmed a latest early Carnian to late Carnian age and reveal, for the first time, a clear link between this plant-bearing continental wet interval, and the CPE in the Turan plate (southern margin of Eurasia) and Iran region. Results of the qualitative and quantitative palynological analysis document an increase in the hygrophytic vegetation elements in the studied area coincident with the one found in the Tethyan same latitude belt suggesting more humid climate in the lower part of the Minakuhi Formation, corresponding to the CPE. The sedimentological and stratigraphical analyses resulted in determination of an interval of fluvial deposits with histosol levels at the basal Miankuhi Formation suggesting the prevalence of humid climate in the studied area by that time. The defined unconformable boundary between the formations is, consequently, interpreted as a result of a sea level fall associated with a climatic shift towards more humidity, decoupling the impact of Eo-Cimmerian collision on the birth of this unconformity in our studied area. The results suggests that this orogenic event is younger than Carnian and positioned somewhere before the Middle-Norian. However, the

exact timing of this event and how it evolved remains controversial. Palynological investigations of the Nayband Formation (Iran Plate), revealed moderately diverse dinoflagellate cyst assemblages which confirmed a middle Norian-Rhaetian age for the studied interval in Iran Plate. Measurement of sedimentary mercury concentrations and Total Organic Carbon (TOC) contents were applied to the four composite sections from the Western Tethys realm to track the hypothesis sources of CPE. Data show increased Hg loading in the Tethyan basins during the CPE. The changes in Hg concentration can be related to coeval LIP volcanism, revealing the close link between these huge volcanic events and profound global climatic changes.

Riassunto

Durante il Carnico (Triassico Superiore), c'è stata una perturbazione climatica registrata a scala globale conosciuta come Carnian Pluvial Episode (CPE) e è datato mediante calibrazione biostratigrafica dall'intervallo Julico 2 e Tuvalico 2. Il CPE è stato un intervallo di cambiamento climatico verso condizioni più umide. La presenza di diverse escursioni isotopiche negative del carbonio (NCIE) suggeriscono l'iniezione nel sistema oceano-atmosfera di una grande quantità di CO2 impoverita di ^{13}C, che potrebbe essere stata indotta da emissioni di gas vulcanici legati al vulcanismo della Wrangellia Large Igneous Province (LIP) o da altri eventi vulcanici coevi a questa. Un dettagliato lavoro sul terreno, studio paleobotanico, palinologico, stratigrafico e sedimentologico sulle successioni del Triassico superiore della Turan Plate (Iran NE) e della placca iraniana per ricercare eventuali segnali del CPE in queste regioni. Il Bacino di Aghdarband (NE Iran), consiste in una successione marina, marino marginale e continentale che documenta una successione sedimentaria, che va dal Triassico medio a quello superiore, e documenta la sedimentazione in bacini tettonicamente molto attivi, in un contesto di convergenza di placche lungo il margine meridionale di Eurasia (Turan Plate). Il nucleo della sinclinale di Aghdarband è dato dalla Formazione di Miankuhi, una sequenza di sedimenti fini silicoclastici con alla base un distinto intervallo continentale. Questo intervallo basale continentale giace con una netta superficie erosiva sulla sottostante Sina Formation. Le analisi paleobotaniche delle successioni del Triassico superiore del bacino di Aghdarband hanno portato all'identificazione di un'associazione di fossili vegetali provenienti dalla facies continentale basale della Formazione di Miankuhi, dominata da radici e organi vegetativi di *Neocalamites iranensis* n. sp., con pochi semi e fossili di piante di affinità botanica indefinita. Palinomorfi ben conservati da questo parte ha permesso di definire un'età Carnica (tardo Julico-Tuvalico) per questo intervallo stratigrafico rivelando, per la prima volta, un chiaro legame tra questa parte della successione e il CPE nel margine meridionale dell'Eurasia (Turan Plate) e nella intera regione iraniana. I risultati dell'analisi palinologica qualitativa e quantitativa documentano l'aumento degli elementi di vegetazione igrofita nell'area studiata coincide con quello riscontrato durante il CPE in altre località al margine della Tetide alla stessa latitudine, suggerendo anche qui una fase climatica più umida. Le analisi sedimentologiche e stratigrafiche hanno inoltre messo riconosciuto, nella parte basale della Formazione di Miankuhi, sedimenti fluviali associati suggerendo la prevalenza del clima umido nell'area studiata in quel momento. Il limite netto ed erosivo tra le formazioni di Sina e Miankuhi, tradizionalmente interpretato come evidenza della fase collisionale cosiddetta Eo-Cimmerica è, di qui interpretato come il risultato di una caduta relativa del livello del mare. La fase

collisionale Eo-Cimmerica deve essere quindi datata tra il Carnico (post-CPE) e il Norico medio. La tempistica esatta di questo evento e come si sia strutturato temporalmente rimane tuttavia controversa. I risultati delle indagini palinologiche della Formazione di Nayband (Iran Plate), hanno rivelato associazioni di dinoflagellati che hanno confermato un'età Norico-Retica per l'intervallo studiato. Le concentrazioni di mercurio sedimentario rapportandole con il contenuto di carbonio organico totale (TOC) sono stati applicati alle quattro sezioni composite della Tetide occidentale per tracciare la causa del CPE. I dati mostrano incrementi nella concentrazione del mercurio nei bacini della Tetide occidentale durante il CPE. I cambiamenti nella concentrazione di Hg possono essere correlati al vulcanismo di LIP, lo stretto legame tra questi enormi eventi vulcanici e i profondi cambiamenti climatici globali.

1. Introduction

The present thesis is focused on the geochemical, paleobotanical, palynological, stratigraphical, and sedimentological study of the Upper Triassic (Carnian) successions in Iran (Turan plate and Iran plate) and Western Tethys regions. During the early Late Triassic (Carnian), a phase of global climatic change and biotic turnover, called Carnian Pluvial Episode (CPE; Simms and Ruffell, 1989), occurred which is defined by an interval of environmental change towards more humid conditions (Simms and Ruffell, 1989; Preto et al., 2010; Dal Corso et al., 2015, 2018) that interrupted the predominantly arid climate of the Triassic (Fig. 1, 2) (Kutzbach and Gallimore, 1989; Parrish, 1993; Sellwood and Valdes, 2006; Boucot et al., 2013; Scotese, 2013; Kustatscher et al., 2018; Mancuso et al., 2021). The CPE is accompanied by sea level changes (e.g., Franz et al., 2014; Gattolin et al., 2015), global warming (e.g., Trotter et al., 2015; Sun et al., 2016; Hornung et al., 2007a, 2007b; Rigo and Joachimski, 2010), increased continental weathering (Rostási et al., 2011), demise of carbonate platforms (e.g., Keim et al., 2006; Hornung et al., 2007b; Breda et al., 2009; Stefani et al., 2010; Lukeneder et al., 2012), deepening of the CCD (Rigo et al., 2007) and locally oxygen depletion in marginal marine settings (e.g., Keim et al., 2006; Hornung et al., 2007b; Soua, 2014). Paleontological data suggest that the CPE was a major time of extinction and may be linked to the Carnian explosive diversification of many key modern groups of plants and animals (e.g., Simms et al., 1995; Rigo et al., 2007; Balini et al., 2010; Chen et al., 2015; Dal Corso et al., 2018, 2020; Benton et al., 2018; Bernardi et al., 2018; Baranyi et al., 2019). Multiple negative carbon isotope excursions (NCIEs) within the CPE interval are recorded by marine and terrestrial organic matter (e.g., Dal Corso et al., 2012, 2015, 2018; Muttoni et al., 2014; Mueller et al., 2016a, 2016b). These NCIEs, which have been also found in other settings outside Western Tethys (Sun et al., 2016, 2019; Miller et al., 2017; Jin et al., 2019; Fu et al., 2020; Tomimatsu et al., 2021), are likely associated with injections of large amount of ^{13}C-depleted CO_2 into the Carnian ocean-atmosphere-soil system that could have been induced by volcanic gas emissions related to Wrangellia Large Igneous Province (LIP) volcanism, or other coeval volcanic events (Furin et al., 2006; Greene et al., 2010; Dal Corso et al., 2012, 2015, 2018, 2020; Xu et al., 2014; Mueller et al., 2016a; Sun et al., 2016; Nozaki et al., 2019; Tomimatsu et al., 2021). An alternative scenario is the relationship between climate crisis and volcanism of a Large Igneous Province. Some researchers (Hornug et al., 2005, 2007a, b; Krystyn et al., 2019; Chu et al., 2020), have linked the CPE (or some of the sedimentological evidence such as the siliciclastic input, anoxia, or the demise of carbonate platforms) with the major plate restructuring taking

place during the Upper Triassic. Particularly, the age of CPE overlaps that of the Eo-Cimmerian orogeny and this led to the postulation f a cause-and-effect relationship between the collision of part of the Cimmerian plates with Laurasia and the formation of a belt following the collision with an effect similar to that of the formation of the Himalayan chain, i.e. an important effect of monsoonal climate circulation. The onset of the CPE is very well constrained in many stratigraphic sections from Tethys domain to Panthalassa or, inside Pangea, from western Eurasia to South America (e.g., Gianolla et al., 1998; Neri et al., 2007; Rigo et al., 2007; Dal Corso et al., 2012, 2015, 2018; Barany et al., 2018, 2019; Jin et al., 2020; Fu et al., 2020; Mancuso et al., 2020; 2021). There are, however, several areas where this wet episode has not been clearly documented as along the southern margin of the Eurasia (Turan Plate) and the Iran Plate. Among the Upper Triassic successions found in Iran region, the Carnian sediments have a limited expansion due to the occurrence of Cimmerian orogeny and they also suffer from a precise age determination. The development of Carnian sequences in Iran (Ghorbani, 2019) are, therefore, confined to some small segments in Zagros, Alborz Mountain Range (N Iran), Central Iran, and Kopeh-Dagh Basin (NE Iran).

The first phase of this project is focused on the geochemical analyses (sedimentary mercury concentration and Total Organic Carbon content) of the Carnian strata from western Tethys domain for tracking hypothesized sources of CPE paleoenvironmental perturbations (Fig. 3). Sedimentary mercury (Hg), usually normalized for TOC content since Hg is closely associated with OM in sediments, has been considered as a promising tool for tracking volcanic activity during intervals of mass extinctions and global palaeoenvironmental changes. Nevertheless, Hg mobilization is also controlled by other factors.

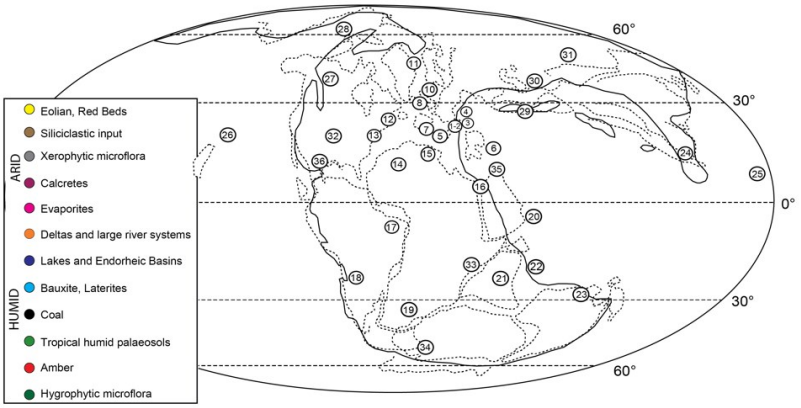

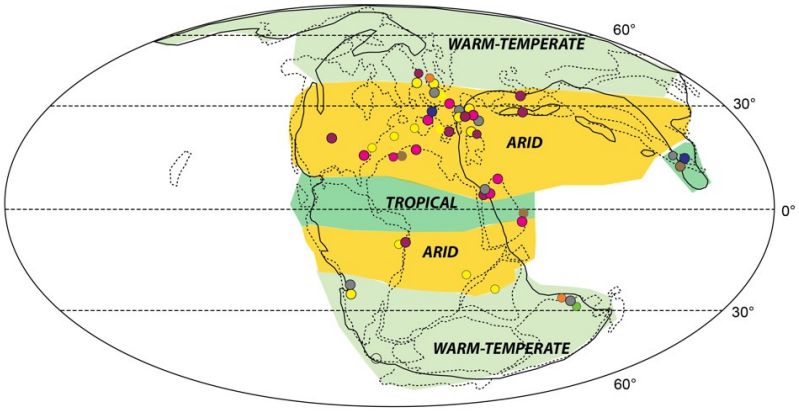

EARLY CARNIAN (Julian 1)

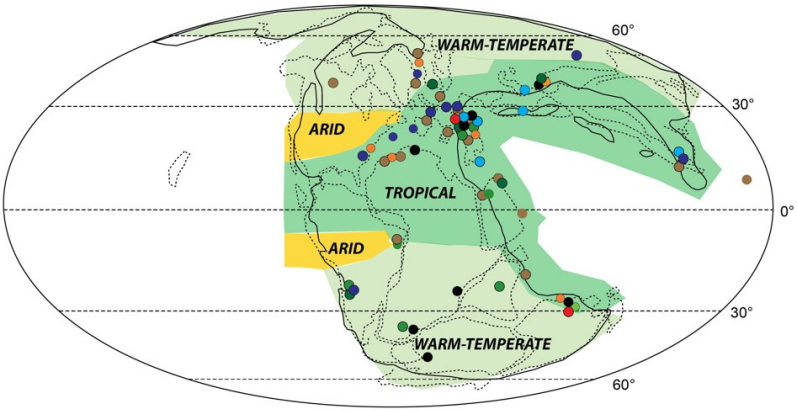

CPE (Julian 2-Tuvalian 1)

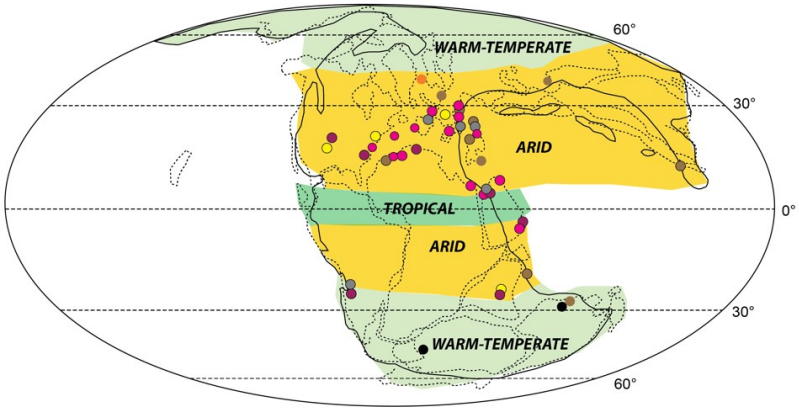

LATE CARNIAN (Tuvalian 2-3)

Previous page: **Figure 1.** Paleogeographic maps for the Triassic Period (modified from Dal Corso et al., 2020) with climatic zones defined by primary and secondary climatic indicators (after Preto et al., 2010; Boucot et al., 2013; Kustatscher et al., 2018; Dal Corso et al., 2020; Mancuso et al., 2021). Localities: 1) Dolomites (Italy); 2) Julian Alps (Italy, Slovenia); 3) Transdanubian Range (Hungary); 4) Northern Calcareous Alps (Austria); 5) Lagonegro Basin (Italy); 6) Antalya (Turkey); 7) Iberia (Spain); 8) United Kingdom; 9) Central European Basin; 10) Barents sea; 11) Jameson Land (Greenland); 12) Fundy Basin (Canada); 13) Richmond and Taylorsville basins (United States); 14) Essaouira Basin (Morocco); 15) Jeffara Basin (Tunisia); 16) Levant Basin (Jordan, Israel); 17) Paraná Basin (Brasil); 18) Ishigualasto and Cujo basins (Argentina); 19) Karoo Basin (South Africa); 20) Oman; 21) Rewa Basin (India); 22) Spiti (India); 23) Carnarvon Basin (Australia); 24) Nanpanjiang Basin (China); 25) Panthalassa (Japan); 26) Wrangellia and Panthalassa (Canada and United States); 27) British Columbia (Canada); 28) Alaska; 29) CEIM (Iran); 30) Aghdarband Basin (Iran); 31) Madygen Basin (Kyrgyzstan); 32) Chinle (Southwestern USA); 33) Selous Basin (Tanzania); 34) Transantarctic Mts. (Antarctica); 35) Arabian Plate (Iraq).

Terrestrial biomass burning or oxidation, and increased detrital inputs (rock weathering and soil erosion) into the basins, or more in general, changes in the size of the terrestrial Hg reservoir, can account for changes of Hg concentrations in the marine reservoir (e.g., Vandal et al., 1993; Martínez-Cortizas et al., 1999; Santos et al., 2002; Them et al., 2019; Dal Corso et al., 2020). In this phase of project, we analysed Hg and total organic carbon (TOC) concentrations in four Carnian marine sedimentary sequences of the Western Tethys to evaluate whether enhanced volcanic activity coincided with the CPE's C-cycle and hydrological perturbations

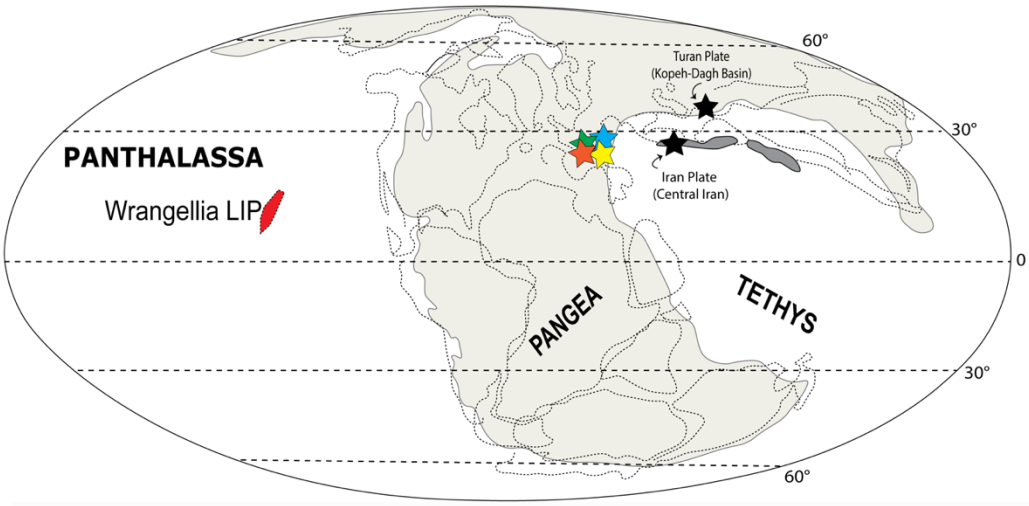

Figure 2. Late Triassic Paleogeography (from Dal Corso et al., 2020). Black stars represent the studied areas in Turan Plate (Kopeh-Dagh Basin, NE Iran) and Iran Plate (Central Iran). Light-Colored stars represent the Western Tethys studied areas including Southern Alps (Dolomites and Julian Alps, Italy), Northern Calcareous Alps (Lunz area, Austria), and Transdanubian Range (Balaton Highland, Hungary).

The second phase of the present PhD project is divided into two sections in order to characterize the sedimentary evolution/depositional conditions, more accurate ages, and paleoclimate records of the Upper Triassic successions of the NE Iran, Turan Plate (upper Sina and the lowermost Miankuhi formations) and and Iran Plate (Tabas Block, Central Iran: Nayband Formation) using a multidisciplinary approach involving the palynological, paleobotanical, and sedimentological assessments (Fig. 3).

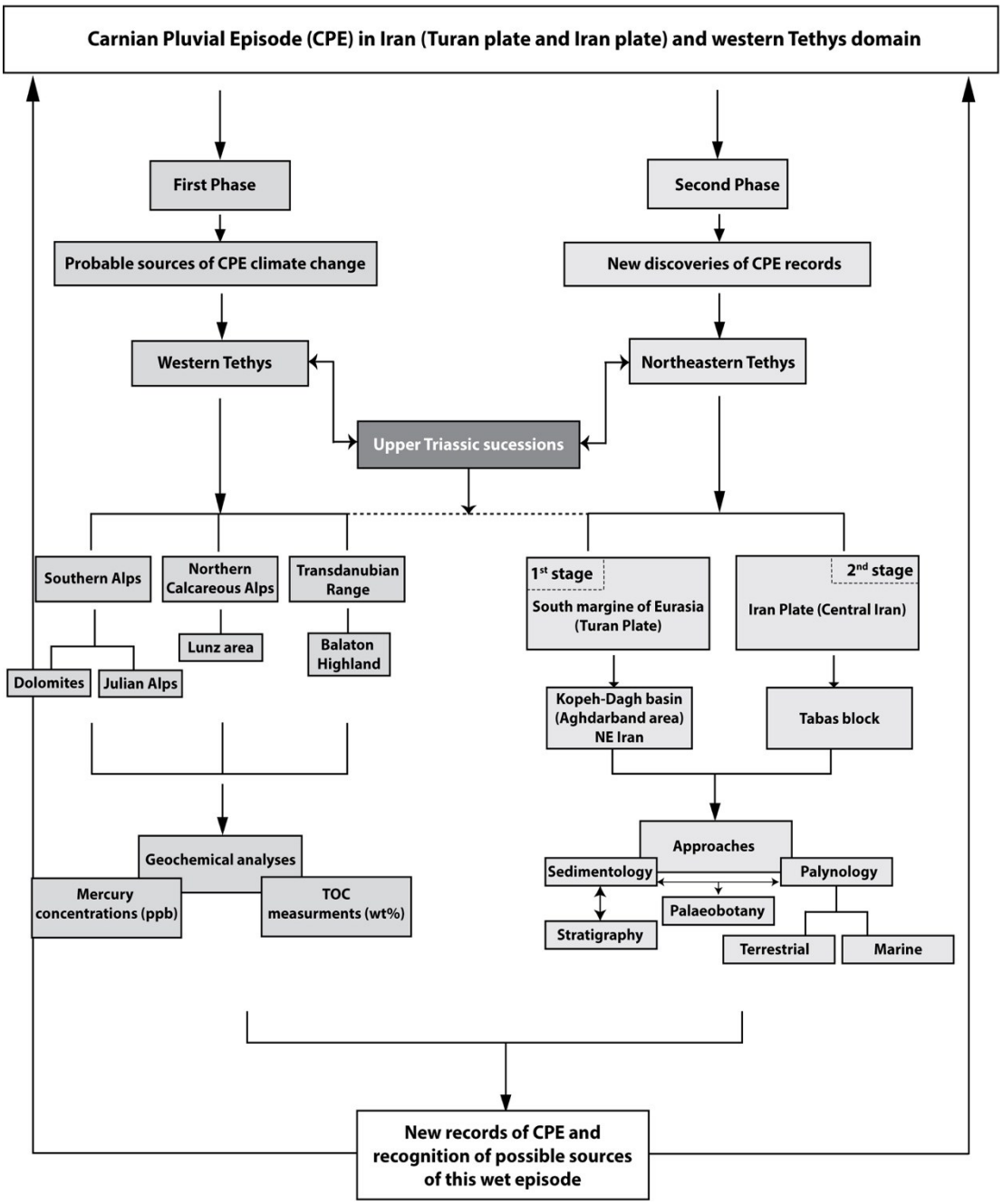

Figure 3. Research process flowchart.

2. Geological setting

2.1. Western Tethys Realm

The Tethyan oceans evolved throughout the Mesozoic and into the Cenozoic within the area bounded by Eurasia to the north and the continents comprising Gondwanaland to the west, south, and east (e.g. Africa, India, Antarctica, and Australia). The western part of this oceanic domain, the Western Tethys, occupies the region between Eurasia, Africa, and Arabia (Fig. 4) and is arguably one of the most complex components of the Tethyan system, characterized by multiple phases of rifting, seafloor spreading, subduction, and collision (Hosseinpour et al., 2016). Reconstructions of the Western Tethys are best expressed by separating the area into two major boundary domains (Atlantic and Tethyan domains) and a series of small basins, which opened and subducted between these two main tectonic realms (Fig. 5) (Handy et al., 2010; Hosseinpour et al., 2016). The Atlantic domain includes the Central, North Central, North, and Northeast Atlantic, and the Tethyan domain includes the Vardar Ocean and western Neotethys. The smaller basins or sub-domains are the Pyrenean Rift and Bay of Biscay, the Ligurian Ocean, Piemont Ocean, the Valais Ocean, the Ionian Sea, and inner Tauride Ocean (Fig. 5). The Piemont-Ligurian and Valais Oceans (Alpine Tethys) are the western extension of the Neotethys, which opened as a result of fragmentation of northern Gondwana and the separation of Eurasia from the African plate. Closure of these oceanic basins and consequent collisional events led to the formation of the major orogenic belts and massive nappe stacking now exposed in the Dinarides, Pennines, Apennines, and Alps (Stampfli and Borel, 2002; Schmid et al., 2008; Handy et al., 2010; Hosseinpour et al., 2016). The Alps were developed from the Cretaceous onwards by the collision between the Adriatic (Austroalpine-Southalpine) and European (Penninic-Helvetic) continental margins. The Austroalpine-Penninic wedge is the core of the collisional belt, a fossil subduction complex which floats on the European lower plate (e.g., Schettino and Turco, 2011).

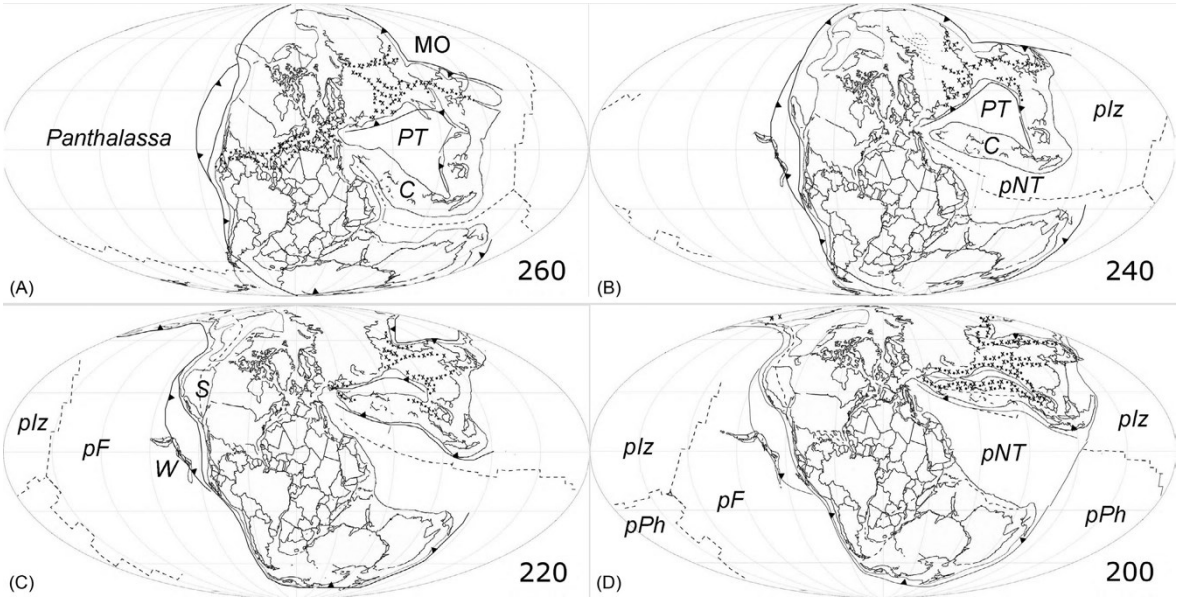

Figure 4. Plate tectonic evolution from the late Permian to the earliest Jurassic (260–200 Ma). Plate boundaries: subduction zones = *lines with barbs*, midocean ridges = *dashed lines*, and continental colli- sion zones = *small x's*. Plates: *C*, Cimmeria; *MO*, Mongol-Okhotsk Ocean; *pF*, proto-Farallon; *pIz*, proto-Izanagi; *pNT*, proto-NeoTethys; *pPh*, protoPhoenix; *PT*, PaleoTethys; *S*, Stikinia; *W*, Wrangellia (Scotese and Schettino, 2017).

According to the direction of tectonic transport, the Alps may be subdivided into two belts of differing size, age and geological meaning: 1) the Europe-vergent belt, a thick collisional wedge of Cretaceous-Neogene age, consisting of continental and minor oceanic units radially displaced towards the Molasse foredeep and European foreland; 2) the Southern Alps, a minor, shallower (non-metamorphic) and younger (Neogene) thrust-and-fold belt displaced to the south (Adria-vergent), which developed within the Alpine hinterland of the Adriatic upper plate, far from the oceanic suture. These belts are separated by the Periadriatic (Insubric) lineament, a major fault system of Oligocene-Neogene age (Dal Piaz et al., 2003).

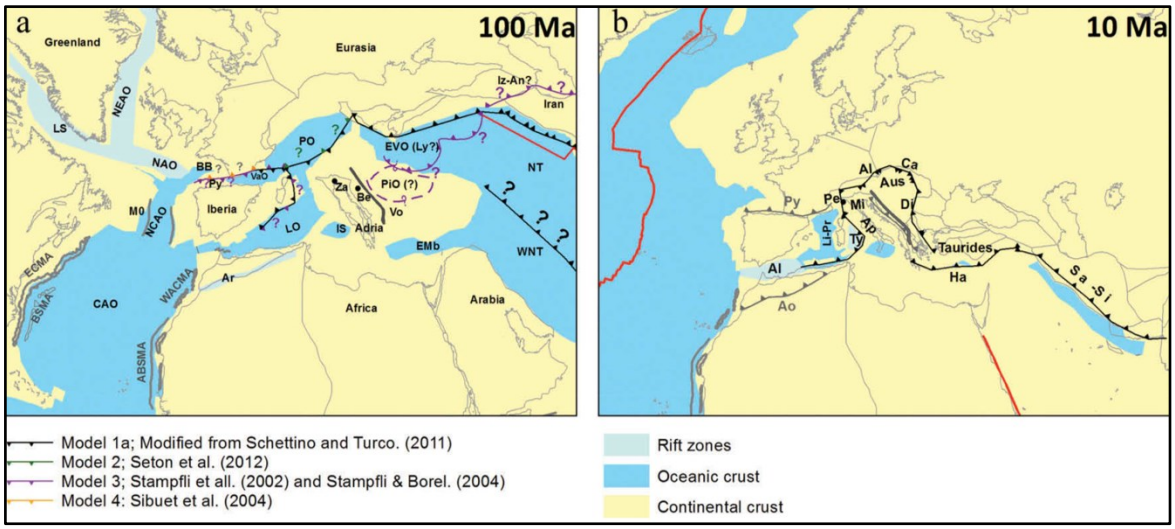

Figure 5. Location of various geographic, geological, tectonic, and geophysical features in the Western Tethys and surrounding areas presented in two different phases. A. Early Cretaceous time showing the early stages of the Alpine compressional phase. B. Collision and formation of orogenic belts are shown in late Miocene time. Subduction zones (black), mid-ocean ridges (red), and magnetic anomalies (grey) are reconstructed by Hosseinpour et al. (2016). LS, Labrador Sea; NEAO, Northeast Atlantic Ocean; NAO, North Atlantic Ocean; NCAO, North Central Atlantic ocean; CAO, Central Atlantic Ocean; ECMA, East Coast magnetic Anomaly; BSMA, Black Spur Magnetic Anomaly; WACMA, West African Coast Magnetic Anomaly; ABSMA, African Black Spur Magnetic Anomaly; BB, Bay of Biscay; Py, Pyrenees; VaO, Valais Ocean; PO, Piemont Ocean; LO, Ligurian Ocean; Ar, Atlas rift; IS, Ionian Sea; EMb, Eastern Mediterranean basin; PiO, Pindos Ocean; EVO, Eastern Vardar Ocean; Ly, Lycian; Vo, Vardar Ophiolites; Iz-An, Izmir-Ancara; NT, Neotethys; WNT, Western Neotethys; Al, Alboran; Ao, Atlas orogenic belt; Li-Pr, Liguro-Provençal; Ty, Tyrrhenian Sea; Pe, Pennines; Ap, Apennines; Al, Alps; Ca, Carpathians; Aus, Austroalpine; Di, Dinarides; Ha, Hellenic arc; Sa-Si, Sanandaj-Sirjan; Za, Zagreb; Be, Belgrade; Mi, Milano. Refer to text of Hosseinpour et al. (2016) for further explanations of each domain/feature.

2.1.1. Southern Alps

2.1.1.1. Dolomites

The Dolomites region is a spectacularly exposed portion of the Southern Alps, a northern Italian chain derived from the comparatively gentle deformation of the Tethyan passive continental margin of Adria (Fig. 6). Although the sedimentary succession ranges in age from Middle Permian to Cretaceous, the geological landscape is largely dominated by the majestic Triassic carbonates, making the area a classical one for the early Mesozoic stratigraphy (Bosellini et al., 2003). During the Middle–Late Triassic, the area occupied a northern equatorial position in the western margin of the Tethys Ocean (Fig. 2) (Muttoni et al., 2015). The Carnian (Julian–Tuvalian) succession of the Dolomites (Fig. 7) begins with the San

Cassiano Formation (Julian). The relative modal composition of packstones and grainstones in the San Cassiano Formation, which reflects the composition of the carbonate producers on the coeval platforms (Cassian Dolomite), show high contents of microbial elements (Preto, 2012). Such microbial-dominated composition abruptly changes in the uppermost part of the San Cassiano Formation–lowermost Heiligkreuz Formation, in correspondence with the negative carbon-isotope excursion that marks the onset of the CPE (Dal Corso et al., 2012, 2018). Ooids and skeletal grains become the most abundant components, and the microbial carbonates reduce to < 10% of rock volume (Gattolin et al., 2015). This change in facies is interpreted as evidence for the crisis of the highly productive early Carnian microbially dominated platforms, which were replaced by less productive metazoan ramps (Gattolin et al., 2015; Dal Corso et al., 2015).

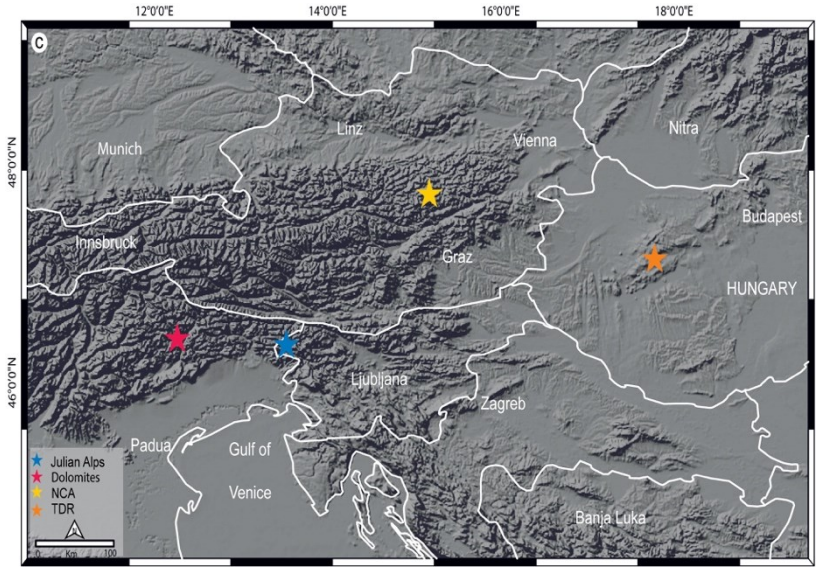

Figure 6. Map of the study area. The stars represent studied sections. Abreviations: NCA = Northern Calcareous Alps, TDR = Transdanubian range.

Above the San Cassiano Formation, the coarse silicislastics, clays, and marls mixed with skeletal and oolitic carbonates of the Heiligkeuz Formation were deposited (Neri et al., 2007; Breda et al., 2009; Stefani et al., 2010). The Heiligkreuz Formation is locally > 100 m thick and represents the rapid infilling of the early Carnian basins as a consequence of the increasing continental runoff during the CPE. It is followed stratigraphically by the clays and dolomites of the Travenanzes Formation (Tuvalian), which was deposited in a marginal marine dryland coastal system (Breda and Preto, 2011).

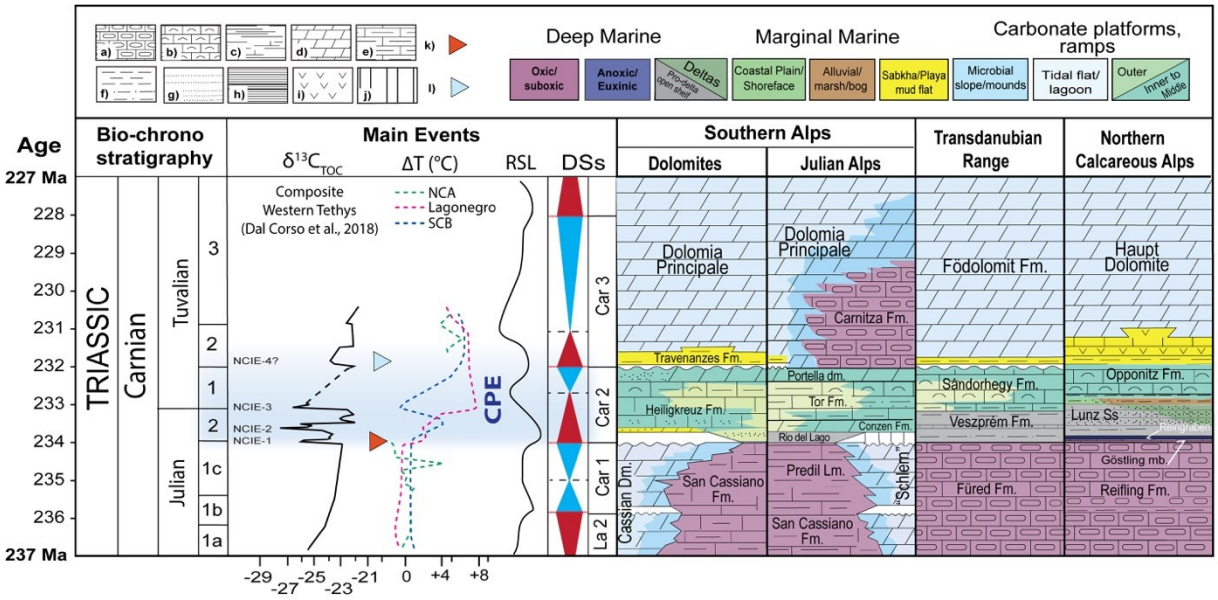

Figure 7. Lithostratigraphic scheme for the Carnian formations in the studied areas along with negative carbon isotope excursions (Dal Corso et al., 2015, 2018), paleotemperature (After Sun et al., 2016), sequence stratigraphy (Modified from Stefani et al., 2010), ages (GTS, 2020), and Relative Sea Level (RSL). The red triangular shows the demise of microbial carbonate platforms and the blue one represents the recovery. Abbreviations: Julian 1a = *Daxatina canadensis* zone, Julian 1b = *Trachyceras aon* zone, Julian 1c = *Trachyceras aonoides* zone, Julian 2 = *Austrotrachyceras austriacum* zone; Tuvalian 1 = *Tropites dilleri* zone , Tuvalian 2 = *Tropites subbullatus* zone , Tuvalian 3 = *Anatropites spinosus* zone, Lithology: a = Cherty limestone, b =Bioclastic limestone, c = Limy marlstone, d = Dolomite, e = Marly limestone, f = Siltstone, g = Sandstone, h = Black shale, i = Evaporites, j = Hiatus, NCA= Northern Calcareous Alps, SCB = South China Block.

Two stratigraphic sections (Milieres and Heiligkreuz) in the Dolomites, which together form a composite section of the entire Heiligkreuz Formation, were sampled and geochemically analysed as part of the second phase of this research.

2.1.1.2. Julian Alps (Cave del Predil area)

The locality studied in the Julian Alps is the classical Cave del Predil area (formerly "Raibl"), near Tarvisio, where the historical type-area of the Carnian stage has been defined (Mojsisovics, 1879; Assereto et al., 1968; Liebermann, 1980) (Fig. 6). In this area, a well-preserved carbonate platform-basin depositional system records microbial platform demise, basin infilling by siliciclastics, transition to mixed terrigenous-skeletal carbonate ramp system, and finally microbial carbonate platform recovery (De Zanche et al., 2000; Gianolla et al., 2003; Caggiati et al., 2018; Dal Corso et al., 2018). The carbonate platform (Schlern Dolomite or "Dolomia Metallifera" Auctorum) is a high-relief microbial buildup and is

interfingered the black laminated limestone of the Predil Limestone (Julian). Above, a thick (> 1000 m) succession of silt and marl alternates with lime mudstone to packstone, locally dolomitized, with abundant skeletal grains (Rio del Lago, Conzen, Tor Formations and Portella Dolomite, upper Julian to lower Tuvalian: De Zanche et al., 2000). The remaining portion of the Tuvalian is represented by mainly nodular, cherty lime mudstone of the Carnitza Formation, which lies conformably on top of the Portella Dolomite (Fig. 6; Gianolla et al., 2003; Caggiati et al., 2018) (Fig. 7). The age of the Cave del Predil section is constrained by ammonoids, conodonts, and sporomorphs (De Zanche et al., 2000; Gianolla et al., 2003; Roghi, 2004; Dal Corso et al., 2018).

In the Cave del Predil area, the Rio Conzen and neighboring Rio delle Cascate sections (De Zanche et al., 2000; Roghi, 2004) have been sampled for geochemical analyses. The sections are very close to each other and a good correlation between them can be achieved with marker beds. They encompass the Predile Dolomite, the Rio del Lago, the Conzen, and part of the Tor formations.

2.1.2. Transdanubian Range (TDR, Balaton Highland)

The Transdanubian Range (TDR) located in the NW part of the Carpathian-Pannonian Basin is the northwestern segment of the ALCAPA terrane (Alpine-West Carpathian- Pannonian) (Fig. 6). During the Late Triassic the TDR formed a segment of the passive Western Tethys margin and was situated between the Northern Calcareous Alps and the Southern Alps (Haas et al., 1995) (Fig. 2). The ALCAPA terrane reached its present-day position due to its eastward escape from the Alpine sector in the Paleogene-early Miocene (mainly Oligocene) (e.g., Kázmér and Kovács, 1985; Csontos et al., 1992; Fodor et al., 1999) and a significant counter-clockwise rotation (e.g., Márton and Fodor, 2003). The TDR is made up predominantly of Triassic formations with a total thickness of 3–4 km (Fig. 7). During Early Carnian a significant change in the lithofacies occurred in the Balaton Highland in the TDR as pelagic limestones (Füred Limestone) passes into a thick marl succession (Veszprém Marl Formation (VMF)) with a marked siliciclastic input (Fig. 7) (Budai and Haas, 1997; Rostási et al., 2011; Dal Corso et al., 2018; Baranyi et al., 2019). This major change in the sedimentation is associated with the CPE climatic shift from arid to more humid conditions as documented by clay mineralogy (Rostási et al., 2011) and by palynomorph assemblages (Baranyi et al., 2019). In the Balaton Highland, the VMF with a variety of thickness (from 100 to 600 m) is comprised of four members: Mencshely Marl Member, Nosztor Limestone Member, Buhimvolgy Breccia

Member and Csicso Marl Member. The basal part of the Veszprém Marl (Mencshely Marl Member), included of a relatively thick marl-dominated succession with some intercalations of sandstone, is separated from the pelagic marls of the upper part (Csicso Marl Member) by a 20 m-thick pelagic limestone member (Nosztor Limestone) (Csillag, 1995). Above, shales with variable carbonate content (Sándorhegy Formation) record the infill of the intraplatform basins during the late Carnian (Tuvalian) and apparently levelled the topography, on which the peritidal Main Dolomite was deposited. The stratigraphic successions of the Transdanubian Range are biostratigraphically well constrained with ammonoids, sporomorphs, and conodonts (Budai et al., 1999). In the second phase of this research samples from two core materials (Met-1 and Bfü-1; Rostási et al., 2011) are geochemically analysed for the mercury concentrations and TOC measurements.

2.1.3. Northern Calcareous Alps (Lunz area)

The Lunz area, located in the eastern Northern Calcareous Alps (Fig. 6), is well-known for containing coal seams with numerous remnants of Late Triassic plant fossils and reptiles (Verloop, 1908; Tollmann, 1976; Dobruskina, 1998; Pott et al., 2008). This area was located at the northwestern rim of the Tethys in the Carnian (Haas, 1991) (Fig. 2). The early Carnian stratigraphy of the Lunz nappe of the Northern Calcareous Alps (Austria, Fig. 6 for location) is a succession of carbonate–siliciclastic sedimentary rocks that records the evolution of the basin from deep-water to delta and carbonate shelf (Rüffer and Bechstädt, 1998) (Fig. 7). The Upper Ladinian–Lower Julian deep-water nodular limestones of the Reifling Fm. are overlain by the laminated dark mudstones and grainstones of the Göstling Fm., which testify to decreasing carbonate input and increasing oxygen depletion in the basin (Hornung et al., 2007b). The lithological change between the Reifling and the Göstling Fms. occurs approximately at the Julian 1–Julian 2 boundary (Fig. 7). Above this level, an increase in clayey interbeds precedes the transition to the Reingraben Fm., a succession of shales that contains sporomorphs of the Julian 2 (Aulisporites astigmosus assemblage; Roghi et al., 2010) (Fig. 7). The proportion of shale and dark mudstone increases towards the overlying coarse terrigenous Lunz Fm. (Köppen, 1997), consisting of deltaic sandstones and siltstones with abundant plant debris (Pott et al., 2008). The infilling of the basins of the Northern Calcareous Alps was completed by deposition of the siliciclastic succession (ca. 400 m-thick) of the Lunz Fm., which was followed by carbonate shelf sedimentation of the Opponitz Fm. (Fig. 7). Samples for the geochemical analyses come from two stratigraphic sections: Steinbach section and Polzberg

section. The Steinbach section encompasses the Reifling Fm. and part of the Göstling Fm. while in the Polzberg section the uppermost part of the Göstling Fm. and the lower part of the Reingraben Fm. are exposed.

2.2. Northern Tethys Realm

Sengör (1979) has shown that during the Late Triassic to Middle Jurassic interval "Tethys" actually consisted of two main oceans separated by a relatively thin, either continuous or broken, continental strip that bisected the Tethyan domain in a roughly east-west direction (Fig. 5, 8). Because during this time interval rocks representing this "intra-Tethyan" continent belonged neither to Laurasia nor to Gondwana-Land, Sengör (1979) has named it the *Cimmerian Continent,* after the Cimmerii, the earliest known inhabitants of the Crimea and the North Dobrudja, where the first pieces of evidence for the existence of the Cimmerian Continent had been discovered (Suess, 1909). Sengör (1979) has argued that the Cimmerian Continent represented a strip that began rifting from the northern margin of Gondwana- Land during the ?Permo-Triassic and rotated in a counterclock-wise fashion until Middle Jurassic time. While obliterating the original Permo-Triassic Pangean gap, now commonly referred to as Paleo-Tethys after Stöcklin (1974) usage for its Iranian segment, "in front" of the Cimmerian Continent, this rotation opened an oceanic complex corresponding largely with Suess' original Tethys (Neo-Tethys in the present terminology) in its "wake," as it swept across the Tethyan domain much like a windshield wiper. Thus, the recommended definition of Paleo-Tethys is that it is the original triangular oceanic embayment of the Permo-Triassic Pangea that came into exisence as a byproduct of the Pangean assembly. Neo-Tethys, on the other hand, is the ocean, or the complex of oceans, that opened to the south of Paleo-Tethys, as a consequence of the counterclock- wise rotation of the Cimmerian Continent, between it and Gondwana-Land (Fig. 8). This tectonic formulation of the Paleo-Tethys concept follows the original paleobiogeographic concept of

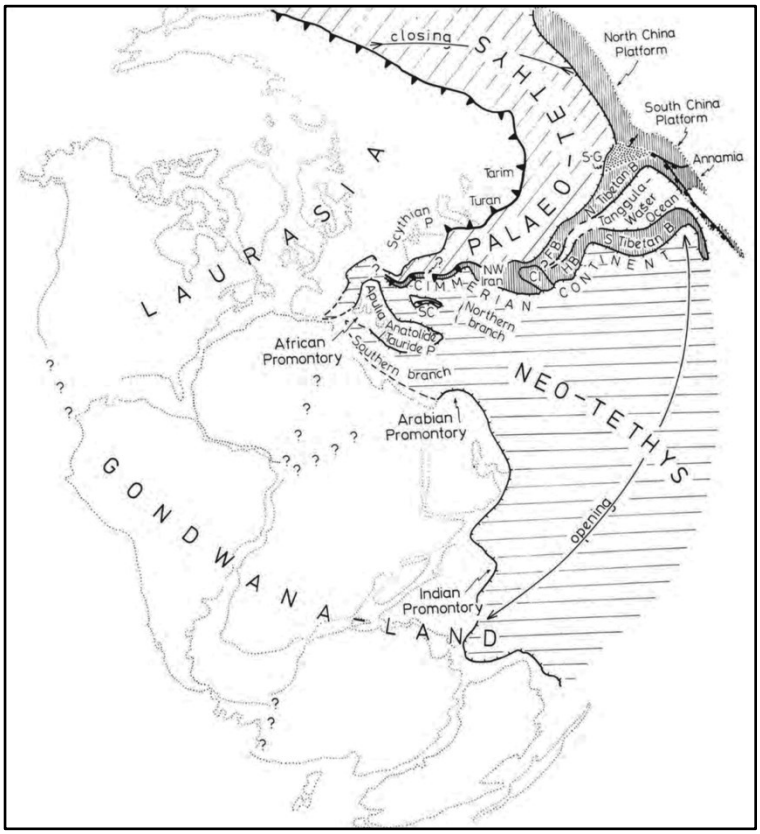

Figure 8. Semi-schematic illustration of the Tethyan domain during the early Mesozoic. This Semi-schematic figure is intended only to illustrate the fundamental idea behind the "double-ocean" concept of Tethys. To see the updated reconstruction of the early Mesozoic shape of the Cimmerian Continent and its location within the Tethyan triangle see the figure 1 of chapter 1, 2, and 3 of the present thesis. SC is the Sakarya Continent, FB is the Farah Block, and HB is the Helmand Block sensu lato. After Sengör et al. (1984).

Kahler's in the sense that the existence of the tectonic Paleo-Tethys is a necessary condition for its successor, Neo- Tethys, and it was located north of and parallel with the latter.

In the light of these definitions, Trümpy's (1982, p. 715) criticism reflects a basic misunderstanding of the concepts of Paleo- and Neo-Tethys. He notes that in the western Mediterranean "the Paleo- and Neo-Tethys distinction becomes unclear," which is easily understandable because Paleo-Tethys never extended into the western Mediterranean, so there can be no such distinction as Paleo- and Neo-Tethys in that region. The various oceanic areas that Triimpy believes ought to be called Neo-Neotethys or Neo-Neo-Neotethys should one follow the Paleo- and Neo-Tethys distinction are actually areas outside Tethys in a tectonic sense and should not be given Tethys-based names.

2.2.1. Southern Eurasia, Turan Plate, Northeast Iran (Kopeh-Dagh basin, Aghdarband area)

The Iranian block(s) was (were) located at the northern margin of the Gondwana land in Paleozoic and remained in this position until the Late Permian–Early Triassic when the Cimmerian blocks (including Central Iran, Afghanistan, Karakoram and Qiangtang) drifted from Gondwana and started to migrate toward Eurasia (Guest et al., 2006; Muttoni et al., 2009; Mattei et al., 2016) (Fig. 2), leading to the northward subduction of the Paleotethys Ocean beneath the Eurasia. The closure of Paleotethys (collision of the Central Iranian microcontinent to the southern margin of Eurasia, also called as Turan Plate) happened in Late Triassic–Early Jurassic time, resulting in the Eo-cimmerian orogeny (Berberian and King, 1981; Guest et al., 2006; Muttoni et al., 2009; Zanchi et al., 2009, 2016; Hollingsworth et al., 2010; Zanchetta et al., 2013; Berra and Angiolini, 2014; Robert et al., 2014; Mattei et al., 2014, 2017).

Following the collision of the Iran Plate and southern margin of Eurasia (Turan Plate), the Kopet-Dagh Basin was formed on the southern margin of the Eurasian Plate from the Jurassic to the Neogene (Brunet et al., 2003) (Fig. 9 A, B). The Paleotethys suture zone in northeastern Iran corresponds to the boundary between the Kopet-Dagh fold-and-thrust belt to the NE, and the eastern prolongation of the Alborz range to the SW (Robert et al., 2014) (Fig. 9B).

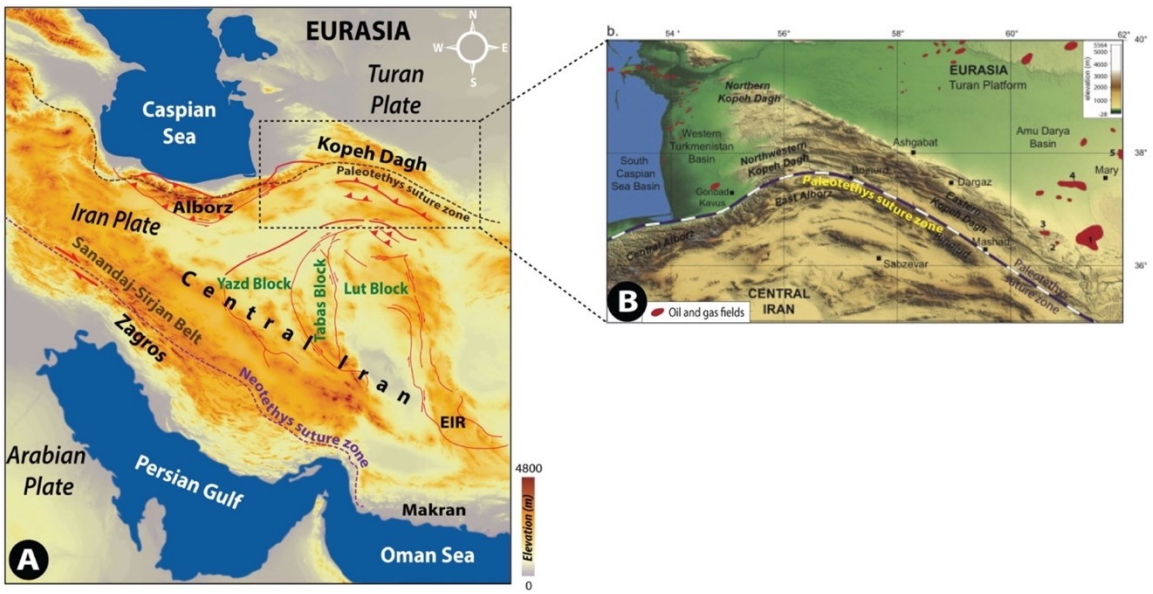

Figure 9. A. Topographic map (ETOPO 1 data) of Iran showing the Main structural zones of the area (after Stocklin & Nabavi, 1973; Berberian and King, 1981; Allen et al., 2004, 2006, 2011; Morley et al., 2009; Nozaem et al., 2013; Calzolari et al., 2016): EIZ: Eastern Iran zone. **B.** Topographic map of the Kopet Dagh range from ASTER GDEM data (Robert et al., 2014). The Paleotethys suture zone is indicated on this map.

The structural zone of Kopeh-Dagh (KD) is about 600 km long and located along the border of Iran and Turkmenistan in northern Central Iran (Fig. 9A). This zone is limited to the west by the Caspian Sea and the Alborz mountain chain, to the south by Central Iran block, and to the north and northeast by the Eurasian Amu Darya Basin (Fig. 9A, B).

The oldest rocks exposed in the KD are within the Fariman–Darreh Anjir complexes (Permian) (Zanchetta et al., 2013 and references therein) and the Aghdarband erosional window (Zanchi et al., 2016 and references therein), a basin which developed in an arc setting resulting from the northward subduction of the Palaeotethys Ocean below the southern margin of Eurasia (Ruttner, 1991, Alavi et al., 1997). These Paleozoic formations with the Triassic successions of the KD were severely deformed during the Eo-cimmerian orogeny and were unconformably covered by the Middle Jurassic Kashafrud Formation (Taheri et al., 2009; Zanchetta et al., 2013, Zanchi et al., 2016; Balini et al., 2019). The Triassic succession of Aghdarband crops out between the upper Palaeozoic basement of the Kopeh-Dagh to the north (Northern Unit) and a thick N-verging thrust stack to the south (Southern Unit) (Fig. 10).

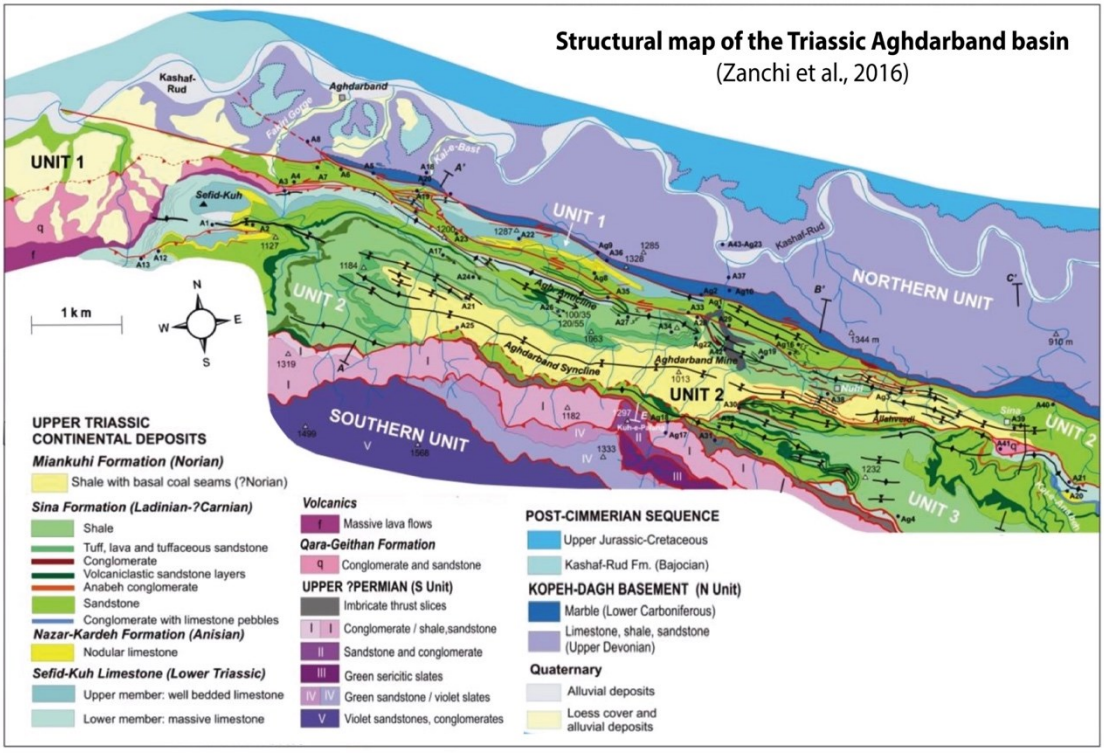

Figure 10. Geological map of the Aghdarband Area showing the three tectonic units and the various formations of the Aghdarband Basin (Zanchi et al., 2016).

The central part of the study area is subdivided in three tectonic units, namely unit 1, unit 2 and unit 3 from north to south (Fig. 10). The Triassic succession of Aghdarband basin is more than 1 km-thick and spans from the Olenekian to the Rhateian (Sefid-Kuh Limestone, Nazar-Kardeh Formation, Sina Formation and Miankuhi Formation, Ghal'eh Qabri shales) (Fig. 11). A substantial *systematic* study on the central and eastern part of the Aghdarband Basin (units 1–3) was performed by Ruttner (1991), who represented a detailed geological map at 1:12,500 scale (Ruttner, 1991: pl. 1). The 1st sub-phase of the first stage of the present PhD research was carried out in unit 2 of the Aghdarband Basin, where the most complete stratigraphic succession of the area is recorded.

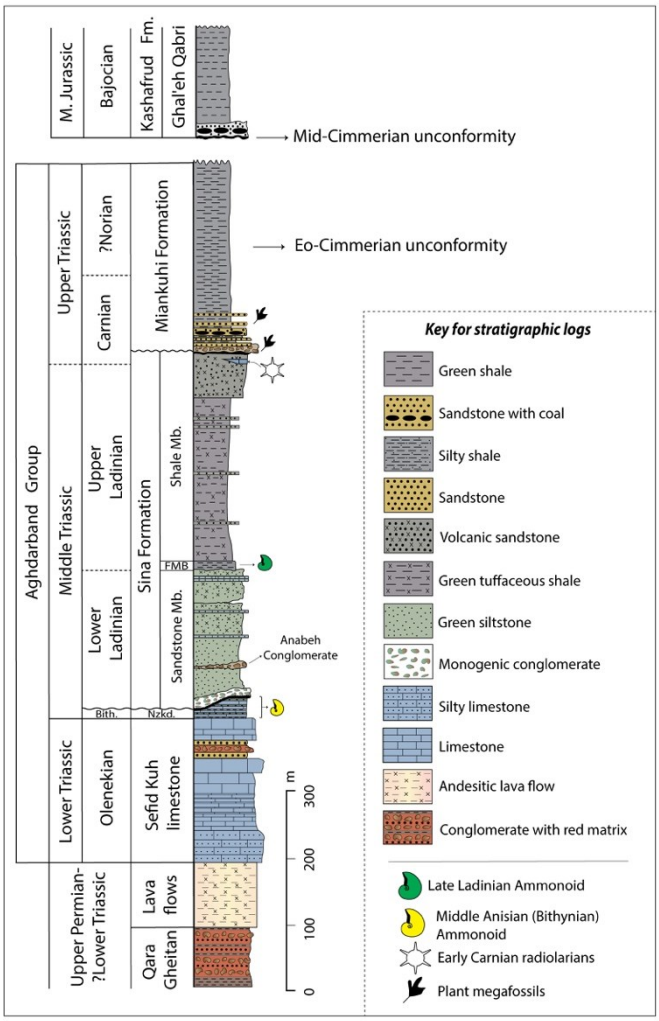

Figure 11. General lithostratigraphic column of the Triassic sequence of the Aghdarband Basin (modified from Ruttner, 1991, 1993; Zanchi et al., 2016; Balini et al., 2019).

2.2.2. *Iran Plate (Central Iran, Tabas Block)*

As a result of the collision of parts of the Cimmerian continent collage in particular the Iran Plate with Eurasia, or in more precise terms, the Turan Plate (e.g., Sengör, 1990), the former carbonate platforms, developed on the crustal blocks of the Cimmerian continent (e.g., Shotori Formation), became subaerially exposed and deeply weathered, which is indicated by palaeokarst and a widespread bauxite horizon. Subsequently, parts of the Iran Plate strongly subsided to form several basins, which were filled with predominantly siliciclastic sediments. This type of sedimentation, represented by the Shemshak Group (Aghanabati, 1998, 2004), persisted over large parts of Central Iran from the Norian to the Toarcian, at which time it was replaced by shallow water carbonates of the Badamu Formation (e.g., Seyed-Emami, 1971). In the late Triassic, Central Iran (CI) as an extensive land located between Paleothetys and Neothetys suture zones (Stöcklin 1968), was consisting of several normal faults due to tectonic movements and extensional regime while, it was a stable platform throughout Paleozoic (Davoudzadeh and Schmidt, 1985). As a significant sector of CI, the Central-East-Iran microplate (CEIM; Takin, 1972) occupied the northeast of the Urumieh–Dokhtar magmatic Belt (UDMB) and is surrounded by Sistan, Naein and Baft ophiolitic suture zones, Doroone fault and Kashmar-Sabzevar ophiolites (Fig. 12). This microplate encompasses different structural components that are not similar in lithostratigraphic aspects and they are separated by major faults (Soffel et al., 1996). These blocks are including Lut Block, Yazd Block, Anarak-Khur Block, and the Kerman-Tabas Block, (See Berberian and King, 1981; Berberian et al., 1982; Davoudzadeh, 1997; Soffel et al., 1996 for geological overviews) (Fig. 12 A).

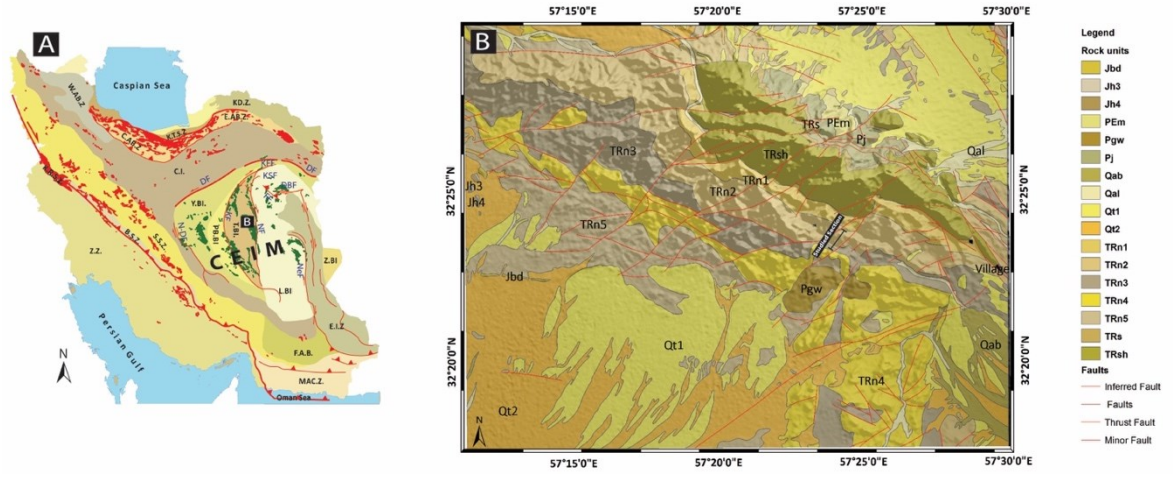

Previous page: **Figure 12. A.** Distribution of Triassic deposits in Iran. Triassic deposits of East-Central Iran and the other zones have been shown in green and orange, respectively. Its base map illustrates the main structural

zones of Iran plateau and major faults of CEIM block (after Allen et al., 2004, 2011; Berberian, 1983; Berberian and King, 1981; Calzolari et al., 2016; Morley et al., 2009; Nozaem et al., 2013; Stöcklin and Nabavi, 1973): B.S.Z: Bisutun sub-zone; C.AB.Z: Central Alborz zone; E.AB.Z: Eastern Alborz zone; W.AB.Z: Western Alborz zone; C.I: Central Iran; E.I.Z: Eastern Iran zone; Z.Z: Zagros zone; S.S.Z: Sanandaj-Sirjan zone; F.A.B: Forearc basin; K.R.S.Z: Kermanshah Radiolarite sub-zone; K.T.S.Z: Khazar-Talesh sub-zone; KD.Z: Koppeh-Dagh zone; L.BI: Lut Block; T.BI: Tabas Block; PB.BI: Posht-e-Badam Block; Y.BI: Yazd Block; MAC.Z: Makran zone; Z.BI: Zabol Block; DBF: Dasht-e-Bayaz Fault; DF: Doruneh Fault; FF: Ferdows Fault; KF: Kuhbanan Fault; KFF: Kuh-e-Faghan fault; KSF: Kuh-e-Sarhangi fault; NF: Naybandan Fault; N-DF: Nain-Dehshir Fault; NeF: Neh Fault. **B:** Simplified geological map of the studied area (Modified from Naybandan geology map (scale: 1:100000), Provided by the Geological Survey of Iran, 1981); Its base map is Digital Elevation Model (DEM). Rock unit description: PEm: Phyllitic, sandy siltstone, shale; Pj: Conglomerate, sandstone, and shale; TRn1: Recessive dark grey-green shale, arkose laterite at base Gelkan Member; TRn2: Shale, sandstone, thin orange weathering limestone fossiliferous Bidestan Member; TRn3: Recessive shale and sandstone, grey-green Howz-e-Sheikh Member; TRn4: Cliff-forming, grey, fossiliferous, reefal limestone Howz-e-Khan Member; TRn5: Silty sandstone, shale shaly siltstone, thin limestone, coal seams; TRs: Orthoquartzite and laterite at base, oolitic limestone, yellow and red shaly limestone; TRsh: Massive dolostone, light coloured, thin grey; Jbd: Shale and thin limestone, thick oolitic limestone at top; Jh3: Sandstone, shale, (intercalated), thin coal seams; Jh4: Shale, siltstone, recessive, minor sandstone; Pgw: Rhyolitic-dacitic (welded) tuff; Qab: Alluvium in braided channels and flood plains; Qal: Alluvium in major stream channels or immediately adjacent; Qt1: Alluvium in older terraces; Qt2: Alluvium in young terraces; (PE: Pre Cambrian; Pj: Permian; TR: Triassic; J: Jurassic; Pg: Paleogene; Q: Quaternary).

The second stage of the first phase of this research is conducted on the Tabas Block from Central Iran, where Mesozoic and Paleozoic sedimentary strata are well-developed (Soffel et al., 1996). The Upper Triassic successions of Tabas Block, Nayband Formation, have been palynologically investigated from a section, called as Sar-Chelenoh, 8 km west of Naybandan village and in the vicinity of Sar-Chelenoh village in the middle part of the Tabas block near its eastern border (Nayabandan fault) (Fig. 12 B). Nayband Formation, is composed of mixed carbonate-siliciclastic deposits. The lower contact of the Nayband Formation leads to Middle Triassic ancient karst called Shotori Formation and the upper contact ambiguously ends up with the Lower Jurassic Ab-e Haji Formation due to the high facies similarity between the Upper Triassic (Nayband Formation) and Lower Jurassic succession (Ab-e Haji Formation) (Kluyver et al., 1983) (Figure 13).

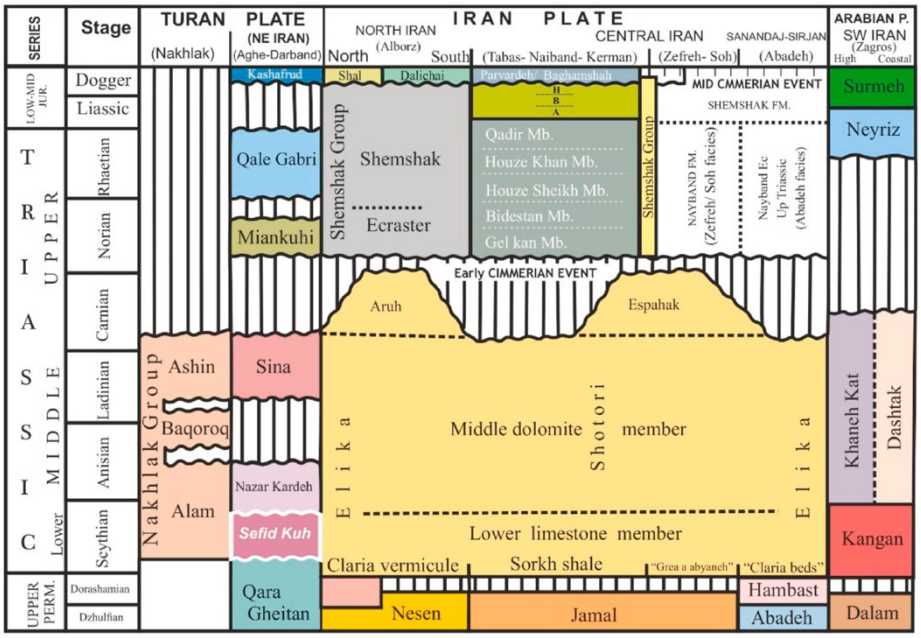

Figure 13. Lithostratigraphic scheme of Triassic deposits in Iran and position of the Miankuhi Formation in relation with upper and lower sequences (modified after Seyed-Emami, 2003. A=Abe-Haji Formation, B=Badamu Formation and H=Hojedk Formation) (Liaghat et al., 2021).

3. Material and methods

3.1. Paleobotany

The studied macroflora come from a stratigraphic section called Allahverdi (35.98°N, 60.87°E; from Aghdarband area (Turan Plate, Kopeh-Dagh basin, NE Iran). The plant fossil assemblage is composed of 28 specimens, generally preserved as compressions or impressions. Since sphenophytes are very delicate, their remains are mostly preserved as internal casts and impressions. Thus, only a macromorphological study was carried out. The fossils are stored in the palaeontological collection of Piero Leonardi Museum of Paleontology and Prehistory (MPL: Museo di Paleontologia e Preistoria Piero Leonardi) in Ferrara, Italy. Hand specimens were photographed with a Nikon 3200D digital camera and microscope Leica 165C equipped with Leica 170HD camera.

3.2. Palynology

108 samples were collected from the Aghdarband basin (NE Iran) and Tabas Block (Central Iran). Samples were macerated and treated with HCl, HF and HNO3. After washing and sieving

(15 μm), the residue was stored in water. Slides were prepared with special glue (Entellan) and are stored in the Department of Physics and Earth Sciences of the Ferrara University.
The microscope slides were investigated under a Leica DM750 light microscope, and the index species were photographed using the Leica ICC50 W digital camera.

3.3. Geochemical analyses

3.3.1. Hg as a volcanic proxy

The distribution pattern of mercury (Hg) in sediments has recently been considered as a promising tool for the interpretation of paleoclimatic and paleoecologic conditions and also for tracking hypothesized sources of paleoenvironmental perturbations in various sites. Several studies performed on the application of Hg proxy in Phanerozoic environmental crises and oceanic anoxic events (OAEs) related to documented or assumed Large Igneous Province (LIP) emplacements as mechanisms of controlling Hg cycling (e.g., Sanei et al., 2012; Percival et al., 2015; Thibodeau et al., 2016; Grasby et al., 2017; Scaife et al., 2017; Wang et al., 2018; Fantasia et al., 2018). Nevertheless, many experts have highlighted the role of biomass burning, increased detrital inputs (rock weathering and soil loss), and/or some combination of them in the interpretation of Hg concentrations during geological events with widespread climatic and biological perturbations (e.g., Vandal et al., 1993; Martínez-Cortizas et al., 1999; Santos et al., 2002; Them et al., 2019).

The use of Hg as a volcanic tracer is based on the known emission of the element from modern volcanoes to the atmosphere and oceans, and the relatively long atmospheric residence time of gaseous elemental mercury (0.5–2 years; Schroeder and Munthe, 1998; Blum et al., 2014), allowing it to be distributed globally before being deposited in sediments (Fig. 10: Slemr et al., 1985; Pyle and Mather, 2003) (Fig. 14). Mercury is expelled into the atmosphere from several sources including the oceans, biomass burning, rock weathering, soil erosion and volcanism (e.g., Blum et al., 2014, Grasby et al., 2017; Schuster et al., 2018, Them et al., 2019). Elemental Hg (Hg^0), which is the dominant form of mercury in atmosphere, can be directly absorbed by the vegetation and soils followed by oxidation and/or transformed to oxidized reactive Hg^{+2}, soluble in water and, therefore, enriched in the rain and is typically deposited during rainfall (e.g. Schroeder and Munthe, 1998; Witt et al., 2008). Mercury reaches to the ocean through direct atmospheric deposition and/or terrestrial riverine runoff (e.g., Holmes et al., 2010; Amos et al., 2014) while it has also the potential of being frequently recycled in the environment (e.g., Driscoll et al., 2013; Them et al., 2019) prior the sequestration in marine sediments (as

reviewed by Fitzgerald and Lamborg, 2014). The majority of riverine-derived Hg, however, is deposited in shallow proximal locations (e.g., Amos et al., 2014; Them et al., 2019).

In marine environments, dissolved Hg^{+2} may be affected by some of the biotic and abiotic processes resulting in the formation of organic-Hg complexes. The organic matter (OM) is one of the main sinks of mercury in the ocean system, with respecting to this and also the role of climate warming in the enhancement of biological production, the Hg scavenging through enhanced organic-rich particles under such a climate condition (e.g., CPE) could be increased and then deposited in the seabed through time (e.g., Vandal et al., 1993; Outridge et al., 2007; Stern et al., 2009; Sanei et al., 2012; Grasby et al., 2013). This model is well substantiated by the significant positive correlation between increasing trend of OM and Hg observed in modern sediments (Gehrke et al., 2009; Outridge et al., 2007; Ruiz and Tomiyasu, 2015; Sanei et al., 2014). Furthermore, mercury can also be adsorbed through sulfide production and preservation in which the dissolved Hg in sediment pore water can be scavenged by many components of the solid phase of the bottom sediments, particularly by pyrite and/or other sulphides complexes (Benoit et al., 1999; Niessen et al., 2003).In an environment with low organic scavenging capacity, the oxidized Hg^{+2} remains in solution and is, eventually, adsorbed onto clays and transported from land to sea; hence clay minerals as the alternative mercury sinks are capable of elevating Hg concentrations in argillaceous sediments which may suggest the increased flux of volcanogenic Hg from continents into the oceans. In this case, Hg and Al_2O_3 are expected to impose a pattern of covariation, as for example observed in some sections across the KPg boundary (e.g. Sial et al., 2013, 2016), and/or during the T-OAE interval (e.g., Percival et al., 2015; Fantasia et al., 2018).

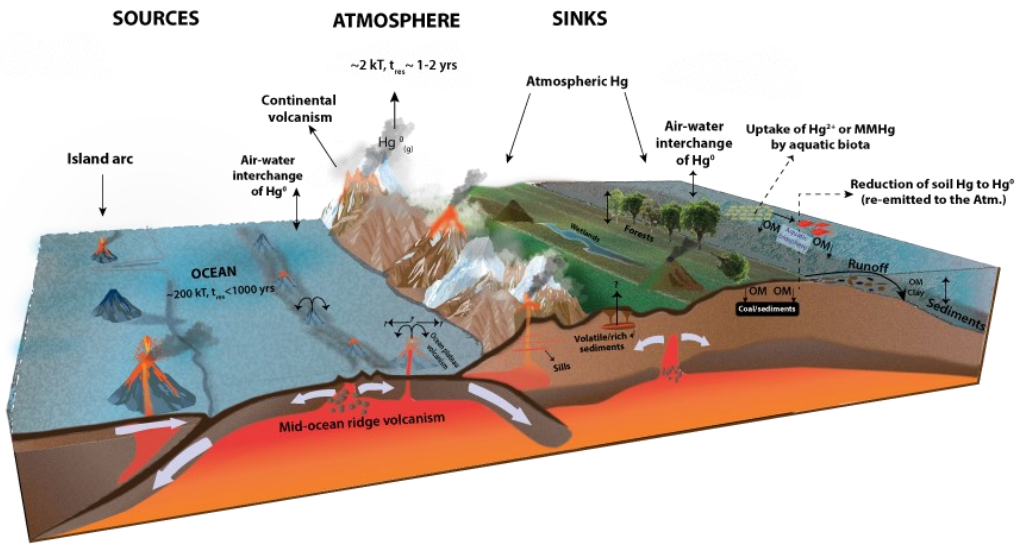

Figure 14. Simplified illustration of the global mercury cycle, adapted from Percival and others (2015). Processes affecting the source, sink, and transportation of mercury through the ocean–atmosphere system are indicated as follows: **1** – Volcanic emission of mercury, chiefly as inert gaseous elemental mercury (Hg^0) to the atmosphere; **2** – Hydrothermal emission of Hg to the ocean at mid-ocean ridges; **3** – Presumed equivalent release of hydrothermal Hg to the ocean from submarine ocean plateau volcanism, similar to that at mid-ocean ridges; **4** – Possible emission of thermogenic Hg to the atmosphere following heating of organic-rich sediments by intruding sills; **5** – Deposition of atmospheric Hg to land, water, or forest canopy, either as particulate Hg (dry deposition) or soluble oxidized mercury (Hg^{2+}) following interaction between atmospheric Hg^0 and atmospheric oxidizing agents such as halogen, nitrile, ozone, and hydroxyl radicals (wet deposition); **6** – Air–water interchange of Hg^0; **7** – Conversion of mercury species between Hg^0, Hg^{2+}, MMHg (monomethylmercury) and DMHg (dimethylmercury) through multiple biotic and abiotic reactions in aquatic environments (for example, Fitzgerald and others, 2007; Selin, 2009; Bowman and others, 2015; summarized in Munthe and others, 2009); **8** – Reduction of soil Hg to Hg^0, which is subsequently re-emitted to the atmosphere; **9** – Interchange of mercury between soil and forest canopy through emission of soil Hg and decay of leaves that have taken up Hg; **10** – High abundance of sulfate- and/or iron-reducing bacteria in reduced wetland environments promoting methylation of Hg^{2+} to organophilic MMHg, which can adsorb onto organic matter; **11** – Deposition of sediments in Hg–OM complexes to soils, peats, or coals; **12** – Riverine runoff (and potentially deposition) into lacustrine or marine environments of detrital Hg bound to either organic matter or clay minerals; **13** – Uptake of Hg^{2+} or MMHg by aquatic biota; **14** – Bioaccumulation of organophilic MMHg up the food chain; **15** – Deposition of bioaccumulated Hg into sediments as Hg–OM complexes; **16** – Potential remobilization and release of sedimentary Hg into the aquatic realm. Atmospheric and oceanic residence times of Hg are indicated (Slemr and others, 1985; Gill and Fitzgerald, 1988).

3.3.1.1. Hg analyses

A total of 243 samples from western Tethyan sections were processed and analyzed for Hg concentrations using a Mercury Analyzer with PYRO-915 Pyrolyzer, Lumex, at the University of Oxford, using the method described by Bin et al. (2001). For each basin, sections were analyzed from a few meters below the base of negative CIE to a few meters above the top of negative CIE. Samples were powdered with an agate mortar. Powdered sample (50 - 250 mg) was weighed into a glass boat before being placed into the pyrolyzer (set at Mode 1) and heated to 700°C. Volatilized elementary Hg was collected by gold amalgamation trap before being detected and calculated via spectral analyses. Throughout the measurement sequences, 74 paint-contaminated soil (NIST 2587; 290 ppb Hg) standards were analyzed, using masses ranging from 10 to 90 mg, to calibrate the Lumex.

The analysed standards indicate reproducibility was generally better than 10% for Hg concentrations. TOC normalization of Hg was applied when TOC was above or equal to 0.2% following the approach recommended by Grasby et al. (2013, 2015). Organic carbon $\delta^{13}C$ data (Dal Corso et al., 2015; 2018) are coupled to the new Hg data, and Hg/Al has been calculated using published elemental data of Baranyi et al. (2019), which were measured on the same core material.

3.3.2. Analysis of total organic carbon (TOC)

A Soli TOC Cube (Elementar Analysensysteme, Hanau, Germany) was used for the determination of Total Organic Carbon (TOC) in rock samples. The analyzer is equipped with two combustion units: a dynamic heater able to raise the temperature from ambient to 900 °C and a post-combustion zone kept at a constant temperature of 800°C, containing a platinum catalyst to achieve complete oxidation of all combustion products released by the dynamic heater. Combustion takes place in pure oxygen at a flow rate of 150 ml/min. The formed CO_2 is detected by an infrared detector. About 500 mg of each sample were weighed into stainless steel crucibles that were heated prior to analysis to avoid contamination by C residues. Values are reported as the mean of duplicate analysis. The sample weight depended on the C content and could be extended up to 1 g in case C contents were too small. A standard of calcium carbonate ($CaCO_3$, Calciumcarbonat, Elementar Analysensysteme, Hanau, Germany) and a soil standard ($CaCO_3$, Bodenstandard, Elementar Analysensysteme, Hanau, Germany) were analyzed prior, between, and after each run. TOC was determined by using temperature programming, described as “temperature-dependent differentiation of total carbon” (DIN

19539) as described by Natali et al. (2020). The dynamic temperature ramping method starts at about 100 °C. After introducing the sample, the temperature increases with a rate of 90 °C / minute to 600 °C for the determination of TOC. The average standard deviation (SD), based on replicate analyses of nine samples and a soil standard (Bodenstandard) was +/-0.02 wt%.

References

Afshar-Harb, A., 1994 - Geology of Kopet Dagh. *Treatise on the Geology of Iran*, 11, 1-275.

Aghanabati, S. A., 1998 - Jurassic Stratigraphy of Iran, *Vols 2. Geological Survey of Iran, Tehran*.

Aghanabati, S. A., Saidi, A., Ghasemi-Nejad, E., Ahmadzadeh, H. M., and Dabiri, O., 2004 - Palinozonation of basal part of the Shemshak Group deposits (Upper Triassic) in North Alborz domain on the basis of dinoflagellates. *www.SID.ir. Development,* 7(4), 2-14 [in Persian].

Alavi, M., Vaziri, H., Seyed-Emami, K., and Lasemi, Y., 1997 - The Triassic and associated rocks of the Nakhlak and Aghdarband areas in central and northeastern Iran as remnants of the southern Turanian active continental margin. *Bulletin of the Geological Society of America*, 109(12): 1563-1575.

Allen, M., Jackson, J., and Walker, R., 2004 - Late Cenozoic reorganization of the Arabia-Eurasia collision and the comparison of short-term and long-term deformation rates. *Tectonics*, *23*(2).

Allen, M. B., Blanc, E. J., Walker, R., Jackson, J., Talebian, M., and Ghassemi, M. R., 2006 - Contrasting styles of convergence in the Arabia-Eurasia collision: Why escape tectonics does not occur in Iran. *special papers-Geological Society of America*, pp. 409-579.

Allen, M. B., Kheirkhah, M., Emami, M. H., and Jones, S. J., 2011 - Right-lateral shear across Iran and kinematic change in the Arabia—Eurasia collision zone. *Geophysical Journal International*, 184(2), 555-574.

Amos, H. M., Jacob, D. J., Kocman, D., Horowitz, H. M., Zhang, Y., Dutkiewicz, S., ... and Sunderland, E. M., 2014 - Global biogeochemical implications of mercury discharges from rivers and sediment burial. *Environmental science & technology*, *48*(16), 9514-9522.

Arche, A., Lopez-Gomez, J., 2014 - The Carnian Humid Event in Western Europe: New data from Iberia and correlation with the Western Neotethys and Eastern North America–NW Africa regions. *Earth Science Reviews*, 128, 196-231.

Assereto, R., Desio, A., Di Colbertaldo, D., and Passeri, L.D., 1968 - Note illustrative della Carta Geologica d'Italia alla scala 1:100.000. *Foglio 14, Tarvisio, Servizio Geologico d'Italia*. pp. 1–70.

Balini M., Nicora A., Zanchetta S., Zanchi A., Marchesi R., Vuolo I., Hosseiniyoon M., Norouzi M. and Soleimani S., 2019 - Olenekian to Early Ladinian stratigraphy of the western part of the Aghdarband window (Kopeh-Dag, NE Iran) . *Rivista Italiana di Paleontologia e Stratigrafia*, 125(1): 283-315.

Balini, M., Lucas, S.G., Jenks, J.F., Spielmann, J.A., 2010 - Triassic ammonoid biostratigraphy: an overview. *Geological Society Special Publication*. 334, 221–262.

Balini, M., Nicora, A., Berra, F., Garzanti, E., Levera, M., Mattei, M., Muttoni, G., Zanchi, A., Bollati, I., Larghi, C., Zanchetta, S., Salamati, R., and Mossavvari, F., 2009 - The Triassic stratigraphic succession of Nakhlak (central Iran) a record from an active margin. *Geological Society Special Publication*, 312(1): 287-321.

Baranyi, V., Kürschner, W.M., Ruffell, A., Mark, W., and Miller, C.S. 2018 - A continental record and climatic implications. *Journal of the Geological Society*, 176: 149-166.

Baranyi, V., Miller, C. S., Ruffell, A., Hounslow, M. W.,and Kürschner, W. M., 2019 - A continental record of the Carnian Pluvial Episode (CPE) from the Mercia Mudstone Group (UK): palynology and climatic implications. *Journal of the Geological Society*, 176(1), 149-166.

Baranyi, V., Rostási, Á., Raucsik, B., and Kürschner, W.M., 2019 - Palynology and weathering proxies reveal climatic fluctuations during the Carnian Pluvial Episode (CPE) (Late Triassic) from marine successions in the Transdanubian Range (western Hungary): *Global and Planetary Change*. v. 177, p. 157-172.

Benoit JM, Gilmour, C.C., Mason, R.P., and Heyes, A., 1999 - Sulfide controls on mercury speciation and bioavailability to methylation bacteria in sediment pore waters. *Environ Sci Technol*. 33: 951–957.

Benton, M. J., Bernardi, M., and Kinsella, C., 2018 - The Carnian Pluvial Episode and the origin of dinosaurs. *Journal of the Geological Society*, *175*(6), 1019-1026.

Berberian, M., & King, G.C.P., 1981 - Towards a Paleogeography and Tectonic Evolution of Iran. *Canadian Journal of Earth Sciences*, 18(2): 210-265.

Berberian, F., Muir, I. D., Pankhurst, R. J., & Berberian, M., 1982 - Late Cretaceous and early Miocene Andean-type plutonic activity in northern Makran and Central Iran. *Journal of the Geological Society*, 139(5), 605-614.

Berberian, M., 1983 - Continental deformation in the Iranian Plateau. *Geological Survey of Iran publications*.

Bernardi, M., Gianolla, P., Petti, F.M., Mietto, P., and Benton, M.J., 2018 - Dinosaur diversification linked to the Carnian Pluvial Episode: *Nature Communications*, v. 9, p. 1-10.

Berra, F., and Angiolini, L, 2014 - The evolution of the Tethys region throughout the Phanerozoic: A brief tectonic reconstruction. *AAPG special volumes*, p. 1-27.

Bin, C., Xiaoru, W., and Lee, F.S.C., 2001 - Pyrolysis coupled with atomic absorption spectrometry for the determination of mercury in Chinese medicinal materials: *Analytica Chimica Acta*, v. 447, p. 161-169.

Boersma M. and van Konijnenburg-van Cittert J.H.A., 1991 - Late Triassic plant megafossils from Aghdarband (NE-Iran). In: A.W. Ruttner (Ed.) - The Triassic of Aghdarband (AqDarband), NE-Iran, and its pre-Triassic frame. *Abhandlungen Der Geologischen Bundesanstalt*, 38: 223-252.

Bosellini, A., Gianolla, P., and Stefani, M., 2003 - Geology of the Dolomites. Episodes 26, 181-185.

Boucot, A.J., Xu, C., Scotese, C.R., and Morley, R.J., 2013 - Phanerozoic climate: an atlas of lithologic indicators of climate. *SEPM Concepts Sedimentol. Paleontol*. 11.

Blum, J. D., Sherman, L. S., and Johnson, M. W., 2014 - Mercury isotopes in earth and environmental sciences. *Annual Review of Earth and Planetary Sciences*, *42*, 249-269.

Breda, A., Preto, N., 2011 - Anatomy of an Upper Triassic continental to marginal-marine system: The mixed siliciclastic-carbonate Travenanzes Formation (Dolomites, Northern Italy). *Sedimentology*. 58, p. 1613–1647.

Breda, A., Preto, N., Roghi, G., Furin, S., Meneguolo, R., Ragazzi, E., Fedele, P., and Gianolla, P., 2009. The Carnian Pluvial Event in the Tofane area (Cortina d'Ampezzo, Dolomites, Italy). *Geol. Alps*. 6, 80–115.

Brunet, F.F., Korotaev, M. V., Ershov, A. V., and Nikishin, A.M., 2003 - The South Caspian Basin: A review of its evolution from subsidence modelling. *Sedimentary Geology*, 156(1-4): 119-148.

Brusatte, S.L., Benton, M.J., Ruta, M., Lloyd, G.T., 2008 - Superiority, competition, and opportunism in the evolutionary radiation of the dinosaurs. *Science*, 321, 1485–1488.

Budai, T., Császár, G., Csillag, G., Dudko, A., Koloszár, L., Majoros, G., 1999 - Geology of the Balaton Highland. *Occasional Papers, 197. Geological Institute of Hungary, Budapest*, pp. 1–257.

Budai, T., Haas, J., 1997 - Triassic sequence stratigraphy of the Balaton Highland, Hungary. *Acta Geol. Hung.* 40 (3), 307–335.

Caggiati, M., Gianolla, P., Breda, A., Celarc, B., and Preto, N., 2018 - The start-up of the Dolomia Principale/Hauptdolomit carbonate platform (Upper Triassic) in the eastern Southern Alps. *Sedimentology*. 65, 1097–1131.

Calzolari, G., Rossetti, F., Seta, M. Della, Nozaem, R., Olivetti, V., Balestrieri, M.L., Cosentino, D., Faccenna, C., Stuart, F.M., and Vignaroli, G., 2016 - Spatiotemporal evolution of intraplate strike-slip faulting: The Neogene-Quaternary Kuh-e-Faghan Fault, central Iran. *Bulletin of the Geological Society of America*, 128(3-4): 374-396.

Cao, W., Zahirovic, S., Flament, N., Williams, S., Golonka, J., and Müller, R. D., 2017 - Improving global paleogeography since the late Paleozoic using paleobiology. *Biogeosciences*, 14(23), 5425-5439.

Charbonnier, G., Adatte, T., Follmi, K.B., and Suan, G., 2020 - Effect of intense weathering and postdepositional degradation of organic matter on Hg/TOC proxy in organic-rich sediments and its implications for deep-time investigations. *Geochemistry, Geophysics, Geosystems*, 21, e2019GC008707.

Chen, Y, Krystyn, L., Orchard, M.J., Lai, X.-L., and Richoz, S., 2015 - A review of the evolution, biostratigraphy, provincialism and diversity of Middle and early Late Triassic conodonts. *Papers in Palaeontology*, 2, 235–263.

Chu, D., et al., 2020, Ecological disturbance in tropical peatlands prior to marine Permian-Triassic mass extinction: *Geology*, v. 48, p. 288-292.

Corsin, P., and Stampfli, G., 1977 - La Formation de Shemshak dans L'elburz Oriental (Iran) Flore-Stratigraphie-Paléogéographie. *Geobios*, 10: 509-571.

Csontos L., Nagymarosy A , Horváth F. and Kováč M., 1992 - Tfertiary evolution of the Intra-Carpathian area: a model. *Tectonophysics*, 208,221-241.

Csillag, G., Budai, T., Gyalog, L., and Koloszár, L., 1995 - Contribution to the upper Triassic geology of the Keszthely Mountains (Transdanubian Range), western Hungary. *Acta Geologica Hungarica*, *38*(2), 111-129.

Dal Corso, J., Bernardi, M., Sun, Y., Song, H., Seyfullah, L.J., Preto, N., Gianolla, P., Ruffell, A., Kustatscher,

E., Roghi, G., Merico, A., Hohn, S., Schmidt, A.R., Marzoli, A., Newton, R.J., Wignall, P.B., and Benton, M.J., 2020 - Extinction and dawn of the modern world in the Carnian (Late Triassic). *Science Advances*. 6(38): eaba0099.

Dal Corso, J., Gianolla, P., Newton, R.J., Franceschi, M., Roghi, G., Caggiati, M., Raucsik, B., Budai, T., Haas, J., and Preto, N., 2015 - Carbon isotope records reveal synchronicity between carbon cycle perturbation and the "Carnian Pluvial Event" in the Tethys realm (Late Triassic). *Global and Planetary Change* 127, 79–90.

Dal Corso, J., Gianolla, P., Rigo, M., Franceschi, M., Roghi, G., Mietto, P., Manfrin, S., Raucsik, B., Budai, T., Jenkyns, H.C., Reymond, C.E., Caggiati, M., Gattolin, G., Breda, A., Merico, A., and Preto, N., 2018 - Multiple negative carbon-isotope excursions during the Carnian Pluvial Episode (late Triassic). *Earth Sci. Rev*. 185, 732–750.

Dal Corso, J., Mietto, P., Newton, R.J., Pancost, R.D., Preto, N., Roghi, G., and Wignall, P.B., 2012 - Discovery of a major negative δ13C spike in the Carnian (Late Triassic) linked to the eruption of Wrangellia flood basalts. Geology 40, 79–82.

Dal Corso, J., Mills, B.J., Chu, D., Newton, R.J., Mather, T.A., Shu, W., Wu, Y., Tong, J., and Wignall, P.B., 2020b - Permo–Triassic boundary carbon and mercury cycling linked to terrestrial ecosystem collapse: *Nature Communications*, v. 11, p. 1-9.

Dal Corso, J., Preto, N., Kustatscher, E., Mietto, P., Roghi, G., and Jenkyns, H.C, 2011 - Carbon-isotope variability of Triassic amber, as compared with wood and leaves (Southern Alps, Italy). *Palaeogeography, Palaeclimatology, Palaeoecology* 302, 187– 193.

Dal Piaz, G. V., Bistacchi, A., and Massironi, M., 2003 - Geological outline of the Alps. *Episodes*, 26(3), 175-180.

Datta, P.M., 2005 - Earliest mammal with transversely expanded upper molar from the Late Triassic (Carnian) Tiki Formation, South Rewa Gondwana Basin, India. *Journal of Vertebrate Paleontology*, 25, 200–207.

Davoudzadeh, M., and Schmidt, K., 1985 - Contribution to the paleogeography, stratigraphy and tectonics of the Cretaceous and Paleocene of Iran. *Neues Jahrbuch Für Geologie Und Paläontologie. Abhandlungen*, 169(3): 284-306.

De Zanche, V., Gianolla, P., Mietto, P., Siorpaes, C., Vail, P.R., 1993 - Triassic sequence stratigraphy in the Dolomites (Italy). *Mem. Sci. Geol*. 45, 1–27.

De Zanche, V., Gianolla, P., and Roghi, G., 2000 - Carnian stratigraphy in the Raibl/Cave del Predil area (Julian Alps, Italy). *Eclogae Geologicae Helvetiae*. 93, 331–347.

Dickens, G.D., O'Neil, J., Rea, D.K., and Owen, R.M. 1995 - Dissociation of methane hydrate as a cause of the carbon isotope excursion at the end of the Paleocene. *Paleoceanography*, 10, 965–971.

Diefendorf, A. F., Mueller, K. E., Wing, S. L., Koch, P. L., and Freeman, K. H., 2010 - Global patterns in leaf 13C discrimina- tion and implications for the studies of past and future climate. Proc. *Nat. Acad. Sci*. 107, 5738–5743.

Dobruskina, I.A., 1998 - Lunz flora in the Austrian Alps - A standard for Carnian floras In: *Palaeogeography, Palaeoclimatology, Palaeoecology*, 143 (4): 307–345.

Donofrio, D.A., 1991 - Radiolaria and Porifera (spicula) from the Upper Triassic of Aghdarband (NE-Iran). *Abhandlungen Der Geologischen Bundes-Anstalt*, 38, 205-222.

Dosztály, L., S. Kovács, T. and Budai, 1989 - Pécsely, Meggy hegy quarry. *In XXI Europea Micropalaeontological Colloquium, Guidebook*.

Driscoll, C. T., Mason, R. P., Chan, H. M., Jacob, D. J., and Pirrone, N., 2013 - Mercury as a global pollutant: sources, pathways, and effects. *Environmental science & technology*, 47(10), 4967-4983.

Dunhill, A.M., Foster, W.J., Sciberras, J., and Twitchett, R.J., 2017 - Impact of the Late Triassic mass extinction on functional diversity and composition of marine ecosystems. *Palaeontology*, 10.1111/pala.12332.

Eftekharnezhad, J., and Behroozi, A., 1991 - Geodynamic significance of recent discoveries of ophiolites and late Paleozoic rocks in NE-Iran (including Kopet Dagh). *Abhandlungen Der Geologischen Bundesanstalt*, 38, 89-100.

Fantasia, A., Föllmi, K. B., Adatte, T., Bernárdez, E., Spangenberg, J. E., and Mattioli, E., 2018 - The Toarcian oceanic anoxic event in southwestern gondwana: an example from the Andean Basin, northern Chile. *Journal of the Geological Society*, *175*(6), 883-902.

Fitzgerald, W.F., and Lamborg, C.H., 2014 - Geochemistry of mercury in the environment. In: Treatise of Geochemistry, vol. 11, 2nd edition, pp. 91–129.

Fodor L, Csontos L, Bada G, Gyo¨rfi I, and Benkovics L., 1999 - Tertiary tectonic evolution of the Pannonian basin system and neigh- bouring orogens: a new synthesis of palaeostress data. In: Durand B, Jolivet L, Horvath F, Seranne M. (eds) The Mediterranean Basins: tertiary extension within the Alpine Orogen. *Geological Society Special Publications*. 156:295–334.

Franz, M., Kustatscher, E., Heunisch, C., Niegel, S., and Röhling, H.G., 2019 - The Schilfsandstein and its flora; arguments for a humid mid-Carnian episode? *Journal of the Geological Society*, 176(1): 133-148.

Franz, M., Nowak, K., Berner, U., Haunisch, C., Bandel, K., Rohling, H.G., and Wolfgramm, M., 2014 - Eustatic control on epicontinental basins: the example of the Stuttgart Formation in the Central European Basin (Middle Keuper, Late Triassic). *Global and Planetary Change*, 122, 305–329.

Fu, X., Wang, J., Wen, H., Wang, Z., Zeng, S., Song, C., Chen, W., and Wan, Y., 2020 - A possible link between the Carnian Pluvial Event, global carbon-cycle perturbation, and volcanism: New data from the Qinghai-Tibet Plateau: *Global and Planetary Change*, v. 194, 103300.

Furin, S., Preto, N., Rigo, M., Roghi, G., Gianola, P., Crowley, J.L. and Bowring, S.A., 2006 - High- precision U–Pb zircon age from the Triassic of Italy: implications for the Triassic time scale and the Carnian origin of calcareous nannoplankton and dinosaurs. *Geology*, 34:1009–1012.

Fürsich, F. T., Wilmsen, M., Seyed-Emami, K., Cecca, F., and Majidifard, M. R., 2005 - The upper Shemshak Formation (Toarcian–Aalenian) of the Eastern Alborz (Iran): Biota and palaeoenvironments during a transgressive–regressive cycle. *Facies*, *51*(1-4), 365-384.

Fürsich, F. T., Wilmsen, M., Seyed-Emami, K., and Majidifard, M. R., 2009 - The Mid-Cimmerian tectonic event (Bajocian) in the Alborz Mountains, Northern Iran: evidence of the break-up unconformity of the South Caspian Basin. *Geological Society, London, Special Publications*, 312(1), 189-203.

Galimov, E.M., 2006 - Isotope organic geochemistry. *Org. Geochem*. 37, 1200–1262.

Gallet, Y., Besse, J., Krystyn, L., Thaveniaut, H., and Marcoux, J., 1994 - Magnetostratigraphy of the Mayerling section (Austria) and Erenkolu Mezarlik (Turkey) section: Improvement of the Carnian (Late Triassic) magnetic polarity time scale. *EPSL*. 125, 173–191.

Garzanti, E., and Gaetani, M., 2002 - Unroofing history of late paleozoic magmatic arcs within the “Turan Plate”

(Tuarkyr, Turkmenistan). *Sedimentary Geology*, 151(1-2), 67-87.

Gattolin, G., Preto, N., Breda, A., Franceschi, M., Isotton, M., and Gianolla, P., 2015 - Sequence stratigraphy after the demise of a high-relief carbonate platform (Carnian of the Dolomites): Sea-level and climate disentangled. *Palaeogeography, Palaeoclimatology, Palaeoecology,* 423:1–17.

Gawlick, H.-J., 2000 - Paläogeographie der Ober-Trias Karbonatplattform in den nördlichen Kalkalpen. Mitteilungen der Gesellschaft der Geologie- & Bergbaustudenten Österreich 44, 45–95.

Gehrke, G.E., Blum, J.D., and Meyers, P.A., 2009 - The geochemical behaviour and iso- topic composition of Hg in a mid-Pleistocene western Mediterranean sapro- pel. Geochim. osmochim. Acta 73, 1651–1665.

Ghasemi-Nejad, E., Head, M.J., and Zamani, M., 2008 - Dinoflagellate cysts from the Upper Triassic (Norian) of northeastern Iran. *Journal of Micropalaeontology*, 27(2), 125-134.

Ghorbani, M., 2019 - Lithostratigraphy of Iran (p. 274). *Springer International Publishing*.

Gianolla P., Morelli C., Cucato M. & Siorpaes C., 2018 - Note Illustrative della Carta Geologica d'Italia alla scala 1: 50.000, Foglio 016, Dobbiaco, pp. 1-283. ISPRA, 20 2018, Roma.

Gianolla, P., De Zanche, V., and Roghi, G., 2003 - An Upper Tuvalian (Triassic) Platform-Basin System in the Julian Alps: the Start-up of the Dolomia Principale (Southern Alps, Italy). *Facies* 49, 135–150.

Gianolla, P., Ragazzi, E., and Roghi, G., 1998 - Upper Triassic amber from the Dolomites (Northern Italy). A paleoclimatic indicator?: *Rivista Italiana di Paleontologia e Stratigrafia*, v. 104, p. 381-390.

Gill, G. A., and Fitzgerald, W. F., 1988 - Vertical mercury distributions in the oceans. *Geochimica et Cosmochimica Acta*, 52(6), 1719-1728.

Góczán, F., Oravecz-Scheffer, A., and Csillag, G., 1991 - The stratigraphic characterization of the Cordevolian and Julian Formations of Csukréti Ravine, *Balatoncsicsó. Földt. Int*. Évi Jel. 241–323.

Góczán, F., Oravecz–Scheffer, A., 1996a - Tuvalian sequences of the Balaton Highland and the Zsámbék Basin, Part I: Litho-, bio- and chronostratigraphic subdivision. *Acta Geologica Hungarica*. 39 (/1), 1–31.

Góczán, F., Oravecz–Scheffer, A., 1996b - Tuvalian sequences of the Balaton Highland and the Zsámbék Basin, Part II: Characterization of sporomorph and foraminifer assemblages, biostratigraphic, palaeogeographic and geohistoric conclusions. *Acta Geologica Hungarica* 39/1, 33–101.

Grasby, S.E., Beauchamp, B., Bond, D.P.G., Wignall, P.B., Talavera, C., Galloway, J.M., Piepjohn, K., Reinhardt, L., and Blomeier, D., 2015 - Progressive environmental deterioration in northwestern Pangea leading to the latest Permian extinction: *Geological Society of America Bulletin*, v. 127, p. 1331–1347.

Grasby, S.E., Sanei, H., Beauchamp, B., and Chen, Z., 2013 - Mercury deposition through the Permo–Triassic biotic crisis: *Chemical Geology*, v. 351, p. 209-216

Grasby, S. E., Shen, W., Yin, R., Gleason, J. D., Blum, J. D., Lepak, R. F., ... and Beauchamp, B., 2017 - Isotopic signatures of mercury contamination in latest Permian oceans. *Geology*, *45*(1), 55-58.

Grasby, S.E., Them II, T.R., Chen, Z., Yin, R., and Ardakani, O.H., 2019 - Mercury as a proxy for volcanic emissions in the geologic record: Earth-Science Reviews, v. 196, 102880.

Greene, A.R., Scoates, J.S., Weis, D., Katvala, E.C., Israel, S., Nixon, G.T., 2010 - The architecture of oceanic plateaus revealed by the volcanic stratigraphy of the accreted Wrangellia oceanic plateau. *Geosphere*. 6, 47–73.

Guest, B., Stockli, D. F., Grove, M., Axen, G. J., Lam, P. S., & Hassanzadeh, J., 2006 - Thermal histories from the central Alborz Mountains, northern Iran: implications for the spatial and temporal distribution of deformation in northern Iran. *Geological Society of America Bulletin*, 118(11-12), 1507-1521.

Haas, J., Budai, T., 1999 - Triassic sequence stratigraphy of the Transdanubian Central Range (Hungary). *Geologica Carpathica*. 50/6, 459–475.

Haas, J., Budai, T., 2004 - Dunántúli-középhegységi egység. In: Haas, J. (Ed.), Magyarország geológiája, Triász. *ELTE Eötvös Kiadó, Budapest*, pp. 25–124.

Haas, J., Kovács, S., Krystyn, L., and Lein, R., 1995 - Significance of late Permian–Triassic facies zones in terrane reconstructions in the Alpine–North Pannonian domain: *Tectonophysics*, v. 242, p. 19–40.

Haas, J., Budai, T., and Raucsik, B., 2012 - Climatic controls on sedimentary environments in the Triassic of the Transdanubian Range (Western Hungary). *Palaeogeogr. Palaeoclimatol. Palaeoecol*. 353–355, 31–44.

Hallam, T., 1995 - Major Bio-Events in the Triassic and Kurassic. In: Walliser, O.H., Global Events and Event Stratigraphy, *Springer-Verlag Berlin Heidelberg New York*., pp. 265–283.

Handy, M., Schmid, S., Bousquet, R., Kissling, E. and Bernoulli, D., 2010 - Recoiling plate-tectonic reconstructions of Alpine Tethys with the geological-geophysical record of spreading and subduction in the Alps, *Earth-Science Reviews*, 102, 121-158.

Harb, A.A., 1979 - The stratigraphy, tectonics and petroleum geology of the Kopet Dagh region, Northern Iran. PhD Teshis, Imperial College London (University of London).

Hesselbo, S. P., Jenkyns, H. C., Duarte, L. V., and Oliveira, L. C., 2007 - Carbon-isotope record of the Early Jurassic (Toarcian) Oceanic Anoxic Event from fossil wood and marine carbonate (Lusitanian Basin, Portugal). *Earth Planet. Sci. Lett*. 253, 455– 470.

Hochuli, P.A., Frank, S.M., 2000 - Palynology (dinoflagellate cysts, spore-pollen) and stratigraphy of the Lower Carnian Raibl Group in the Eastern Swiss Alps. *Eclogae Geol. Helv*. 93, 429– 443.

Hollingsworth, J., Fattahi, M., Walker, R., Talebian, M., Bahroudi, A., Bolourchi, M. J., ... and Copley, A., 2010 - Oroclinal bending, distributed thrust and strike-slip faulting, and the accommodation of Arabia–Eurasia convergence in NE Iran since the Oligocene. *Geophysical Journal International*, *181*(3), 1214-1246.

Holmes, C. D., Jacob, D. J., Corbitt, E. S., Mao, J., Yang, X., Talbot, R., and Slemr, F., 2010 - Global atmospheric model for mercury including oxidation by bromine atoms. *Atmospheric Chemistry and Physics*, *10*(24), 12037-12057.

Holz, M., 2015 - Mesozoic paleogeography and paleoclimates – A discussion of the diverse greenhouse and hothouse conditions of an alien world. *Journal of South American Earth Sciences*. 61, 91–107.

Hornung, T., Brandner, R., 2005 - Biochronostratigraphy of the Reingraben Turnover (Hallstatt Facies Belt): local black shale events controlled by regional tectonics, *climatic change and plate tectonics*. Facies 51, 460–479.

Hornung, T., Brandner, R., Krystyn, L., Joachimski, M.M. and Keim, L., 2007b - Multistratigraphic constraints on the NW Tethyan "Carnian Crisis". *New Mexico Museum of Natural History Bulletins*, 4:9–67.

Hornung, T., Krystyn, L. and Brandner, R., 2007a - A Tethys-wide mid-Carnian (Upper Triassic) carbonate productivity crisis: Evidence for the Alpine Reingraben Event from Spiti (Indian Himalaya)? *Journal of Asian Earth Sciences*, 30:285–302.

Hosseinpour, M., Williams, S., Seton, M., Barnett-Moore, N., and Müller, R. D. (2016) - Tectonic evolution of western Tethys from Jurassic to pres- ent day: Coupling geological and geophysical data with seismic tomography models. *International Geology Review*, *58*(13), 1616–1645.

Jin, X., Gianolla, P., Shi, Z., Franceschi, M., Caggiati, M., Du, Y., and Preto, N., 2020 - Synchronized changes in shallow water carbonate production during the Carnian Pluvial Episode (Late Triassic) throughout Tethys. *Global and Planetary Change*, 184, 103035.

Jin, X., McRoberts, C.A., Shi, Z., Mietto, P., Rigo, M., Roghi, G., Manfrin, S., Franceschi, M., and Preto, N., 2019 - The aftermath of the CPE and the Carnian–Norian transition in northwestern Sichuan basin, South China. *J. Geol. Soc. London*. 176, 179–196.

Kázmér, M. and Kovács, S., 1985 - Permian-Paleogene paleogeography along the Eastern part of the Insubric-Periadriatic Lineament system: evidence for continental escape of the Bakony-Drauzug Unit. *Acta Geol. Hung*.. 28(1-2): 71-84.

Keim, L., Brandner, R., Krystyn, L., and Mette, W., 2001 - Termination of carbonate slope progradation: an example from the Carnian of the Dolomites, Northern Italy. *Sedimentary Geology*, 143(3-4), 303-323.

Keim, L., Schlager, W., 2001 - Quantitative compositional analysis of a Triassic carbonate platform (Southern Alps, Italy). *Sediment. Geol.* 139, 261–283.

Keim, L., Spötl, C., and Brandner, R., 2006 - The aftermath of the Carnian carbonate platform demise: a basinal perspective (Dolomites, Southern Alps). Sedimentology 53, 361–386.

Kemp, TS., 2005 - The origin and evolution of mammals. Oxford, UK: *Oxford University Press*. 331 p.

Klausen, T.G., and Mørk, A., 2014 - The Upper Triassic paralic deposits of the De Geerdalen Formation on Hopen: Outcrop analog to the subsurface Snadd Formation in the Barents Sea. *AAPG Bulletin*, 98(10): 1911-1942.

Kluyver, H. M., Tirrul, R., Chance, P. N., Johns, G. W., Meixncr, H. M., 1983 - Explanatory text of the Naybandan Quadrangle Map 1: 250,000 *Geol. Surv. Iran Geol. Quad*., J8, pp. 1-143.

Kolar-Jurkovšek, T., Gaździcki, A., and Jurkovšek, B., 2005 - Conodonts and foraminifera from the "Raibl Beds" (Carnian) of the Kararvanke Mountains, Slovenia: stratigraphical and paleontological implications. *Geol. Quart*. 49/4, 429–438.

Kolar-Jurkovšek, T., Jurkovšek, B., 2010 - New paleontological evidence of the Carnian strata in the Mežica area (Karavanke Mountains, Slovenia): conodont data for the Carnian Pluvial Event. *Palaeogeography, Palaeoclimatology, Palaeoecology*. 290, 81–8.

Köppen, A., 1997 - Faziesentwicklung in der frühen Obertrias Mitteleuropas-ein sequenzstratigraphischer Vergleich. *Gaea Heidelbergensis* 2, 1–233.

Korte, C., Kozur, H., and Veizer, J., 2005 - δ13C and δ18O values of Triassic brachiopods and carbonate rocks as proxies for coeval seawater and palaeotemperature. *Palaeogeography, Palaeoclimatology,*

Palaeoecology. 226, 287–306.

Kovács, S., L. Krystyn, S. Szabó, L. Dosztály, and T. and Budai, 1991 - The Ladinian/Carnian boundary in the Balaton Upland, Hungary. *Symp. Trias. Strat.*

Kozur, H., Mock, R., 1991 - New Middle Carnian and Rhaetian Conodonts from Hungary and the Alps. Stratigraphic importance and tectonic implications for the Buda Mountains and adjacent areas. *Jb. Geol.* B.-A. 134/2, 271–297.

Kozur, H.W. & Bachmann, G.H., 2010 - The Middle Carnian Wet Intermezzo of the Stuttgart formation (Schilfsandstein), Germanic Basin. *Palaeogeography, Palaeoclimatology, Palaeoecology*, 290:107–119.

Kristan-Tollmann, E., Haas, J., and Kovács, S., 1991 - Karnische Ostracoden und Conodonten der Bohrung Zsámbék–14 im Transdanubischen Mittelgebirge (Ungarn). *Jubiläumsschrift 20 Jahre Geologische Zusammenarbeit Österreich–Ungarn*, 193–220.

Krystyn, L., and Tatzreiter, F., 1991 - Middle Triassic ammonoids from Aghdarband (NE-Iran) and their paleobiogeographical significance. *Abhandlungen Der Geologischen Bundesanstalt*, 38, 139-165.

Krystyn, L., 1978 - Eine neue Zonengliederung im alpin-mediterranen Unterkarn. *Schrift. Erdwiss. Komm. Österr. Ak. Wiss*., v. 4, pp. 37-75, Wien.

Krystyn, L., 1991 - Die Fossillagerstätten der alpinen Trias: Exkursionsführer. *Universität Wien*, p. 61.

Krystyn, L., Balini, M., Aghababalou, B. S., and Hairapetian, V., 2019 - Norian ammonoids from the Nayband Formation (Iran) and their bearing on Late Triassic sedimentary and geodynamic history of the Iran Plate. *Rivista Italiana di Paleontologia e Stratigrafia*, *125*(1).

Kürschner, W.M., Herngreen,W., 2010 - Triassic palynology of central and northwestern Europe: a review of palynofloral diversity patterns and biostratigraphic subdivisions In: Lucas, S.G. (Ed.) The Triassic Timescale. *Geol. Soc. Spec. Publ*. 334, 263–283.

Kustatscher e., ash s.r., Karasev e., Pott c., vajda v., yu J. and Mcloughlin s., 2018 - Flora of the late triassic. in: tanner l. (ed.), the late triassic World. *springer, cham*, pp. 545–622.

Kutzbach, J.E., Gallimore, R.G., 1989 - Pangaean Climates' Megamonsoons of the Megacontinent. *J. Geophys. Res.* 94, 3341–3357.

Leonardi P., Polo, C., 1952 - La fauna cassiana di Cortina d'Ampezzo. Parte 2., Cefalopodi. *Memorie dell'Istituto Geologico dell'Università di Padova*, 17, 3–27.

Lewan, M.D., 1983 - Effects of thermal maturation on stable organic carbon isotopes as determined by hydrous pyrolysis of Woodford Shale. *Geochim. Cosmochim. Acta*. 47, 1471–1479.

Liaghat, M., Adabi, M. H., Swennen, R., Mohammadi, Z., and Alijani, H., 2021 - An integrated facies, diagenesis and geochemical analysis along with sequence stratigraphy of the Lower Triassic Aghe-Darband basin (north-east Iran). *Journal of African Earth Sciences*. 173, 103952.

Lieberman, H. M., 1978 - Carnitza Formation — ein neuer Begriff für Oberkarnische Beckenkalke der südlichen Kalkalpen bei Raibl (Cave del Predil, Italien). *Mitt. Ges. Geol. Bergbaustud. Österr*. 25, 35–60.

Lieberman, H.M. 1980 - The suitability of the Raibl sequence as a stratotype for the Carnian Stage and the Julian Substage of the Triassic. *Newsletters on Stratigraphy*, 36: 35-42.

Lindström, S., Sanei, H., Van De Schootbrugge, B., Pedersen, G. K., Lesher, C. E., Tegner, C., Heunisch, C., Dybkjær, K., and Outridge, P.M., 2019 - Volcanic mercury and mutagenesis in land plants during the end-Triassic mass extinction: *Science advances*, v. 5, eaaw4018.

Lucas, S.G., Luo, Z., 1993 - Adebasileus from the Upper Triassic of West Texas: The Oldest Mammal. *Journal of Vertebrate Palaeontology*. 13, 309–334.

Lucas, S.G., Tanner, L.H., 2015 - End-Triassic nonmarine biotic events. *Journal of Palaeogeography*. 4, 331–348.

Lukeneder S., Lukeneder A., Harzhauser M., Islamoglu Y., Krystyn L., and Lein R., 2012 - A delayed carbonate factory breakdown during the Tethyan-wide Carnian Pluvial Episode along the Cimmerian terranes (Taurus, Turkey). *Facies*, 58, 279–296.

Lukeneder, S., Lukeneder, A., 2014 - A new ammonoid fauna from the Carnian (Upper Triassic) Kasimlar Formation of the Taurus Mountains (Anatolia, Turkey). *Palaeontology*. 57, 357–396.

Lunn, G. A., 2020 - Dating and correlation of the Baluti Formation, Kurdistan, Iraq: Implications for the regional recognition of a Carnian "marker dolomite", and a review of the Triassic to Early Jurassic sequence stratigraphy of the Arabian Plate. *Journal of Petroleum Geology*, *43*(1), 109-125.

Lunn, G. A., Miller, S., and Samarrai, A., 2019 - DATING AND CORRELATION OF THE BALUTI FORMATION, KURDISTAN, IRAQ: Implications for the regional recognition of a Carnian "marker dolomite", and a review of the Triassic to Early Jurassic sequence stratigraphy of the Arabian Plate. *Journal of Petroleum Geology*, *42*(1), 5-36.

Mancuso, A.C., Benavente, C.A., Irmis, R.B., and Mundil, R., 2020 - Evidence for the Carnian Pluvial Episode in Gondwana: New multiproxy climate records and their bearing on early dinosaur diversification. *Gondwana Res*. 86, 104–125.

Mancuso, A.C., Dihl Horn, B.L., Benavente, C.A., Schultz, C.L., and Irmis, R.B., 2021 - The paleoclimatic context for South American Triassic vertebrate evolution, *Journal of South American Earth Sciences*. 103321.

Mandl, G. 2000 - The Alpine sector of the Tethyan shelf – Examples of Triassic to Jurassic sedimentation and deformation from the Northern Calcareous Alps. *Mitteilungen der Österreichischen Geologischen Gesellschaft.* 92, 61–77.

Maron, M., Muttoni, G., Dekkers, M.J., Mazza, M., Breda, A., Krijgsman, W., and Rigo, M., 2017 - Contribution to the magnetostratigraphy of the Carnian: new magneto-biostratigraphic constraints from Pignola-2 and Dibona marine sections, Italy. *Newsletter in Stratigraphy*, 50, 187–203.

Martinez-Cortizas, A., Pontevedra-Pombal, X., Garcıa-Rodeja, E., Novoa-Munoz, J. C., and Shotyk, W., 1999 - Mercury in a Spanish peat bog: archive of climate change and atmospheric metal deposition. *Science*, *284*(5416), 939-942.

Martinez-Peréz, C., Cascales-Minana, B., Plasencia, P., Botella, H., 2014 - Exploring the major depletions of conodont diversity during the Triassic. *Historical Biology*, 27, 503–507.

Márton, E., and Fodor, L., 2003 - Tertiary paleomagnetic results and structural analysis from the Transdanubian Range (Hungary): rotational disintegration of the Alcapa unit. *Tectonophysics*, *363*(3-4), 201-224.

Masetti, D., Neri, C., and Bosellini, A., 1991 - Deep-water asymmetric cycles and progradation of carbonate platforms governed by high-frequency eustatic oscillations (Triassic of the Dolomites, Italy): *Geology*, v. 19, p. 336-339.

Mattei, M., Muttoni, G., Cifelli, F., 2014 - A record of the Jurassic massive plate shift from the Garedu Formation of central Iran. *Geology*, 42(6): 555–558.

Mattei, M., Cifelli, F., Alimohammadian, H., Rashid, H., Winkler, A., and Sagnotti, L., 2017 - Oroclinal bending in the Alborz Mountains (Northern Iran): New constraints on the age of South Caspian subduction and extrusion tectonics. *Gondwana Research*, *42*, 13-28.

Matthews, K.J., Maloney, K.T., Zahirovic, S., Williams, S.E., Seton, M., and Müller, R.D., 2016 - Global plate boundary evolution and kinematics since the late Paleozoic. *Global and Planetary Change*, 146: 226-250.

McKirdy, D.M., Powell, T.G., 1974 - Metamorphic alteration of carbon iso- topic composition in ancient sedimentary organic matter: new evidence from Australia and South Africa. *Geology*, 2, 591–595.

Mietto P., Manfrin S., Preto N., Rigo M., Roghi G., Furin S., Gianolla P., Posenato R., Muttonii G., Nicora A., Buratti N., Cirilli S., Spötl C., Ramezani J., and Bowring S.A., 2012 - The Global Boundary Stratotype Section and Point (GSSP) of the Carnian Stage (Late Triassic) at Prati di Stuores/Stuores Wiesen section (Southern Alps, NE Italy). *Episodes*, v. 35/3, pp. 414-430.

Mietto, P., Manfrin, S., Preto, N., Rigo, M., Roghi, G., Furin, S., Gianolla, P., Posenato, R., Muttoni, G., Nicora, A., Buratti, N., Cirilli, S., Spötl, C., Ramezani, J., and Bowring, S.A., 2012 - The Global Boundary Stratotype Section and Point (GSSP) of the Carnian Stage (Late Triassic) at Prati di Stuores/Stuores Wiesen section (Southern Alps, NE Italy). *Episodes* 35/3 414–430.

Miller, C.S., Peterse, F., da Silva, A.-C., Baranyi, V., Reichart, G.J. & Kürschner, W., 2017 -Astronomical age constraints and extinction mechanisms of the Late Triassic Carnian crisis. *Scientific Reports*, 2557.

Moix, P., Vachard, D., Jamesallibon, R., Wernli, R., Kozur, H., and Stampfli, G., 2013 - Palaeotethyan, Neotethyan and Hulu-Pindos series in the Lycian Nappes (SW Turkey): Geodynamical Implications. The Triassic System: New Developments in Stratigraphy and Paleontology: *Bulletin* 61, 61, 401.

Mojsisovics, E. von, 1879 - Die Dolomit-Riffe von Sudtirol und Venetien. In: Hölder, A. (Ed.). Beiträge zur Bildungsgeschichte der Alpen. Wien. 552.

Mojsisovics, E.M. von, 1882 - Die Cephalopoden der mediterranen Triasprovinz. *Abh. K. K. Geol. Reichsanst*., v. 10, pp. 1-332, Wien.

Morley, C.K., Kongwung, B., Julapour, A.A., Abdolghafourian, M., Hajian, M., Waples, D., Warren, J., Otterdoom, H., Srisuriyon, K., and Kazemi, H., 2009 - Structural development of a major late Cenozoic basin and transpressional belt in central Iran: The Central Basin in the Qom-Saveh area. *Geosphere*, 5(4): 325-362.

Mueller, S., Hounslow, M.W., Kürschner, W.M., 2016b - Integrated stratigraphy and palaeoclimate history of the Carnian Pluvial Event in the Boreal realm; new data from the Upper Triassic Kapp Toscana Group in central Spitsbergen (Norway). *J. Geol. Soc*. 173, 186–202.

Mueller, S., Krystyn, L., and Kürschner, W.M., 2016a - Climate variability during the Carnian Pluvial Phase – a quantitative palynological study of the Carnian sedimentary succession at Lunz am See, Northern Calcareous Alps, Austria. *Palaeogeography, Palaeoclimatology, Palaeoecology*. 441, 198–211.

Muttoni, G., Gaetani, M., Kent, D. V., Sciunnach, D., Angiolini, L., Berra, F., ... & Zanchi, A., 2009 - Opening of the Neo-Tethys Ocean and the Pangea B to Pangea A transformation during the Permian. *GeoArabia*, *14*(4), 17-48.

Muttoni, G., Mazza, M., Mosher, D., Katz, M.E., Kent, D.V., and Balini, M., 2014 - A Middle–Late Triassic (Ladinian–Rhaetian) Carbon and Oxygen isotope record from the Tethyan Ocean. *Palaeogeography, Palaeoclimatology, Palaeoecology,* 399, 246–259.

Muttoni, G., Tartarotti, P., Chiari, M., Marieni, C., Rodelli, D., Dallanave, E. and Kirscher, U. 2015 - Paleolatitudes of Late Triassic radiolarian cherts from Argolis, Greece: Insights on the paleogeography of the western Tethys. *Palaeogeography, Palaeoclimatology, Palaeoecology,* 417: 476–490.

Nagy Z.R., 1999 - Platform-basin transition and depositional models for the Upper Triassic (Carnian) Sándorhegy Limestone, Balaton Highland, Hungary. *Acta Geologica Hungarica*, 42/3: 267-299.

Nakada, R, Ogawa, K., Suzuki, N., Takahashi, S., Takahashi, Y., 2015 - Late Triassic compositional changes of aeolian dusts in the pelagic Panthalassa: Response to the continental climatic change. *Palaeogeography, Palaeoclimatology, Palaeoecology*, 393, 61-75.

Natali, C., Bianchini, G., Carlino, P., 2020 - Thermal stability of soil carbon pools: Inferences on soil nature and evolution: *Thermochimica Acta*, v. 683, 178478.

Neri, C., Gianolla, P., Furlanis, S., Caputo, R., Bosellini, A., 2007 - Note Illustrative della Carta Geologica d'Italia alla scala 1:50.000, Foglio 029 Cortina d'Ampezzo. SystemCart (200 p). A.P.A.T, Roma.

Newham, E., Benson, R., Upchurch, P., Goswami, A., 2014 - Mesozoic mammaliaform diversity: The effect of sampling corrections on reconstructions of evolutionary dinamics. *Palaeogeography, Palaeoclimatology, Palaeoecology,* 412, 32–44.

Niessen, S., Foucher, D., Clarisse, O., Fischer1, J.C., Mikac, N., Kwokal, Z., Fajon, V. and Horvat M., 2003 - Influence of sulphur cycle on mercury methylation in estuarine sediment (Seine estuary, France). *J Phys IV* 107:953–956.

Nozaem, R., Mohajjel, M., Rossetti, F., Della Seta, M., Vignaroli, G., Yassaghi, A., Salvini, F., and Eliassi, M., 2013 - Post-Neogene right-lateral strike-slip tectonics at the north-western edge of the Lut Block (Kuh-e-Sarhangi Fault), Central Iran. *Tectonophysics*, 589: 220-233.

Oberhauser, R., 1991 - Triassic foraminifera from the Faqir Marl Bed of the Sina Formation (Aghdarband Group, NE-Iran). *Abhandlungen der Geologischen Bundesanstalt*, 38: 201-204.

Ogg, J.G., 2015 - The mysterious Mid-Carnian 'Wet Intermezzo' global event. *Journal of Earth Science*, 26, 181–191.

Outridge, P. M., Sanei, H., Stern, G. A., Hamilton, P. B., and Goodarzi, F., 2007 - Evidence for control of mercury accumulation rates in Canadian High Arctic lake sediments by variations of aquatic primary productivity. *Environmental Science & Technology*, *41*(15), 5259-5265.

Parrish, J.T., 1993 - Climate of the Supercontinent Pangea. J. Geol. 101, 215–233. Planderová, E., 1980. Palynomorphs from Lunz Beds and from black clayey shales in basement of Vienna Basin (borehole LNV-7). *Geol. Carpath*. 31, 267–294.

Paterson, N.W., Mangerud, G., Cetean, C.G., Mørk, A., Lord, G.S., Klausen, T.G., and Mørkved, P.T., 2016 - A multidisciplinary biofacies characterisation of the Late Triassic (late Carnian-Rhaetian) Kapp Toscana Group on Hopen, Arctic Norway. *Palaeogeography, Palaeoclimatology, Palaeoecology*, 464,

16-42.

Payne, J.L., Turchyn, A.V., Paytan, A., DePaolo, D.J., Lehrmann, D.J., Yu, M., Wei, J., 2010 - Calcium isotope constrains on the end-Permian mass extinction. *PNAS* 107, 8543–8548.

Percival, L.M.E., Witt, M. L. I., Mather, T. A., Hermoso, M., Jenkyns, H. C., Hesselbo, S. P., Al-Suwaidi, A. H., Storm, M. S., Xu, W., Ruhl, M., 2015 - Globally enhanced mercury deposition during the end-Pliensbachian extinction and Toarcian OAE: A link to the Karoo–Ferrar Large Igneous Province, *Earth and Planetary Science Letters*, v. 428, p. 267-280.

Percival, L.M.E., C. Jenkyns, H., A. Mather, T., J. Dickson, A., J. Batenburg, S., Ruhl, M., P. Hasselbo S., Barclay, R., Jarvis, I., A. Robinson, S, Woelders, L., 2018 - Does large igneous province volcanism always perturb the mercury cycle? Comparing the records of Oceanic Anoxic Event 2 and the end-Cretaceous to other Mesozoic events: American Journal of Science, v. 318, p. 799-860,Pisa, G., Marinelli, M., and Viel, G., 1980, Infraraibl Group: a proposal (Southern Calcareous Alps, Italy): *Rivista Italiana di Paleontologia e Stratigrafia*, v. 85, p. 983-1002.

Pott, C., Krings, M., and Kerp, H., 2008 - The Carnian (Late Triassic) flora from Lunz in Lower Austria: Paleoecological considerations: *Palaeoworld*, v. 17, p. 172-182.

Preto N., 2012 - Petrology of carbonate beds from the stratotype of the Carnian (Stuores Wiesen section, Dolomites, Italy): the contribution of platform-derived microbialites. *Geo.Alp*, v. 9, pp. 12-29.

Preto, N., Breda, A., Dal Corso, J., Spötl, C., Zorzi, F., Frisia, S., 2015 - Primary dolomite in the Late Triassic Travenanzes Formation, Dolomites, Northern Italy: Facies control and possible bacterial influence. Sedimentology, 62, 697–716.

Preto, N., Gianolla, P., Franceschi, M., Gattolin, G., Riva, A., 2017 - Geometry and evolution of Triassic high-relief, isolated microbial platforms in the Dolomites, Italy: The Anisian Latemar and Carnian Sella platforms compared. *AAPG Bulletin*, 101, 475–483.

Preto, N., Hinnov, L., 2003 - Unrevealing the origin of carbonate platform cyclothems in the Upper Triassic Durrenstein Formation (Dolomites, Italy). *Journal of Sedimentary Research*, 73, 774–789.

Preto, N., Kustatscher, E., Wignall, P.B., 2010 - Triassic climates—state of the art and perspectives. *Palaeogeography, Palaeoclimatology, Palaeoecology*, 290, 1–10.

Preto, N., Roghi, G., Gianolla, P., 2005 - Carnian stratigraphy of the Dogna area (Julian Alps, northern Italy): tesserae of a complex palaeogeography. *Bull. Soc. Geol*. It., 124, 269–279.

Pyle, D. M., and Mather, T. A., 2003- The importance of volcanic emissions for the global atmospheric mercury cycle. *Atmospheric Environment*, *37*(36), 5115-5124.

Retallack, G.J., Veevers, J.J., and Morante, R., 1996 - Global coal gap between Permian-Triassic extinction and Middle Triassic recovery of peat-forming plants, *Geological Society of America Bulletin*, v. 108 (2), p. 195-207.

Ricou, L.E., 1994 - La thétys reconstruite: plaques, blocs continentaux et leurs limites depuis 260 ma de l'amérique centrale à l'asie du sud-est. *Geodinamica Acta*, 7(4), 169-218.

Ridgwell, A., Schmidt, D.N., 2010 - Past constraints on the vulnerability of marine calcifiers to massive carbon dioxide relase. *Nat. Geo*. 3, 196–200.

Riding, R., Liang, L., Braga, J.C., 2014 - Millennial-scale ocean acidification and late Quaternary decline of

cryptic bacterial crusts in tropical reefs. *Geobiology*, 12, 387–405.

Rigo M, Mazza M, Karádi V, and Nicora A., 2018 - New Upper Triassic conodont biozonation of the Tethyan Realm. In: Tanner, L. H. (ed.), The Late Triassic World, *Earth in a Time of Transition, Springer, Berlin*. p. 189-235.

Rigo, M., Joachimski, M.M., 2010 - Palaeoecology of Late Triassic conodonts: constraints from oxygen isotopes in biogenic apatite. *Acta Palaeontol. Pol.* 55, 471–478.

Rigo, M., Preto, N., Roghi, G., Tateo, F., and Mietto, P., 2007 - A rise in the Carbonate Compensation Depth of western Tethys in the Carnian (Late Triassic): deep-water evidence for the Carnian Pluvial Event. *Palaeogeography, Palaeoclimatolology, Palaeoecology*, 246, 188–205.

Robert, A.M.M., Letouzey, J., Kavoosi, M.A., Sherkati, S., Müller, C., Vergés, J., and Aghababaei, A., 2014 - Structural evolution of the Kopeh Dagh fold-and-thrust belt (NE Iran) and interactions with the South Caspian Sea Basin and Amu Darya Basin. *Marine and Petroleum Geology*, 57, 68-87.

Roghi, G., 2004. Palynological investigations in the Carnian of Cave del Predil area (once Raibl, Julian Alps). *Review of Palaeobotany and Palynology*, p. 132, 1–35.

Roghi, G., Gianolla, P., Minarelli, L., Pilati, C., Preto, N., 2010 - Palynological correlation of Carnian humid pulses throughout western Tethys. *Palaeogeography, Palaeoclimatolology, Palaeoecology*. 290, 89–106.

Rostási, Á., Raucsik, B., Varga, A., 2011 - Palaeoenvironmental controls on the clay mi- neralogy of Carnian sections from the Transdanubian Range (Hungary). *Palaeogeography, Palaeoclimatolology, Palaeoecology*. 300, 101–112.

Rruhl, M., Kürschner, W.M., 2011 - Multiple phases of carbon cycle distur- bance from large igneous province formation at the Triassic–Jurassic transition. Geology, 39, 431–434.

Ruffell, A., Simms, M.J., Wignall, P.B., 2016 - The Carnian Humid Episode of the late Triassic: a review. *Geol. Mag*. 153, 271–284.

Ruiz, W. L. G., and Tomiyasu, T., 2015 - Distribution of mercury in sediments from Kagoshima Bay, Japan, and its relationship with physical and chemical factors. *Environmental Earth Sciences*, 74(2), 1175-1188.

Rüffer, T., and Bechstãdt, T., 1998 - Triassic sequence stratigraphy in the western part of the Northern Calcareous Alps (Austria): in: de Graciansky, P.-C, Hardenbol, J., Jacquin, T., Vail, P.R. (Eds.), Mesozoic and Cenozoic Sequence Stratigraphy of European Basins. *SEPM Special Publications*, v. 60, p.

Ruhl, M., Bonis, N.R., Reichard, G.J., Sinninghe Damsté, J.S., and Kürschner, W.M., 2011 - Atmospheric carbon injection linked to End-Triassic Mass Extinction. Science, 333, 430–434.

Russo, F., Neri, C., Mastandrea, A., Baracca, A., 1997. The mudmound nature of the Cassian platform margins of the Dolomites. A case history: the Cipit boulders from Punta Grohmann (Sasso Piatto Massif, Northern Italy). *Facies*. 36, 25–36.

Ruttner, A.W, 1984 - The pre-Liassic basement of the eastern Kopet Dagh Range. *Neues Jahrbuch für Geologie und Paläontologie-Abhandlungen*, 168: 256-268.

Ruttner, A.W., 1988 - The coal deposits of Agdarband (Aq Darband) NE-Iran and its geological frame In: Second Mining Symposium Iran (Kerman). Ministry of Mines and Metals, Tehran, 183-202.

Ruttner, A.W., Brandner, R., & Kirchner, E., 1991 - Geology of the Aghdarband area (kopet Dagh, NE-Iran). *Abhandlungen Der Geologischen Bundesanstalt*, 38, 7-79.

Ruttner, A. W., 1993 - Southern borderland of Triassic Laurasia in north-east Iran. *Geologische Rundschau*, 82(1), 110-120.

Sanei, H., Grasby, S.E., and Beauchamp, B., 2012 - Latest Permian mercury anomalies: *Geology*, v. 40, p. 63-66.

Sanei, H., Outridge, P. M., Stern, G. A., and Macdonald, R. W., 2014 - Classification of mercury–labile organic matter relationships in lake sediments. *Chemical Geology*, *373*, 87-92.

Santos, E. C. O., Câmara, V. M., Jesus, I. M., Brabo, E. S., Loureiro, E. C. B., Mascarenhas, A. F. S., and Silveira, I. M., 2002 - A contribution to the establishment of reference values for total mercury levels in hair and fish in Amazonia. *Environmental Research*, 90(1), 6-11.

Saxby, J.D., Stephenson, L.C., 1987 - Effect of an igneous intrusion on oil shale at Rundle (Australia). *Chemical Geology*, 63, 1–16.

Scaife, J.D., Ruhl, M., Dickson, A. J., Mather, T. A., Jenkyns, H. C., Percival, L. M. E., Hesselbo P., Cartwright J., Eldrett, J. S., Bergman, S. C., and Minisini, D., 2017 - Sedimentary mercury enrichments as a marker for submarine large igneous province volcanism? Evidence from the Mid-Cenomanian event and Oceanic Anoxic Event 2 (Late Cretaceous): *Geochemistry, Geophysics, Geosystems*, v. 18, p. 4253-4275.

Schettino, A., and Turco, E., 2011 - Tectonic history of the western Tethys since the Late Triassic: Geological Society of America Bulletin, v. 123, no. 1–2, p. 89–105.

Schlager, W., Schöllnberger, W., 1974 - Das Prinzip stratigraphischer Wenden in der Schichtfolge der Nördlichen Kalkalpen. Mitt. *Österr. Geol. Ges*. 66–67 (165–193).

Schmid, S.M., Bernoulli, D., Fügenschuh, B., Matenco, L., Schefer, S., Schuster, R., Tischler, M., and Ustaszewski, K., 2008 - The Alpine-Carpathian-Dinaridic orogenic system: Correlation and evolution of tectonic units, *Swiss Journal of Geosciences*, v. 101, no. 1, p. 139–183.

Schroeder, W.H., Munthe, J., 1998 - Atmospheric mercury: An overview. *Atmos. Environ*. 32 (5), 809–822.

Schulz, O., 1970 - Vergleichende petrographische Untersuchungen an Karnischen Sedimenten der Julischen Alpen. Gailtaler Alpen und des Karwendels. *Verh. Geol. B. A* 1970, 165–229.

Schuster, P. F., Schaefer, K. M., Aiken, G. R., Antweiler, R. C., Dewild, J. F., Gryziec, J. D., ... and Zhang, T., 2018 - Permafrost stores a globally significant amount of mercury. *Geophysical Research Letters*, *45*(3), 1463-1471.

Scotese, C.R., 2013 - Map Folio 45, Late Triassic (Carnian, 222.6 Ma), Paleomap, PaleoAtlas for ArcGIS, volume 3, Triassic and Jurassic Paleogeographic, Paleoclimatic and Plate Tectonic Reconstructions, *PALEOMAP Project, Evanston, IL.*

Scotese, C. R., and A. Schettino. "Late Permian-Early Jurassic paleogeography of western Tethys and the world." *Permo-Triassic salt provinces of Europe, North Africa and the Atlantic margins*. Elsevier, 2017. 57-95.

Sellwood, B.W., Valdes, P.J., 2006 - Mesozoic climates: General circulation models and the rock record. *Sediment. Geol*. 190, 269–287.

Şengör, A.M.C., 1979 - Mid-Mesozoic closure of Permo--Triassic Tethys and its implications. *Nature*, 279: 590-593.

Şengör, A.M.C., 1984 - The Cimmeride orogenic system and the tectonics of Eurasia. *Geological Society of America Special Paper*, 195: 82.

Şengör, A.M.C., 1990 - A new model for the late Palaeozoic-Mesozoic tectonic evolution of Iran and implications for Oman. *Geological Society Special Publication*, 49(1): 797-831.

Seyed-Emami, K., 1971 - The Jurassic Badamu Formation in the Kerman region, with some remarks on the Jurassic stratigraphy of Iran. *Geological Survey of Iran, Report*, *19*(1-80), 264.

Seyed-Emami, K., 2003 - Triassic in Iran. *Facies*, 48(1), 91-106.

Seyed-Emami, K., Fuersich, F. T., Wilmsen, M., Majidifard, M. R., & Shekarifard, A., 2009 - Upper Triassic (Norian) cephalopods from the Ekrasar Formation (Shemshak Group) of Northern Alborz, Iran. *Rivista Italiana di Paleontologia e Stratigrafia*, 115(2).

Sheikholeslami, M.R., and Kouhpeyma, M., 2012 - Structural analysis and tectonic evolution of the eastern Binalud Mountains, NE Iran. *Journal of Geodynamics*, 61: 23-46.

Shen, H., Wang, H., Shen, C., Wu, J., Zhu, Y., Shi, W., Zhang, X., and Ying, Z., 2020 - Effect of atmosphere of SO2 coexisted with oxidizing gas on mercury removal under oxy-fuel condition, *Chemosphere*, v. 259, 127525.

Sial, A. N., Lacerda, L. D., Ferreira, V. P., Frei, R., Marquillas, R. A., Barbosa, J. A., ... and Pereira, N. S., 2013 - Mercury as a proxy for volcanic activity during extreme environmental turnover: The Cretaceous–Paleogene transition. *Palaeogeography, Palaeoclimatology, Palaeoecology*, *387*, 153-164.

Sial, A. N., Chen, J., Lacerda, L. D., Frei, R., Tewari, V. C., Pandit, M. K., ... and Pereira, N. S., 2016 - Mercury enrichment and Hg isotopes in Cretaceous–Paleogene boundary successions: Links to volcanism and palaeoenvironmental impacts. *Cretaceous Research*, *66*, 60-81.

Simms, M.J., Ruffel, A.H., Johnson, L.A., 1995 - Biotic and climatic changes in the Carnian (Triassic) of Europe and adjacent areas. In: Fraser, N.C., Sues, H.-D. (Eds.), In The Shadow Of The Dinosaurs: Early Mesozoic Tetrapods. *Cambridge University Press*, pp. 352–365.

Simms, M.J., Ruffell, A.H., 1989 - Synchroneity of climatic change and extinctions in the Late Triassic. *Geology*, 17, 265–268.

Simms, M.J., Ruffell, A.H., 1990 - Climatic and biotic change in the Late Triassic. *Journal of the Geological Society of London* 147, 321–327.

Simoneit, B.R.T., Brenner, S., Peters, K.E., Kaplan, I.R., 1978 - Thermal alteration of Cretaceous black shale by basaltic intrusions in the Eastern Atlantic. *Nature*, 273, 501–504.

Slemr, F., Schuster, G., & Seiler, W., 1985 - Distribution, speciation, and budget of atmospheric

mercury. *Journal of atmospheric chemistry*, *3*(4), 407-434.

Soffel, H. C., Schmidt, S., Davoudzadeh, M., and Rolf, C., 1996 - New palaeomagnetic data from Central Iran and a Triassic palaeoreconstruction. *Geologische Rundschau*, 85(2), 293-302.

Soua, M., 2014 - Early Carnian anoxic event as recorded in the southern Tethyan margin, Tunisia: an overview, *International Geology Review*, 56:15, 1884-1905.

Soussi, M., Niedzwiedzki, G., Talanda, M., Drozdz, D. Sulej, T. Boukhalfa, K., Mermer, J., and Blazejowski, B. 2017 - Middle Triassic (Anisian-Ladinian) Tejra red beds and Late Triassic (Carnian) carbonate sedimentary records of southern Tunisia, Saharan Platform: Biostratigraphy, sedimentology and implication on regional stratigraphic correlations. *Marine and Petroleum Geology*, 79, 222-256.

Stampfli, G.M. and Borel, G.D., 2002 - A plate tectonic model for the Paleozoic and Mesozoic constrained by dynamic plate boundaries and restored synthetic oceanic isochrons. *Earth Planet. Sci. Lett.*, 196, 17-33.

Stefani, M., Furin, S., and Gianolla, P., 2010 - The changing climate framework and depositional dynamics of the Triassic carbonate platforms from the Dolomites. *Palaeogeography, Palaeoclimatology, Palaeoecology*, 290, 43–57.

Stern, G. A., Sanei, H., Roach, P., Delaronde, J., and Outridge, P. M., 2009 - Historical interrelated variations of mercury and aquatic organic matter in lake sediment cores from a subarctic lake in Yukon, Canada: further evidence toward the algal-mercury scavenging hypothesis. *Environmental science & technology*, 4*3*(20), 7684-7690.

Stöcklin, J., 1968 - Structural history and tectonics of Iran: a review. *American Association of Petroleum Geologists Bulletin*, 52 (1968), pp. 1229-1258.

Stöcklin, J., 1974 - Possible Ancient Continental Margins in Iran In: The Geology of Continental Margins:873-887. *Springer Berlin Heidelberg*.

Stöcklin, J., and Nabavi, M.H., 1973 - Tectonic map of Iran. *Geological Survey of Iran*, 1, 5.

Stur, D., 1868 - Beiträge zur Kenntniss der Geologischen Verhältnisse der Umgegend von Raibl und Kaltwasser. Jhb. K. K. *Geol. Reichsanst*., v. 18, pp. 71-122, Wien.

Suess, E., 1867 - Raibl. In: E. Suess, E., und Mojsisovics, E.M.v. – Studien über die Gliederung der Trias und Jurabildungen in den östichen Alpen. Jhb. K. K. *Geol. Reichsanst*., v. 17/4, pp. 554-582, Wien.

Suess, E., 1909 - Das Antlitz der Erde. Tempsky, Wien, 111/2, 789 pp.

Sun, Y., Wignall, P., Joachimski, M.M., Bond, D.P.G., Grasby, S.E., Lai, X.L., Wang, L.N., Zhang, Z.T., and Sun, S., 2016 - Climate warming, euxinia and carbon isotope perturbations during the Carnian (Triassic) Crisis in South China. *Earth and Planetary Science Letters*, 444, 88–100.

Sun, Y.D., Richoz, S., Krystyn L., Zhang Z.T., and Joachimski, M.M., 2019 - Perturbations in the carbon cycle during the Carnian Humid Episode: carbonate carbon isotope records from southwestern China and northern Oman: *Journal of the Geological Society*, v. 176, p. 167–177.

Svensen, H., Planke, S., Malthe-Sørenssen, A., Jamtveit, B., Myklebust, R., Rasmussen Eidem, T., Rey, S.S., 2004 - Release of methane from a vol- canic basin as mechanism for initial Eocene global warming. *Nature*, 429, 542–545.

Svensen, H., Planke, S., Polozov, A.G., Schmidbauer, N., Corfu, F., Podladchikov, Y.Y., and Jamtveit, B., 2009 - Siberian gas venting and the end-Permian environmental crisis: *Earth and Planetary Science Letters*, v. 277, p. 490–500.

Takin, M., 1972 - Iranian geology and continental drift in the Mid- dle East. *Nature*, 235 (5334):147–150.

Them, T.R., Jagoe, C.H., Caruthers, A.H., Gill, B.C., Grasby, S.E., Gröcke, D.R., Yin, R., and Owens, J.D., 2019 - Terrestrial sources as the primary delivery mechanism of mercury to the oceans across the Toarcian Oceanic Anoxic Event (Early Jurassic): *Earth and Planetary Science Letters*, v. 507, p. 62-72.

Taheri, J., Fürsich, F. T., and Wilmsen, M., 2009 - Stratigraphy, depositional environments and geodynamic significance of the Upper Bajocian–Bathonian Kashafrud Formation, NE Iran. *Geological Society, London, Special Publications*, *312*(1), 205-218.

Thibodeau, A. M., Ritterbush, K., Yager, J. A., West, A. J., Ibarra, Y., Bottjer, D. J., ... and Corsetti, F. A., 2016 - Mercury anomalies and the timing of biotic recovery following the end-Triassic mass extinction. *Nature Communications*, *7*(1), 1-8.

Tollmann, A., 1976 - Analyse des klassischen nordalpinen Mesozoikums: Stratigraphie, Fauna und Fazies der Nördlichen Kalkalpen XV, *Deuticke Wien*, v. 2, 580 p.

Tomimatsu, Y., Nozaki, T., Sato, H., Takaya, Y., Kimura, J.I., Chang, Q., Naraoka, H., Rigo, M., and Onoue, T., 2021 - Marine osmium isotope record during the Carnian “pluvial episode”(Late Triassic) in the pelagic Panthalassa Ocean, *Global and Planetary Change*, v. 197, 103387.

Tozer, A., 1967 - A standard for Triassic time. *Geological Survey of Canada Bulletin*, 156, pp. 1-103.

Trotter, A.J., Williams, S.I., Nicora, A., Mazza, M., and Rigo, M., 2015 - Long-term cycles of Triassic climate change: A new d18O record from conodont apatite: *Earth and Planetary Science Letters*, v. 415, p. 165–174.

Trümpy, R., 1982 - Das PhSnomen Trias. - *Geol. Rdsch*., 71, 711-723, Stuttgart.

Urlichs, M., 1974 - Zur Stratigraphie und Ammonitenfauna der Cassianer Schichten von Cassian (Dolomiten/Italien). *Schrift. Erdwiss. Komm. Österr. Ak. Wiss*., v. 2, pp. 207-222, Wien.

Urlichs, M., 1994 - Trachyceras Laube 1869 (Ammonoidea) aus dem Unterkarn (Obertrias) der Dolomiten (Italien), *Stuttg. Beitr. Naturk., ser. B (Geol. Paläont.)*, v. 217, pp. 1-55, Stuttgart.

Urlichs, M., 2017 - Revision of some stratigraphically relevant ammonoids from the Cassian Formation (Latest Ladinian-Early Carnian, Triassic) of St. Cassian (Dolomites. Italy). *N. Jb. Geol. Paläont*. Abh., 283/2: 173-204.

Vaez-Javadi, F., 2004 - Persicostrobus Vaez-Javadi n. gen. a new Equisetalean strobilus from the Triassic of Iran. *Rivista Italiana di Paleontologia e Stratigrafia*, 110: 715-718.

Vandal, G. M., Fitzgerald, W. F., Boutron, C. F., & Candelone, J. P., 1993 - Variations in mercury deposition to Antarctica over the past 34,000 years. *Nature*, 362(6421), 621-623.

Verloop, J.H., 1908 - Profil der Lunzer Schichten in der Umgebung von Lunz, *Zeitschrift deutscher geologischer Gesellschaft, Monatsberichte*, v. 60, p. 81-89.

Wang, X., Cawood, P.A., Zhao, H., Zhao, L., Grasby, S.E., Chen, Z.Q., Wignall, P.B., Lv, Z., and Han, C., 2018 - Mercury anomalies across the end Permian mass extinction in South China from shallow and deep water depositional environment: *Earth and Planetary Science Letters*, v. 496, p. 159-167.

Wessely, G., 2006 - Niederösterreich-Geologie der Österreichischen Bundesländer, *Vienna, Austria, Verlag der Geologische Bundesanstalt*, 416 p.

Wilmsen, M., Fürsich, F.T., Seyed-Emami, K., Majidifard, M.R., and Taheri, J., 2009 - The Cimmerian Orogeny in northern Iran: Tectono-stratigraphic evidence from the foreland. *Terra Nova*, 21(3), 211-218.

Witt, M. L. I., Mather, T. A., Pyle, D. M., Aiuppa, A., Bagnato, E., and Tsanev, V. I., 2008 - Mercury and halogen emissions from Masaya and Telica volcanoes, Nicaragua. *Journal of Geophysical Research: Solid Earth*, 113(B6).

Wörhmann, S.F. von, 1894 - Die Raibler Schichten nebst kritischer Zusammenstellung ihrer Fauna, *Jahrbuch der Kaiserlich-Koniglichen Geologischen Reichsanstalt*, v. 43 (1893), p. 617-768.

Xu, G., Hannah, J. L., Stein, H. J., Mørk, A., Vigran, J. O., Bingen, B., ... and Lundschien, B. A., 2014 - Cause of Upper Triassic climate crisis revealed by Re–Os geochemistry of Boreal black shales. *Palaeogeography, Palaeoclimatology, Palaeoecology*, *395*, 222-232.

Zanchetta, S., Berra, F., Zanchi, A., Bergomi, M., Caridroit, M., Nicora, A., and Heidarzadeh, G., 2013 - The record of the Late Palaeozoic active margin of the Palaeotethys in NE Iran: Constraints on the Cimmerian orogeny. *Gondwana Research*, 24(3-4), 1237-1266.

Zanchi, A., Zanchetta, S., Balini, M., and Ghassemi, M.R., 2016 - Oblique convergence during the Cimmerian collision: Evidence from the Triassic Aghdarband Basin, NE Iran. *Gondwana Research*, 38: 149-170.

Zanchi, A., Zanchetta, S., Garzanti, E., Balini, M., Berra, F., Mattei, M., and Muttoni, G., 2009 - The Cimmerian evolution of the Nakhlak-Anarak area Central Iran and its bearing for the reconstruction of the historyof the Eurasian margin. *Geological Society Special Publication*, 312(1): 261-286.

Zeng, Z., Zhu, H., Yang, X., Zeng, H., Hu, X., and Xia, C. 2019 - The Pangaea Megamonsoon records: Evidence from the Triassic Mungaroo Formation, Northwest Shelf of Australia. *Gondwana Research*, 69, 1-24.

Zhang, Y., Li, M., Ogg, J., Montgomery, P., Huang, C., Chen, Z.-Q., Shi, Z., Enos, P. and Lehrmann, D.J., 2015 - Cycle- calibrated magnetostratigraphy of middle Carnian from South China: Implications for Late Triassic time scale and termination of the Yangtze Platform. *Palaeogeography, Palaeoclimatology, Palaeoecology*, 436:135–166.

Zhou, T.S., & Zhou, H.Q., 1983 - Triassic nonmarine strata and flora of China. *Bull. Chin. Acad. Geol. Sci*, 5, 95-110.

Chapter 1

Mercury deposition in Western Tethys during the Carnian Pluvial Episode (Late Triassic)

submitted to *Scientific Reports*

Mercury deposition in Western Tethys during the Carnian Pluvial Episode (Late Triassic)

Mina Mazaheri-Johari[1]*, Piero Gianolla[1], Tamsin A. Mather[2], Joost Frieling[2], Daoliang Chu[3], Jacopo Dal Corso[3]*

[1]Department of Physics and Earth Sciences, University of Ferrara, Ferrara, Italy.

[2]Department of Earth Sciences, University of Oxford, South Parks Road, Oxford, UK.

[3]State Key Laboratory of Biogeology and Environmental Geology, School of Earth Sciences, China University of Geosciences, Wuhan, China.

*emails: mzhmni@unife.it; j.dalcorso@cug.edu.cn

Abstract

The Late Triassic Carnian Pluvial Episode (CPE) was a time of biological turnover and environmental perturbations. Within the CPE interval, C-isotope and sedimentary records indicate multiple pulses of depleted carbon into the atmosphere-ocean system linked to discrete enhancements of the hydrological cycle. Data suggest a similar cascade of events to other extinctions, including being potentially driven by the emplacement of Wrangellia large igneous province (LIP). The age of Wrangellia overlaps that of the CPE, but a direct link between volcanism and CPE's pulses remains elusive. We present sedimentary Hg concentrations from the Western Tethys successions to resolve volcanic activity through the previously established CPE global negative C-isotope excursions (NCIEs). Higher Hg concentrations and Hg/TOC are recorded just before and during NCIEs and siliciclastic inputs. The depositional setting suggests volcanic Hg inputs into the basins over the NCIEs rather than increases of Hg drawdown or riverine transport. Differences in Hg and Hg/TOC signals between the basins could be linked to coeval LIP

style or temporal resolution of the sedimentary successions. Overall, our new data provide support for a link between pulses of Wrangellia LIP, the NCIEs, and humid phases that mark the CPE in the Western Tethys.

Introduction

The Carnian Pluvial Episode (CPE, Late Triassic) was an interval of global warming and an enhanced hydrological cycle couple to extinctions and major radiations among terrestrial and marine taxa, giving rise to new modern-style ecosystems [1,2,11,3–10]. The CPE lasted for 1.2–1.6 Myrs, in the late Julian–early Tuvalian of the Carnian [12–14] (Fig. 1), and was marked by repeated carbon-cycle perturbations, as evidenced by multiple negative carbon-isotope excursions (NCIEs) [5,6,21,22,7,13,15–20]. The NCIEs indicate large injections of ^{13}C-depleted carbon into the exogenic C-cycle reservoirs, each of which just precedes increases of continental runoff, as chiefly observed in the successions of the Western Tethys, and changes in carbonate sedimentation [6,7,19,23,24]. Understanding the triggers of the CPE is crucial given its important juncture in Earth history and the parallels with the cascade of events associated with other mass extinctions. Coeval volcanic activity has previously been invoked as a cause for the CPE's NCIEs, both in terms of direct C emissions and as a trigger for positive C-cycle feedbacks (e.g., release of ^{13}C-depleted C from ocean floor clathrates) [5,13,15]. The emplacement of the Wrangellia oceanic plateau, a submarine large igneous province (LIP), has been the main candidate for this scenario [5,7,8,15,16,21,22]. However, besides age overlap [25] and Os isotope data from deep water successions of Panthalassa that show Wrangellia started in the Early Carnian *Trachyceras* ammonoid Zone, hereafter referred to as Julian 1 [22], further evidence for volcanic activity in the sedimentary record has been lacking. Hence, a direct temporal link between LIP volcanism and the environmental changes has been difficult to substantiate. Sedimentary Hg concentrations have been used to track volcanic activity during intervals of mass extinction and global environmental change [26–28]. Though other factors can at least partially control Hg deposition in terrestrial and marine settings [29,30], increases of sedimentary Hg concentration at or directly below the level of mass extinction, C-cycle and/or environmental perturbations have been used as evidence for the influence of volcanism [28]. Here we analysed Hg and total organic carbon (TOC) concentrations in four Carnian marine sedimentary sequences of the Western Tethys to evaluate whether enhanced Hg loading and volcanic activity coincided with the C-cycle and hydrological perturbations across the CPE.

Study area

We analyzed 243 mudstone and shale samples for Hg and TOC from 4 different areas of the Western Tethys realm: Southern Alps (Dolomites and Julian Alps) in Italy, Northern Calcareous Alps (Lunz) in Austria, and Transdanubian Range (Balaton) in Hungary (Fig. 1). The studied successions encompass the CPE and are well-calibrated with ammonoid, conodont, and sporomorph biostratigraphy [6,7,31]. In the Dolomites, 20 samples are from Milieres section and 30 samples from Heiligkreuz section, encompassing the Heiligkreuz Fm. (*A. austriacum–T. dilleri* ammonoid zones = Julian 2–Tuvalian 1) [6,7]. In the Julian Alps, 58 samples have been collected at Cave del Predil (Rio Conzen and Rio delle Cascate sections). The succession encompasses the Predil Dolomite, the Rio del Lago Fm., the Conzen Fm., and part of the Tor Fm. (*Trachyceras–A. austriacum* zones = Julian 1–2) [7,31]. In the Transdanubian Range, a total number of 73 samples have been analyzed from two cores (BFÜ-1 and MET-1; Rostási et al., 2011). 39 samples are from BFÜ-1 and 34 samples from MET-1, covering the Füred Limestone and the Veszprém Marl Fm. (*Trachyceras–A. austriacum*). In the Northern Calcareous Alps (Austria), we have analyzed 62 samples from Steinbach and Polzberg sections [6,17], encompassing the Reifling Fm., the Göstling Mb. and the Reingraben Fm. (*Trachyceras–A. austriacum* zone = Julian 1–2). A detailed description of the studied successions is in the Supplementary Information.

Results

In the studied sections of the Western Tethys, the measured Hg concentrations are <100 ppb, except those of the Northern Calcareous Alps included the highest values (up to 526 ppb) (Fig. 2 and 3). The average Hg concentration (29 ppb) in the Carnian rocks of the Western Tethys is lower than that measured in some modern sediments [32] (average Hg = *ca.* 40–60 ppb) and in clastic rocks covering other Phanerozoic events linked to major volcanic activity [28] (average Hg = 62.4 ppb), but is closer to the average Hg concentrations found in limestones across the

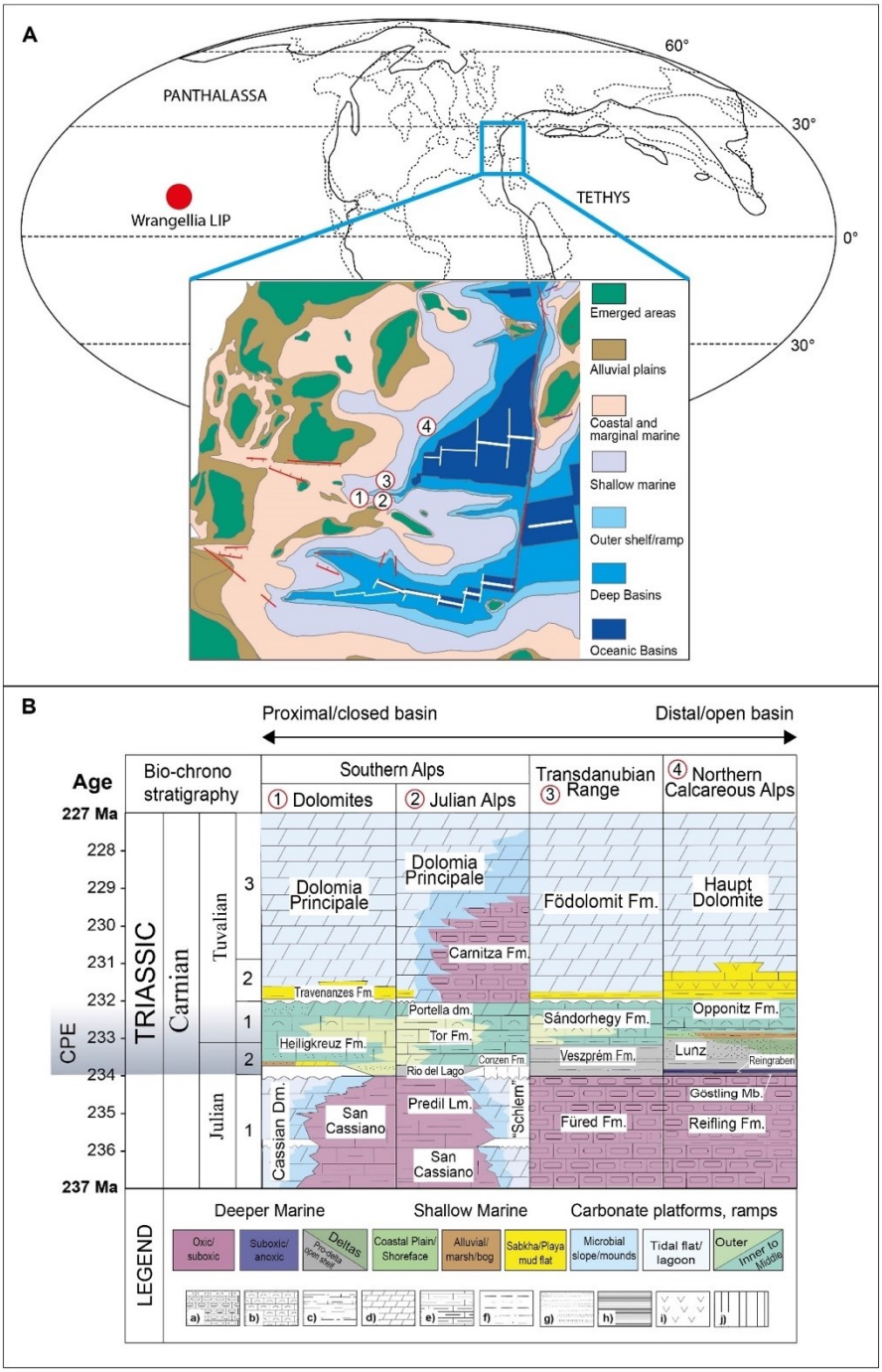

Figure 1. A) Late Triassic palaeogeography and position of the studied successions in the Western Tethys (1=Dolomites; 2=Julian Alps; 3=Transdanubian Range; 4=Northern Calcareous Alps); modified after ref.[14], B) Lithostratigraphic scheme for the Carnian formations in the studied areas. Julian 1 = *Trachyceras* zone, Julian 2 = *Austrotrachyceras austriacum* zone; Tuvalian 1 = *Tropites dilleri* zone , Tuvalian 2 = *Tropites subbullatus* zone , Tuvalian 3 = *Anatropites spinosus* zone. Lithology: a = Cherty limestone, b =Bioclastic limestone, c = Limy marlstone, d = Dolomite, e = Marly limestone, f = Siltstone, g = Sandstone, h = Black shale, i = Evaporites, j = Hiatus.

same Phanerozoic events [28] (average Hg = 34.3 ppb). All Hg and TOC results are in the Supplementary Tables S1–4 and Supplementary Figures S1–S4.

Low Hg concentrations are also coupled to generally low TOC values (<1 wt%), with only 11% of the samples showing TOC above 1 wt% (Fig. 2). Hg and TOC data are concentrated in a narrow range of values (Fig. 2). Hg/TOC values for TOC > 0.2 wt%, i.e., above the recommended lower limit for TOC normalisation [28], are on average lower (38.2 ppb/wt%) than those recorded during other Phanerozoic events (average Hg/TOC = 71.9 ppb/wt%) linked to major volcanic activity, although most among them are linked to subareal LIPs [28].

In the composite section of the Dolomites, the Hg concentrations are very low (Supplementary Table S1 and Fig. S1; Fig. 3), with a maximum value of 33 ppb and an average of 9.2 ppb. Hg only shows a slight increase (from 6.5 to 27 ppb) in the upper part of the section, upper Dibona Member of Heiligkreuz Formation, and reaches its maximum values (33 ppb) at meters 40–50, within the NCIE-3 (Fig. 3). TOC values range from 0.1 wt% to 20.5 wt%. Two high TOC of 9.2wt%. and 20.4 wt% are linked to the presence of abundant wood particles. In the upper part of the section (40–60 m, NCIE-3), an increase in Hg/TOC to > 20 ppb/wt% is recorded at the NCIE-3 and is parallel to the rise in Hg concentrations (Fig. 3).

Hg concentrations of the Julian Alps are low (Supplementary Table S2 and Fig. S2; Fig. 2), with a maximum value of 27 ppb and an average of 10 ppb. TOC is also low, with values ranging from 0.2wt% to 0.8wt%. Just before and at the end of the NCIE-2, Hg and Hg/TOC values show 3- to 6-fold increases in the Julian Alps, as Hg values rise from < 5 ppb up to 30 ppb and Hg/TOC from *ca.* 14 ppb/wt% up to max 49 ppb/wt% (from 435 to 440 meters) (Fig. 3).

Hg values through the Balaton Highland boreholes of the Transdanubian Range show a maximum value of 61 ppb (Supplementary Table S3 and Fig. S3) with an average of 25.5 ppb (Fig. 2). A sharp Hg increase (from 5.7 to 61 ppb) is recorded in the upper Füred Limestone and the base of Mencshely Marl Member of Veszprem Formation (from 400 to 340 meters) where the NCIE-1 starts (Fig. 3). Most of TOC data are below 1 wt%. Hg/TOC shows a major increase (from 9.5 to 113 ppb/wt%) at the onset of the NCIE-1 (between 400 to 340 meters; Fig. 3).

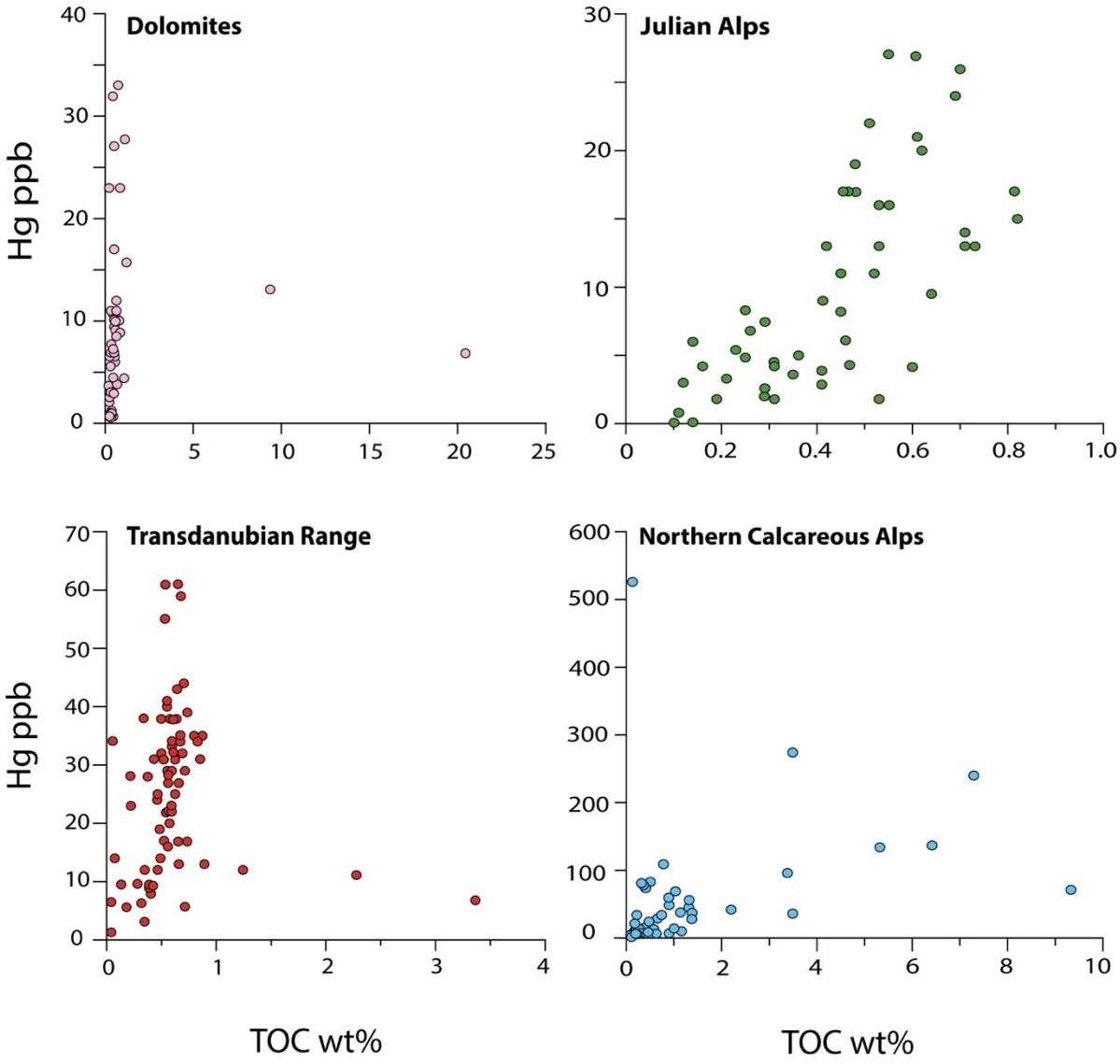

Figure 2. Hg *vs* TOC values from the studied successions of the Western Tethys (Figure 1).

In the Lunz composite section of the Northern Calcareous Alps, the Hg concentrations vary from 2 to 526 ppb (Supplementary Table S4 and Fig. S4), with most of the data lower than 150 ppb. A sharp increase in Hg is observed from 7 (ppb) in the lowermost part of the Reifling Fm. (at 3.5 meter) to 78 (ppb) in the upper part of Reifling Fm. (at 5 meter), where the onset of the NCIE-1 is recorded (Fig. 3). Hg reaches its maximum value (526 ppb) in the uppermost Reifling Formation. By the start of the Göstling Formation (onset of CPE at Julian 1 – Julian 2 boundary) at 9.6 meters, the third increase of Hg (from 4.3 to 274 ppb) is recorded. Throughout the Göstling Fm., sporadic sharp increases of Hg (127, 358, and 240 ppb at 10.8, 15.8, and 17

meters, respectively) are observed (Fig. 3). TOC content varies from 0.2 to 9.30 wt%, with most of the values below 2.5 wt%. The Hg/TOC is consistently lower than the average value (average~55 ppb/wt% in Hg/TOC ratios with TOC>0.2) with major spikes in the uppermost parts of Reifling Fm. (from 5 to 10 meters) coincident with the start of the NCIE-1 (Fig. 3). Notably, the very high Hg values (> 300 ppb, with a max of 526 ppb) occurring within the Göstling Mb. are associated with too low TOC (< 0.2 wt%) for normalization (see Supplementary Fig. S4).

Discussion

In modern and ancient sediments Hg is preferentially bound to organic matter, and for this reason Hg is generally normalized to TOC content [28,32]. In the studied successions, Hg and Hg/TOC overall show similar trends and peaks (Fig. 3), suggesting that higher Hg deposition is not predominantly controlled by variations in TOC content. TOC concentrations are generally low and fall within a narrow range of values (Fig. 2), making it challenging to evaluate the exact relationships between Hg and TOC through the different sample sets.

Particular environmental and depositional conditions can enhance local drawdown of Hg and its accumulation in sediments without the need for an actual net increase of atmospheric Hg input (e.g., ref. [32]). Marine redox chemistry is a controlling factor in Hg burial. For example, the development of strong euxinic (free sulfide) conditions may lead to enhanced pyrite formation, which may facilitate Hg inclusions [32–35]. However, the samples analysed here are all similar mudstones, thus excluding a lithological control (e.g., limestone *vs* clastic) on Hg concentration [26,36]. A small number of marl samples from the Northern Calcareous Alps have very high Hg concentrations and relatively low TOC values (Fig. 2 and 3), which could indicate the presence of Hg bound to other sulfide-mineral phases, e.g., pyrite [29]. Nevertheless, in the Northern Calcareous Alps—but also in all the other studied basins—there is no evidence of (semi-)permanent euxinic conditions, in which a sulfide Hg host could be more prevalent [32,35], as shown, for example, by the presence of bioturbation and benthic fauna (*Halobia* and benthic foraminifera [37]) found in the same strata that record the Hg spikes.

A general shift in basin-wide depositional style, from carbonate-dominated to mainly terrigenous sedimentation, is observed in the Northern Calcareous Alps and Transdanubian Range at the onset of the CPE that followed the initial C-isotope perturbations and is related to increased continental runoff driven by an enhancement of the hydrological cycle [6], but the

Hg/TOC peaks in the Northern Calcareous Alps and Transdanubian Range start before and continue through the facies change (Fig. 3). In the Transdanubian Range, this sedimentological change was also accompanied by a change in clay mineralogy, with the increase of kaolinite in the Veszprém Marls [38]. Hg could be captured by clay minerals, as observed across the Cretaceous – Palaeogene boundary and the Toarcian OAE [26]. However, in the Carnian sequences, the Hg (and Hg/TOC) starts to rise before the change in clay mineralogy, and published Al concentrations measured on the same samples from MET-1 core [20] show no relation to Hg (Supplementary Figure S3). Hence, although part of the Hg could be hosted in other, still unidentified minerals, the absence of euxinic facies and changes in clay mineralogy directly correlated to Hg variations suggest that in the studied basins Hg is preferentially hosted in organic matter, as in the majority of modern and ancient sediments [28,32].

Differences in position, Hg concentrations and magnitude of the Hg/TOC spikes are observed between basins. In the Northern Calcareous Alps and the Transdanubian Range, a substantial rise of Hg/TOC is recorded at the onset of the NCIE-1, while in the Southern Alps a Hg/TOC increase is not apparent in the same stratigraphic interval (Fig. 3). Subsequent Hg/TOC increases occur during NCIE-2 in the Transdanubian Range and the Julian Alps, and during NCIE-3 in the Dolomites (Fig. 3). Collectively, this suggests that in the western Tethys Hg/TOC increased during the early stages of NCIE-1 in the Northern Calcareous Alps and Transdanubian Range, just before and during the late stage of NCIE-2 in the Julian Alps and Transdanubian Range, and in the early stages of NCIE-3 in the Dolomites.

Different Hg and Hg/TOC signals could arise due to local differential diagenesis, as intense weathering and post-depositional oxidation of organic matter can change Hg concentrations in sediments and Hg/TOC values [29,39]. Enrichments in Hg and Hg/TOC may be controlled by early diagenetic degradation of organic matter, potentially amplifying the Hg/TOC ratios, especially in samples with very low TOC [40]. The detected Hg/TOC spikes are in samples with TOC content ≥0.2 wt% and parallel enrichments in absolute Hg concentrations (Fig. 3). Moreover, previous biomarker and RockEval analyses, clay mineralogy, colour alteration index of conodont apatite, and sporomorphs coloration indicate immaturity to low thermal maturity for the analysed samples in the Southern Alps, Transdanubian Range, and Northern Calcareous Alps [5,7,17,38].

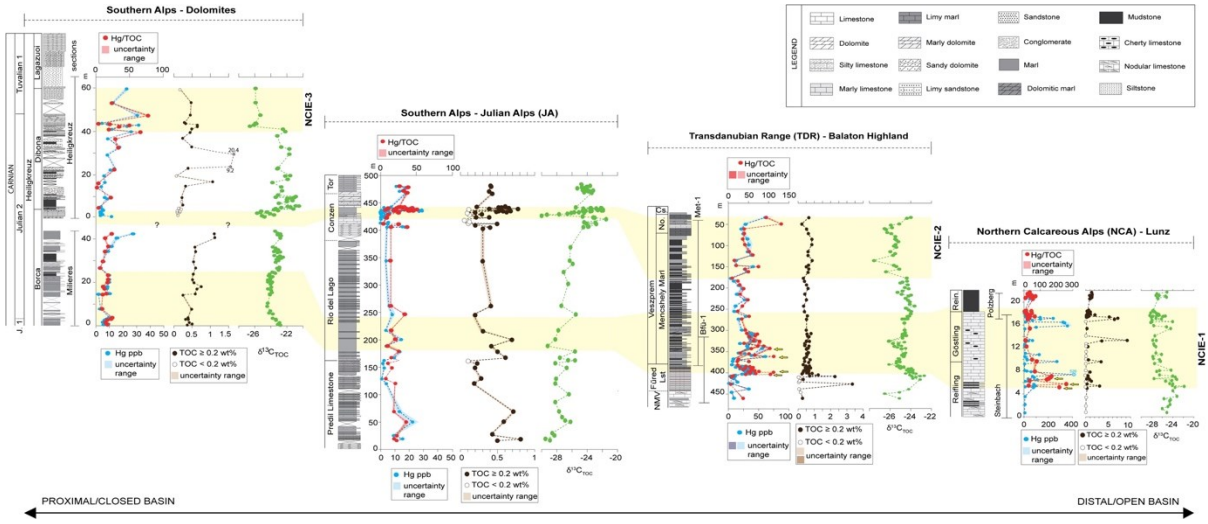

Figure 3. Hg, Hg/TOC, and C-isotope data from the Western Tethys. Hg has been normalized for TOC > 0.2wt% (Fig. 2). C isotope data and stratigraphic correlations are from ref. [5–7]. The 10% Hg concentration uncertainty is indicated on each Hg data plot in the form of shaded, semitransparent bounds; the ±0.02 wt% uncertainty on TOC measurements is also shown by semitransparent bounds; and the uncertainty envelope for each Hg/TOC value is shown on each Hg/TOC plot by a pale red field. Note that the TOC uncertainty bounds are visible only for section Julian Alps (JA) at this scale. The yellow arrows indicate the onset of Hg/TOC peaks in the NCA and TDR before and through the facies change.

Therefore, we find it unlikely that degradation of organic matter was responsible for the Hg/TOC signal, and we conclude that the observed anomalies in both Hg and Hg/TOC across different basins, likely record actual changes in Hg input into the depositional environment, and not local changes in Hg drawdown and/or diagenesis.

The terrestrial Hg reservoir can modulate global marine Hg deposition [29,30]. As one of the main reservoirs of exogenic Hg cycle, soil erosion and oxidation of terrestrial organic matter following extensive collapse of vegetation on land can result in an increase of Hg input into the marine depositional environments [32]. However, there is no evidence for such modulation during the CPE. The Carnian marks the formation of thick productive coal measures after a global "coal gap" that started at the Permian–Triassic Mass Extinction [41], and witnessed the appearance and spread of many new land plant groups [8] and the extensive development of soils in the Western Tethys [42,43], suggesting an overall expansion of the flora rather than a collapse.

Enhanced hydrological cycle during the CPE resulted in the expansion of large riverine systems in Pangea [8,44,45] and consequent increases of terrigenous inputs in many basins, where these spikes of continental runoff are the distinctive signature of the CPE. The transport of terrestrial material into the basins could increase Hg concentrations in marine sediments. However, higher Hg concentrations and Hg/TOC are recorded just before, at the onset, and during the NCIEs, which all precede siliciclastic inputs [6]: As said before, in the Northern Calcareous Alps (Lunz) and in the Transdanubian Range (Balatonfüred) Hg and Hg/TOC start to increase at the onset of the NCIE, before the $\delta^{13}C_{TOC}$ reaches its minimum values, while the subsequent increases occur during NCIE-2 in the Transdanubian Range, just before and at the end of NCIE-2 in the Julian Alps as well as early stages of NCIE-3 in the Dolomites. This implies that the episodic enhancement of continental runoff was not responsible for the initial, pre-NCIEs increases of Hg loading into the basins. However, the increased siliciclastic input that followed the initial Hg and NCIE onset, could have resulted in the transport of additional Hg in later stages of the NCIEs intervals (e.g., increases of Hg at the end of the NCIE-2 in the Julian Alps).

As for other LIP-related events, a huge amount of Hg was plausibly released by the Carnian Wrangellia oceanic plateau at the time of the CPE. Given the temporal overlap between Wrangellia LIP and the CPE, substantiated by biostratigraphic, radioisotopic, and geochemical data [8,22,25,46], and in the absence of clear evidence for other dominant Hg drawdown and transport mechanisms, it is plausible to assume a volcanic origin of the additional Hg during

the CPE. Wrangellia erupted a minimum of 1×10^6 km^3 of basalts in the Panthalassa ocean (Fig. 1) at a latitude of about 10–15°N [16,22]. The remnants of Wrangellia now outcrop in northwestern America, but coeval oceanic intraplate basalts are also present in east Asia (Sambosan and Taukha belts), which could have been part of the same LIP [22]. Os isotope data from pelagic successions of Japan show a sharp $^{187}Os/^{188}Os$ increase in the Julian (Fig. 4), that is interpreted as unradiogenic Os input from Wrangellia emplacement [22].

As with other similar oceanic plateaus [26,36], dispersal of Hg during the initial submarine phase of Wrangellia was likely predominantly marine. Current evidence suggests that a lower proportion of the records across events coeval to the emplacement of LIPs with submarine or mixed submarine/subaerial activity, show a clear Hg/TOC perturbation, compared to the records across events coeval with subaerial continental LIPs (e.g., the Siberian Traps), i.e., with atmospheric Hg dispersal, show a Hg perturbation [26]. The amplified Hg signal associated with continental flood basalts may in part result from volcanic intrusions into sedimentary sequences, with coals and evaporites [47]. This potentially liberates a large quantity of previously bound Hg through melting and combustion [48], adding to the more simple magmatic degassing thought to dominate Hg release from oceanic igneous plateaus. Moreover, the oceanic residence time of Hg is shorter (<1000 yrs) than the mixing time, whilst in the atmosphere Hg in the vapor phase has a relatively longer residence time (0.5–2 yrs) compared to the mixing time and atmospheric Hg can thus be easily dispersed globally in contrast to oceanic Hg [49]. As a result, Hg emitted from submarine volcanism is expected to be less efficiently and uniformly dispersed than atmospheric Hg [26,36]. Indeed, the magnitudes of the Hg/TOC peaks at events coeval with submarine LIPs (e.g., OAE 1a, OAE 1b, OAE 2) tend to be smaller (up to 200 ppb/wt%) [28,36,50,51] compared to those associated with continental explosive LIPs (e.g., up to 600 ppb/wt% for the Siberian Traps) [26]. These lower magnitudes are comparable to the Hg/TOC peaks found in the Carnian (Fig. 3 and 4). Hence, differential Hg and Hg/TOC signals in the different studied basins of the Western Tethys might be related to Wrangellia volcanic style, resulting in a less efficient distribution of Hg in different depositional settings. It might be hypothesized that the semi-restricted basins of the Southern Alps limited direct Hg marine influx to these basins, in contrast to the more open marine settings of the Northern Calcareous Alps and Transdanubian Range (Fig. 1). It is known that the Wrangellia switched between submarine and subaerial activity [8]. The switch in eruptive style to subaerial [52] has not been dated yet [8], but may have resulted in a wider atmospheric Hg dispersal, and anomalous Hg/TOC in a wider variety of continental to marine environments [26].

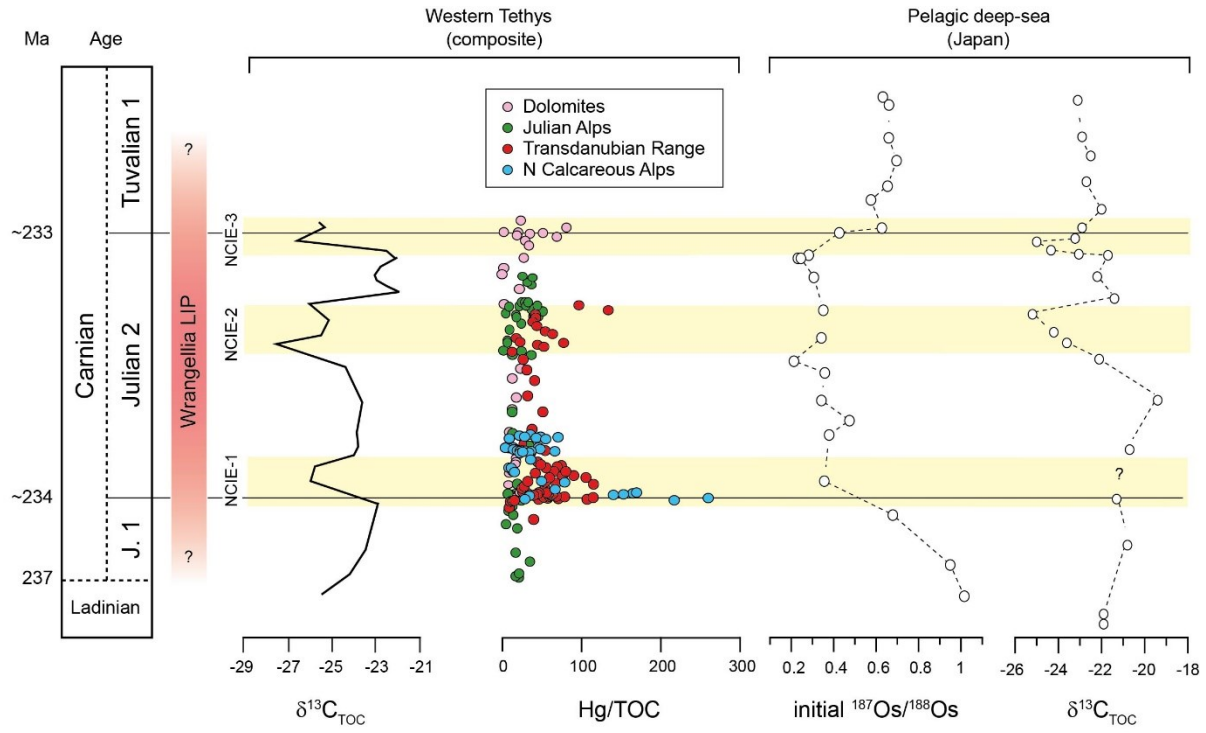

Figure 4. A comparison of our Western Tethys composite Hg/TOC stratigraphy with Os-isotopes through the same period associated with the Carnian Pluvial Episode recorded in Japan. Os and C-isotope data from Panthalassa are from ref. [22]. C-isotope data from the Western Tethys are from ref. [7]. The approximate period of the Wrangellia LIP emplacement is taken from ref. [6,8-9,14,16,25,48].

Alternatively, the lack of a Hg enrichments at the NCIE-1 in the Dolomites and Julian Alps could be explained by stratigraphic features and sampling resolution (Fig. 5). At Milieres-Dibona section (Dolomites), the onset of the NCIE-1 could be missing as the sediments below the isotope anomaly do not outcrop in the area (see ref. [6]). This is due to the fact that the uppermost San Cassiano – lowermost Heiligkreuz basinal succession of the Dolomites is represented by fine-grained shales that are easily eroded and covered by vegetation. We therefore cannot exclude the possibility that the covered sediments at the base of the section might have prevented sampling of the first Hg spike, and the onset of the NCIE-1 [6]. In the Julian Alps, the temporal and stratigraphic sampling resolution across the NCIE-1 is limited because the sections are extremely expanded, almost vertical and poorly accessible. Here, the NCIE-1 is defined by only 4 samples, i.e., the same samples also measured for Hg, collected in ~70 meters of succession. As observed in the Transdanubian Range and Northern Calcareous Alps, Hg/TOC are not constant within the body of the NCIE-1, and the short-lived spikes may have been missed in the Julian Alps (Fig. 5).

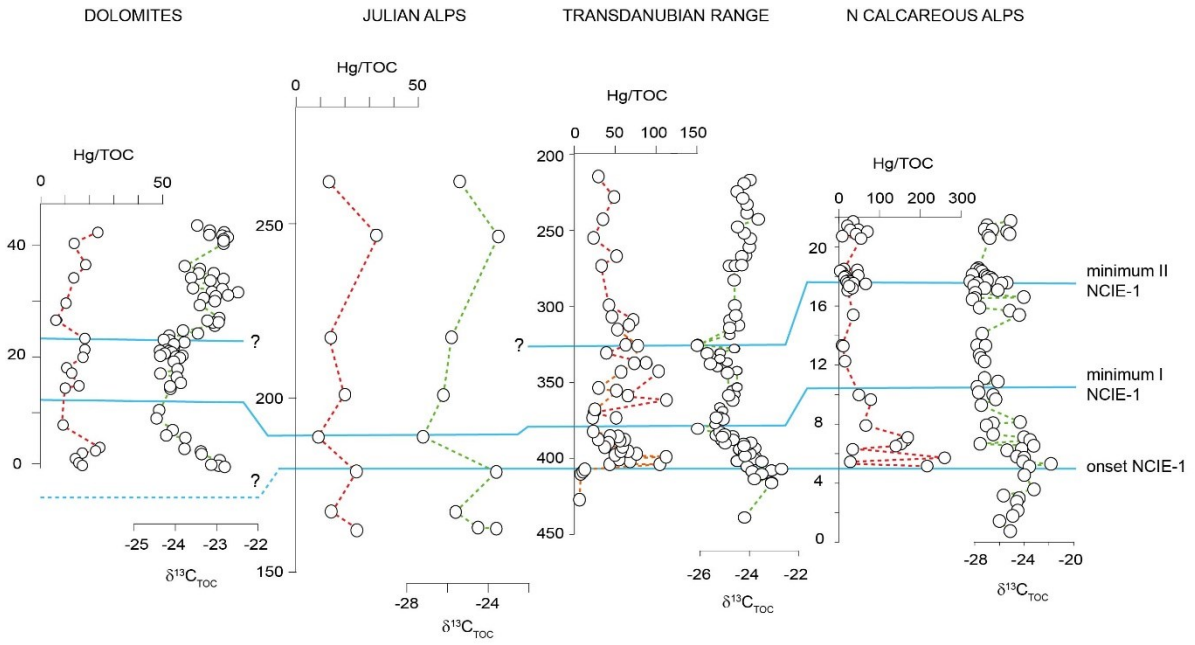

Figure 5. Detail of Hg/TOC and $\delta^{13}C_{TOC}$ data across the NCIE-1 in the studied basins of the Western Tethys. The Hg/TOC spike associated with the NCIE-1 of the CPE could be missing in the Southern Alps (Dolomites and Julian Alps) because of the incompleteness of the succession and lower sampling resolution.

Conclusions

Our new data show pulses of increased Hg loading in the Western Tethys during the early Late Triassic CPE. The pulses occur in correspondence to NCIEs, but the Hg/TOC record is different in different basins. A rise of Hg/TOC is recorded in the more distal, open, and complete basin successions of the Northern Calcareous Alps (Austria) and the Transdanubian Range (Hungary) at the onset of the first NCIE of the CPE, but the same spike is not recorded during the same interval in the more proximal restricted basins of the Southern Alps (Italy). This geographical distribution might be an artifact of incomplete sections or low temporal sampling resolution. However, it is also consistent with a primary signal as major interbasinal differences in Hg concentrations and Hg/TOC are recorded during other Mesozoic LIP events linked to emplacements of oceanic plateaux, and are explained by the relatively inefficient dispersal of Hg from submarine volcanism [26,27,53]. Overall, our data is consistent with the hypothesis that pulses of Wrangellia volcanic activity triggered multiple injections of

isotopically light C into the atmosphere-ocean system and associated environmental perturbations.

Methods

Hg analysis. A total of 243 samples were analysed for Hg concentrations using a Lumex RA-915 Portable Mercury Analyser with PYRO-915 Pyrolyzer at the University of Oxford, using the method described by ref. [54]. Samples were powdered with an agate mortar, then an aliquot of 50 – 250 mg was weighed into a glass boat before being placed into the pyrolyzer and heated to 700°C. Volatilized elementary Hg was quantified via atomic absorption spectrometry. At the start of each run and throughout the measurement sequences (every 10 samples), paint-contaminated soil (NIST 2587; 290 ppb Hg) standards were analysed, using masses ranging from 10 to 90 mg, to calibrate the Lumex. The analysed standards indicate reproducibility was generally better than 10% for Hg concentrations. TOC normalization of Hg was applied when TOC was above or equal to 0.2% following the approach recommended by ref. [28]. For the Transdanubian Range Hg/Al has been calculated using published elemental data of ref. [20], which were measured on the same core material. The Hg data are coupled to the organic carbon $\delta^{13}C$ data previously generated on the same samples [6,7].

Analysis of total organic carbon (TOC). An Elementar Soli TOC Cube was used to determine Total Organic Carbon (TOC) in rock samples at the University of Ferrara. The analyser is equipped with two combustion units: a dynamic heater able to raise the temperature from ambient to 900 °C and a post-combustion zone kept at a constant temperature of 800°C, containing a platinum catalyst to achieve complete oxidation of all combustion products released by the dynamic heater. Combustion takes place in pure oxygen at a flow rate of 150 ml/min. An infrared detector detects the formed CO_2. About 500 mg of each sample were weighed into stainless steel crucibles that were heated prior to analysis to avoid contamination by C residues. Values are reported as the mean of duplicate analysis. The sample weight depended on the C content and could be extended up to 1g in cases where the C contents were low (equal or below 0.1 wt%). A standard of calcium carbonate ($CaCO_3$, Calciumcarbonat, Elementar) and a soil standard ($CaCO_3$, Bodenstandard, Elementar with approximately 1.3% C content) were analysed prior, between, and after each run. Temperature-dependent differentiation of total carbon (DIN19539) has been applied for determining the total organic carbon content as described by ref. [55]. The dynamic temperature ramping method starts at about 100 °C. After introducing the sample, the temperature is increased at a rate of 90 °C / minute

up to 600 °C for the determination of TOC. The average standard deviation (SD), based on replicate analyses of nine samples and a soil standard (Bodenstandard), was +/-0.02 wt%.

References

1. Schlager, W. & Schöllnberger, W. Das Prinzip stratigraphischer Wenden in der Schichtfolge der Nördlichen Kalkalpen. *Mitteilungen der Geol. Gesellschaft Wien* 66–67, 165–193 (1974).
2. Simms, M. J. & Ruffell, A. H. Synchroneity of climatic change and extinctions in the Late Triassic. *Geology* 17, 265–268 (1989).
3. Simms, M. J. & Ruffell, A. H. Climatic and biotic change in the late Triassic. *J. - Geol. Soc.* 147, 321–327 (1990).
4. Hornung, T. & Brandner, R. Biochronostratigraphy of the Reingraben Turnover (Hallstatt Facies Belt): Local black shale events controlled by regional tectonics, climatic change and plate tectonics. *Facies* 51, 460–479 (2005).
5. Dal Corso, J. *et al.* Discovery of a major negative δ13C spike in the Carnian (Late Triassic) linked to the eruption of Wrangellia flood basalts. *Geology* 40, 79–82 (2012).
6. Dal Corso, J. *et al.* Carbon isotope records reveal synchronicity between carbon cycle perturbation and the 'Carnian Pluvial Event' in the Tethys realm (Late Triassic). *Glob. Planet. Change* 127, 79–90 (2015).
7. Dal Corso, J. *et al.* Multiple negative carbon-isotope excursions during the Carnian Pluvial Episode (Late Triassic). *Earth-Science Reviews* 185, 732–750 (2018).
8. Dal Corso, J. *et al.* Extinction and dawn of the modern world in the Carnian (Late Triassic). *Sci. Adv.* 6, (2020).
9. Trotter, J. A., Williams, I. S., Nicora, A., Mazza, M. & Rigo, M. Long-term cycles of Triassic climate change: A new δ18O record from conodont apatite. *Earth Planet. Sci. Lett.* 415, 165–174 (2015).
10. Ruffell, A., Simms, M. J. & Wignall, P. B. The Carnian Humid Episode of the late Triassic: A review. *Geol. Mag.* 153, 271–284 (2016).
11. Mancuso, A. C., Benavente, C. A., Irmis, R. B. & Mundil, R. Evidence for the Carnian Pluvial Episode in Gondwana: New multiproxy climate records and their bearing on

early dinosaur diversification. *Gondwana Res.* 86, 104–125 (2020).

12. Zhang, Y. *et al.* Cycle-calibrated magnetostratigraphy of middle Carnian from South China: Implications for Late Triassic time scale and termination of the Yangtze Platform. *Palaeogeogr. Palaeoclimatol. Palaeoecol.* 436, 135–166 (2015).

13. Miller, C. S. *et al.* Astronomical age constraints and extinction mechanisms of the Late Triassic Carnian crisis. *Sci. Rep.* 7, (2017).

14. Bernardi, M., Gianolla, P., Petti, F. M., Mietto, P. & Benton, M. J. Dinosaur diversification linked with the Carnian Pluvial Episode. *Nat. Commun.* 9, (2018).

15. Sun, Y. D. *et al.* Climate warming, euxinia and carbon isotope perturbations during the Carnian (Triassic) Crisis in South China. *Earth Planet. Sci. Lett.* 444, 88–100 (2016).

16. Sun, Y. D., Richoz, S., Krystyn, L., Zhang, Z. T. & Joachimski, M. M. Perturbations in the carbon cycle during the carnian humid episode: Carbonate carbon isotope records from southwestern China and Northern Oman. *J. Geol. Soc. London.* 176, 167–177 (2019).

17. Mueller, S., Krystyn, L. & Kürschner, W. M. Climate variability during the Carnian Pluvial Phase - A quantitative palynological study of the Carnian sedimentary succession at Lunz am See, Northern Calcareous Alps, Austria. *Palaeogeogr. Palaeoclimatol. Palaeoecol.* 441, 198–211 (2016).

18. Mueller, S., Hounslow, M. W. & Kürschner, W. M. Integrated stratigraphy and palaeoclimate history of the Carnian Pluvial event in the Boreal realm; new data from the upper triassic kapp toscana group in central Spitsbergen (Norway). *J. Geol. Soc. London.* 173, 186–202 (2016).

19. Jin, X. *et al.* The aftermath of the CPE and the Carnian–Norian transition in northwestern Sichuan basin, South China. *J. Geol. Soc. London.* 176, 179–196 (2019).

20. Baranyi, V., Miller, C. S., Ruffell, A., Hounslow, M. W. & Kürschner, W. M. A continental record of the carnian pluvial episode (CPE) from the mercia mudstone group (UK): Palynology and climatic implications. *J. Geol. Soc. London.* 176, 149–166 (2019).

21. Fu, X. *et al.* A possible link between the Carnian Pluvial Event, global carbon-cycle perturbation, and volcanism: New data from the Qinghai-Tibet Plateau. *Glob. Planet. Change* 194, (2020).

22. Tomimatsu, Y. *et al.* Marine osmium isotope record during the Carnian “pluvial episode” (Late Triassic) in the pelagic Panthalassa Ocean. *Glob. Planet. Change* 197, (2021).

23. Hornung, T., Krystyn, L. & Brandner, R. A Tethys-wide mid-Carnian (Upper Triassic) carbonate productivity crisis: Evidence for the Alpine Reingraben Event from Spiti (Indian Himalaya)? *J. Asian Earth Sci.* 30, 285–302 (2007).

24. Gattolin, G. *et al.* Sequence stratigraphy after the demise of a high-relief carbonate platform (Carnian of the Dolomites): Sea-level and climate disentangled. *Palaeogeogr. Palaeoclimatol. Palaeoecol.* 423, 1–17 (2015).

25. Furin, S. *et al.* High-precision U-Pb zircon age from the Triassic of Italy: Implications for the Triassic time scale and the Carnian origin of calcareous nannoplankton and dinosaurs. *Geology* 34, 1009–1012 (2006).

26. Percival, L. M. E. *et al.* Does large igneous province volcanism always perturb the mercury cycle? Comparing the records of Oceanic Anoxic Event 2 and the end-cretaceous to other Mesozoic events. *Am. J. Sci.* 318, 799–860 (2018).

27. Lindström, S. *et al.* Volcanic mercury and mutagenesis in land plants during the end-Triassic mass extinction. *Sci. Adv.* 5, (2019).

28. Grasby, S. E., Them, T. R., Chen, Z., Yin, R. & Ardakani, O. H. Mercury as a proxy for volcanic emissions in the geologic record. *Earth-Science Reviews* 196, (2019).

29. Them, T. R. *et al.* Terrestrial sources as the primary delivery mechanism of mercury to the oceans across the Toarcian Oceanic Anoxic Event (Early Jurassic). *Earth Planet. Sci. Lett.* 507, 62–72 (2019).

30. Dal Corso, J. *et al.* Permo–Triassic boundary carbon and mercury cycling linked to terrestrial ecosystem collapse. *Nat. Commun.* 11, 2962 (2020).

31. Roghi, G., Gianolla, P., Minarelli, L., Pilati, C. & Preto, N. Palynological correlation of Carnian humid pulses throughout western Tethys. *Palaeogeogr. Palaeoclimatol. Palaeoecol.* 290, 89–106 (2010).

32. Shen, J. *et al.* Sedimentary host phases of mercury (Hg) and implications for use of Hg as a volcanic proxy. *Earth Planet. Sci. Lett.* 543, (2020).

33. Benoit, J. M., Gilmour, C. C., Mason, R. P. & Heyes, A. Sulfide controls on mercury speciation and bioavailability to methylating bacteria in sediment pore waters.

Environ. Sci. Technol. 33, 951–957 (1999).

34. Niessen, S. *et al.* Influence of sulphur cycle on mercury methylation in estuarine sediment (Seine estuary, France). in *Journal De Physique. IV : JP* 107, 953–956 (2003).

35. Sanei, H., Grasby, S. E. & Beauchamp, B. Latest permian mercury anomalies. *Geology* 40, 63–66 (2012).

36. Scaife, J. D. *et al.* Sedimentary Mercury Enrichments as a Marker for Submarine Large Igneous Province Volcanism? Evidence From the Mid-Cenomanian Event and Oceanic Anoxic Event 2 (Late Cretaceous). *Geochemistry, Geophys. Geosystems* 18, 4253–4275 (2017).

37. Tollmann, A. *Analyse des klassischen nordalpinen Mesozoikums: Stratigraphie, Fauna und Fazies der Nördlichen Kalkalpen*. (Deuticke Wien, 1976).

38. Rostási, Á., Raucsik, B. & Varga, A. Palaeoenvironmental controls on the clay mineralogy of Carnian sections from the Transdanubian Range (Hungary). *Palaeogeogr. Palaeoclimatol. Palaeoecol.* 300, 101–112 (2011).

39. Charbonnier, G., Adatte, T., Föllmi, K. B. & Suan, G. Effect of Intense Weathering and Postdepositional Degradation of Organic Matter on Hg/TOC Proxy in Organic-rich Sediments and its Implicationsfor Deep-Time Investigations. *Geochemistry, Geophys. Geosystems* 21, (2020).

40. Jones, D. S., Martini, A. M., Fike, D. A. & Kaiho, K. A volcanic trigger for the late ordovician mass extinction? Mercury data from south china and laurentia. *Geology* 45, 631–634 (2017).

41. Retallack, G. J., Veevers, J. J. & Morante, R. Global coal gap between Permian-Triassic extinction and Middle Triassic recovery of peat-forming plants. *Bull. Geol. Soc. Am.* 108, 195–207 (1996).

42. Gianolla, P., Ragazzi, E. & Roghi, G. Upper Triassic amber from the Dolomites (Northern Italy). A paleoclimatic indicator? *Riv. Ital. di Paleontol. e Stratigr.* 104, 381–390 (1998).

43. Preto, N. & Hinnov, L. A. Unraveling the origin of carbonate platform cyclothems in the Upper Triassic Dürresntein Formation (Dolomites, Italy). *J. Sediment. Res.* 73, 774–789 (2003).

44. Arche, A. & López-Gómez, J. The Carnian Pluvial Event in Western Europe: New data from Iberia and correlation with the Western Neotethys and Eastern North America-NW Africa regions. *Earth-Science Reviews* 128, 196–231 (2014).

45. Klausen, T. G., Nyberg, B. & Helland-Hansen, W. The largest delta plain in Earth's history. *Geology* 47, 470–474 (2019).

46. Greene, A. R. *et al.* The architecture of oceanic plateaus revealed by the volcanic stratigraphy of the accreted Wrangellia oceanic plateau. *Geosphere* 6, 47–73 (2010).

47. Svensen, H. *et al.* Siberian gas venting and the end-Permian environmental crisis. *Earth Planet. Sci. Lett.* 277, 490–500 (2009).

48. Wang, X. *et al.* Mercury anomalies across the end Permian mass extinction in South China from shallow and deep water depositional environments. *Earth Planet. Sci. Lett.* 496, 159–167 (2018).

49. Schroeder, W. H. & Munthe, J. Atmospheric mercury - An overview. in *Atmospheric Environment* 32, 809–822 (1998).

50. Charbonnier, G. & Föllmi, K. B. Mercury enrichments in lower Aptian sediments support the link between Ontong Java large igneous province activity and oceanic anoxic episode 1a. *Geology* 45, 63–66 (2017).

51. Sabatino, N. *et al.* Mercury anomalies in upper Aptian-lower Albian sediments from the Tethys realm. *Palaeogeogr. Palaeoclimatol. Palaeoecol.* 495, 163–170 (2018).

52. Greene, A. R. *et al.* The architecture of oceanic plateaus revealed by the volcanic stratigraphy of the accreted Wrangellia oceanic plateau. *Geosphere* 6, 47–73 (2010).

53. Percival, L. M. E. *et al.* Mercury evidence for pulsed volcanism during the end-Triassic mass extinction. *Proc. Natl. Acad. Sci. U. S. A.* 114, 7929–7934 (2017).

54. Bin, C., Xiaoru, W. & Lee, F. S. C. Pyrolysis coupled with atomic absorption spectrometry for the determination of mercury in Chinese medicinal materials. *Anal. Chim. Acta* 447, 161–169 (2001).

55. Natali, C., Bianchini, G. & Carlino, P. Thermal stability of soil carbon pools: Inferences on soil nature and evolution. *Thermochim. Acta* 683, 178478 (2020).

Acknowledgments

We thank G. Roghi, N. Preto and M. Caggiati for assistance in the field. We acknowledge G. Bianchini, G.M. Salani, and V. Brombin for the help with TOC analysis. MM-J and PG acknowledges FAR 2018-2019 founding of the University of Ferrara. TAM and JF acknowledge funding from ERC consolidator grant (ERC-2018-COG-818717-V-ECHO).

Author contributions

JDC and PG designed the study. PG and JDC collected the samples. MM-J prepared the samples. MM-J, JF and TM carried out Hg analysis. All the authors discussed the data and conclusions of the study. MM-J, JDC and PG wrote the manuscript with inputs from all co-authors.

Competing interests

The authors declare no competing interests.

Additional information

Correspondence and requests for materials should be addressed to MM-J and JDC.

Chapter 2

A monotypic stand of *Neocalamites iranensis* n. sp. from the Carnian Pluvial Episode (Late Triassic) of the Aghdarband area, NE Iran (Turan Plate)

Published in the the Rivista Italiana di Paleontologia e Stratigrafia on July 2021

A monotypic stand of *Neocalamites iranensis* n. sp. from the Carnian Pluvial Episode (Late Triassic) of the Aghdarband area, NE Iran (Turan Plate)

Mina Mazaherijohari[1], Evelyn Kustatscher[2,3], Guido Roghi[4], Ebrahim Ghasemi-Nejad[5], Piero Gianolla[1]

[1]Department of Physics and Earth Sciences, University of Ferrara, Via G. Saragat 1, Ferrara 44100, Italy. E-mail: mzhmni@unife.it, piero.gianolla@unife.it

[2] Department of Earth and Environmental Sciences, Paleontology & Geobiology, Ludwig-Maximilians-Universität München, Richard-Wagner-Straße 10, 80333 München, Germany. E-mail: Evelyn.Kustatscher@naturmuseum.it

[3] SNSB-Bayerische Staatssammlung für Paläontologie und Geologie, Richard-Wagner-Straße 10, 80333 München, Germany. E-Mail: Evelyn.Kustatscher@naturmuseum.it

[4] Institute of Geosciences and Earth Resources - CNR, Via Gradenigo 6, Padova 35131, Italy. E-mail: guido.roghi@igg.cnr.it

[5]Department of Geology, Faculty of Science, University of Tehran, Enghelab Square, Tehran, Iran. E-mail: eghasemi@khayam.ut.ac.ir

Abstract

The Aghdarband Basin in the Kopeh-Dagh Range (NE Iran) is one of the most important areas for unraveling the evolution of the Turan plate (southern margin of Eurasia) during the last phase of the closure of the Paleotethys and to reconstruct the history of the Cimmerian blocks just before their collision with Eurasia during the early Late Triassic. The youngest sediments affected by the Early Cimmerian orogeny are those of the Upper Triassic Miankuhi Formation, which covers unconformably the Upper Triassic (lower Carnian) marine beds of the Sina Formation by an interval of continental facies including local conglomerates, cross-bedded sandstones, mudstone layers, silty shales, an up to one-meter-thick coal layer with plant remains, and shales. The plant assemblages represent a relatively wide variety of different forms (sphenophytes, ginkgophytes, conifers, and *incertis sedis*), documenting wetlands with lush vegetation typical of warm and humid environments. In this study, we describe a plant fossil assemblage from the base of the Miankuhi Fm., dominated by roots and vegetative organs of *Neocalamites iranensis* n. sp., with few plant fossils of uncertain botanical affinity.

Palynological investigations of the basal part of the Miankuhi Formation confirm a latest early Carnian to late Carnian age for this interval and reveal, for the first time, a clear link between this plant-bearing bed, and a time of global environmental changes, the Carnian Pluvial Episode. This is the first report of the Carnian Pluvial Episode in the Turan plate (southern margin of Eurasia) and Iran.

Keywords: Kopeh-Dagh Range, Triassic, coal deposits, sphenophytes, fossil plants, CPE.

Introduction

Plant macrofossils are common in Iran, although most plant remains are of Rhaetian or Jurassic age (e.g., Vaez-Javadi 2013a and refs. therein). Among the first authors to describe and enlist Late Triassic to Middle Jurassic plant fossils from Iran were Göppert (1861), Stur (1886), Schenk (1887), and Krasser (1891). The best studied area is the Alborz Mountains (e.g., Krasser 1891; Kilpper 1971, 1975; Bernard & Miller 1976; Schweitzer 1978; Vassiliev 1984; Schweitzer & Kirchner 1995, 1996, 1998, 2003; Schweitzer et al. 1997, 2000, 2009; Vaez-Javadi & Syooki 2002; Vaez-Javadi 2004, 2008; Vaez-Javadi & Abbasi 2012) as the Rhaeto-Liassic successions of Dorud (e.g., Barnard 1965, 1976), Amol area (Popa et al. 2012), Karmozd, and Zirab (e.g., Kilpper 1964, 1968, 1971; Kimyai 1972), located in the Central Alborz Mountains, are rich in plant fossils.

Most studies describe diverse and abundant plant fossil assemblages that were mainly collected close to mined coal seams. The Aghdarband Coal Bed (Miankuhi Formation) from the Aghdarband area is an example of such a plant-bearing horizon in the Kopeh-Dagh Range, Northeast Iran. Boersma & Van Konijnenburg-van Cittert (1991) were so far the first and only ones to describe Triassic plant fossils from the Aghdarband area. The authors recognized a variety of sphenophytes (*Neocalamites*), ginkgophytes (*Sphenobaiera*), conifers (*Podozamites*), and incertis sedis (*Taeniopteris*, *Carpolithes*), including new species *Podozamites paucinervis*. The plant fossils were collected at several outcrops either from the Aghdarbad Coal Bed at the base of the Miankuhi Formation, or from a coal horizon at the base of the Ghal'eh Qabri Shales. In situ trunks in vertical, standing position were mentioned (Ruttner 1991), but not described. The composition of the plant fossil assemblages from the basal coal layer of Miankuhi Formation (Boersma & Van Konijnenburg-van Cittert 1991) and the poorly preserved marine palynomorphs (dinoflagellate cysts; Ghasemi-Nejad et al. 2008) suggested a Norian age for the coal bed, whereas our palynological analyses yielding terrestrial palynomorphs support a Carnian age for the base of the Miankuhi Formation (see below). The

plant-bearing basal part of the Ghal'eh Qabri Shales were assigned putatively to the Rhaetian (Boersma & Van Konijnenburg-van Cittert 1991).

This study aims to provide an overview of the fossiliferous horizon yielding in situ plant fossils from the coal layer of the Miankuhi Formation, to discuss plant fossils previously found in the area, and to describe the first plant fossils of Iran dated confidentially as Carnian, representing the Carnian Pluvial Episode (CPE).

Geological setting

Cimmeria as an extended deformed zone comprising several microcontinent blocks, rifted from Gondwana at the end of the Paleozoic (e.g., Sengör 1979, 1984, 1990; Stampfli & Borel 2002; Angiolini et al. 2007) and collided with Eurasia during the Triassic (e.g., Stöcklin 1974; Sengör 1979, 1984, 1990; Ricou 1994; Stampfli & Borel 2002; Wilmsen et al. 2009; Zanchi et al. 2009a, 2009b) (Fig. 1). The collision of the Iranian microplate as part of the Cimmerian blocks with the southern margin of Eurasia (Turan Plate) during the Late Triassic/Early Jurassic defines one of the major compressional events of the Iranian platform, named as Cimmerian collision, which caused the closure of the Paleotethys Ocean (e.g., Stöcklin 1974; Sengör 1979, 1984; Stampfli & Borel 2002; Wilmsen et al. 2009; Zanchi et al. 2009a, 2009b). The Eo-Cimmerian orogeny affected the Kopeh-Dagh Basin in the southern margin of the Eurasian Plate (NE Iran) and subsequent Middle Jurassic rifting led to the development of more than 7 km thick sequence of gently folded rocks of Jurassic to Paleogene sediments in this basin (e.g., Afshar-Harb 1979; Davoudzadeh & Schmidt 1985; Milanovsky 1991; Afshar-Harb 1994; Brunet et al. 2003; Garzanti & Gaetani 2002; Mahboubi et al. 2010; Robert et al. 2014). The Kopeh-Dagh intracontinental range stretches for about 700 kilometers in a WNW–ESE

Figure 1: Late Triassic paleogeography (about 230 Ma, redrawn from Matthews et al. 2016; Cao et al. 2017). The red area corresponds to the studied location (Turan Plate). NTO: Neotethys Ocean; MTO: Mesotethys Ocean; PTO: Paleotethys Ocean.

direction east of the Caspian Sea, and lies in the northeast of Iran and south of Turkmenistan (Fig. 2A, B). The basement of the Kopeh-Dagh Range (pre-Jurassic sediments) crops out in the eastern part of the belt and within the Aghdarband erosional window due to the erosion of the gently folded overlying Jurassic–Paleogene beds by the river Kashaf-Rud and other drainage systems to the south (Ruttner 1984, 1991). The Aghdarband area occupied the southern part of the Kopeh-Dagh Range which was located at about 35–45ºN during the Late Triassic (~230 Ma) (Mattei et al. 2014; Muttoni et al. 2015; Matthews et al. 2016; Cao et al. 2017) and its sediments are principally Triassic in age (e.g., Ruttner 1984, 1988, 1991; Baud et al. 1991a; Boersma & Van Konijnenburg-van Cittert 1991; Donofrio 1991; Alavi et al. 1997; Ghasemi-Nejad et al. 2008; Balini et al. 2009, 2019) (Fig. 2C). The well-dated Triassic successions of Aghdarband were deposited in a back-arc setting associated with the northward subduction of the Paleotethys Ocean along the southern margin of Eurasia and are strongly deformed as a result of the Cimmerian orogeny (Ruttner 1991; Alavi et al. 1997; Zanchi et al. 2009a; Sheikholeslami & Kouhpeyma 2012; Zanchetta et al. 2013). There is still considerable ambiguity about the precise time of deformation of the Aghdarband area although extensive field analyses by Zanchi et al. (2016) proposed a pre-Bajocian age for the deformation. This basin, formed within the framework of an extensional-transtensional tectonic regime, is subdivided into three main structural units named unit 1, 2, and 3 from north to south (Ruttner 1991; Zanchi et al. 2016). Unit 1 is characterized by folding and faulting deformation while thrusting characterizes the units 2 and 3 (Zanchi et al. 2016). A substantial *systematic* study on the central and eastern part of the Aghdarband Basin (units 1–3) was performed by Ruttner

(1991), who represented a detailed geological map at 1:12,500 scale *(*Ruttner 1991: pl. 1*)*. The present study was carried out in unit 2 of the Aghdarband Basin, where the most complete stratigraphic succession of the area is recorded.

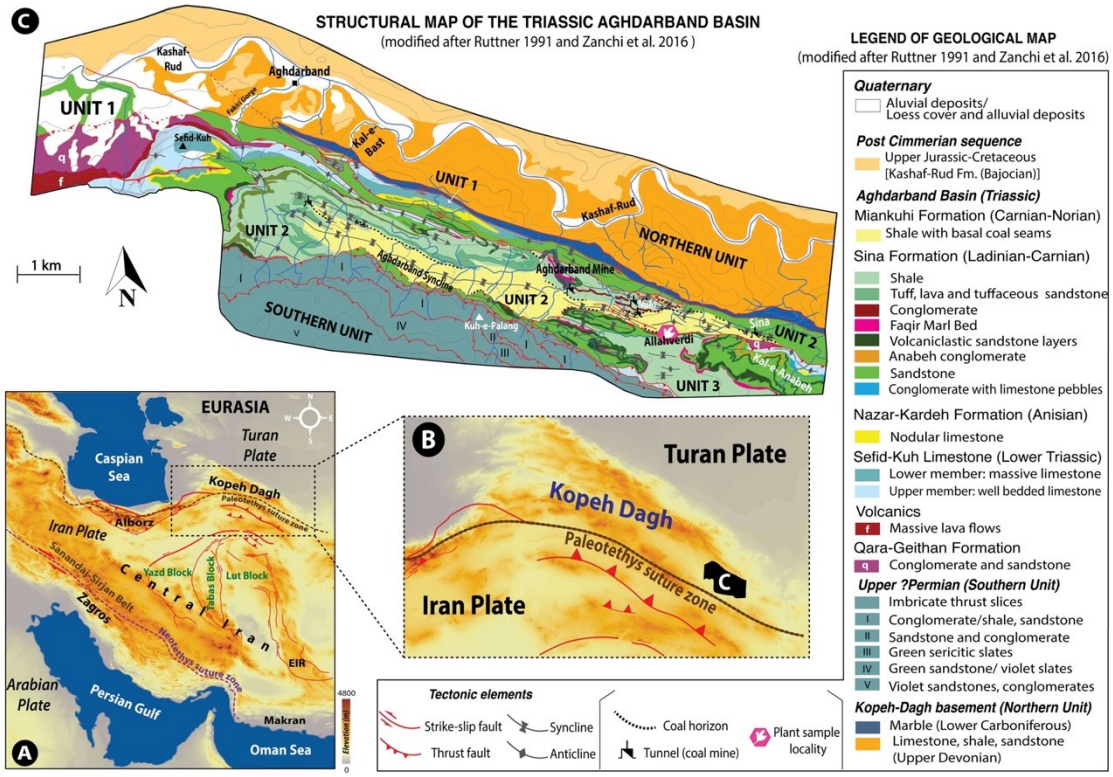

Figure 2: A: Main structural zones of the area (after Stöcklin & Nabavi 1973; Berberian & King 1981; Allen et al. 2004, 2011; Morley et al. 2009; Nozaem et al. 2013; Calzolari et al. 2016): EIZ: Eastern Iran zone. **B:** Detail of the Kopeh-Dagh Range and the location of the studied area (Aghdarband Basin). **C:** Geological map of the Aghdarband Area showing the three tectonic units and the various formations of the Aghdarband Basin (modified after Ruttner 1991; Zanchi et al. 2016).

Revised Stratigraphy

The Triassic stratigraphy of the tectonic unit 2 is represented by four distinct formations which are, in ascending stratigraphic order, the Sefid-Kuh Limestone, the Nazar-Kardeh Formation, the Sina Formation, and the Miankuhi Formation (Fig. 3). The Lower Triassic Sefid-Kuh Limestone (Baud et al. 1991a; Balini et al. 2019) overlies the ?late Permian–Early Triassic volcanoclastic conglomerates of the Qara-Qeitan Formation (Ruttner 1991; Eftekharnezhad & Behroozi 1991; Baud et al. 1991a; Alavi et al. 1997; Balini et al. 2009; Zanchi et al. 2016). Up-section, relatively deep-water fossiliferous cherty limestones of the Nazar-Kardeh Formation were deposited due to a sudden deepening at the end of the Olenekian in the units 1 and 2. The Nazar-Kardeh Formation with a Bithynian age (Krystyn & Tatzreiter 1991; Balini et al. 2019)

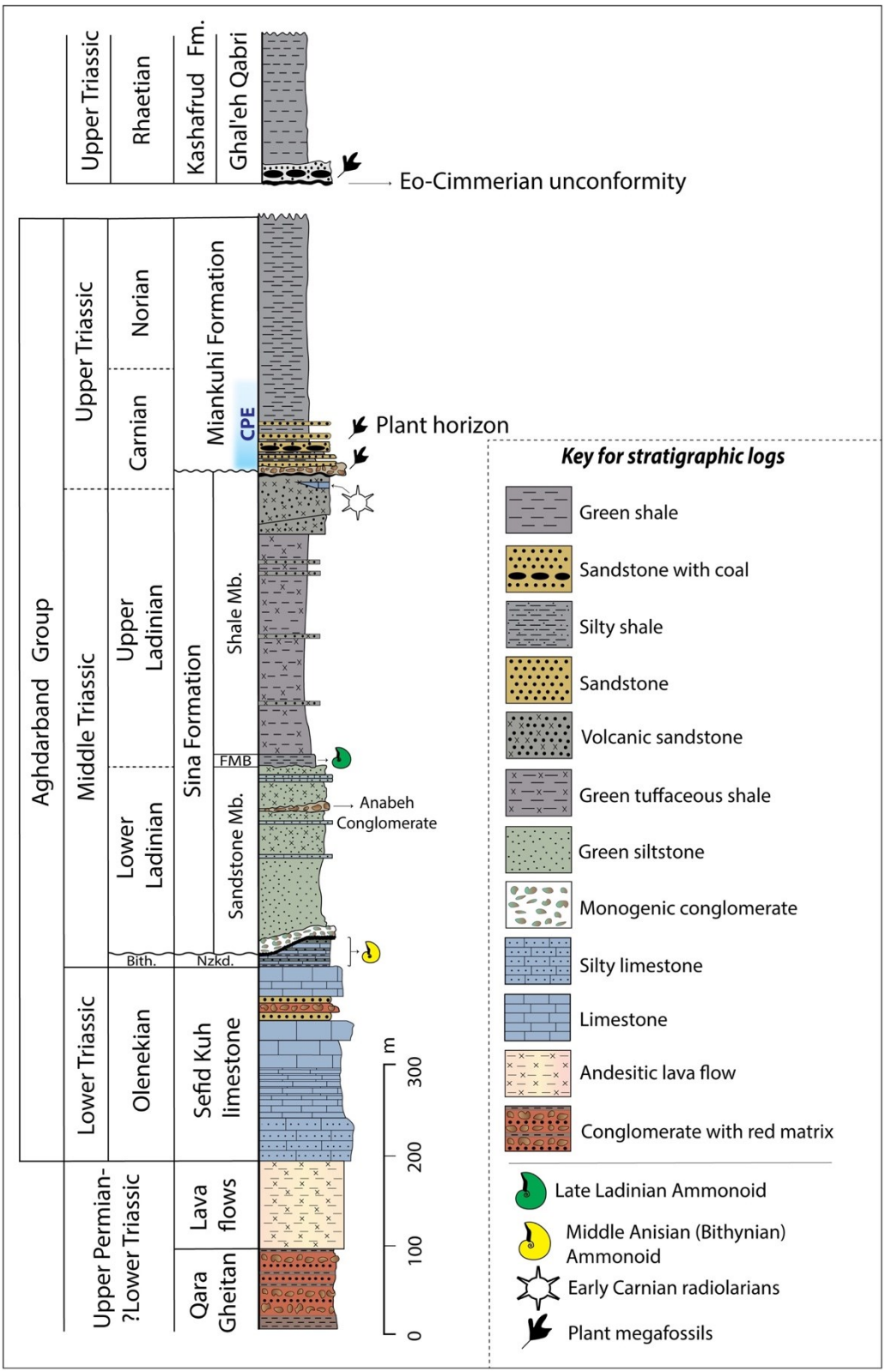

Figure 3: the General lithostratigraphic column of the Triassic sequence of the Aghdarband Basin (modified from Ruttner 1991, 1993; Zanchi et al. 2016; Balini et al. 2019).

is unconformably capped by a relatively thick sequence of volcaniclastic-turbiditic units, named Sina Formation, which is divided into two members (Ruttner 1991; Baud et al. 1991b): the Sandstone Member comprises conglomerates and green tuffaceous sandstones, and the overlying Shale Member contains red ammonoid-bearing marls (Faqir Marl Bed) and tuffaceous shales. A quick change to a coarsening upward succession, combined with the end of volcanic activity during early Carnian times, is recorded in the uppermost Sina Formation. The age of the Sina Formation spans from the early Ladinian to the early Carnian (Ruttner 1991; Krystyn & Tatzreiter 1991; Donofrio 1991). The Sina Formation is separated from the overlying Miankuhi Formation by an unconformity documented by continental sediments resting on the marine shale. The base of the Miankuhi Formation is characterized by conglomerates, cross-bedded sandstones, mudstones with minor sandstone lenses, sandstone layers, silty shales, and an up to one-meter thick coal layer documenting a wet alluvial plain environment. Upwards, the Miankuhi Formation is composed of brown-colored shales with some interbedded siltstone and/or fine-grained sandstone (Ruttner 1991, fig. 12b). These shales were thought to be completely barren of fossils (Ruttner 1984, 1991), but a poor assemblage of benthonic foraminifers has been found at the base of the monotonous shales (Oberhauser 1991), reflecting extremely adverse living conditions. Furthermore, the lowermost Miankuhi Formation yielded plant megafossils (Boersma & Van Konijnenburg-van Cittert 1991) and poorly preserved marine palynomorphs (Ghasemi-Nejad et al. 2008) considered of Norian age. The described dinoflagellate cyst assemblage (*Hebecysta*, *Heibergella*, *Rhaetogonyaulax, Sverdrupiella*) is, however, not restricted to the Norian and has also been reported from the Carnian (e.g., Bucefalo Palliani & Buratti 2006).

Zanchetta et al. (2013) proposed a U-Pb zircon age of 217.1 ± 1.8 Ma for a magmatic intrusion (Torbat-e-Jam Granite) into the deformed coal-bearing terrigenous successions of the Miankuhi Formation in the north of Torbat-e-Jam, suggesting a minimum age of middle Norian and probably a Carnian to middle Norian age for this formation. The results of our palynological investigations on the basal part of the Miankuhi Formation confirm a latest early Carnian (Julian 2) to late Carnian (Tuvalian) age for this part of the succession (see Age assignments for details). This composition of the terrestrial palynomorph assemblages and their age indications, along with the stratigraphical and sedimentological observations, change the position of the unconformable contact between the Miankuhi Fm. and the underlying Sina Fm. from its traditional place (Ruttner 1984, 1991; Baud et al. 1991b; Zanchi et al. 2016; Balini et al. 2019) immediately below the coal bed to the base of the conglomerate layers. Additionally, records of plant fossils below and above the coal bed provide adequate proof for the existence

of a continuous continental succession and a clear wet interval at the base of the Miankuhi Formation starting with the conglomerate layers. Nevertheless, the contact between the two formations is often tectonized due to active faulting and syn-sedimentary tectonic control over short distances in the area during the Triassic (Zanchi et al. 2016). Up-section, the Miankuhi Formation is separated from the basal black shales (Ghal'eh Qabri Shales) of the Kashaf-Rud Formation by an angular unconformity representing the Eo-Cimmerian orogeny (Ruttner 1991). A transgressive white sandstone layer at the base of the Ghal'eh Qabri Shales contains another coal level with Rhaetian plant remains (Boersma & Van Konijnenburg-van Cittert 1991).

Materials and methods

The studied macroflora is from a stratigraphic section called Allahverdi (35.98°N, 60.87°E; Fig. 2C). The plant fossil assemblage comprises 28 specimens, generally preserved as compressions or impressions. Sphenophytes are very delicate; their remains are mostly preserved as internal casts and impressions. The fossils are stored in the paleontological collection of Piero Leonardi Museum of Paleontology and Prehistory (MPL: Museo di Paleontologia e Preistoria Piero Leonardi) in Ferrara, Italy. Hand specimens were photographed with a Nikon 3200D digital camera and palynomorphs with a Leica 165C microscope equipped with Leica 170HD camera.

The macroflora of the Aghdarband area

At least four taxa were distinguished based on macromorphological analyses of the macroremains; they belong to the sphenophytes and to plant groups of unknown botanical affinity.

Division SPHENOPHYTA

Order **Equisetales** Dumortier, 1829

Family Equisetaceae Michaus, ex DC, 1804

Genus *Neocalamites* Halle, 1908

Neocalamites iranensis Kustatscher, Mazaheri-Johari et Roghi n. sp.

Pl. 1, figs. A–E; Pl. 2, figs. A–D

Etymology. Named after the country where the remains were discovered for the first time, Iran.

Holotype: MPL 9303 (Pl. I, fig. A), showing a stem fragment with at least two nodes from which arise a whorl of leaves, here designated.

Paratype: MPL 9304 (Pl. I, fig. B), showing the distribution and length of the leaves, here designated.

Additional material. Seven specimens, MPL 9305, 9306, 9307, 9308, 9309, 9310, 9311.

Type locality. Allahverdi outcrop, 35.98°N, 60.87°E, Aghdarband Basin, Iran.

Type horizon. Miakuhi Formation, Julian 2 to Tuvalian, Carnian, Late Triassic.

Repository. Museum of Paleontology and Prehistory Piero Leonardi, Ferrara, Italy.

Diagnosis. Stem articulated, with a smooth surface and distinct closely arranged vascular bundles. Lateral branches arising in whorls from non-swollen nodes. Leaves linear, entire-margined arranged in whorls of very numerous leaves; leaf bases consistent with leaf width, free up to the attachment at the nodal level. One to two internode vascular bundles per vallecular canal and leaf; no distinct midrib in leaves.

Description. The plant assemblage is dominated by leafless and leafy stems and putative branches, leaf whorls, and internal casts belonging to the sphenophyte genus *Neocalamites*. The stem fragments are up to 112 mm long and 55 mm wide in compression (MPL 9312–9313, Pl. I, figs. C–D), straight, with no evidence of tapering, and with densely disposed longitudinal grooves (corresponding to the vascular bundles) at a concentration of up to 18/cm (MPL 9313, Pl. I, fig. D). Some internodes are 35 mm long (MPL 9303, Pl. I, fig. A) but the maximum length of internodes exceeds 90 mm since in some fragments no complete internodes are observed (MPL 9313, Pl. I, fig. D). Smaller fragments have been interpreted as lateral branches (MPL 9314, Pl. I, fig. E). Nor lateral branches nor stems show any evidence of thickening at the nodal level. The internodes of the lateral branches are 3–5 mm wide and up to 15 mm long. When three-dimensionally preserved the stems appear secondarily compressed, with the vascular bundles of two successive internodes alternating (MPL 9315-9316, Pl. II, figs. A–B). Leaves are long, linear, straight, entire-margined, 0.8–1.4 mm wide, at least 85 mm long with no distinct vein (MPL 9304, Pl. I, fig. B; MPL 9317, Pl. II, fig. C). The leaf bases are consistent in width with the leaf width and free up to the attachment to the node (MPL 9303, Pl. I, fig. A, MPL 9318, Pl. II, fig. D). The leaves radiate evenly from the node; they are attached to the stem in a whorl. Information on leaf traces is missing since no cortex with leaf traces has been found. Each whorl consists of at least 40 leaves since in the most complete specimens more than 20 leaves were counted in up to half of a whorl (MPL 9318, Pl. II, fig. D). The number of vascular bundles corresponds to twice to three times the number of leaves in each whorl.

Comparisons with specimens from Iran. The stem fragments from the Rhaetian and Jurassic sediments of Iran assigned to *Neocalamites meriani* are in most cases very narrow, 3–15 mm in diameter (e.g., Schweitzer et al. 1997; Vaez-Javadi 2013a), although a maximum diameter of 35 mm is possible (e.g., Corsin & Stampfli 1977), and the number of leaves per whorl is very few (6–14 leaves; Tab. 1). This makes an assignment to *Neocalamites merianii* questionable (for discussion see below). *Neocalamites iranensis* resembles the specimens described by Kilpper (1964, pl. I, fig. 5) as *Neocalamites* sp. cf. *N. carrerei* (Zeiller) Halle in the distance between the vascular bundles (0.5 mm) but differs in the presence of distinct leaf bases and the higher number of leaves (more than 40 against ~25).

The specimens assigned by Kilpper (1964, pl. I, fig. 4) and Parvacideh & Vaez Javadi (2015, pl. I, fig. 2) putatively to *Neocalamites hoerensis* (Schimper) Halle are not well-enough preserved for a comparison with our specimens. The specimens described by Sadovnikov (1976, pl. I, figs. 5–7) as *Neocalamites hoerensis* from the Rhaetian–Middle Jurassic of Ziran (Iran) differs in having narrower stems and less vascular bundles (Tab. 1). The specimens are too badly preserved to permit a better comparison. *Neocalamites iranensis* n. sp. differs from *Neocalamites* sp. A sensu Boersma & Van Konijnenburg-van Cittert (1991) in having a narrower stem diameter (up to 12 mm wide), shorter internodes (5–13 mm), enlarged nodes, twelve leaves per whorl and the expanded base of the leaves in the latter (Tab. 1).

Neocalamites iranensis n. sp. resembles *Neocalamites ishpushtensis* Jacob et Shukla from the Jurassic of northern Afghanistan in the linear shape and the free attachment of the leaves at nodal level (Tab. 1). They differ, however, because of the narrower stems (5 mm), the swollen nodes, the lower number of leaves (6) per node, and the shorter but wider leaves (2 x 50–60 mm). Our specimens resemble *Neocalamites ishpushtensis* as described by Schweitzer et al. (1997) from the lower Middle Jurassic of Iran and Afghanistan in the non-thickened nodes and the long leaves that are not basally fused. However, the specimens from Schweitzer et al. (1997) differ from our specimens in the lower number of leaves, the smaller width and length of the stems, the costate outer surface, and the slightly lanceolate leaf shape with a pointed apex and a restricted basis (Tab. 1). *Neocalamites iranensis* n. sp. can be distinguished from the specimens assigned by Saadat-Nejad et al. (2010) to *Neocalamites ishpushtensis* by the much narrower stem (4 mm against up to 55 mm), and the shorter length (maximum 25 mm against minimum 85 mm) and narrower width (0.5–1 mm against 0.8–1.4 mm) of the leaves. The specimen figured by Khalilizadeh et al. (2020; fig. 10E, 12E) as *Neocalamites ishpushtensis*

		stem width (mm)	internode length (mm)	cortex	costae	nodes	vascular bundles	leaves / whorl	leaf shape	leaf length (mm)	leaf width (mm)	leaf bases	leaf apex	leaf traces	veins	annotations
This paper	*Neocalamites iranensis*	up to 55 mm wide	35–90	smooth	absent	no thickening	18/cm	at least 40	straight, linear	>85	0.4–1.4	free, consistent with leaf width	unknown	unknown	unknown	
Kilpper (1964)	*Neocalamites* cf. *carrerei*	20					20/cm	25						1 mm diameter		
Kilpper (1964)	*Neocalamites hoerensis*	15	>20				16/cm									
Fakhr (1977)	*Neocalamites hoerensis*	25–30	up to 90				14–16/cm									
Parvacideh & Vaez Javadi (2015)	*Neocalamites* cf. *hoerensis*	14.7–15.7	24													
Sadovnikov (1976)	*Neocalamites hoerensis*		>50				10–20/cm		narrow, thin						indistinct	
Sadovnikov (1986)	*Neocalamites hoerensis*	<50	<110			expanded in branches	10–25/cm	<50	linear	120	0.5–2.5 mm	free to the bases		rounded–elongated	single	
Vaez-Javadi (2016)	*?Neocalamites hoerensis*	9					20–21/cm									just stem with vascular bundles, not well enough to describe the species
Corsin & Stampfli (1977)	*Neocalamites merianii*	10–35	18–26		pronounced	slightly swollen				>35	1.5–2			2 mm		
Vaez-Javadi (2013)	*Neocalamites merianii*	20–25	19		distinct, 8–10 mm wide			6	linear, parallel margins	>20	1–1.5					
Vaez-Javadi (2013)	*Neocalamites* cf. *merianii*	2–2.5	19		3–4 ribs			6	linear, parallel margins	>20	1–1.5					
Vaez-Javadi (2012a)	*Neocalamites* cf. *merianii*	2–2.5	19		3–4 ribs				linear, parallel margins	>20	1–1.5					
Vaez-Javadi (2016)	*Neocalamites* cf. *merianii*	4						10	linear, parallel margins	>15						
Schweitzer et al. (1997)	*Neocalamites* cf. *merianii*	2–4	20	n.a.	pronounced, at 0.6 mm distance	swollen		12–14	straight, parallel margins, arise perpendicularly		1	broad			indistinct	vascular bundles are probably described as costae
Jacob & Shukla (1955)	*Neocalamites ishpushtensis*	5	20	n.a.	pronounced	swollen		6?	linear	50–60	2	free			clear midrib	vascular bundles are probably described as costae
Schweitzer et al. (1997)	*Neocalamites ishpushtensis*	3–21	20–50	costate		no thickening	distinct, straight	>25	slightly lanceolate, maximum width at the middle part	50–120	2–5	free to the basis, restricted in width	acute	circular, 0.5–1 mm diameter	distinct midrib	vascular bundles are probably described as costae
Saadat-Nejad et al. (2010)	*Neocalamites ishpushtensis*	4	25		present		at 0.5 mm distance		linear, narrow	>25	0.5–1	free, base slightly restricted				
Khalilizade et al. (2020)	*Neocalamites ishpushtensis*					slightly swollen										
Corsin & Stampfli (1977)	*Neocalamites* sp.	40–50														
Boersma & Van Konijnenburg-van Cittert (1991)	*Neocalamites* sp. A	12	5–13		scarcely ribbed	slightly enlarged		12		>46	2	expanded (up to 3 mm)				

Table 1: Comparison of the new species *Neocalamites iranensis* n. sp. with the other *Neocalamites* species from the Triassic and Jurassic of Iran and Afghanistan.

differs in the distinct thickening of the nodes; the missing of a description does not enable us to make a more detailed comparison. It has, however, to be noted that what Jacob et al. (1955) and Schweitzer et al. (1997) described as ridges and furrows correspond rather to the vascular bundles, and thus to characters of the inner structure of the stem, than to the costae of the outer surface (Tab. 1).

Comparisons with other species of *Neocalamites*. *Neocalamites iranensis* n. sp. differs from the type species *Neocalamites lehmannianus* (Goeppert) Weber from the Rhaetian–Lower Jurassic of Germany in the single or opposite attachment of the branches, the narrower but longer internodes, the swollen nodes, the lower number (12–48) of leaves per whorl, the broader leaves (1–2.5 mm) and the distinct midrib of the latter. The most closely resembling species is *Neocalamites horridus* Zan et al. from the Upper Triassic of China because of its abundant, linear leaves with a free base and the only slightly swollen nodes but it differs because of the unbranched stems, the striations and prickles on the outer surface and the distinct midrib on the leaves. It resembles also *Neocalamites carrerei* (Zeiller) Halle from the Rhaetian of Tonkin (North Vietnam), but well-known also from the Ladinian–Carnian of China (e.g., Sze, 1933, 1949, 1956; Xingxue, 1995), because of the linear to filiform leaves with a free attachment to the node and a similar frequency of vascular bundles. The type material differs, however, because of the lower vascular bundles vs. leaf scars ratio (1–2 times against 2–3 times in *Neocalamites iranensis* n. sp.), and the distinctly higher number (80–100 against >40 in our specimens) and wider (1–1.5 against 0.4–1.4 mm) leaves each whorl. Moreover, the leaves have a distinct vein in the Rhaetian type species. *Neocalamites iranensis* n. sp. differs from most *Neocalamites* species in missing a swelling of the nodes. One of the few exceptions that does not show swellings either is *Neocalamites virginensis* (Fontaine) Berry from the Triassic of USA but the latter has much narrower (5 mm) and shorter (15–20 mm) internodes, a lower number of leaves per node (<24) and wider leaves (1–2.5 mm) with a broad midvein (3–4 mm). Another main character of *Neocalamites iranensis* n. sp. is the indistinct midrib, which it has in common with *Neocalamites minutus* Gee et al. from the Upper Jurassic of Switzerland and

Plate I

Plate I: *Neocalamites iranensis* n. sp. A. Stem fragment with at least two nodes from which arise a whorl of leaves, holotype (MPL 9303). B. Distribution and length of the leaves of a half whorl, paratype (MPL 9304). C. Stem fragments with impressions of the vascular bundles (MPL 9312). D. Largest stem fragment with impressions of the vascular bundles (MPL 9313). E. Small lateral branch fragments with leaves (MPL 9314). Scale bars: A–E= 2 cm.

Neocalamites suberosus (Artabe et Zamuner) Bomfleur et al. from the Middle Triassic of Argentina. It differs, however, in the slightly swollen nodes, the narrower and shorter internodes, and the higher number of narrower and shorter leaves. The new species differs from *Neocalamites suberosus* in having wide and shallow grooves on the external surface resulting in a costate external structure of the stem, and the shorter (> 30 mm) but broader (2–4 mm) leaves. The only other Triassic species, *Neocalamites merianii* from the Middle–lower Upper Triassic of Europe, resembles the new species in the arrangement in whorls of the branches

and the general dimensions of the internodes, although the lateral branches are much thicker in the specimens from Germany. The two species differ, however, because the outer surface can be costate and the node is generally swollen in *Neocalamites merianii*. Moreover, in the latter species, the leaves are present only on the lateral shoots (see Pott et al. 2008), whereas both the primary and lateral shoots are covered by leaves in the new species, and the leaves are broader and have a distinct midrib in *Neocalamites merianii*.

Genus *Radicites* Potonié, 1893

***Radicites* sp.**

Pl. 2, fig. E

Material. Five specimens

Description. The main root axis is up to 50 mm long and 4 mm wide (MPL 9319, Pl. 2, fig. E). The secondary roots of 11–20 mm length and 1 mm width arise at an angle of 50–55°. The secondary roots do not show any rootlets or ramifications.

Discussion. *Radicites* is a genus used generally for compound root remains of unknown sphenophyte affinity with typically a mm thick main root and several secondary roots. Heer (1877, pl. 75, fig. 3; pl. 26, fig. 3) identified similar structures as roots of *Equisetites arenaceus* (Jaeger) Schenk from the Carnian of Neue Welt (Switzerland) because of their frequent association with the latter. Linck (1943) described a stratigraphic section with several in situ "Wurzelböden" [root horizons] in the Schilfsandstein of Mühlbach (Germany), Kräusel & Leschik (1959, pl. 10, text-fig. 2; pl. 5, fig. 37) even described roots and stems arising from a rhizome. Kelber (1990, pl. 56, fig. 96; 1999, pl. 364, fig. 9) and Kelber & Hansch (1995, pl. 131, figs. 281–2) described horizons with several generations of *Equisetites* roots in the Erfurt Formation (Ladinian) of Germany. Sometimes the younger generation penetrates the "fossils" of the older, sediment-covered organic remains. These structures were interpreted as various successive root horizons representing several generations evolving in an ever-changing deltaic area of the Lower Keuper. Bock (1969, pl. 72–74) described *Anabacaulus duplicatus* Emmons as root systems of equisetaleans associated with, but not anatomically connected to, *Neocalamites delewarensis* Bock.

Plate II

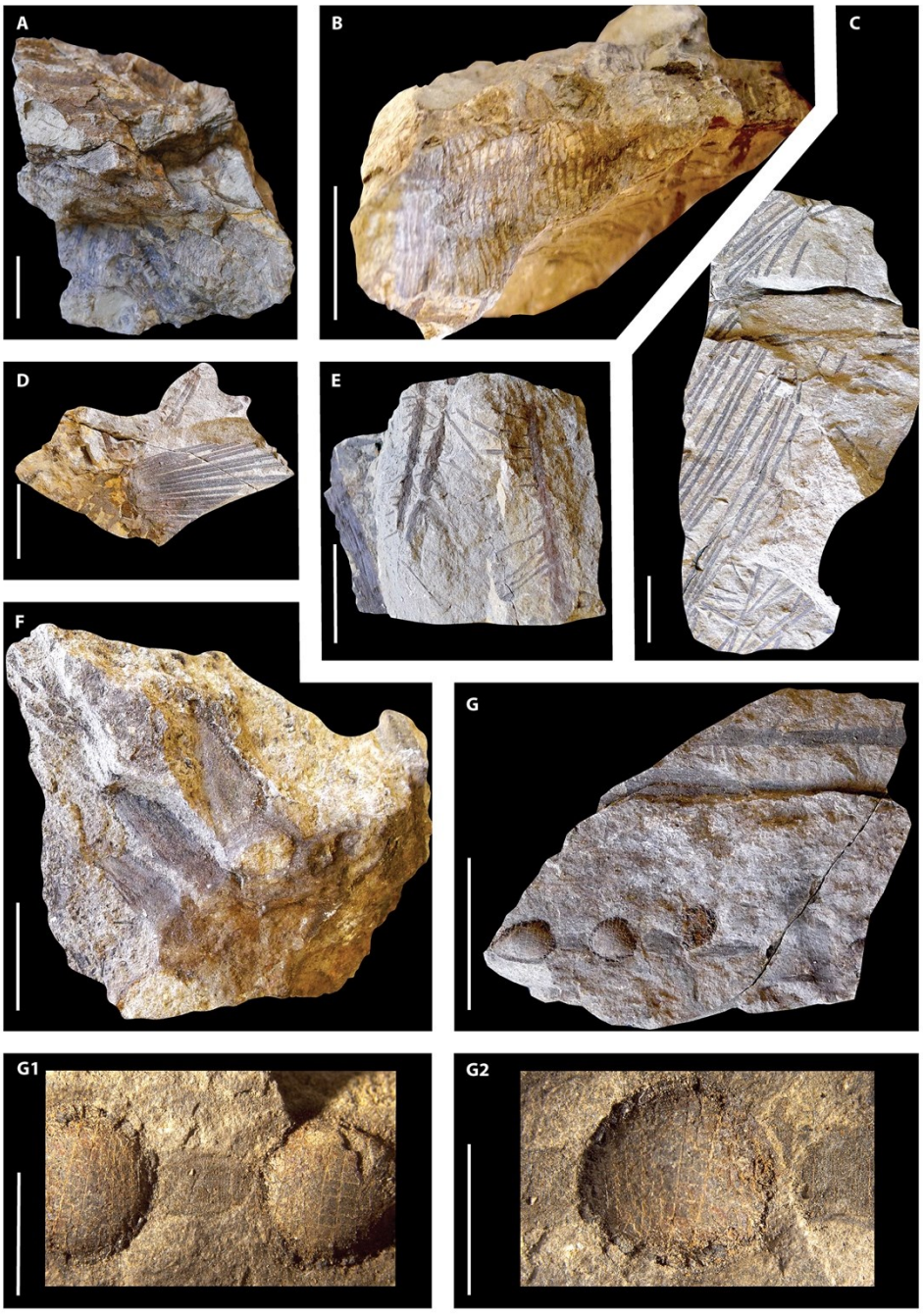

Plate II: *Neocalamites iranensis* n. sp. A. Three-dimensional preservation of a compressed stem (MPL 9315). B. Three-dimensional preservation of a compressed stem showing the vascular bundles at the nodal level (MPL 9316). C. Parallel arising linear leaves (MPL 9317). D. Whorl of leaves arising at nodal level (MPL 9318). E. *Radicites* sp., compound roots (MPL 9319). F. Triangular structures of unknown botanical affinity (MPL 9320). G. Three roundish structures in various sections (MPL 9321). G1–G2: Details of the structures showing the desiccation structures of the organic material. Scale bars: A–G= 2 cm, G1–G2= 0.5 cm.

The simple structures of the roots, as well as a comparison with remains from the Triassic of Europe (e.g., Kelber & Hansch 1995; Kustatscher & Van Konijnenburg-van Cittert 2008) suggest a sphenophyte affinity. Since the only sphenophyte so far described in these fossiliferous horizons, is *Neocalamites iranensis* n. sp., an affinity with this species is most likely. Although the roots do not show holes that perforate older fossils, an autochthonous origin of the remains is postulated since the root fragments are distributed three-dimensionally and at various levels within the rock slabs (e.g. MPL 9319, Pl. 2, fig. E).

The genus *Radicites* has been reported repeatedly from Rhaetian and Jurassic sediments of Iran and Afghanistan (e.g., Sadovnikov 1976; Schweitzer et al. 1997, 2009; Vaez-Javadi 2013a). The typical longitudinal striate structure of *Radicites sulcatus* Sadovnikov has not been observed in our specimens. Since the fragments are small, we prefer not to assign them to any species.

Additional material

Pl. II, fig. F–G

Two specimens are not assignable to any species but are here figured since they could represent the only non–sphenophyte remains in the assemblage. Specimen one (MPL 9320, Pl. II, fig. F) is 50 mm long and 53 mm wide. It is composed of three elongated structures of 38–42 mm length and 9–11 mm width; the basal part of each element is enlarged and has a diameter of 12–13 mm. At least one of the elements seems subdivided in longitudinal striae and could show also a transversal line. The specimen seems composed of three shoots or axes that are basally connected or fused. These structures appear hollow. The possible longitudinal and transversal interruptions could suggest it to belong to some sphenophytes. It cannot be excluded that it could be a part of a sphenophyte axis with lateral shoots arising from a nodal element. In this case, it could be a part of a sphenophyte axis with lateral shoots arising from a nodal element. In this case, it could perhaps belong to *Neocalamites iranensis* and represent the proof that this species was articulated with a whorl of lateral axes arising at nodal level. Since the fragment is not well-preserved, we prefer to keep it for now distinguished from the *Neocalamites iranensis*. Another rock slab (MPL 9321, Pl. 2, figs. G1–2) contains three elements with an elliptical (9.3 x 6.3 mm) to roundish section (6–7 mm) with a 0.8–1 mm thick coaly layer characterized by cracks with a quadrangular, blocky pattern filled by mineral layers. The latter structure can occur during the conservation of thick coaly layers, especially if the organic material is transformed in vitrinite. These structures could represent remains of seeds, considering the general shape and dimension; a clear integument and seed structure, is however, missing.

Similar structures were also observed for root nodules, such as for example in *Equisetites burchardtii* Schimper from the Wealden near Bückeburg, northern Germany (Schenk, 1871), where they occur in large masses in palaeosols associated with *Equisetites* roots. Putative root nodules assigned to *Equisetites arenaceous* of the Middle–Late Triassic of Germany are, however, generally bigger in dimension, up to 10 cm in diameter (EK, pers. observ.). In case these structures are isolated root nodules, this would support the presence of the monotypic sphenophyte stand. In case these would be seeds, they could belong to plants growing closely nearby or could have been transported over some distance to the depositional environment, and belong, thus, to allochthonous elements.

Age assignment

Ruttner (1991) described coal seams and "hanging sandstone" with well-preserved plant remains. A distinct plant assemblage was described from the outcrops 76/94, 76/95, and 75/19, including *Neocalamites* sp. A sensu Boersma & Van Konijnenburg-van Cittert (1991), *Sphenobaiera* sp. A, *Taeniopteris* sp. A, *Podozamites paucinervis* Boersma et Van Konijnenburg-van Cittert, *Podozamites* sp., *Carpolithes* cf. *cinctus* Nathorst, and undetermined seed scales. The plant assemblage was interpreted as putatively Norian in age (Boersma & Van Konijnenburg-van Cittert 1991). Balini et al. (2019) proposed a general Late Triassic age for the Miakuhi Formation based on the stratigraphical position of the unit which overlies unconformably the Sina Formation.

Palynological analyses were carried out for the first time both in the Sina and Miankuhi formations and the better-preserved specimens are presented on Plate III. The terrestrial sporomorph assemblage of the Upper Sina Formation (Shale Member) is dominated by cycads (*Cycadopites* sp.; Pl. III, fig. 8), conifers (*Triadispora* sp., *Lunatisporites* sp., *Araucariacites* sp.) as well as sporadic ferns (*Concavisporites* sp., *Dictyophyllidites mortonii*, *Trachysporites* sp., *Todisporites minor*, *Deltoidospora* sp.; Pl. III, figs. 1–3, 7) and sphenophytes (*Calamospora* sp.). The sporomorph assemblage of the lowermost part of the Miankuhi Formation is characterized by the co-occurence of *Aulisporites astigmosus* (Pl. III, figs. 5–6), *Spiritisporites* sp. (Pl. III, fig. 4), *Equisetosporites* sp. (Pl. III, fig. 9), *Chasmatosporites* sp., and *Annulispora* sp. which allows us to define a latest early Carnian to late Carnian age, corresponding to the Carnian Pluvial Episode, for the lower part of the formation containing the coal levels and thus for both the new outcrop as well as for the outcrops 76/94, 76/95, and 75/19 of Boersma & Van Konijnenburg-van Cittert (1991).

Plate III

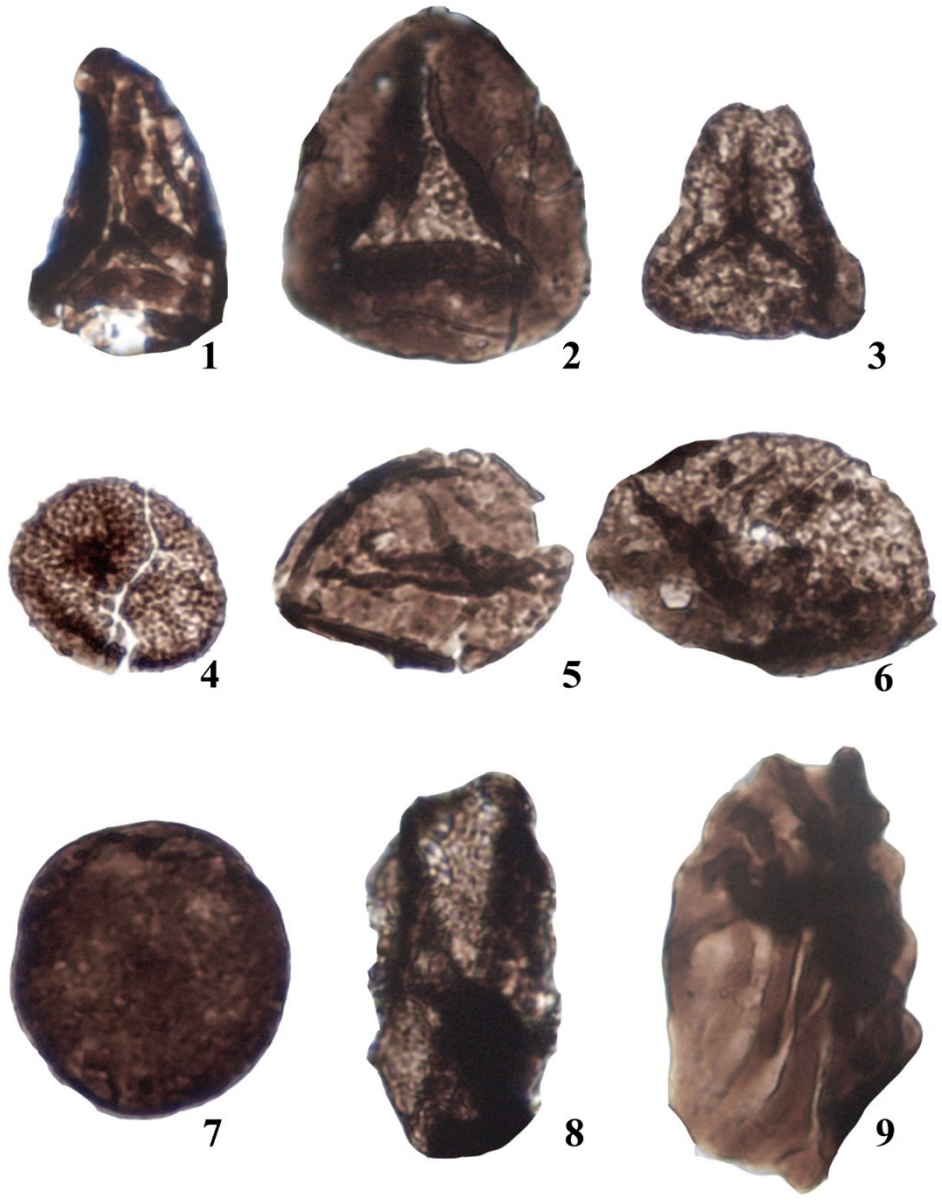

Plate III: Sporomorphs of the plant yielding horizon. Each taxon name is followed by the section name, sample number, slide number, length of specimens, and stage coordinates for a Leica DM750 light microscope. **1)** *Concavisporites* sp.; Kal-e-Bast section; KB 4 I; slide I; length 36.8 µm; K16/1; **2)** *Dictyophyllidites mortonii* (de Jersey) Playford et Dettman, 1965; Kal-e-Bast section; KB 4 I; slide I; length 43.2 µm; H52; **3)** *Trachysporites* sp.; Kal-e-Bast section; KB 4 I; slide I; length 30.4 µm; F25/4; **4)** *Spiritisporites* sp.; Kal-e-Bast section; KB 2; slide I; length 25.2 µm; M71/1; **5-6)** *Aulisporites astigmosus* (Leschik) Klaus, 1960; Kal-e-Bast section; KB 4 I; slide I; N. 5: length 35 µm; N. 6: length 43.2 µm; N.5: W65, N.6: R40; **7)** *Todisporites minor* Couper, 1958; Kal-e-Bast section; KB 4 II; slide II; length 32 µm; Q4; **8)** *Cycadopites* sp.; Kal-e-Bast section; KB 4 I; slide II; length 49.6 µm; O54; **9)** *Equisetosporites* sp.; Kal-e-Jom'eh section; MKJ 13; slide III; length 54.4 µm; G56/2.

Discussion

Comparison between micro- and macrofloras of the Miankuhi Formation

Although the plant fossil assemblage described in this study represents a monotypic stand of sphenophytes (*Neocalamites iranensis* n. sp.), the surrounding coeval plant fossil localities 76/94, 76/95, and 75/19 of Boersma & Van Konijnenburg-van Cittert (1991), yielded a wider range of plant remains, including sphenophytes, ferns, and a variety of gymnosperms. Additional information on the regional flora, present during this moment, is given by the sporomorphs. Comparing the composition of the terrestrial sporomorphs with that of the macroplant assemblage from the same layer in the Miankuhi Formation, it becomes evident that for most of the identified spores and pollen there is a good relationship. In the microflora the genera *Aulisporites*, *Spiritisporites* and *Chasmatosporites* have been produced by Bennettitales, Cycadales or Ginkgoales (Kräusel and Schaarschmidt 1966; Balme 1995; Paterson et al. 2016), which are also known from the macroplant remains due to the presence of the genera *Pterophyllum* (Bennettitales), *Taeniopteris* (Bennettitales or Cycadales), and *Sphenobaiera* (Ginkgoales). The conifer pollens are of unknown botanical affinity; among the macroremains the shoots of *Podozamites* are the only representatives of this plant group. The sphenophyte, monotypic in our assemblages but also present in the surrounding outcrops by *Neocalamites*, correspond to *Calamospora* in the microflora.

There are, however, also elements among the sporomorphs, belonging to taxa that are not found so far among the macroremains. To these belong *Annulispora*, a typical bryophyte spore (e.g., Koppelhus 1991; Paterson et al. 2016). Their missing in the macrofossil record is, however, not very surprising considering the low preservation potential of mosses in the fossil record (e.g., Taylor et al. 2009; Heinrichs et al. 2018). Conifers and seed ferns must have been more abundant and diverse in the flora, considering the presence of the genera *Triadispora*, *Lunatisporites* and *Araucariacites* among the palynomorphs. Also, *Equisetosporites* belongs putatively to a group of plants not represented in the macroplant assemblage, the gnetophytes, ephedrales, or angiospermids (e.g., Pocock & Vasanthy 1988; Osborn et al. 1993; Lindström et al. 2016). The typical spore genera, *Todisporites*, and other baculate/apiculate forms could be linked to the macroremains by *Cladophlebis*. The recorded microflora, therefore, represents a much more luscious vegetation during the deposition time of the fossiliferous horizon of the Miankuhi Formation than shown so far by the macrofossil record only, because it reflects the regional flora.

Paleoenvironmental considerations

The occurrence of sphenophytes is connected with humid habitats in the vicinity of rivers and lakes (Batten 1974, Abbink et al. 2004). Many of the arborescent Carboniferous taxa (*Calamites*) were important components of the peat-forming vegetation; they colonized, however, also riverbanks or disturbed areas (DiMichele & Hook 1992). Extant *Equisetum* plants colonize a broad spectrum of habitats, ranging from humid to dry, although most taxa prefer humid habitats or areas in which sufficient groundwater is available. It is, therefore, reasonable to conclude that Mesozoic sphenophytes probably grew in the more humid habitats. The fact that most sphenophytes are clonal permits them to form more or less extensive (monotypic) stands along the margins of water bodies, where clonal plants are often especially successful. Rhizomes are effective in sustaining the plants during periods of flooding, erosion, or sediment accumulation since the resources stored in the rhizomatous system facilitate aerial shoot regeneration if the aerial parts of the plant are destroyed (Pott et al. 2008). Vegetative reproduction by means of fragmentation, as suggested for example for the Triassic sphenophyte *Equisetites arenaceus*, may have been advantageous under these conditions (Pott et al. 2008). The branch fragments may have been transported by water, and ultimately started new clones in other areas.

Zan et al. (2012) described *Neocalamites horridus* as growing in large, closely packed stands consisting of completely monopodial aerial stems, which would have provided an interlocking support similar to that of modern-day stands of large *Equisetum* species or bamboo. Similar considerations can be made also on *Neocalamites iranensis* n. sp. considering their monotypical occurrence in our fossiliferous levels.

It is believed that *Neocalamites*-type plants prefer moist habitats but could stand slightly drier conditions than *Equisetites*-type of plants (Barbacka 2009, 2011), although *Neocalamites* remains were also found in sediments deposited under swamp conditions. This makes them swamp dwellers during the Jurassic (Barbacka et al. 2015, 2016; Popa, pers. comm. 2021). The presence of a monotypic stand of (autochtonous) sphenophytes of the *Neocalamites* type supports the hypothesis that these plants grew in a rather humid environment and could have been among the primary producers of the coal layers at the base of the Miankuhi Formation, similarly to their Carboniferous relatives.

Comparisons with coeval floras

Floras of the Carnian Pluvial Episode (CPE) are generally characterized by diverse plant assemblages that reflect floras growing under generally humid conditions and in swampy

fluvial to deltaic depositional environments (e.g., Dobruskina 1994; Kelber & Hansch 1995; Pott et al. 2008; Kustatscher et al. 2018). The Lunz flora, the most famous European flora of the CPE, has been deposited in a swampy, paralic environment, which gave origin to thick coal layers. It is characterized by a rich and very diverse flora with plant fossils referable to a great diversity of species belonging to numerous plant groups. Ferns and cycads/bennettitaleans are very abundant, whereas sphenophytes, conifers, and putative ginkgophytes are less common (e.g., Dobruskina 1994, 1998; Pott et al. 2008, Pott & Krings 2010; Kustatscher et al. 2018 and references therein). The coeval Schilfsandstein flora of Germany is dominated by sphenophytes and ferns; conifers and bennettitaleans are locally rare to common. The stratigraphic sequence hosting this flora includes multiple paleosol layers with consecutive generations of in situ sphenophyte (*Equisetites*) shoots and rhizomes (Kelber & Hansch 1995), which grew in a fluvio-deltaic setting (Franz et al. 2019; Kustatscher et al. 2018). These monotonous associations of ferns and sphenophytes as well as the occurrences of in situ sphenophytes, together with their sporomorph assemblages, suggest that these floras grew under humid conditions (e.g., Kelber & Hansch 1995; Kustatscher et al. 2018).

The base of the Stockton Formation in North Carolina and Pennsylvania (USA) could also correspond to the CPE. The plant assemblages of this formation are not associated with coal deposits (e.g., Kustatscher et al. 2018). They are diverse and abundant in conifers and cycads/bennettitaleans, whereas ferns and sphenophytes are rare (e.g., Wanner & Fontaine, in Ward, 1900; Bock 1969; Axsmith et al. 1995 and references therein). The paleogeographic position (about 25–30°N) of the European and Northern America floras is, however, much closer to the Equator than the plant assemblage from the Aghdarband Basin and the inner-continental setting of the America floras could account for the missing coal layers.

Paleolatitudinally closer are the Carnian floras of the De Geerdalen Formation in the Scandinavia-Greenland region. The CPE successions are represented by non-marine delta plain deposits (Klausen & Mørk 2014) yielding a rich flora dominated by ferns, bennettitaleans, and seed ferns, whereas sphenophytes and ginkgophytes are also well represented (e.g., Pott 2012; Kustatscher et al. 2018). The Protopivskaya Formation of the Donets Basin and the Kalachevskaya Formation of the Middle and Eastern Asian sub-provinces (north and central Asia; e.g., Kustatscher et al. 2018 and references therein) are dominated by seed ferns (mostly Peltaspermales; up to 30%) and *Glossophyllum*-type leaves (Dobruskina 1994). Marattiales are the dominant ferns in the Urals, Caucasus, and Central Asia, whereas the Dipteridaceae spread at lower latitudes of the East Asian Subprovince (e.g., Sad-Gorod Formation of the Primorye; Volynets & Shorokhova 2007). Sphenophytes are numerous but taxonomically not diverse and

occupy a subordinate position in relation to other plant groups in these subprovinces (Kustatscher et al. 2018). They are, however, a significant component of several assemblages in the northern part of the Chelyabinsk Basin and the Southern Urals (Kirichkova 1969) and in the Bukobay Formation of the Ilek River Basin (Brick 1952), where the plants grew in rather humid environments of alluvial plains, delta plains and shallow lacustrine environments during the Carnian (Kochnev 1934; Brick 1936; Sixtel 1961, 1962; Dobruskina 1995). The CPE-deposited layers of the Madygen flora yielded both seed ferns but also various spore-producing plants including lycophytes and bryophytes, typical for humid environments (e.g., Dobruskina 1995; Moisan et al. 2011, 2012; Moisan & Voigt 2013).

The Carnian deposits of the Southern East Asia Subprovince (Kustatscher et al. 2018) include plant assemblages from the Daqiaodi Formation of the Yongren, Yunnan, and Yunnan-Sichuan border area, the Jiuligang Formation of Nanzhang, Hubei, and the Jiapeila Formation of Tibet (Zhou & Zhou 1983; Fansong 1983, 1990). The flora is abundant in sphenophytes, ferns, seed ferns, and cycads/bennettitaleans and resembles the Schilfsandstein flora of Western Europe (Zhou & Zhou 1983; Kustatscher et al. 2018). The Indonesian Carnian flora is dominated by sphenophytes, ferns, and cycads/bennettitaleans (Kon'no 1972; Vakhrameev et al. 1978). Carnian floras from Japan; i.e., the Yamaguti plant assemblages from the Momonoki and Aso formations of the Mine Group (Ôishi 1932a, 1932b, 1940; Ôishi & Takahashi 1936; Takahashi 1951) are abundant in ferns, conifers, and cycads/bennettitaleans, whereas sphenophytes are rare (Volynets & Shorokhova 2007).

This shows how diverse the plant fossil assemblages are generally during the Carnian and especially during the Carnian Pluvial Episode. Moreover, local conditions in Germany (e.g., Kelber & Hansch 1995) and Russia (e.g., Brick 1952) during the CPE gave origin to similar monotypic stands of sphenophytes, mostly in fluvio-deltaic settings.

Conclusions

The Carnian Pluvial Episode was a time of global environmental changes. The extent of the biological turnover in marine and terrestrial ecosystems associated with these events is, however, still not well understood, although a substantial reduction in genus and species richness in many marine groups with the disappearance of up to 33% of all marine genera is proposed (Dal Corso et al. 2020). Within the terrestrial ecosystems, a major turnover is observed during the CPE, associated with a major radiation and diversification event (Bernardi et al. 2018; Dal Corso et al. 2020). Plant fossils evidence a shift of plant associations towards elements more adapted to humid conditions at different latitudes (e.g., Roghi et al. 2010; Preto

et al. 2010; Mueller et al. 2016; Kustatscher et al. 2018), and extensive resin production (Gianolla et al. 1998; Roghi et al. 2006; Schmidt et al. 2012; Seyfullah et al. 2018). The onset of the CPE is very well constrained in many stratigraphic sections from Tethys domain to Panthalassa or, inside Pangea, from western Eurasia to South America (e.g., Dal Corso et al. 2012, 2015, 2018; Barany et al. 2018; Jin et al. 2020; Fu et al. 2020; Mancuso et al. 2020). There are, however, several areas where this event has not been documented as clearly as along the southern margin of Eurasia. The latest early Carnian to late Carnian age assigned to the basal part of the Miankuhi Formation using palynological associations allows to date the fluvial sediments, the coal layer and the plant levels to the CPE. This is the first record of Carnian plant fossils from the NE Iran, and also the first record for the Carnian Pluvial Episode in the Turan Plate, Kopeh-Dagh Range (NE Iran). The monotypic stand of *Neocalamites iranensis* n. sp. gives a glimpse into a peculiar microenvironment established under local conditions, during a period characterized by a high abundance in precipitation. The plant fossils from the surrounding areas (Boersma & Van Konijnenburg–van Cittert 1991) and the palynological record from the Miankuhi Formation give some ideas of the composition of the regional flora, including other plant groups, such as bryophytes, lycophytes, ferns, cycads, bennettitaleans, ginkgoaleans, and conifers, typical for the Carnian Pluvial Episode.

Acknowledgments

We are very grateful to Natalia Zavialova (Moscow) for her help with the Russian species of *Neocalamites* (translations and identification of the various characters). Mihai Popa (Bucharest, Romania), Zhuo Feng (Kunming, China) and Elke Schneebeli-Hermann (Zürich, Switzerland) helped with the literature research. Thanks also to Giovanni Muttoni (Milano) for the discussion about the paleolatitude position of the Turan plate during the Triassic and Angela Bertinelli (Perugia) for information about radiolarians. We also gratefully acknowledge the cooperation of colleagues from the Geological Survey of Iran, Mashhad branch, particularly Jafar Taheri, Abradat Maafi, and Maryam Hosseiniyoon for assistance in fieldwork. Mine Engineer Hajiyan (from the company of Maadan Khavar) is also acknowledged for providing hospitality at the Aghdarband Coal mine during our fieldwork. Mihai Popa (Budapest) and an anonymous reviewer are thanked for their very helpful and constructive remarks. Sadly, we recently learned of the untimely and unexpected death of our dear colleague and co-author Ebrahim Ghasemi-Nejad. The painful news left us dismayed and saddened, with him we lost a talented scientist, a great friend who introduced us to the outstanding geology of Iran. We will miss him, as will his students, his colleagues and above all his family.

References

Abbink O.A., Van Konijnenburg-van Cittert J.H.A. & Visscher H. (2004) - A sporomorph ecogroup model for the Northwest European Jurassic - Lower Cretaceous: Concepts and framework. *Geologie en Mijnbouw/Netherlands Journal of Geosciences*, 83(1): 17–38.

Afshar-Harb A. (1979) **-** The Stratigraphy, Tectonics and Petroleum Geology of the Koppeh-Dagh Region, Northern Iran**.** Unpublished Ph.D. thesis. Imperial College of Science and Technology, London (1979), 316 pp.

Afshar-Harb A. (1994) - Geology of Kopet Dagh. *Treatise on the Geology of Iran*, 11: 1–275.

Alavi M., Vaziri H., Seyed-Emami K. & Lasemi Y. (1997) - The Triassic and associated rocks of the Nakhlak and Aghdarband areas in central and northeastern Iran as remnants of the southern Turanian active continental margin. *Bulletin of the Geological Society of America*, 109(12): 1563–1575.

Allen M., Jackson J. & Walker R. (2004) - Late Cenozoic reorganization of the Arabia-Eurasia collision and the comparison of short-term and long-term deformation rates. *Tectonics*, 23(2).

Allen M.B., Kheirkhah M., Emami M.H. & Jones S.J. (2011) - Right-lateral shear across Iran and kinematic change in the Arabia-Eurasia collision zone. *Geophysical Journal International*, 184(2): 555–574.

Angiolini L., Gaetani M., Muttoni G., Stephenson M.H. & Zanchi A. (2007) - Tethyan oceanic currents and climate gradients 300 m.y. ago. *Geology*, 35(12): 1071–1074.

Axsmith B.J., Taylor T.N., Delevoryas T. & Hope R.C. (1995) - A new species of *Eoginkgoites* from the Upper Triassic of North Carolina, USA. *Review of Palaeobotany and Palynology*, 85(3-4): 189–198.

Balini M., Nicora A., Berra F., Garzanti E., Levera M., Mattei M., Muttoni G., Zanchi A., Bollati I., Larghi C., Zanchetta S., Salamati R. & Mossavvari F. (2009) - The Triassic stratigraphic succession of Nakhlak (central Iran) a record from an active margin. *Geological Society Special Publication*, 312(1): 287–321.

Balini M., Nicora A., Zanchetta S., Zanchi A., Marchesi R., Vuolo I., Hosseiniyoon M., Norouzi M. & Soleimani S. (2019) - Olenekian to Early Ladinian stratigraphy of the western part of the Aghdarband

window (Kopeh-Dag, NE Iran) . Riv. It. Palaeontol. Strat., 125(1): 283–315.

Balme B.E. (1995) - Fossil in situ spores and pollen grains: an annotated catalogue. *Review of Palaeobotany and Palynology*, 87: 81–323.

Baranyi V., Kürschner W.M., Ruffell A., Mark W. & Miller C.S. (2018) - A continental record of the Carnian Pluvial Episode (CPE) from the Mercia Mudstone Group (UK). palynology and climatic implications. *Journal of the Geological Society*, 176: 149–166.

Barbacka M. (2009) - Sphenophyta from the Early Jurassic of the Mecsek Mts., Hungary. *Acta Palaeobotanica*. 49(2): 221–231.

Barbacka M. (2011) - Biodiversity and the reconstruction of Early Jurassic flora from the Mecsek Mountains (southern Hungary). *Acta Palaeobotanica*, 51(2): 127–179.

Barbacka M., Püspöki Z., Bodor E., Forgács Z., Hámor-Vidó M., Pacyna G., McIntosh R.W. (2015) - Palaeotopography related plant succession stages in a coal forming deltaic succession in early Jurassic in Hungary. *Palaeogeography, Palaeoclimatology, Palaeoecology,* 440: 579–593.

Barbacka M., Popa M.E., Mitka J., Bodor E., Puspoki Z., McIntosh R.W. (2016) - A quantitative approach for identifying plant ecogroups in the Romanian early Jurassic terrestrial vegetation. *Palaeogeography, Palaeoclimatology, Palaeoecology,* 446: 44–54.

Barnard P.D.W. (1965) - Flora of the Shemshak Formation. Part 1. Liassic plants from Dorud. *Revista Italiana di Paleontologia e Stratigrafia*, 71(4): 1123–1168.

Barnard P.D.W. & Miller J.C. (1976) - Flora of the Shemshak Formation (Elburz, Iran). 3. *Middle Jurassic (Dogger) Plants from Katumbargah, Vasek Gah and Imam Manak. Palaeontographica B*, 155: 31–117.

Batten D.J. (1974) - Wealden palaeoecology from the distribution of plant fossils. *Proceedings of the Geologists' Association*, 85(4): 433–458.

Baud A., Brandner R. & Donofrio D.A. (1991a) - The Sefid Kuh Limestone-A late Lower Triassic Carbonate Ramp (Aghdarband, NE-Iran). In: Ruttner A.W. (Ed.) - The Triassic of Aghdarband (AqDarband), NE-Iran, and its Pre-Triassic Frame. *Abhandlungen der Geologischen Bundes-Anstalt*, *38*: 111–123.

Baud A., Stampfli G. & Stephen D. (1991b) - The Triassic Aghdarband Group: Volcanism and geological evolution. In: Ruttner A.W. (Ed.) - The Triassic of Aghdarband (AqDarband), NE-Iran, and its Pre-Triassic Frame. *Abhandlungen der Geologischen Bundes-Anstalt*, *38*: 125–137.

Berberian M. & King G.C.P. (1981) - Towards a Paleogeography and Tectonic Evolution of Iran. *Canadian Journal of Earth Sciences*, 18(2): 210–265.

Bernardi M., Gianolla P., Petti F.M., Mietto P. & Benton M.J. (2018) - Dinosaur diversification linked with the Carnian Pluvial Episode. *Nature Communications*, 9: 1499.

Bock W. (1969) - The American Triassic flora and global distribution. *Geological Center Research Series*, 3:1–357.

Boersma M. & Van Konijnenburg-van Cittert J.H.A. (1991) - Late Triassic plant megafossils from Aghdarband (NE-Iran). In: A.W. Ruttner (Ed.) - The Triassic of Aghdarband (AqDarband), NE-Iran, and its pre-Triassic frame. *Abhandlungen der Geologischen Bundes-Anstalt*, 38: 223–252.

Brick M.I. (1936) - The first finding of the Lower Triassic flora in Middle Asia. *Transactions of Geological Institute of the USSR Academy of Sciences*, 5: 161–174.

Brick M.I. (1952) - Iskopaemaja flora i stratigrafija nižnemezozojskich otloženij bassejna srednego tečenija r. Ilek v Zapadnom Kazachstane. *Gosudarstvennoe Izd. Geologičeskoj Literatur*: 1–116.
Brunet F.F., Korotaev M.V., Ershov A.V. & Nikishin A.M. (2003) - The South Caspian Basin: A review of its evolution from subsidence modelling. *Sedimentary Geology*, 156(1-4): 119–148.

Bucefalo Palliani R. & Buratti N. (2006) - High diversity dinoflagellate cyst assemblages from the Late Triassic of southern England: new information on early dinoflagellate evolution and palaeogeography. *Lethaia* , 39: 305–312.

Calzolari G., Rossetti F., Seta M., Della Nozaem R., Olivetti V., Balestrieri M.L., Cosentino D., Faccenna C., Stuart F.M. & Vignaroli G. (2016) - Spatio-temporal evolution of intraplate strike-slip faulting: The Neogene-Quaternary Kuh-e-Faghan Fault, central Iran. *Bulletin of the Geological Society of America*, 128(3-4): 374–396.

Cao W., Zahirovic S., Flament N., Williams S., Golonka J. & Müller D.R. (2017) - Improving global paleogeography since the late Paleozoic using paleobiology. *Biogeosciences*, 14(23): 5425–5439.

Corsin P. & Stampfli G. (1977) - La Formation de Shemshak dans l'Elburz Oriental (Iran) Flore-Stratigraphie-Paléogéographie. *Geobios*, 10: 509–571.

Dal Corso J., Mietto P., Newton R.J., Pancost R.D., Preto N., Roghi G. & Wignall P.B. (2012) - Discovery of a major negative $\delta^{13}C$ spike in the Carnian (Late Triassic) linked to the eruption of Wrangellia flood basalts. *Geology*, 40(1): 79–82.

Dal Corso J., Gianolla P., Newton R.J., Franceschi M., Roghi G., Caggiati M., Raucsik B., Budai T., Haas J. & Preto N. (2015) - Carbon isotope records reveal synchronicity between carbon cycle perturbation and the "Carnian Pluvial Event" in the Tethys realm (Late Triassic). *Global and Planetary Change*, 127: 79–90.

Dal Corso J., Gianolla P., Rigo M., Franceschi M., Roghi G., Mietto P., Manfrin S., Raucsik B., Budai T., Jenkyns H.C., Reymond C.E., Caggiati M., Gattolin G., Breda A., Merico A. & Preto N. (2018) - Multiple negative carbon-isotope excursions during the Carnian Pluvial Episode (Late Triassic). *Earth-Science Reviews*, 185: 732–750.

Dal Corso J., Bernardi M., Sun Y., Song H., Seyfullah L.J., Preto N., Gianolla P., Ruffell A., Kustatscher E., Roghi G., Merico A., Hohn S., Schmidt A.R., Marzoli A., Newton R.J., Wignall P.B. & Benton M.J. (2020) - Extinction and dawn of the modern world in the Carnian (Late Triassic). *Science Advances*, 6(38): eaba0099.

Davoudzadeh M. & Schmidt K. (1985) - Contribution to the paleogeography, stratigraphy and tectonics of the Cretaceous and Paleocene of Iran. *Neues Jahrbuch für Geologie und Paläontologie. Abhandlungen*, 169(3): 284–306.

DiMichele W.A., Hook R.W., Beerbower R., Boy J.A., Gastaldo R.A., Hotton, N., Phillips T.L., Scheckler S.E., Shear W.A. & Sues H.D. (1992) - Paleozoic terrestrial ecosystems. *Terrestrial Ecosystems through Time. University of Chicago Press, Chicago*: 205–325.

Dobruskina I.A. (1994) - Triassic Floras of Eurasia. *Österreichische Akademie der Wissenschaften, Schriftenreihe der Erdwissenschaftlichen Kommissionen*, 10: 1–422.

Dobruskina I.A. (1995) - Keuper (Triassic) Flora from Middle Asia (Madygen, Southern Fergana). *Bulletin New Mexico Museum of Natural History and Science*, 5: 1–49.

Dobruskina I.A. (1998) - Lunz flora in the Austrian Alps - A standard for Carnian floras In: *Palaeogeography, Palaeoclimatology, Palaeoecology*, 143 (4): 307–345.

Donofrio D.A. (1991) - Radiolaria and Porifera (spicula) from the Upper Triassic of Aghdarband (NE-Iran). *Abhandlungen der Geologischen Bundes-Anstalt*, 38: 205–222.

Eftekharnezhad J. & Behroozi A. (1991) - Geodynamic significance of recent discoveries of ophiolites and late Paleozoic rocks in NE-Iran (including Kopet Dagh). *Abhandlungen der Geologischen Bundes-Anstalt*, 38: 89–100.

Fakhr M. S. (1977) - Contribution a l'Étude de la flore rhéto-liassique de la formation de Shemshak de l'Elbourz (Iran). *Mémoires de la section des Sciences.* 5: 178 pp.

Fansong M. (1983) - New materials of fossil plants from the Jiuligang Formation of Jingmen-Dangyang Basin, W. Hubei. *Professional Papers of Stratigraphy and Palaeontology*, 10: 223–238.

Fansong M. (1990) - Some Pteridosperms from Western Hubei in Late Triassic and Their Evolutionary Tendency. *Journal of Integrative Plant Biology*, 32(4).

Franz M., Kustatscher E., Heunisch C., Niegel S. & Röhling H.G. (2019) - The Schilfsandstein and its flora; arguments for a humid mid-Carnian episode? *Journal of the Geological Society*, 176(1): 133–148.

Fu X., Jian Wang J., Wen H., Wang Z., Zeng S., Song C., Chen W. & Wan J. (2020) - A possible link between the Carnian Pluvial Event, global carbon-cycle perturbation, and volcanism: New data from the Qinghai-Tibet Plateau. *Global and Planetary Change*, 194: 103300.

Garzanti E. & Gaetani M. (2002) - Unroofing history of late paleozoic magmatic arcs within the “Turan Plate” (Tuarkyr, Turkmenistan). *Sedimentary Geology*, 151(1-2): 67–87.

Ghasemi-Nejad E., Head M.J. & Zamani M. (2008) - Dinoflagellate cysts from the Upper Triassic (Norian) of northeastern Iran. *Journal of Micropalaeontology*, 27(2): 125–134.

Gianolla P., Ragazzi E. & Roghi G. (1998) - Upper Triassic amber from the Dolomites (Northern Italy). A paleoclimatic indicator? *Rivista Italiana di Paleontologia e Stratigrafia*, 104(3): 381–390.

Göppert H.R. (1861) - Ueber das Vorkommen von Lias-Pflanzen im Kaukasus und der Alborus-Kette:

Abhandlungen der Schlesischen Gesellschaft für vaterländische Literatur. Abtheil. für Naturwissenschaften u. Medicin. 1861:Vol 2, 189–194.

Heer, O. (1876-1877). Flora fossilis Helvetiae. Die vorweltliche Flora der Schweiz. Verlag J. *Wurster & Comp., Zürich*. 182 p. Parts 1,2 (1876):1- 90; Parts 3, 4 (1877):91–182.

Heinrichs J., Feldberg K., Bechteler J., Regalado L., Renner M.A.M., Schäfer-Verwimp A., Gröhn C., Müller P., Schneider H. & Krings M. (2018) - A Comprehensive Assessment of the Fossil Record of Liverworts in Amber. In: Krings M., Harper C.J., Cúneo N.R. & Rothwell G.E. (Eds.), *Transformative Paleobotany*: Academic Press, Amsterdam, pp. 213–252.

Jacob K., Shukla B.N. & West W.D. (1955) - Jurassic Plants from the Saighan Series of northern Afghanistan and their paleoclimatological and paleogeographical significance. *Memoirs of the Geological Survey of India*, *Palaeontographica Indica*, 33 (2): 1–64.

Jin X., Gianolla P., Shi Z., Franceschi M., Caggiati M., Du Y. & Preto N. (2020) - Synchronized changes in shallow water carbonate production during the Carnian Pluvial Episode (Late Triassic) throughout Tethys. *Global and Planetary Change*, 184: 103035.

Kelber K.P. (1990) - Die versunkene Pflanzenwelt aus den Deltasümpfen Mainfrankens vor 230 Millionen Jahren: *Beringeria*, 1: 1–67.

Kelber K.P. & Hansch W. (1995) - Keuperpflanzen – Die Enträtselung einer über 200 Milionen Jahre alten Flora. Museo 11: 1–157.

Khalilizadeh H., Ghaderi A., Ashouri A.R. & Zand-Moghadam H. (2020) - Plant macrofossils, ichnofossils, facies analysis and palaeoenvironment interpretation of the Hojedk Formation in the north of Kerman (Central Iran). *Journal of Stratigraphy and Sedimentology Researches University of Isfahan*, 35 (4): 1–38.

Kilpper K. (1964) - Über eine Rät/Lias-Flora aus dem nördlichen Abfall des Alburs-Gebirges in Nord-Iran. Teil 1: Bryophyta und Pteridophyta. *Palaeontographica*, 114B: 1–78.

Kilpper K. (1968) - Einige Bennettiteen-Blätter aus dem Lias von Karmozd-Zirab (N-Iran). *Journal of the Linnean Society of London, Botany*, 61(384): 129–135.

Kilpper K. (1971) - Über eine Rät/Lias-Flora aus dem nördlichen Abfall des Alburs-Gebirges in Nord-

Iran. Teil 2: Ginkgophyten-Belaubung. *Palaeontographica Abteilung B*: 89–102.

Kilpper K. (1975) - Paläobotanische untersuchungen in Nord-Iran. I. Nachweis nichtmariner Obertrias am Nordabfall des Alburs-Gebirges. 1. Grossform der Pflanzenfunde von seltenen Gattungen. *Review of Palaeobotany and Palynology*, 19(2): 139–153.

Kimyai A. (1972) - Fossil flora of Shemshak Formation, Garmabdar area. *Journal of Science, Tehran University*, 3(2): 7–25.

Kirichkova A.I. (1969) - Materials for the study of the Lower Mesozoic flora of the Eastern Urals. *Trudy Vsesoyuznogo Neftjanogo Geologo Razved Instituta*, 268: 270–349.

Klausen T.G. & Mørk A. (2014) - The Upper Triassic paralic deposits of the De Geerdalen Formation on Hopen: Outcrop analog to the subsurface Snadd Formation in the Barents Sea. *AAPG Bulletin*, 98(10): 1911–1942.

Kochnev E.A. (1934) - On the study of Jurassic coal-bearing deposits of Fergana. *Materials on Geology of Coal Deposits of Middle Asia*: 5–6.

Kon'no E. (1972) - A new *Chiropteris* and other fossil plants from the Heian System, Korea. *Japanese Journal of Geology and Geography*, 16(1-2): 105–114.

Koppelhus E. (1991) - Palynology of the Lower Jurassic Rønne Formation on Bornholm, eastern Denmark. *Bulletin of the Geological Society of Denmark*, 39: 91–110.

Krasser F. (1891) - Über die fossile Flora der rhätischen Schichten Persiens. *Sitzungsberichte der Österreichischen Akademie der Wissenschaften, Mathematisch-Naturwissenschaftliche Klasse*, 100: 413–432.

Kräusel R. & Leschik G. (1959) - Die Keuperflora von Neuewelt bei Basel. III. Equisetaceen. *Schweizerische Paläontologische Abhandlungen*, 77: 5–19.

Kräusel R. & Schaarschmidt F. (1966) - Die Keuperflora von Neuewelt bei Basel; 4/5: Pterophyllen und Taeniopteriden. *Schweizerische Paläontologische Abhandlungen*, 84: 1–64.

Krystyn L. & Tatzreiter F. (1991) - Middle Triassic ammonoids from Aghdarband (NE-Iran) and their paleobiogeographical significance. *Abhandlungen der Geologischen Bundes-Anstalt*, 38: 139–165.

Kustatscher E. & Van Konijnenburg-van Cittert J.H.A. (2008) - Lycophytes and horsetails from the Triassic flora of Thale (Germany). *Neues Jahrbuch für Geologie und Paläontologie - Abhandlungen*, 250(1): 65–77.

Kustatscher E., Ash S.R., Karasev E., Pott C., Vajda V., Yu J. & McLoughlin S. (2018) - Flora of the Late Triassic. In: Tanner L. (Ed.), The Late Triassic World. *Springer, Cham*, pp. 545–622.
Linck O. (1943) - Fossile Wurzelböden aus dem Mittleren Keuper. *Natur und Volk*, 73: 226–234.

Lindström S., Irmis R.B., Whiteside J.H., Smith N.D., Nesbitt S.J. & Turner A.H. (2016) - Palynology of the upper Chinle Formation in northern New Mexico, U.S.A.: Implications for biostratigraphy and terrestrial ecosystem change during the Late Triassic (Norian-Rhaetian). *Review of Palaeobotany and Palynology*, 225: 106–131.

Mahboubi A., Moussavi-Harami R., Carpenter S.J., Aghaei A. & Collins L.B. (2010) - Petrographical and geochemical evidences for paragenetic sequence interpretation of diagenesis in mixed siliciclastic-carbonate sediments: Mozduran Formation (Upper Jurassic), south of Agh-Darband, NE Iran. *Carbonates and Evaporites*, 25(3): 231–246.

Mancuso A.C., Benavente C.A., Irmis R.B. & Mundil R. (2020) - Evidence for the Carnian Pluvial Episode in Gondwana: New multiproxy climate records and their bearing on early dinosaur diversification. *Gondwana Research*, 86: 104–125.
Mattei M., Muttoni G. & Cifelli F. (2014) - A record of the Jurassic massive plate shift from the Garedu Formation of central Iran. *Geology*, 42(6): 555–558.

Matthews K.J., Maloney K.T., Zahirovic S., Williams S.E., Seton M. & Müller R.D. (2016) - Global plate boundary evolution and kinematics since the late Paleozoic. *Global and Planetary Change*, 146: 226–250.

Milanovsky E.E. (1991) - Rifting and its role in the tectonic structure of the Earth and its Mezo-Cenozoic geodynamics. *Geotektonika (Geotectonics),* 1: 3–20.

Moisan P. & Voigt S. (2013) - Lycopsids from the Madygen Lagerstätte (Middle to Late Triassic, Kyrgyzstan, Central Asia). *Review of Palaeobotany and Palynology*, 192: 42–64.

Moisan P., Voigt S., Pott C., Buchwitz M., Schneider J.W. & Kerp H. (2011) - Cycadalean and bennettitalean foliage from the Triassic Madygen Lagerstätte (SW Kyrgyzstan, Central Asia). *Review*

of Palaeobotany and Palynology, 164(1-2): 93–108.

Moisan P., Voigt S., Schneider J.W. & Kerp H. (2012) - New fossil bryophytes from the Triassic Madygen Lagerstätte (SW Kyrgyzstan). *Review of Palaeobotany and Palynology*, 187: 29–37.

Morley C.K., Kongwung B., Julapour A.A., Abdolghafourian M., Hajian M., Waples D., Warren J., Otterdoom H., Srisuriyon K. & Kazemi H. (2009) - Structural development of a major late Cenozoic basin and transpressional belt in central Iran: The Central Basin in the Qom-Saveh area. *Geosphere*, 5(4): 325–362.

Mueller S., Hounslow M.W. & Kürschner W.M. (2016) - Integrated stratigraphy and palaeoclimate history of the Carnian Pluvial Event in the Boreal realm; new data from the Upper Triassic Kapp Toscana Group in central Spitsbergen (Norway). *Journal of the Geological Society, London*, 173(1): 186–202.

Muttoni G., Tartarotti P., Chiari M., Marieni C., Rodelli D., Dallanave E. & Kirscher U. (2015) - Paleolatitudes of Late Triassic radiolarian cherts from Argolis, Greece: Insights on the paleogeography of the western Tethys. *Palaeogeography, Palaeoclimatology, Palaeoecology*, 417: 476–490.

Nozaem R., Mohajjel M., Rossetti F., Della Seta M., Vignaroli G., Yassaghi A., Salvini F. & Eliassi M. (2013) - Post-Neogene right-lateral strike-slip tectonics at the north-western edge of the Lut Block (Kuh-e-Sarhangi Fault), Central Iran. *Tectonophysics*, 589: 220–233.
Oberhauser R. (1991) - Triassic foraminifera from the Faqir Marl Bed of the Sina Formation (Aghdarband Group, NE-Iran). *Abhandlungen der Geologischen Bundesanstalt*, 38: 201–204.

Ôishi S. (1932a) - Rhaetic plants from Province Nagato (Yamaguchi Prefecture), Japan. *Journal of the Faculty of Science, Hokkaido Imperial University. Ser. 4, Geology and Mineralogy*, 2(1): 51–68.

Ôishi S. (1932b) - The Rhaetic Plants from the Nariwa District, Prov. Bitchû (Okayama Prefecture), Japan. *Journal of the Faculty of Science, Hokkaido Imperial University. Ser. 4, Geology and Mineralogy*, 1(3-4): 257–380.

Ôishi S. (1940) - The Mesozoic Floras of Japan. *Journal of the Faculty of Science, Hokkaido Imperial University. Ser. 4, Geology and Mineralogy*, 5(2-4): 123–480.

Ôishi S. & Takahashi E. (1936) - The Rhaetic Plants from Province Nagato. A Supplement. *Journal of the Faculty of Science, Hokkaido Imperial University. Ser. 4, Geology and Mineralogy*, 3(2): 113–133.

Osborn J.M., Taylor T.N. & de Lima M.R. (1993) - The ultrastructure of fossil ephedroid pollen with gnetalean affinities from the Lower Cretaceous of Brazil. *Review of Palaeobotany and Palynology*, 77(3-4): 171–184.

Parvacideh A. & Vaez Javadi F. (2015) - Plant Macrofossils from the Takht Coal Mine, Minoodasht and its Dating, Relative abundance and Sörensen index in comparison with the other Florizones in Iran and Eurasia. *Journal of Stratigraphy and Sedimentology Researches*, 30(4): 59–86.

Paterson N.W., Mangerud G., Cetean C.G., Mørk A., Lord G.S., Klausen T.G. & Mørkved P.T. (2016) - A multidisciplinary biofacies characterisation of the Late Triassic (late Carnian-Rhaetian) Kapp Toscana Group on Hopen, Arctic Norway. *Palaeogeography, Palaeoclimatology, Palaeoecology*, 464: 16–42.

Pocock S.A.J. & Vasanthy G. (1988) - *Cornetipollis reticulata*, a new pollen with angiospermid features from Upper Triassic (Carnian) sediments of Arizona (U.S.A.), with notes on *Equisetosporites*. *Review of Palaeobotany and Palynology*, 55(4): 337–356.

Pott C. (2012) - The Upper Triassic flora of Svalbard. *Acta Palaeontologica Polonica*, 59(3): 709–740.

Pott C. & Krings M. (2010) - Gymnosperm foliage from the Upper Triassic of Lunz, Lower Austria: an annotated check list and identification key. *Geo.Alp*, 7: 19–38.

Pott C., Kerp H. & Krings M. (2008) - Sphenophytes from the Carnian (Upper Triassic) of Lunz am See (Lower Austria). *Jahrbuch der Geologischen Bundes-Anstalt*, 148(2): 183–199.

Preto N., Kustatscher E. & Wignall P.B. (2010) - Triassic climates - State of the art and perspectives. *Palaeogeography, Palaeoclimatology, Palaeoecology*, 290(1-4): 1–10.

Ricou L.E. (1994) - La Thétys reconstruite: plaques, blocs continentaux et leurs limites depuis 260 Ma de l'Amérique centrale à l'Asie du sud-est. *Geodinamica Acta*, 7(4): 169–218.

Robert A.M.M., Letouzey J., Kavoosi M.A., Sherkati S., Müller C., Vergés J. & Aghababaei A. (2014) - Structural evolution of the Kopeh Dagh fold-and-thrust belt (NE Iran) and interactions with the South Caspian Sea Basin and Amu Darya Basin. *Marine and Petroleum Geology*, 57: 68–87.

Roghi G., Ragazzi E. & Gianolla P. (2006) - Triassic Amber of the Southern Alps (Italy). *Palaios*,

21(2): 143–154.

Roghi G., Gianolla P., Minarelli L., Pilati C. & Preto N. (2010) - Palynological correlation of Carnian humid pulses throughout western Tethys. *Palaeogeography, Palaeoclimatology, Palaeoecology*, 290(1-4): 89–106.

Ruttner A.W. (1984) – The pre-Liassic basement of the eastern Kopet Dagh Range. *Neues Jahrbuch für Geologie und Paläontologie-Abhandlungen*, 168: 256–268.

Ruttner A.W. (1988) – The coal deposits of Agdarband (Aq Darband) NE-Iran and its geological frame In: Second Mining Symposium Iran (Kerman). Ministry of Mines and Metals, Tehran: 183–202.

Ruttner A.W. (1991) – Geology of the Aghdarband Area (Kopet Dag, NE-Iran). In: Ruttner A.W. (Ed) – The Triassic of Aghdarband (AqDarband), NE-Iran and its pre-Triassic frame. *Abhandlungen der Geologischen Bundes-Anstalt,* 38: 7–79.

Ruttner A.W. (1993). Southern borderland of Triassic Laurasia in north-east Iran. *Geologische Rundschau*, *82*(1): 110–120.

Saadat Nejad J., Ghaderi A. & Naeemi Ghasabian N. (2010) – Study and presentation of Toarcian–Bajocian plant macrofossils of Gorakhk- Shandiz Region, North East of Iran. *Sedimentary Facies*, 2(2): 173–203.

Sadovnikov G.N. (1976) – The Mesozoic flora of Alborz and central Iran and its stratigraphic importance. *National Iran Steel Company of Iran, Tehran*: 1–118.

Schenk A. (1871) - Die fossile Flora der norddeutschen Wealdenformation. Theodor Fischer, 66 pp, Cassel.

Schenk A. (1887). Fossile Pflanzen aus der Albourskette, gesammelt von E. Tietze, Chefgeologe der k.k. geologischen Reichsanstalt, in: Uhlworm, O., Haenlein, F.H. (Eds.), *Bibliotheca Botanica,* Abhandlungen aus dem Gesamtgebiete der Botanik: 1–12.

Schmidt A.R., Jancke S., Lindquist E.E., Ragazzi E., Roghi G., Nascimbene P.C., Schmidt K., Wappler T. & Grimaldi D.A. (2012) – Arthropods in amber from the Triassic Period. *Proceedings of the National Academy of Sciences*, 109(37): 14796–14801.

Schweitzer H.J. (1978) – Die räto-jurassischen Floren des Iran und Afghanistans. 5. *Todites princeps*, *Thaumatopteris brauniana* und *Phlebopteris polypodioides*. *Palaeontographica Abteilung B*, 168(1-3): 17–60.

Schweitzer H.J. & Kirchner M. (1995) – Die Rhaeto-Jurassischen Floren des Iran und Afghanistans: 8. Ginkgophyta. *Palaeontographica Abteilung B*, 237: 1–58.

Schweitzer H.J. & Kirchner M. (1996) – Die rhäto-jurassischen Floren des Iran und Afghanistans: 9. Coniferophyta. *Palaeontographica Abteilung B*: 77–139.

Schweitzer H.J. & Kirchner M. (1998). Die rhäto-jurassischen Floren des Iran und Afghanistans. 11. Pteridospermophyta und Cycadophyta I. Cycadales. *Palaeontographica B*, 248 (1-3): 1–85.

Schweitzer H.J. & Kirchner M. (2003) – Die Rhaeto -Jurassischen Floren des Iran und Afghanistans. 13. Cycadophyta III. Bennettitales. *Palaeontographica Abteilung B,* 264(1-6): 1–166.

Schweitzer H.J., Van Konijnenburg-van Cittert J.H.A. & Van der Burgh J. (1997) – The Rhaeto-Jurassic flora of Iran and Afghanistan. 10. Bryophyta, Lycophyta, Sphenophyta, Pterophyta-Eusporangiatae and -Protoleptosporangiatae. *Palaeontographica Abteilung B*: 103–192.

Schweitzer H.J., Kirchner M. & Van Konijnenburg-van Cittert J.H.A. (2000) – The Rhaeto-Jurassic flora of Iran and Afghanistan. 12. Cycadophyta II. Nilssoniales. *Palaeontographica Abteilung B*, 254(1-3): 1–63.

Schweitzer H.J., Schweitzer U., Van Konijnenburg-van Cittert J.H.A,. van der Burgh J. & Ashraf R.A. (2009) – The Rhaeto-Jurassic flora of Iran and Afghanistan. 14. Pterophyta – Leptosporangiatae. *Palaeontographica Abteilung B*, 279(1-6): 1–108.

Şengör A.M.C. (1979) – Mid-Mesozoic closure of Permo–Triassic Tethys and its implications. *Nature*, 279: 590–593.

Şengör A.M.C. (1984) – The Cimmeride orogenic system and the tectonics of Eurasia. *Geological Society of America Special Paper*, 195: 82.

Şengör A.M.C. (1990) – A new model for the late Palaeozoic-Mesozoic tectonic evolution of Iran and implications for Oman. *Geological Society Special Publication*, 49(1): 797–831.

Seyfullah L.J., Beimforde C., Dal Corso J., Perrichot V., Rikkinen J. & Schmidt A.R. (2018) –

Production and preservation of resins–past and present. *Biological Reviews*, *93*(3): 1684–1714.

Sheikholeslami M.R. & Kouhpeyma M. (2012) – Structural analysis and tectonic evolution of the eastern Binalud Mountains, NE Iran. *Journal of Geodynamics*, 61: 23–46.

Sixtel T.A. (1961) – The representatives of the *Gigantopteris* and some accompanying plants from the Madygen Formation of Fergana. *Paleontological Journal*, 1: 151–158.

Sixtel T.A. (1962) – Flora of the Late Permian and Early Triassic in Southern Fergana. *Stratigraphy and Palaeontology of Uzbekistan and Adjacent Areas. Akademia Nauk USSR, Tashkent.(In Russian.)*: 271–414.

Stampfli G.M. & Borel G.D. (2002) – A plate tectonic model for the Paleozoic and Mesozoic constrained by dynamic plate boundaries and restored synthetic oceanic isochrons. *Earth and Planetary Science Letters*, 196(1-2): 17–33.

Stöcklin J. (1974) – Possible Ancient Continental Margins in Iran In: Chreighton, A.B & Drake, C.L. (Eds.), The Geology of Continental Margins:873–887. Springer Berlin Heidelberg.

Stöcklin J. & Nabavi M.H. (1973) – Tectonic map of Iran. *Geological Survey of Iran*, 1: 5.

Stur D. (1886) – Vorlage der von Dr. Wähner aus Persien mitgebrachten fossilen Pflanzen. Verhandlungen der Kaiserlich-Königlichen Geologischen Reichsanstalt, 16: 431-436.

Sze H.C. (1933) - Fossile Pflanzen aus Shensi, Szechuan und Kneichow. *Palaeontologica Sinica,* 1: 1–32.

Sze H.C. (1949) - Die Mesozoische Flora aus der Hsiangchi Kohlen Serie in Westupeh. *Palaeontologia Sinica*, 2: 1–71.

Sze H.C. (1956) - Older Mesozoic plants from the Yengchang Formation, Northern Shensi. *Palaeontologica Sinica*, 139: 92–96.

Takahashi E. (1951) – Descriptive Notes on Some Mesozoic Plants from Province Nagato (Yamaguchi Prefecture). *The Journal of the Geological Society of Japan*, 57(664): 29–33.

Taylor T.N., Taylor E.L. & Krings M. (2009) - Paleobotany: the biology and evolution of fossil plants. Academic Press.

Vaez-Javadi F. (2004) - *Persicostrobus* Vaez-Javadi n. gen. a new Equisetalean strobilus from the Triassic of Iran. *Rivista Italiana di Paleontologia e Stratigrafia*, 110: 715–718.

Vaez-Javadi F. (2008) - Plant macrofossils of Iran. *Department of Environment Press* (in Persian), Tehran, 236 pp.

Vaez-Javadi F. (2013) - Triassic and Jurassic floras and climate of central-east Iran. *Geological Survey of Iran, Rahi Pub*. 261 pp.

Vaez-Javadi F. & Syooki M.G. (2002) - Plant megafossil remains from Shemshak Formation of Jajarm area, NE Alborz, Iran. *Paleobotanist*, 51(1-3): 57–72.

Vaez-Javadi F. & Abbasi N. (2012) - Study of plant macrofossils from Baladeh area (Central Alborz): dating and biostratigraphy. *Journal of Stratigraphy and Sedimentology Researches*, 28(3): 37–64.

Vakhrameev V.A., Dobruskina I.A. & Meyen S.V. (1978) - Paläozoische und mesozoische Floren Eurasiens und die Phytogeographie dieser Zeit. VEB Gustav Fischer Verlag, Jena.

Vassiliev, I. (1984) - *Mesozoic plant fossils from coal areas in Iran*. *V. II. Atlas of Ministry of Mine and Netal*, 2(2), 97 p., 47 plates.

Volynets E.B. & Shorokhova S.A. (2007) - Late Triassic (Mongugai) flora of the Primorye region and its position among coeval floras of Eurasia. *Russian Journal of Pacific Geology*, 1(5): 482–494.

Ward L.F., Fontaine W.M., Wanner A. & Knowlton F.H. (1900) - Status of the Mesozoic floras of the United States: First paper: the older Mesozoic: Vol. 20. US Government Printing Office.

Wilmsen M., Fürsich F.T., Seyed-Emami K., Majidifard M.R. & Taheri J. (2009) - The Cimmerian Orogeny in northern Iran: Tectono-stratigraphic evidence from the foreland. *Terra Nova*, 21(3): 211–218.

Xingxue L. (1995) - Fossil floras of China through the geological ages. Guangzhou: Guangdong Science and Tehnology Press, 144.

Zan S., Axsmith B.J., Escapa I., Fraser N.C., Liu F.X. & Xing D.H. (2012) - A new *Neocalamites* (Sphenophyta) with prickles and attached cones from the Upper Triassic of China. *Palaeoworld*, 21(2):

75–80.

Zanchetta S., Berra F., Zanchi A., Bergomi M., Caridroit M., Nicora A. & Heidarzadeh G. (2013) - The record of the Late Palaeozoic active margin of the Palaeotethys in NE Iran: Constraints on the Cimmerian orogeny. *Gondwana Research*, 24(3-4): 1237–1266.

Zanchi A., Zanchetta S., Berra F., Mattei M., Garzanti E., Molyneux S., Nawab A. & Sabouri J. (2009a) - The Eo- Cimmerian (Late? Triassic) orogeny in North Iran. In M.-F. Brunet, M. Wilmsen & J.W. Granath (Eds) - South Caspian, northern and central Iran sedimentary basins. *Geological Society Special Publication*, 312 (1): 31–55.

Zanchi A., Zanchetta S., Garzanti E., Balini M., Berra F., Mattei M. & Muttoni G. (2009b) - The Cimmerian evolution of the Nakhlak-Anarak area Central Iran and its bearing for the reconstruction of the historyof the Eurasian margin. *Geological Society Special Publication*, 312(1): 261–286.

Zanchi A., Zanchetta S., Balini M. & Ghassemi M.R. (2016) - Oblique convergence during the Cimmerian collision: Evidence from the Triassic Aghdarband Basin, NE Iran. *Gondwana Research*, 38: 149–170.

Zhou T.S. & Zhou H.Q. (1983) - Triassic nonmarine strata and flora of China. *Bull. Chin. Acad. Geol. Sci*, 5: 95–110.

Chapter 3

Evidence of Carnian Pluvial Episode (Late Triassic) from the Aghdarband Basin (Turan Plate, NE Iran)

In preparation to be submitted in Global and Planetary Change

Abstract

The Middle-Upper Triassic Aghdarband Basin, NE Iran, consists of a strongly deformed marine and non-marine succession deposited along the southern margin of Eurasia (Turan Plate) in a highly complex tectonic context. The core of the Aghdarband Syncline consists of a rather monotonous sequence of brown-coloured shales, with intercalations of siltstones and fine-grained sandstones forming the Miankuhi Formation. The shale-dominated Miankuhi Fm. rests on an unconformity surface, separating it from the underlying Sina Formation. A multidisciplinary study based on sedimentological, palynological, and paleobotanical data evidences the depositional environment, sedimentary evolution, and paleoclimate conditions of the upper Sina and the lowermost Miankuhi formations. The palynological association is relatively diverse and well-preserved, yielding sporomorphs of latest early Carnian to late Carnian age in the lowermost part of the Miankuhi Formation. The qualitative and quantitative palynological analysis document a shift from xerophytic associations in the Upper Ladinian (Upper Sina Formation) to hygrophytic elements in the Carnian (Lower Miankuhi Formation). This increase in hygrophytic elements is also observed in coeval Tethyan outcrops at the same latitudinal belt and suggests a more humid climate in the lower part of the Miankuhi Formation, in correspondence with the Carnian Pluvial Episode. The sedimentological and stratigraphical analyses show an evolution from prodelta to delta setting in the Upper Sina Fm, then an unconformity enhanced by an interval of fluvial deposits with histosol levels in the basal Miankuhi Formation supporting the humid climate shift. The unconformable boundary between the Miankuhi and the Sina formations is, consequently, interpreted as a result of the sea-level fall associated with the humid climate shift, decoupling the previously proposed impact of Eo-Cimmerian collision as the origin of this unconformity. This suggests the record of the so-called Eo-cimmerian event in this basin might be related to the tectonic event that deformed the Miankuhi Formation and is probably older than the Middle Norian (217.1 ± 1.8 Ma) but younger than the Late Carnian testifying again a diachronicity in the record of collision. The exact timing and evolution of the Eo-Cimmerian collision remain, however, controversial.

1. Introduction

During the Late Triassic to Early Jurassic Cimmerian Orogeny, the Iran plate collided with the Turan plate and formed a single sedimentary province. There is still considerable controversy regarding the timing and dynamics of this orogenetic process, but it had a profound effect on the Late Triassic and Jurassic sedimentation patterns, giving origin to a series of unconformities (e.g., Stöklin, 1974; Boulin, 1988; Ruttner, 1991; Saidi et al., 1997; Alavi et al., 1997; Stampfli and Borel, 2002; Horton et al., 2008; Fürsich et al. 2009a; Wilmsen et al. 2009a, b; Zanchetta et al., 2013; Zanchi et al., 2016). The effects of this orogeny are also registered in the Aghdarband Basin, which is located in the southern part of the Kopeh-Dagh Range on the Turan Plate (NE Iran) and consists mainly of Triassic rocks (Ruttner 1991; Alavi et al. 1997; Zanchi et al. 2009a, 2016; Sheikholeslami & Kouhpeyma 2012; Zanchetta et al. 2013). The Middle-Upper Triassic succession *of the Aghdarband Basin* consists of deep-water to prodelta-delta volcanoclastic sequences of the Sina Formation (Ruttner 1991; Mazaheri-Jorari et al. 2021) and the shale-dominated Miankuhi Formation (*Ruttner 1991*). The two formations are separated by an unconformable boundary corresponding to the end of the deposition of marine arc-related volcaniclastics in the area (Sina Formation), and according to Ruttner (1991) and Zanchi et al. (2016), it records the onset of the Eo-Cimmerian collision. The Cimmerian compressional event produced wide deformations in the Triassic units of the area, and the Miankuhi Formation is the youngest unit subjected to this deformative event (Alavi, 1991; Alavi et al., 1997; Sheikholeslami and Kouhpeyma, 2013; Zanchetta et al., 2013). Besides the complex tectonic history of the strata, not much is known about the age of the Miankuhi Formation, with the exception of few studies on plant megafossils and marine palynology of its lowermost part suggesting a pre-Rhaetian age (Boersma & Van Konijnenburg-van Cittert 1991*;* Ghasemi-Nejad et al., 2008). The macrofloral composition (sphenophytes, ginkgophytes, conifers, and *incertis sedis*) along with stratigraphical and sedimentological observations in the basal Miankuhi *Formation* support the existence of continental/marginal marine deposits formed under humid climate conditions with an age of Late Carnian age based on pollen associations (Mazaheri-Johari et al., 2021). This shows that the Cimmerian collision as an explanation for this erosional unconformity is insufficient and needs to be reassessed.

The following hypotheses can be proposed for the origin of the unconformity and the coal bearing sediments at the base of the continental deposits of the Miankuhi Formation: (1) An oblique convergence of the Iran plate with the Southern Eurasian margin (Turan Domain) and related transpressional regimes during the Cimmerian collision, causing a vertical uplift of the

Kopeh-Dagh basement (Zanchi et al., 2016), resulted in erosion and accumulation of continental sediments due to the balance between active tectonic regimes and surface processes; (2) The northward movement of Eurasia and the latitudinal shift towards more humid tropic latitudes resulted in a zonal climate control on the sedimentary facies increasing noticeably the sedimentation in the southern margin of Eurasia; (3) A local record of the so-called Carnian Pluvial Episode (CPE), a climatic disturbance with a short duration (Simms and Ruffel, 1989; Ruffel et al. 2015; Miller et al., 2017; Dal Corso et al., 2018; 2020) characterized in marginal marine to continental setting by increase in the runoff, sudden input of immature siliciclastics, stream rejuvenation and fluvial incision, development of paleosols typical of humid climates (Breda et al., 2009; Kozur and Bachmann, 2010;) and a marked sea-level fall (Roghi et al. 2010; Stefani et al., 2010; Arche & Gomez, 2014; Gattolin et al., 2015; Shi et al. 2017; Barrenchea et al. 2018). The detailed qualitative and quantitative palynological data from the Upper Triassic strata of the Aghdarband Basin along with stratigraphical investigations as useful proxies for more precise age dating and paleoclimatological and paleoenvironmental reconstructions, validate the third potential hypothesis for unravelling the origin of this unconformity and the sedimentary evolution of the studied interval.

Three sections comprising Upper Triassic strata from tectonic unit 2 of the Aghdarband Basin (Ruttner 1991; Zanchi et al., 2016) are analyzed palynologically and stratigraphically. Palynostratigraphic zones are established, and their paleoclimatic signals are investigated to interpret and reconstruct the geological evolution of the basin during the time of deposition of the Sina and the Miankuhi formation*s.*

2. Geological setting

The Aghdarband Basin is part of the Turan Plate (Natal'in and Sengör, 2005) (Fig. 1), situated north of the Eo-Cimmerian suture zone, and occupies the southern part of the Kopeh-Dagh Range in Northeast Iran (Fig. 1). During the Late Triassic, it was part of the southern margin of Eurasia, positioned at ~ 35–45ºN latitude (Mattei et al. 2014; Muttoni et al. 2015; Matthews et al. 2016; Cao et al. 2017; Barrier et al., 2018) (Fig. 2). The sedimentation pattern of the studied area is mostly governed by Triassic carbonate-siliciclastic sediments (Fig. 3) which are intensely deformed due to the Cimmerian Orogeny, one of the major orogenic events of the southern Eurasian margin (Turan Plate), when the Iran plate as part of the Cimmerian blocks detached from Gondwana at the end of the Paleozoic and collided with the Turan Plate during Late Triassic/Early Jurassic following the closure of the Palaeotethys ocean (e.g., Stöcklin,

1974; Sengör, 1979, 1984, 1990; Gaetani, 1997; Stampfli & Borel, 2002; Wilmsen et al., 2009; Zanchi et al., 2009; Muttoni et al., 2009; Robinson et al., 2012). The northward subduction of the Paleotethys below the southern margin of Eurasia (Turan Plate) resulted in the formation of an arc setting with Triassic deposits (Ruttner 1991; Balini et al., 2009, 2019) in the Aghdarband Basin (Ruttner 1991; Alavi et al., 1997) (Fig. 2). This basin is structurally divided into three tectonic units (Ruttner 1991; Zanchi et al. 2016): (1) the Southern unit consisting of coarse-grained conglomerates, sandstones, and slates of ?latest Permian to earliest Triassic age (Ruttner 1991; Alavi et al., 1997; Zanchi et al., 2016), (2) the Northern unit as part of the Eurasian arc-related Turan domain (Ruttner 1991; Natal'in and Sengör, 2005; Zanchi et al., 2016) consisting of late Paleozoic rocks, and (3) a central part bounding by the southern and northern units comprised of mostly marine and often fossiliferous Triassic successions (Ruttner 1991; Zanchi et al., 2016; Balini et al., 2019). The central part is further subdivided into three other tectonic units named units 1, 2, and 3 (Fig. 1) from North to South (Ruttner 1991; Zanchi et al. 2016). Most of the sedimentary successions are tectonically deep-deformed in all tectonic units. The deformation style of sediments in unit 1 is represented by folding and faulting controlled by a transpression tectonic regime while thrusting dominated the deformation style of sediments deposited in units 2 and 3 (Ruttner 1991; Zanchi et al., 2016). From the early ‘70s, several studies were conducted *on the* central and eastern part of the Aghdarband Basin by different research groups. The comprehensive studies performed in 1991 by Anton Ruttner are among the most important ones, including a detailed geological map at 1:12,500 scale (Ruttner 1991: pl. 1).

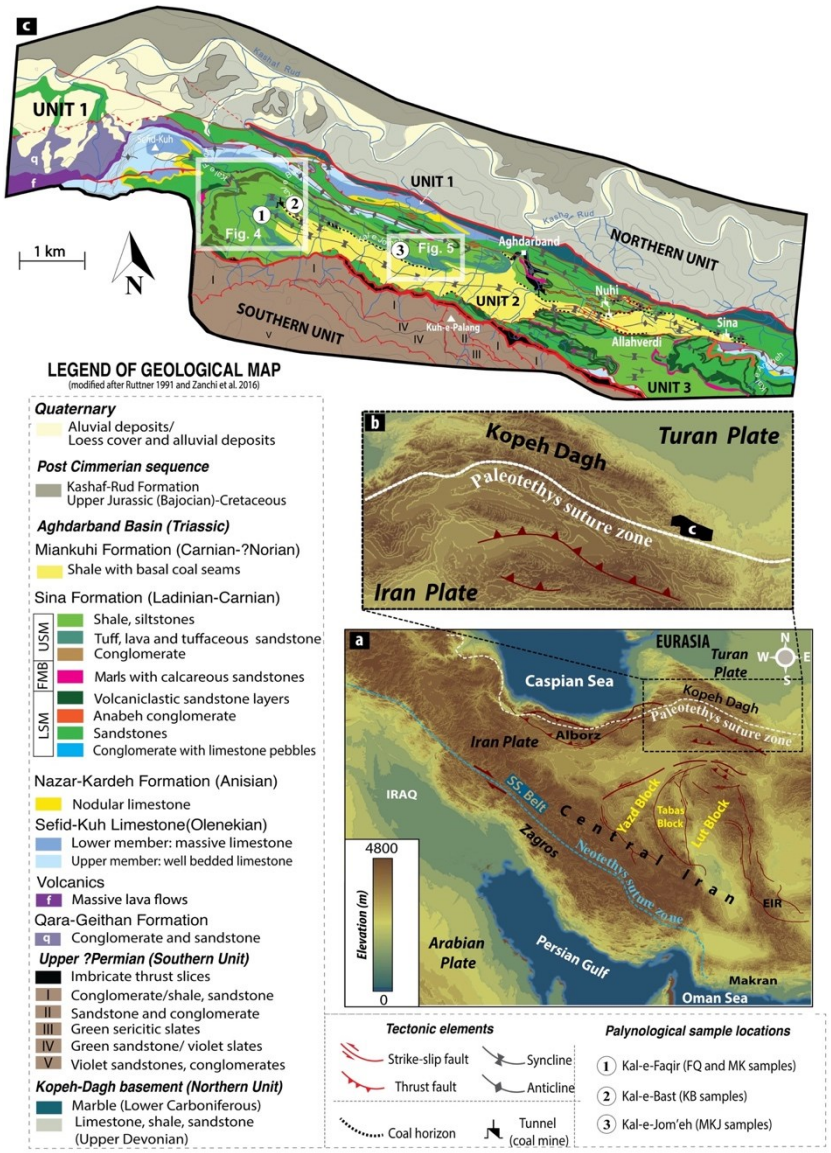

Figure 1: A) Main structural zones of the area (after Stöcklin & Nabavi 1973; Berberian & King 1981; Allen et al 2004, 2011; Morley et al 2009; Nozaem et al 2013; Calzolari et al 2016): EIZ: Eastern Iran zone. **B)** Detail of the Kopeh-Dagh Range and the location of the studied area (Aghdarband Basin). **C)** Geological map of the Aghdarband Area showing the three tectonic units, the various formations of the Aghdarband Basin (modified after Ruttner 1991 and Zanchi et al. 2016), and locations of the studied sections (1: Kal-e-Faqir section, 2: Kal-e-Bast section, 3: Kal-e-Jom'eh section). Abbreviations: SS. Belt: Sanandaj-Sirjan belt; EIR: East Iranian Range; LSM: Lower Sandstone Member; FMB: Faqir Marl Bed; USM: Upper Shale Member.

3. *Methods*

Three stratigraphic sections have been studied in the tectonic unit 2 of the Aghdarband Basin, the Kal-e-Faqir, the Kal-e-Bast, and the Kal-e-Jom'eh sections (Fig. 1). A multidisciplinary approach involving stratigraphy, sedimentology, and palynology has been adopted to provide

a better perspective on sedimentary geology, biostratigraphy, and paleoclimatology of the studied successions. High-definition field-image processing was applied to enhance the sedimentological observations and better define geometric relationships between different stratigraphic units. This image processing method, combined with detailed stratigraphic and sedimentological analyses, gave origin to a revision of the geological map (Figs. 4, 5) for the areas surrounding each section, different from the original map by Ruttner (1991).

Fifty samples were collected for qualitative and quantitative palynological analysis. Rock samples were crushed and treated with HCl (37%) and HF (47%) to dissolve the non-organic material. After washing and sieving (15 μm nylon mesh), the residue was stored in water and then strew mounted onto microscope slides using Entellan glue as the mounting medium. The quantitative analysis was performed by consecutively counting a relative number of grains per sample (Visscher, H., Van der Zwan, 1981), based on the quantity and preservation of the organic residues, to detect floral turnovers along the studied sections. The microscope slides were studied under a Leica DM750 light microscope, and the index species were photographed using a Leica ICC50 W digital camera (Plates I-III). The slides are housed in the Department of Physics and Earth Sciences of the Ferrara University.

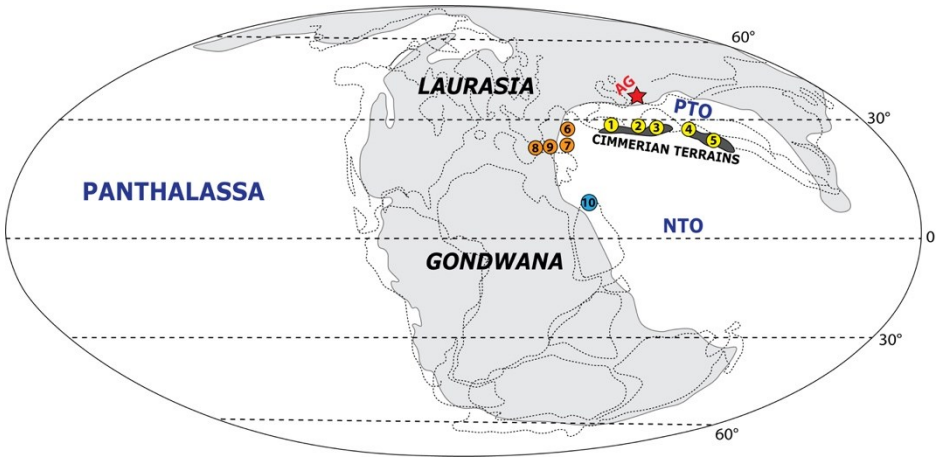

Figure 2: Late Triassic paleogeographic position of the studied area (red star, Aghdarband area) (modified aftetr Stampfli, 2000; Bernardi et al., 2018). Abbreviations: PTO: Paleotethys; NTO: Neotethys; AG: Aghdarband; Localities: 1) Sanandaj-Sirjan; 2) Alborz; 3) Lut (Central Iran); 4) Central Afghanistan; 5) South Tibet; 6) Northern Calcareous Alps; 7) Transdanubian Range (Balaton highland); 8) Julian Alps (Cave del Predil); 9) Dolomites; 10) Arabian Plate (Iraq).

4. Stratigraphy

Triassic successions in Iran are exposed in Central Iran (Tabas, Nayband, Kerman, Zofreh-Soh, Abadeh), North Iran (Alborz), Zagros, and the tectonic window of Aghdarband (Berberian and King, 1981; Ruttner 1991; Alavi et al., 1997; Buryakovsky et al., 2001; Robert et al., 2014) in northeastern Iran. The Triassic rocks of the Aghdarband Basin are characterized by marine and non-marine sediments forming the Aghdarband Group. The Aghdarband Group has been divided into four formations according to their lithological and paleontological content (Ruttner, 1991) (Fig. 3).

The lowermost formation of the Aghdarband Group is the Olenekian to the Middle Anisian Sefid-Kuh Limestone (Ruttner, 1991; Balini et al., 2019) overlying the ?late Permian–Early Triassic volcanoclastic conglomerates of the Qara-Qeitan Formation (Ruttner 1991; Eftekharnezhad & Behroozi 1991;Alavi et al. 1997; Balini et al. 2009; Zanchi et al. 2016; Liaghat et al., 2021). This unit is generally overlain by the relatively deep-water fossiliferous cherty limestones of the Nazar-Kardeh Formation (Nzkd. in Fig. 3), Bithynian in age (Krystyn & Tatzreiter 1991; Balini et al. 2019). These successions (Sefid-Kuh and Nzkd. formations) were deformed and eroded, and subsequently, a tectonically controlled basin was formed. This basin is then filled by a marine, volcanoclastic succession known as the Sina Formation (Ruttner 1991; Baud et al. 1991b; Balini et al., 2019). Moving upwards, the shale-dominated Miankuhi Formation rests on an unconformity surface, separating it from the underlying Sina Formation.

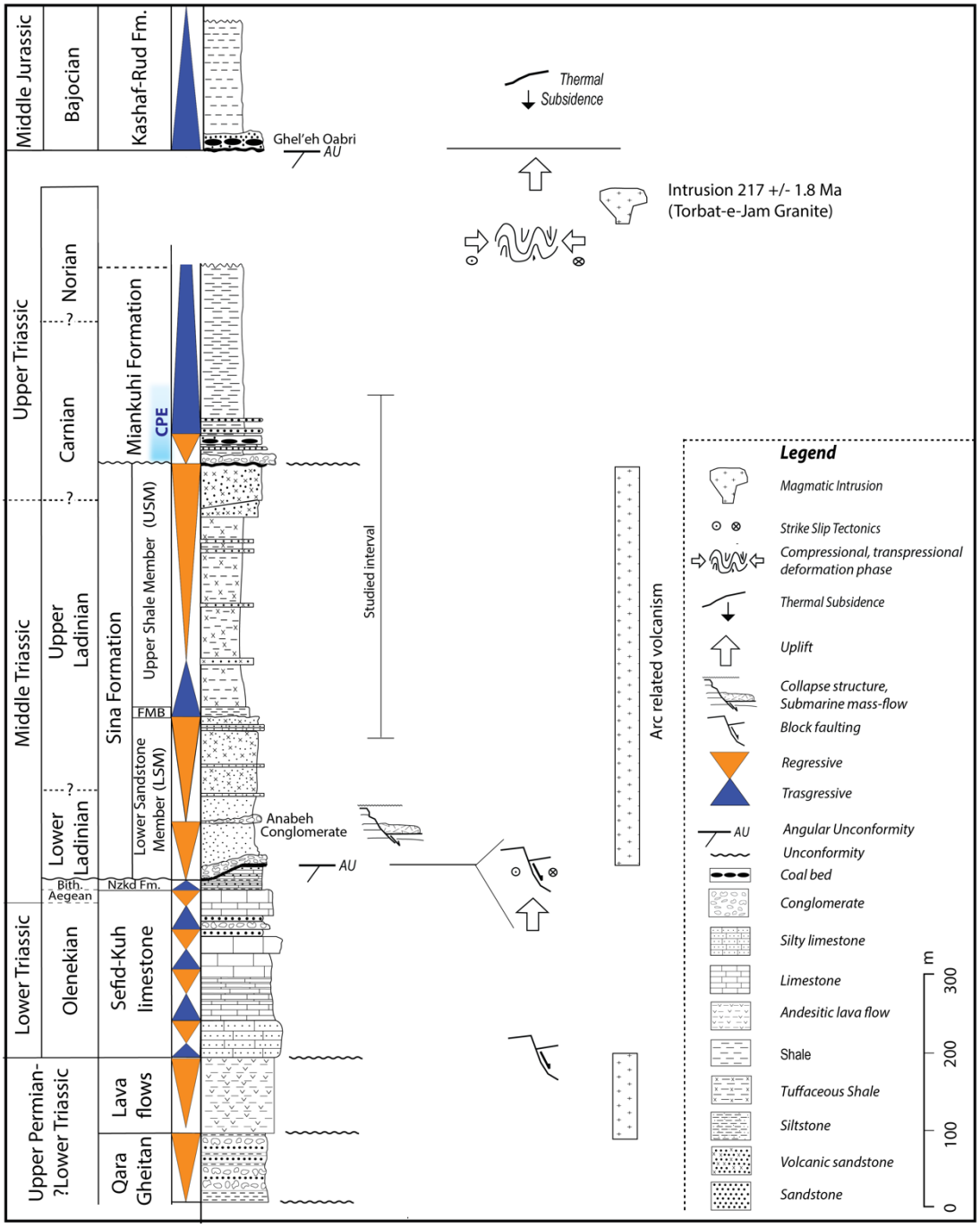

Figure 3: General lithostratigraphic column of the Triassic sequence of the Aghdarband Basin (modified from Ruttner 1991, 1993; Zanchi et al. 2016; Balini et al. 2019). Abbreviations: Bith: Bithynian; Nzkd Fm.: Nazar-Kardeh Formation; FMB: Faqir Marl Bed.

4.1.1 The Sina Formation

The Sina Formation has been investigated in detail in the upper part of the Kal-e-Faqir composite section. This section is the most complete section, covering both the Sina and the Miankuhi formations, and is composed of 5 segments (Fig. 4).

In some localities, there are lines of monogenic conglomerates along the angular unconformity at the base of the Sina Formation (Ruttner 1991; Balini et al., 2019). The lower part of the Sina Formation, named *Lower Sandstone Member* (LSM), is characterized by the prevalence of dark-green, decimeter-thick beds of coarse- to medium-grained volcanoclastic sandstones, brownish on the weathered surface, with dark (green to violet) tuffaceous shale intercalations (in some places up to one meter thick). Sandstones commonly show normal grading and other turbiditic features and are organized in (decameter) thick stacks of beds alternating to minor intervals where greenish to dark greyish pelites prevail. Tuffaceous limestones have also been found. A decameter layer composed of polygenic conglomerate beds and intercalated coarse-grained sandstone crops out in the eastern part of the Aghdarband Basin (Anabeh conglomerate, unit 3; Ruttner 1991; Balini et al., 2019), within the lower LSM. The upper part of the LSM is characterized by a coarsening and thickening upward sequence basically composed of thick-bedded litharenites and calcareous tuffaceous sandstones, producing an easily identifiable cliff. In this part, well-preserved ammonoid remnants have been found.

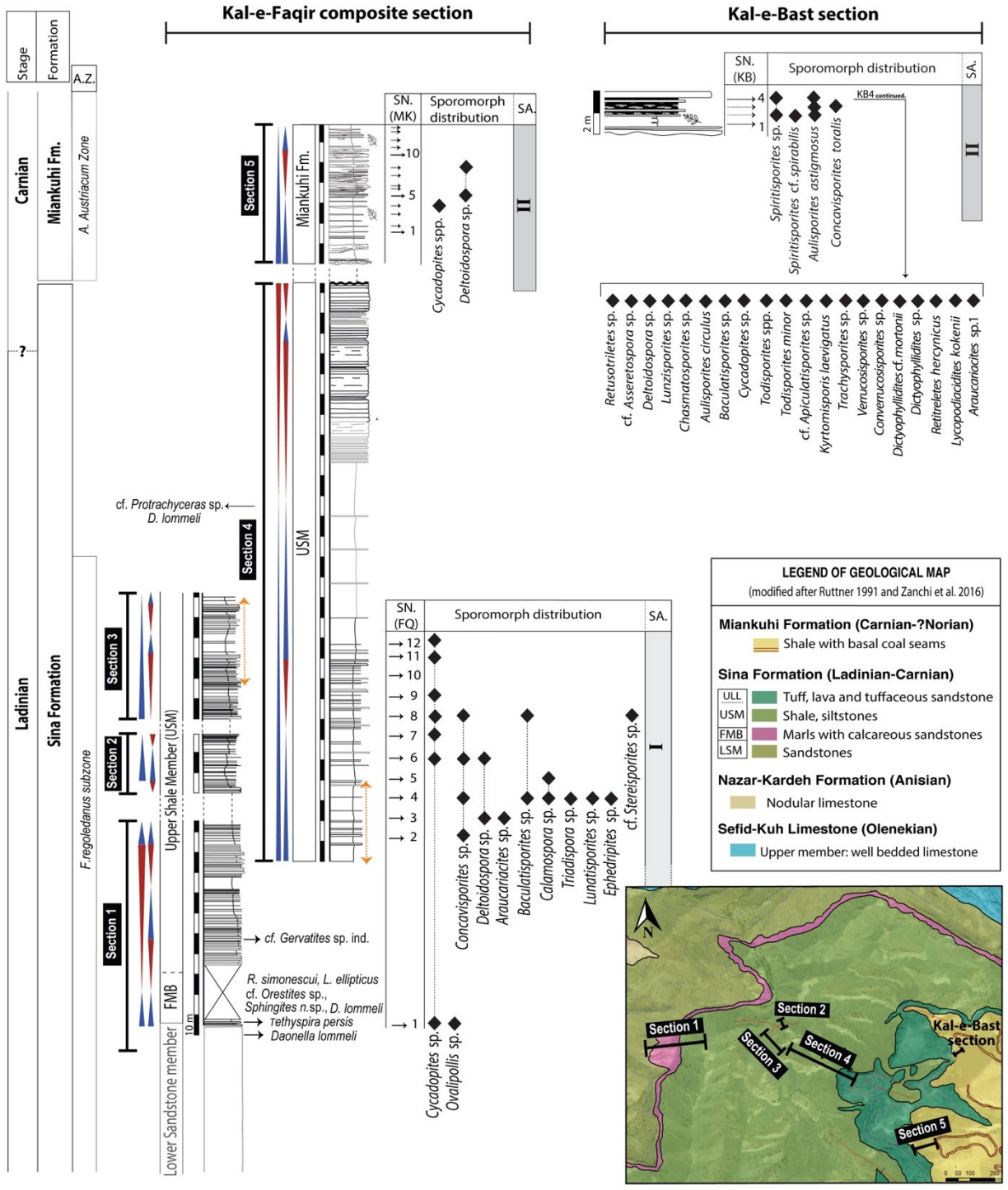

Figure 4: Lithology of the Triassic (Upper Ladinian-Carnian) uppermost Sina and Lowermost Miankuhi formations from the Kal-e-Faqir composite section and the Kal-e-Bast section, Aghdarband, with the re-drawn geological map of the area surrounding the studied sections, and distribution of sporomorph assemblages. Abbreviations: SA. Sporomorph assemblage; SN: Sample number; A.Z.: Ammonoid Zone; *R. simonescui*: *Romanites simonescui*; *L. ellipticus*: *Lobites ellipticus*; *D. lommeli*: *Daonella lommeli*; *A. austriacum*: *Austrotrachycera austriacum*; LSM: Lower Sandstone Member; FMB: Faqir Marl Bed; USM: Upper Shale Membere; ULL: Upper Litharenite Lithofacies.

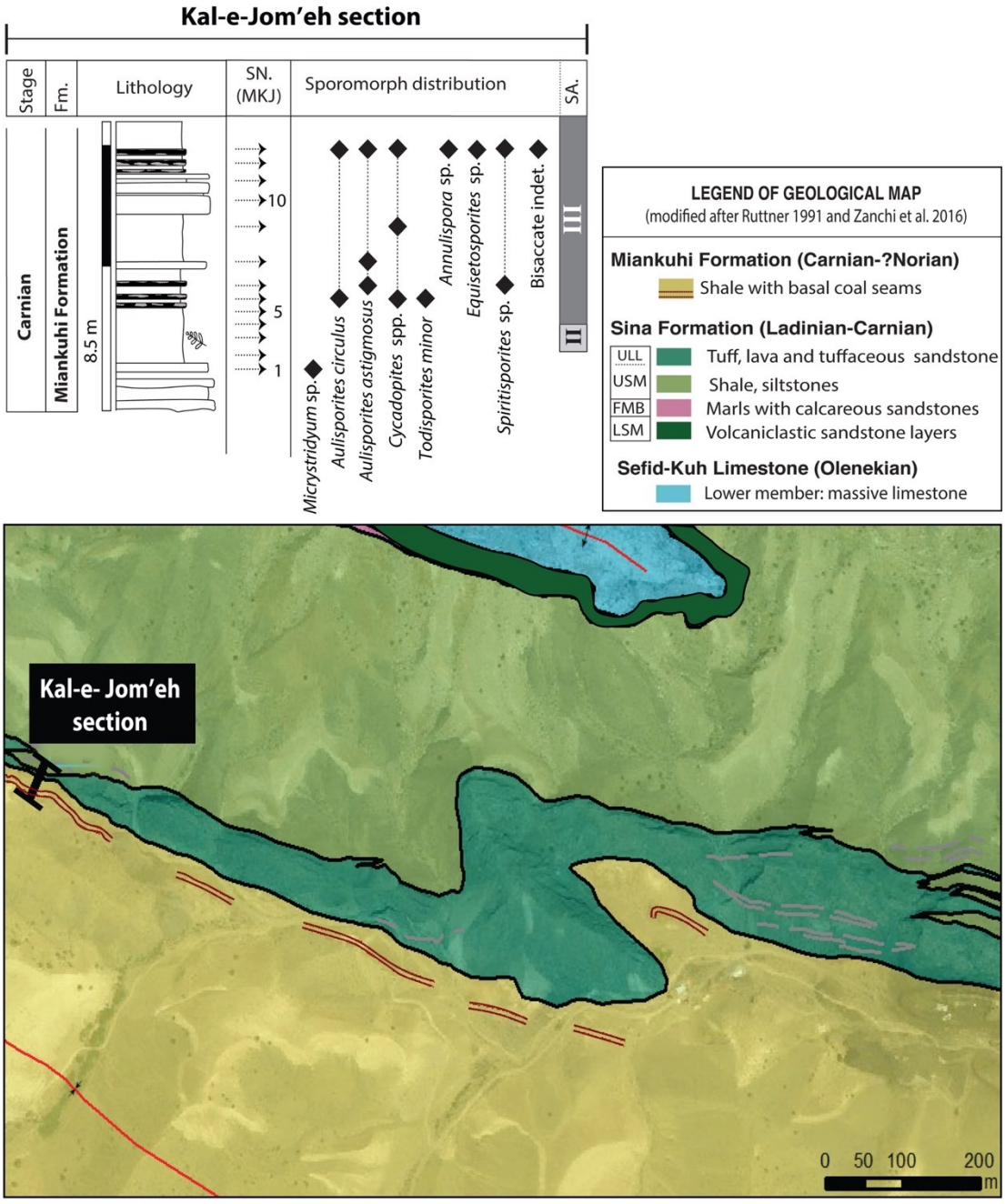

Figure 5: Lithology of the Triassic (Carnian) Lowermost Miankuhi Formation from the Kal-e-Jom'eh section, Aghdarband, with the re-drawn geological map of the area surrounding the studied section and distribution of sporomorph assemblages. Abbreviations: SA. Sporomorph assemblage; SN: Sample number; LSM: Lower Sandstone Member; FMB: Faqir Marl Bed; USM: Upper Shale Membere; ULL: Upper Litharenite Lithofacies.

The sharp reappearing of fine muds above the LSM marks a well-visible ledge (Fig. 6A): it identifies the transition to the Faqir Marl Bed (FMB), composed of greenish calcareous pelites, pink marls, tuffaceous crinoidal packstone, and rare tuffaceous calcareous sandstone

intercalations. Beyond small local changes in thickness, the FMB represents an important marker interval in succession. In addition to crinoids, cephalopods, brachiopods, and pelagic bivalves are also common (Kristan-Tollmann, 1991; Krystyn & Tatzreiter, 1991; Siblik 1991). The unit extends upward for about 25 meters, even if its middle to upper part is often not exposed because of debris cover.

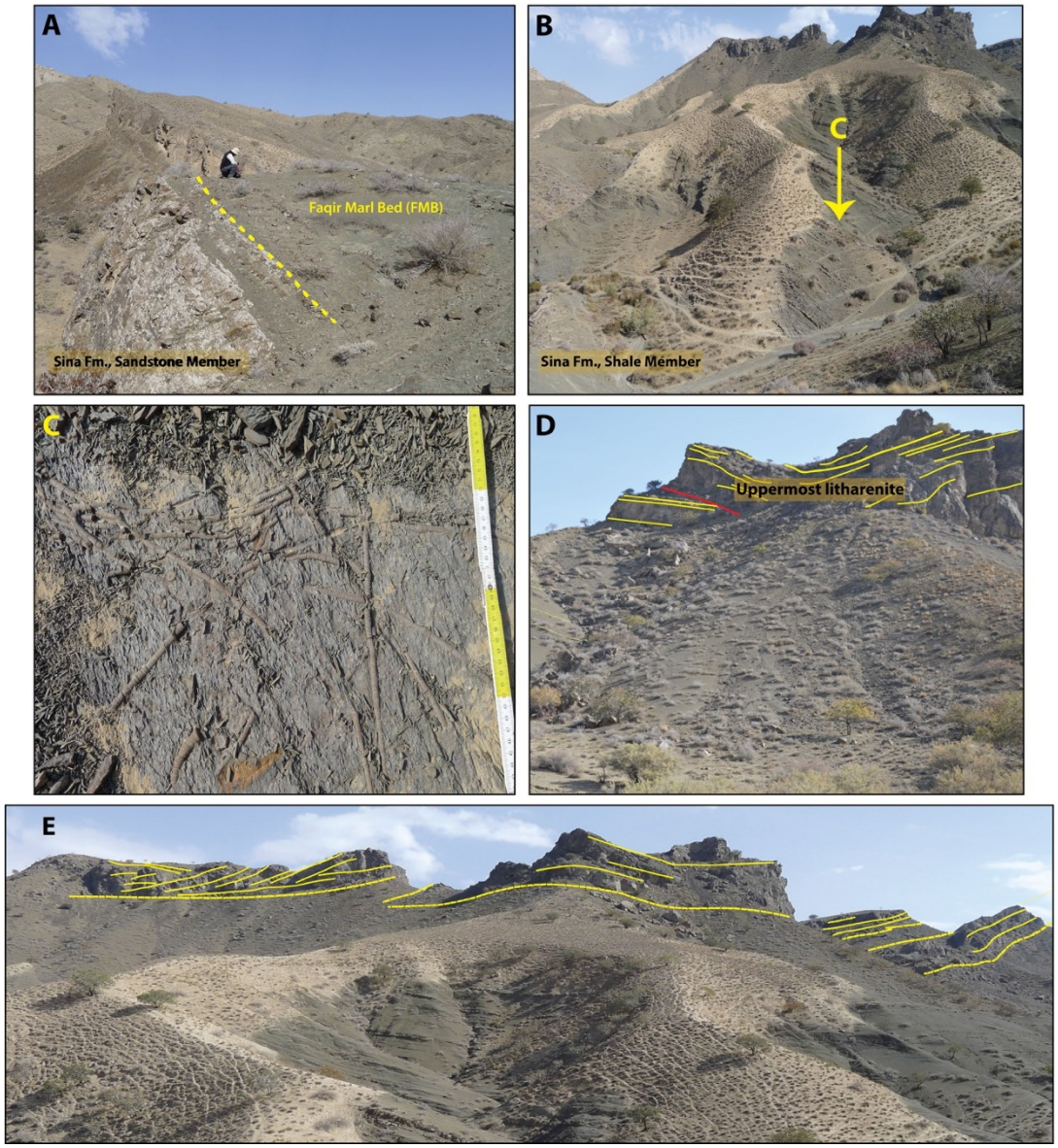

Figure 6: A) The transition from the upper part of the Lower Sandstone Member of the Sina Formation to the Faqir Marl Bed (FMB). **B)** Above the FMB, the Upper Shale Member (USM) has been shown which is characterized by a very thick siliciclastic succession with the fining and thinning upward trend (Upper Shale Member); **C)** Several pelagic crinoids found in some layers of the Upper Shale Member; **D)** The Upper Litharenite lithofacies (ULL) at the topmost USM. **E)** The transition of Upper Shale Member (USM) to the Upper Litharenite lithofacies (ULL) both upward and laterally.

Above the FMB, a very thick siliciclastic succession occurs, named *Upper Shale Member* (USM). Its lower part is commonly composed of greenish shales and siltites, and less common thin-bedded, poorly cemented, dark green to brown tuffaceous sandstone intercalations. About 45 meters upward in the Kal-e-Faqir section, a 10 meters thick, tuffaceous litharenite-rich interval occurs, with plant fragments, flow casts, and other unidirectional tractive current indicators (Ruttner, 1991), in turn followed by pelites with thin sandstone intercalations. Respect to the LSM, an increase in the content of metamorphic and plutonic grains from the crystalline basement has been pointed out (Ruttner 1991; Baud et al., 1991). At 120 m from the base, the member shows a fining and thinning upward trend, with sandstone intercalations becoming increasingly rare (Fig. 6B). On the other hand, thin mudstone to wackestone layers occur intercalated in fine siliciclastics. Several pelagic crinoids (Fig. 6C) have been found in some layers of this interval, together with brachiopods and pelagic bivalves. Toward the top of the USM, the stacking pattern changes again to thickening and coarsening upward, culminating in dm-thick sandstone layers with silty intercalations and the transition to the *Upper Litharenite lithofacies (ULL)* (Fig. 6D). The transition is gradual, occurring both upward and laterally (Fig. 6E). The ULL comprises decameter sets of massive to clinostratified litharenites, commonly with an erosive base, separated by thin intervals where silty intercalations are common. Toward the top of the sandstone unit, erosive channels and accretionary forms have been locally identified. Wood and plant debris are also common in some layers. A lateral transition toward dark shaly pelites also occurs.

4.1.2 The Miankuhi Formation

Polygenic conglomerate beds with a sharp erosive base on the USM mark the unconformity at the base of the Miankuhi Formation. In the Kal-e-Faqir composite section (Fig. 4), the conglomerate is followed upward by a succession of brownish to yellowish pelites with thin, tabular to lenticular sandstone intercalations. Less frequently, siltstones and sandstones (sometimes tuffaceous) show small- and large-scale cross bedding and are organized in sets forming overall lenticular bodies. The last patterns become very common after about 30 m upward in the section (Fig. 7A, B), where channel sandstone bodies in part crosscut themselves, sometimes resulting in amalgamated banks. Polygenic conglomerates at the base of cross-bedded sandstones are also frequent. At 55 m from the base of the unit, the occurrence of large channels decreases, and sandstone bodies are limited to lenticular or tabular thin layers intercalated to brownish pelites where marine benthonic microfauna pointing to a stressful

environment (Oberhauser, 1991). A similar succession has also been reported in the area south of Kal-e-Bast creek (Ruttner 1991), where layers of 2-3 meters thick polygenic conglomerate and cross-bedded coarse sandstone irregularly cut the top of the Sina Formation (i.e., the top litharenite unit) and underneath a one-meter-thick coal seam (Fig. 7C). The latter is also present close to the area where the Kal-e-Faqir composite section was measured and can be correlated to its upper part, while in the Kal-e-Jom'eh section, it occurs together with coaly shales and shales with diagenetic nodules and common plant root traces, intercalated with sandstones (Fig. 7D). Inside this continental interval, histosol levels with marls full of plant debris and thin coal layers have also been observed.

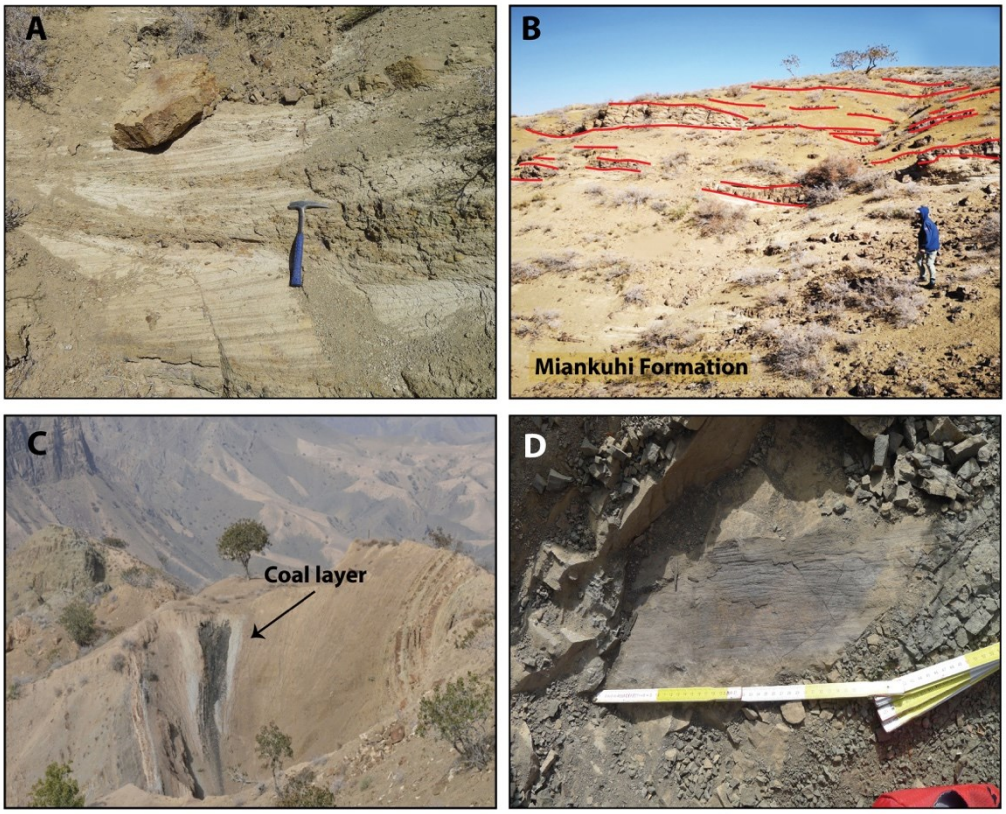

Figure 7: A) Cross bedded sandstones in the lowermost Miankuhi Formation, **B)** Erosive channels in the Miankuhi Fm., **C)** Basal Coal layer of the Miankuhi Formation, **D)** Plant-bearing intervals of Miankuhi Formation.

On the hanging wall of the coal seam, yellowish sandstones and sandy shales occur again for less than 10 meters and fine upward to shale and thin sandstone alternations. The Miankuhi Formation continues upward for about 150 m with a monotonous succession of shales, apparently without any important change in the depositional style. Out of the studied area, this formation is unconformably covered by basal sandstones of the Ghal'eh Qabri Shales, Rhaetian

in age according to Ruttner (1991, 1993) and Boersma & van Konjnenburg-van Cittert (1991) but later assigned to the basal Kashaf-Rud with an age of Bajocian based on ammonoids (Seyed-Emami, 2003).

4.1.3 Facies and basin evolution

The local occurrence of the monogenic conglomerate in the LSM (Balini et al., 2019) overlapping the basal unconformity suggests sedimentation through mass flow processes in marine depocenters, adjacent to topographically higher areas of bypass or where the Lower Triassic to Anisian substrate was still subjected to erosion. The following thick-bedded, mainly volcanoclastic sandstones represent deposition by turbidity currents in a relatively deep-marine environment. The lower part of the LSM can be indeed interpreted as the product of submarine sedimentation during regression in an overall back-arc, tectonically active setting. The middle part of LSM, commonly characterized by tuffaceous shale layers, is instead interpreted as the result of a transgression, while the thickening and coarsening upward stack of litharenite beds at the top of the LSM represents a prograding sandstone lobe leading to the emplacement of a shallower marine setting. As a matter of fact, the transition to the FMB is marked by a condensed, ammonoid-bearing surface that has been interpreted by some authors (Balini et al., 2019) as a drowning unconformity. Baud et al. (1991) interpreted the following-up marls and calcareous shale as the product of sedimentation in a distal, deep ramp environment. However, the transition from FMB to USM can be referred to as a further deepening of the depositional setting, governed by siliciclastic sedimentation and turbidity flow processes. The following-upward succession is characterized by a thinning and fining upward trend that is clearly related to a general transgression, limited upward by a maximum flooding interval, just a few tens of meters below the ULL. Well bedded, laminated to massive sandstones, and shaly to silty intercalations composing the basal part of this last unit are organized in a thickening/coarsening upward stack and pass upward to clinostratified and amalgamated beds of lithoarenite. The overall spatial distribution and organization of facies associations suggest a transition from a prodelta to a delta slope and then to delta front setting. Indeed, erosive channels with accretionary bars recognized in the uppermost part of the ULL could represent distributary channels, while some shaly intercalations lying laterally eastward to the sandstone bodies can be referred to interdistributary bay deposits. Moreover, in an overall view, the ULL is organized in at least three sandstone bodies (Fig. 6E) laterally pinching out to prodelta shales and siltites, with the latter (upper) litharenitic body extended almost on the whole area.

The transition from the Sina to the Miankuhi Formation marks an important sequence boundary. Field observations often show an erosional surface covered by a basal layer of polygenic conglomerates and intercalated sandstones. Alternations of sandstone channels and pelites characterize the initial part of the Miankuhi Formation and can be framed in a distal alluvial plain environment, with common terminal splays and overbank deposits. Fine-grained conglomerates often occupy the lower central part of channels, overlapped by coarse-grained festooned sandstones (Fig. 7A), laterally passing to cross-bedded sandstones representing lateral accretionary sand bars, and upward grading to reddish fine sandstones and siltites. The closeness of channels in the vertical stacking pattern points to low accommodation space for the initial part of the Miankuhi Formation. However, the unit changes upwards to prevailing pelites intercalated with small channels, suggesting an increase in accommodation rates. Moreover, the occurrence of oligotrophic foraminifers and the coal layers point to shifts of the depositional environment towards a marginal marine setting, with a coastal mudflat periodically flooded by the sea and by rivers and rich in paralic swamps where the organic material accumulated. Therefore, about fifty meters of Miankuhi Formation can be framed in a general regressive trend, while at least the upper part of the measured sections (shale-dominated intervals) can be interpreted as a transgression.

5. Biostratigraphy

Conodont samples with *Gondolella costricta* and *Gondolella mombergensis* have been reported by Ruttner (1991) for the lower part of the LSM. Based on the conodont fauna, the lowermost succession is assigned to the lower Ladinian (*Curionii* Zone; Balini et al., 2010). In the middle part of the LSM (tens of meters above the Anabeh conglomerate), *Traumatocrinus caudex* has been found by Ruttner (1991), a species also reported from the upper Ladinian and lower Julian of the Southern Alps and Northern Calcareous Alps (Bittner, 1895; Wohrmann, 1889; Kristan-Tollmann, 1991). The occurrence of *Monophyllites* sp. and *Daonella lommeli* (Ruttner, 1991; Krystyn & Tatzreiter 1991) is consistent with a late Ladinian age for the upper part of the LSM. Frequent findings of some peculiar fossil species in the FMB, such as *Romanites simonescui* among ammonoids and the brachiopod *Tethyspira persis* (Ruttner, 1991 and ref. therein) allow to date the FMB to the uppermost Ladinian (*Frankites regoledanus* ammonoid subzone; Krystyn & Tatzreiter, 1991; Balini et al., 2019). Almost all the USM can be referred to the same substage because of the occurrence of *D. lommeli* and of *Protrachyceras* spp. in the upper part of the member, just below the boundary with the ULL. The latter is lacking useful biostratigraphic fossils, and it cannot be excluded that it covers the lowermost

Julian (*Trachyceras Z*one), as already postulated by Ruttner (1991) also for the presence of an upper Triassic radiolarian and sponge association in the uppermost Sina Fm. (Donofrio, 1991). Except for some benthic foraminifera that only point to a restricted environment, and a poorly preserved aquatic palynomorphs (dinoflagellates) pointing to a Norian (Ghasemi-Nejad et al., 2008) and possibly Carnian age (e.g., Bujak & Fisher 1976; Bucefalo Palliani and Buratti 2006; Mangerud et al., 2019; Mantle et al., 2020) for the lowermost Miankuhi Formation, there is not any useful fossil fauna in the lower part of this unit. Instead, interesting floral and palynomorph associations have been found (Mazaheri-Johari et al., 2021), accurately analyzed and detailed as follows.

a. Palynological analyses

About 50% of the collected and analyzed samples were productive, yielding microspores. Slides are dominated by spores and pollen grains, whereas marine elements are rare. Amorphous organic matter (AOM) is rare and present in a few slides only. Dark brown, mostly angular wood particles with subordinate angular black particles are also present. The palynological assemblages vary noticeably in preservation, although they are generally not well-preserved, precluding precise species identification for all grains. Although many forms have been identified only at the genus level, some important key species have been identified, allowing a biostratigraphic correlation. A total of 30 terrestrial taxa and different types of aquatic palynomorphs are detected, including freshwater algae. The terrestrial taxa are divided into five major plant groups: sphenophytes, ferns, conifers, and cycads. The palynoflora of most assemblages are dominated by representatives of the gymnosperms (ranging from 28 to 75% of the total sum) such as those belonging to the *Cycadopites-Monosulcites*, bisaccates pollen grains, *Ephedripites*, and inaperturate pollen grains. Trilete and indeterminate spores closely follow in abundance (ranging from 17 to 91% of the total sum) (Fig. 8).

5.1.1 Kal-e-Faqir composite section

A total of 12 samples from the USM of the Sina Formation (FQ samples) were collected at regular intervals (sampling step is 10 meters) for palynological investigations. The samples yielded relatively well-preserved assemblages dominated by terrestrial palynomorphs belong to ferns (*Deltoidospora* sp., *Concavisporites* sp., *Baculatisporites* sp.), sphenophytes

Plate I

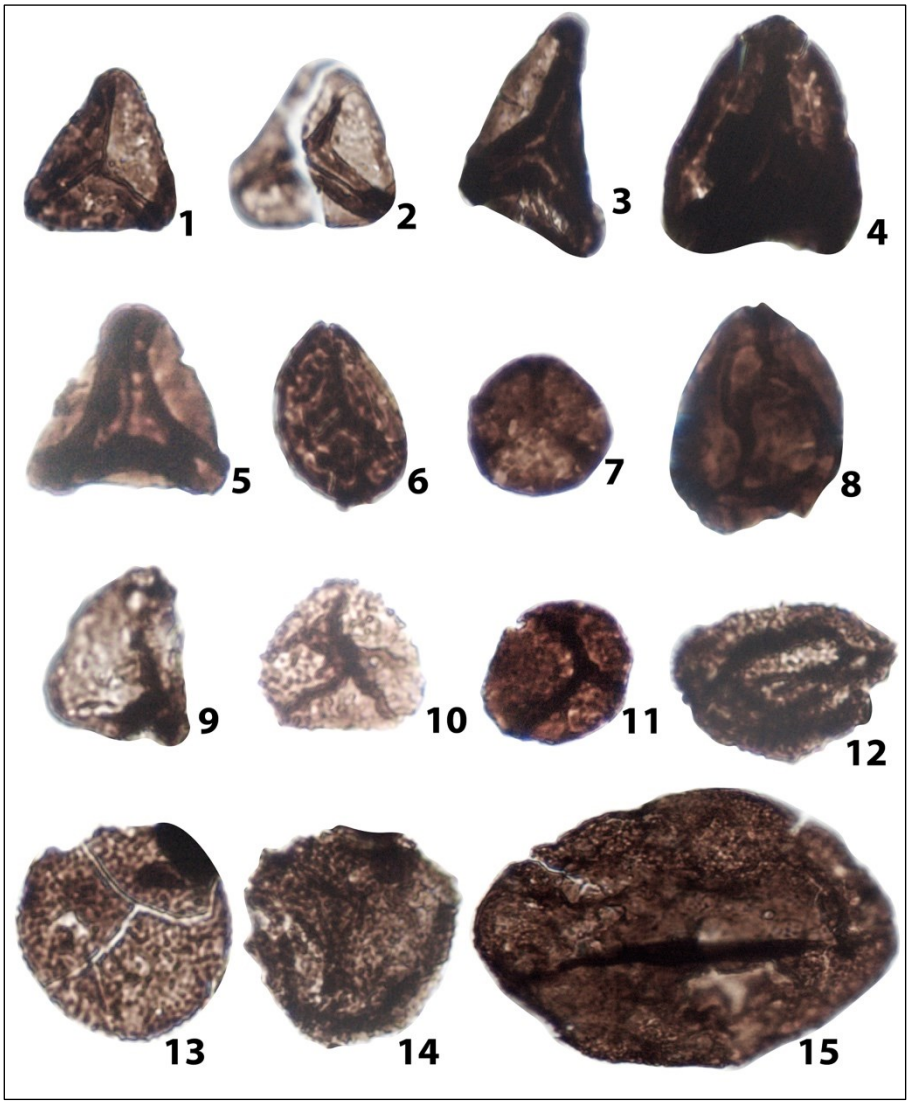

Plate I: Sporomorphs of the plant yielding horizon. Each taxon name is followed by the section name, sample number, slide number, scale, and stage coordinates for a Leica DM750 light microscope. **1-2)** *Concavisporites* sp.; 1: Kal-e-Bast section; KB 3; Slide II; 27 µm high; U58/1; 2: Kal-e-Bast section; KB 3; slide I; 28 µm high; P26/2; **3)** *Concavisporites toralis*; Kal-e-Bast section; KB 4 I; slide II; 42 µm high; V68/4; **4)** *Kyrtomisporis leavigatus*; Kal-e-Bast section; KB 4I; slide II; 38 µm high; J63/2; **5)** *Dictyophyllidites mortonii*; Kal-e-Bast section; KB 4I; slide I; 30 µm diameter; R75; **6)** *Lycopodiacidites kokenii*; Kal-e-Bast section; KB 4I; slide II; 25 µm diameter; W5; **7)** *Retusotriletes hercynicus*; Kal-e-Bast section; KB 4I; slide I; 31 µm diameter; J74/2; **8-9)** *Deltoidospora* sp.; 8: Kal-e-Faqir section; Fq 8; slide I; 40 µm high; N53/3; 9: Kal-e-Bast section; KB 4 I; slide I; 35 µm high; X67; **10)** *Lunzisporites* sp.; Kal-e-Bast section; KB 4 I, slide I; 27 µm diameter; Y67; **11)** Cf. *stereisporites* sp.; Kal-e-Faqir section; Fq 8; slide V; 24 µm diameter; G62/2; **12)** *Araucariacites* sp. 1; Kal-e-Bast section; KB 4 I, slide I; 33 µm diameter; W58/2; **13-14)** *Spiritisporites* cf. *spirabilis;* Kal-e-Bast section; 13: KB 2, slide II; 35 µm diameter; L31; 14: KB 4 I, slide II; 33 µm diameter; M23/4; **15)** Ind. foveolate trilete spore.; Kal-e-Faqir section; FQ 8, slide IV; 95 µm high; H45/1.

(*Calamospora* sp.), cycads/ginkgophytes (*Cycadopites* sp.), and conifers (*Ovalipollis* sp., *Triadispora* sp., *Lunatisporites* sp., *Araucariacites* sp.) (Fig. 4). In the upper part of the Kal-e-Faqir composite section (lowermost Miankuhi Formation), 14 samples were collected (MK samples) at regular intervals (sampling step varying from 2 to 6 meters), yielding spore grains mainly represented by *Deltoidospora* sp. along with *Cycadopites* spp. among the gymnosperms (Fig. 4).

Plate II

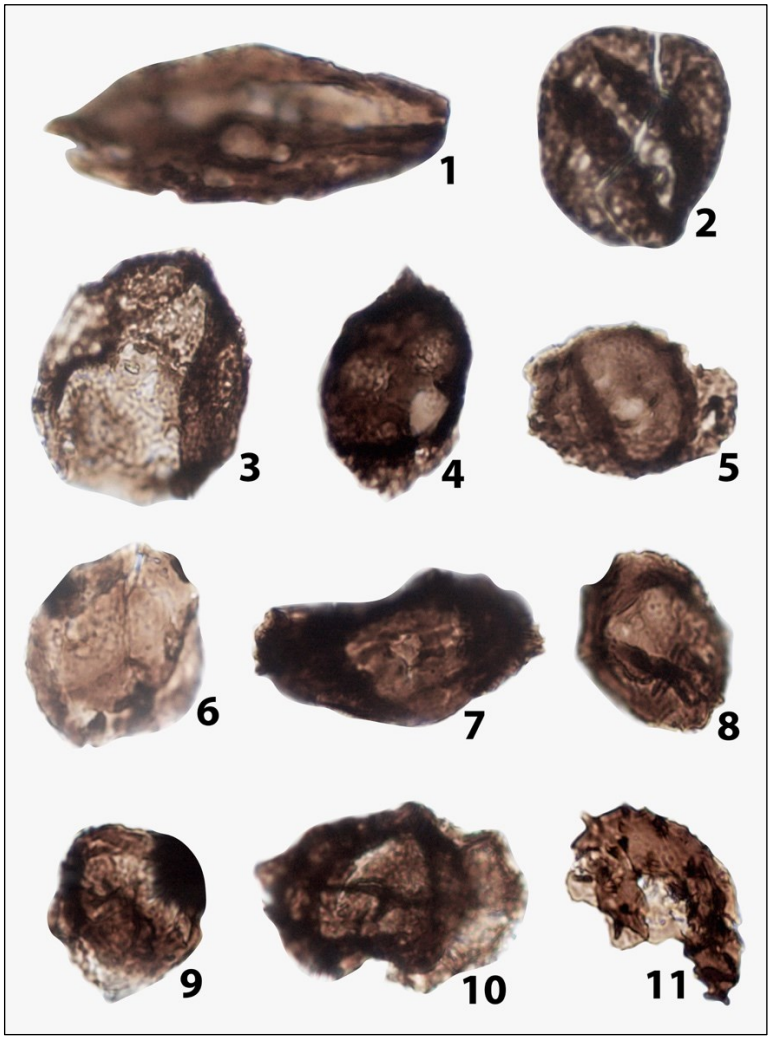

Plate II: 1-3) *Cycadopites* sp.; 1: Kal-e-Faqir section; Fq 4; slide II; 26 µµ high; K42/2; 2: Kal-e-Bast section; KB 4 II; slide II; 30 µm diameter; U6/3; 3: Kal-e-Jom'eh section; MKJ 9; slide II; 56 µµ high; R74; **4)** Cf. *Triadispora* sp.; Kal-e-Faqir section; Fq 4; slide I; 37 µm high; B48/1; **5)** *Triadispora* sp.; Kal-e-Faqir section; Fq 8; slide I; 36 µm high; H29; **6)** *Annulispora* sp.; Kal-e-Jom'eh section; MKJ 13; slide V; 46 µm diameter; M44/4; **7)** *Lunatisporites* sp.; Kal-e-Faqir section; Fq 4, slide I; 29 µm high; P42/2; **8-9) cf.** Circumpolles; Kal-e-Faqir section; 8: Fq 4, slide I; 37 µm diameter; R37/2; 9: Fq 8, slide I; 35 µm diameter; O52/4; **10)** *Chordasporites* sp.; Kal-e-Faqir section; Fq 8, slide II; 34 µm high; N49; **11)** *Baculatisporites* sp.; Kal-e-Faqir section; Fq 8, slide II; 50 µm high; J35/3.

5.1.2 Kal-e-Bast Section

The studied sequence lies in the Kal-e-Bast valley, west of Miankuhi (36.00°N, 60.81°E; Fig. 4) and consists in the lowermost Miankuhi Formation characterized by microconglomerate with shale intercalations, plant-bearing coaly shales, greenish clays with plant roots, coal beds, and sandstone layers. Palynological samples collected from the coal levels (KB samples) yielded a very rich sporomorph assemblage consisting of *Deltoidospora* sp., *Concavisporites toralis*, *Todisporites* spp., *Verrucosisporites* sp., Converrucosisporites sp., *Trachysporites* sp., *Todisporites minor*, *Dictyophyllidites* sp., *Dictyophyllidites* cf. *mortonii, Retitriletes hercynicus*, cf. *Apiculatisporites* sp., *Lycopodiacidites kokenii, Lunzisporites* sp., *Baculatisporites* sp., cf. *Asseretospora* sp., and *Kyrtomisporis laevigatus* along with the species belong to *Spiritisporites* sp., *Spiritisporites* cf. *spirabilis*, *Aulisporites astigmosus*, and *Aulisporites circulus* (Fig. 4). Among the gymnosperms, *Araucariacites* sp.1 and *Cycadopites* sp. are recorded.

5.1.3 Kal-e-Jom'eh Section

The Miankuhi Formation in the Kal-e-Jom'eh section was analyzed with a sampling step varying from 50 cm to 2.5 meters. A total of 13 samples (MKJ samples) being collected and investigated. Most samples are characterized by rich terrestrial and rare marine components. Marine elements (*Micrystridium* sp.) come from the lower part of the measured section, whereas the remaining part of the section is dominated by terrestrial palynomorphs, including the bennettitalean pollen *Aulisporites* (*A. astigmosus* and *A. circulus*), *Cycadopites* spp., and *Spiritisporites* sp.. In the upper part of the succession (sample MKJ 13), the *Equisetosporites* sp. and *Annulispora* sp. were also identified (Fig. 5).

5.2. Palynostratigraphy

Palynological analyses were carried out for this study both in the Sina and Miankuhi formations. Based on the stratigraphic distribution of the various species, three main pollen assemblage could be defined, from the bottom to the top:

- Assemblage 1: It corresponds to the assemblage found in the Sina Formation (Kal-e-Faqir composite section). This assemblage is defined by the presence of *Deltoidospora* sp., *Concavisporites* sp., *Baculatisporites* sp., *Calamospora* sp., *Cycadopites* sp., *Triadispora* sp., *Lunatisporites* sp., and *Araucariacites* sp.

- Assemblage 2: This assemblage is characterized by the presence of *Aulisporites astigmosus*, *A. circulus*, *Spiritisporites spirabilis*, *Chasmatosporites* sp. together with the spore association found in the lowermost part of the Miankuhi Formation in the upper Kal-e-Faqir composite section, in the Kal-e-Bast section, and the Kal-e-Jom'eh section.
- Assemblage 3: This assemblage belongs to the association found in the sample MKJ13 of the Kal-e-Jom'eh section and corresponds to *Aulisporites astigmosus*, *A. circulus, Cycadopites* sp., *Equisetosporites* sp., and *Annulispora* sp., as well as the re-appearance of bisaccates.

The terrestrial sporomorph assemblage of Upper Sina Formation (Shale Member) is dominated by cycad (*Cycadopites* sp.), conifers (*Triadispora* sp., *Lunatisporites* sp., *Araucariacites* sp.) as well as a sporadic fern (*Deltoidospora* sp.) and sphenophyte (*Calamospora* sp.) taxa. The sporomorph assemblage of the lowermost part of the Miankuhi Formation is characterized by the co-occurrence of Bennetttitale, Cycadales, and Ginkgoales (*Aulisporites astigmosus, Chasmatosporites* sp.), conifers, Majonicacea (*Pseudoenzonalasporites summus*), sphenophytes (*Equisetosporites* sp.), and bryophytes (*Annulispora* sp.). The assemblage 1 from Sina Formation confirms an age of late Ladinian for the strata, which is in agreement with the age suggested by Balini et al. (2019) based on ammonoid and bivalve records. Assemblage 2 and 3 allow us to define a latest-Early Carnian to Late Carnian age corresponding to the Carnian Pluvial Episode for the lower part of the Miankuhi Formation (Mazaheri-Johari et al. 2021).

5.3 Correlation with other Carnian palynological associations

Assemblages 1 in the upper Sina Formation contain few diagnostic specimens and can tentatively be correlated with upper Ladinian-lower Carnian associations where these trilete spores are found together with various species of *Lunatisporites*, *Triadispora,* and *Ovalipollis* (Mietto et al. 2012, Van der Eem, 1983). The assemblage 2, found in the Miankuhi Fm. can be correlated with the *Aulisporites astigmosus* assemblage of Roghi et al. (2010), which is Julian 2 in age. *Aulisporites astigmosus* is very important and reported in many palynological studies related to successions belong to the CPE as, for example, in the Veszprém Formation (Balaton Highland) (Barany et al., 2019) and the Raibler Schichten in Northern Calcareous Alps (Kavary, 1966; Jelen and Kušej, 1982; Roghi et al., 2010). In the Julian Alps, Cave del Predil area , *Aulisporites astigmosus* has a stratigrafic range from the Rio del Lago Formation to the Tor Formation (Roghi et al., 2004; Dal Corso et al. 2018). The same assemblage is also

documented in the Heiligkreuz Formation in the Dolomites (Praehauser-Enzenberg, 1970; Roghi, 2004, 2010; Breda et al., 2009). A rich association of *A. astigmosus*, *Cycadopites,* and fern spores also occur in the Schilfsandstein in Germany (Visscher et al., 1994). Fijałkowska-Mader (1999) described similar successions dominated by *Aratrisporites, Calamospora,* and *Aulisporites* from the Schilfsandstein of Poland.

Plate III

Plate III: 1) *Baculatisporites* sp.; Kal-e-Bast section; KB 4 I; slide I; 32 µm diameter; Q63/2; **2)** *Asseretospora* sp.; Kal-e-Bast section; KB 4 I; slide I; 38 µm diameter; X71/2; **3-5)** *Aulisporites astigmosus;* Kal-e-Bast section; 3: KB 2; slide I; 60 µm diameter; Q18/4; 4: KB 4 I; slide I; 60 µm length; Y60/4; 5: KB 4 I; slide II; 35 µm length; V45; **6-7)** *Aulisporites circulus;* 6: Kal-e-Bast section; KB 4 I; slide I; 31 µm diameter; M64; 7: Kal-e-Jom'eh section; MKJ 6; Slide I; 25 µm diameter; L66; **8-9)** *Chasmatosporites* sp.; Kal-e-Bast section; 8: KB 4 I; slide I; 34 µµ diameter; V67/3; 9: KB 4 I, slide I; 39 µm diameter; T66/3; **10)** *Trachysporites* sp.; Kal-e-Bast section; KB 4 I; slide I; 30 µm diameter; F25/4; **11)** *Todisporites* sp.; Kal-e-Bast section; KB 4 I; slide I; 40 µm diameter; T40; **12)** *Todisporites minor*; Kal-e-Jom'eh section; MKJ 6; slide I; 35 µm diameter; G68/3; 1**3)** *Ephedripites* sp.; Kal-e-Faqir section; Fq 4, slide I; 47 µm diameter; F54/1; **14)** *Ovalipollis* sp.; Kal-e-Faqir section; Fq 1; slide 0II; 38 µm high; R34/1; **15)** *Calamospora* sp.; Kal-e-Faqir section; Fq 1; slide 0II; 37 µm high; X44/3.

In the Boreal Realm, *Aulisporites astigmosus* was found in the lower parts of the Tschermakfjellet Formation (Vigran et al. 2014; Mueller et al., 2016), within the Tethyan *T. aonoides* ammonoid zone, so in slightly older sediments in comparison with the southern Tethyan realm. This was interpreted as a diachronous occurrence of *A. astigmosus* zone, occurring first in the Boreal region. The hypothesis was that the *Aulisporites*-producing mother-plant, which was a hygrophytic gymnosperm (Bennettitales, Kräusel & Saarschmidt 1966; Balme 1995) migrated southwards during the time interval of the Carnian Pluvial Event when palaeoenvironmental conditions became favorable for its proliferation in the Tethys realm.

It is also notable that the circumpollen grains and the cavatomonolete spores *Aratrisporites* typical assemblage as *Duplicisporites continuus* assemblage of Roghi (2004) and *Aulisporites-Aratrisporites* acme (Roghi, 2004) and also typical of this age at lower latitudes in Arabian Plate (NE Iraq, Baluti Formation) (Lunn, 2020) are absent or very rare (3%) in our studied interval. The palynological association discovered in Iraq resembles more closely European associations of the Alpine Realm than other assemblages from Iran.

6. Discussion

The Aghdarband area in the Kopeh-Dagh range (NE Iran) has recently attracted huge interest for unraveling the Triassic evolutionary dynamics of the southern margin of Eurasia plate during the final closure of the Paleotethys Ocean and the accretion of Cimmerian terranes to southern Eurasia, and reconstructing its tectonic evolution since the Triassic. The current paper takes a palynological and stratigraphical approach to examine the precise age of the upper Triassic strata and paleoclimatic conditions prevailing during the sedimentation at this time interval in the area with taking a new look at the basin analyses of the studied interval.

After a significant tectonic phase disrupting the middle Anisian paleotopography of the Aghdarband basin, uplifting several sectors and eventually developing structural highs and more subsiding areas, a deep basin environment with common turbidity currents developed in the Ladinian time. This deep basin was filled by the volcanoclastics of the Sina Formation, but the progressive basin infilling was discontinued at different times as a result of relative sea-level oscillations, related both to eustatic variations and to persisting active tectonics. In the

western part of the Aghdarband Basin, a major phase of basin infilling is started from the latest Ladinian time onwards, leading to a progressive decrease in sedimentation depth and a sedimentary environment transition from offshore to delta setting, then to the shallow marginal marine, and mainly fluvial setting. Notably, there could be a good correlation between the transgressive-regressive trends described here in the latest Ladinian and the depositional trends reported from several regions of the Tethys area, such as the Dolomites (cf. depositional sequence La 2 in Hardenbol et al., 1998; Gianolla et al., 1998, 2021; TLa3 in Haq et al., 2018). We believe that there is a clear shallow depositional environment before reaching transition from Sina Fm. to Miankhui Fm. The lower boundary of the latter unit has therefore been placed tens of meters below the original one reported by Ruttner (1991) for the western sector, starting from the basal conglomerates of the Miankhui Fm. (Mazaheri-Johari et al., 2021). The subsequent relative sea-level drop possibly helped establish an opportunity to erode early Julian sets of beds: in a shallow environment with gentle topography, the shoreline could run away seaward in response to sea-level fall, less than tens of meters, resulting in substantial subaerial (and fluvial) exposure and erosion of the previously deposited sediments. Furthermore, the erosive channels in the lower part of the Miankuhi Formation could locally cut each other and older sediments, including upper parts of the Sina Formation, in a vertical direction. Therefore, the unconformity at the base of the Miankuhi Formation could represent a time gap of about two million years at most which is not such a large gap in time reported in other studies (Ruttner, 1991; Seyed-Emami (2003); Zanchi et al., 2016; Balini et al., 2019; Liaghat et al., 2021). A significant sea-level drop is documented during the CPE interval worldwide (e.g., Roghi et al. 2010; Stefani et al., 2010; Arche & Gomez, 2014; Mueller et al., 2014; Gattolin et al., 2015; Franz et al., 2015; Zhang et al., 2015; Shi et al. 2017; Barrenechea et al. 2018) and this enhanced erosion could be associated with this global sea-level fall.

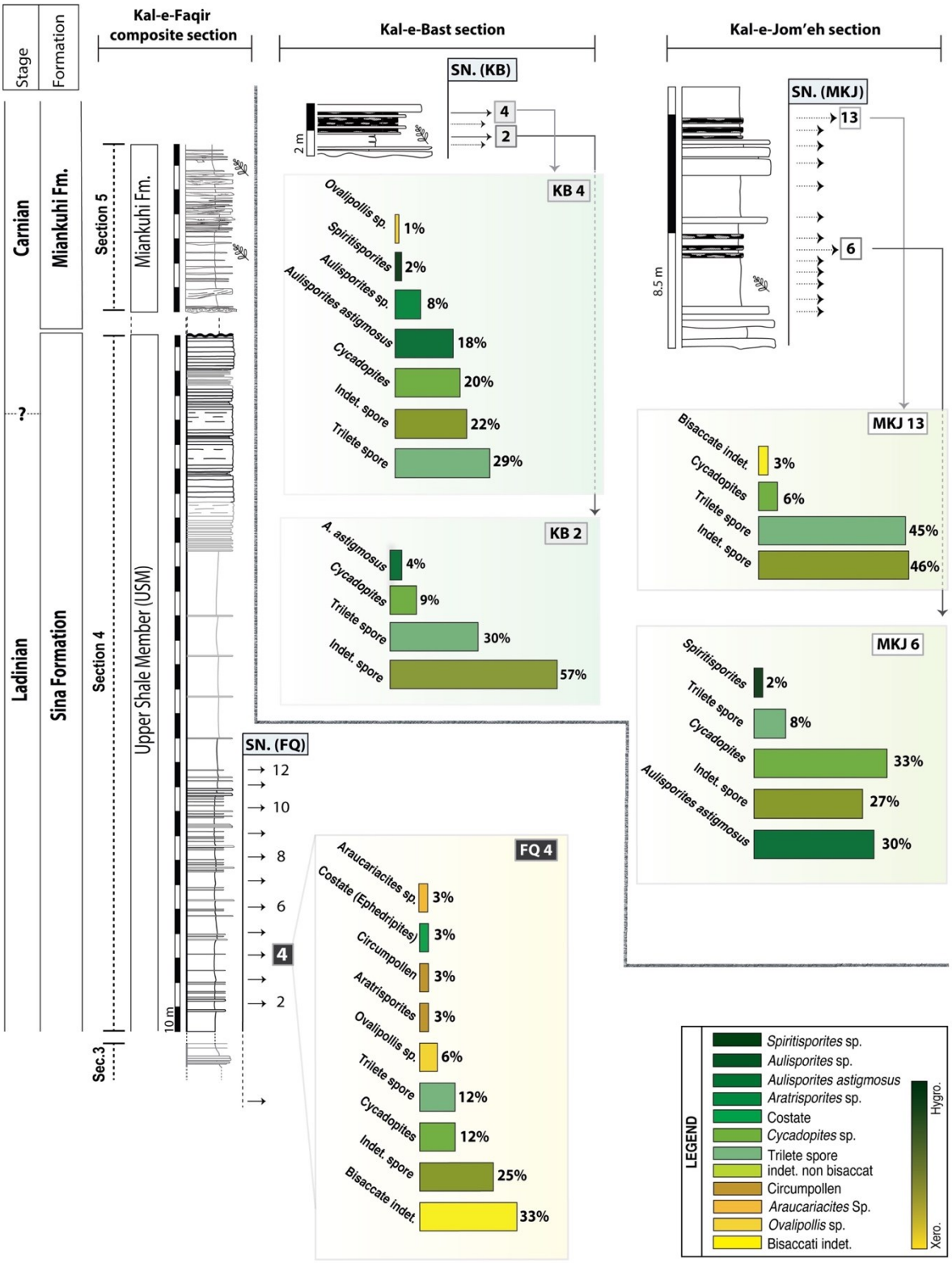

Figure 8: Quantitative results of discovered palynomorphs from Uppermost Sina Formation in the Kal-e-Faqir composite section (FQ4 sample), and lowermost Miankuhi Formation in the Kal-e-Bast (KB2 and KB4 samples) and Kal-e-Jom'eh (MKJ6 and MKJ13 samples) sections. Greenish colors indicate hygrophytic elements and yellowish ones show xerophytic sporomorphs. Abbreviations: SN: Sample number; Sec. 3: section 3; *A. astigmosus*: *Aulisporites astigmosus*; Indet: indetermined.

The reinterpretation of the stratigraphical and sedimentological patterns in this study allowed us to reconsider the extent of the unconformity previously related to the Cimmerian event, both in terms of sedimentary and time gap.

A U-Pb zircon age of 217.1 ± 1.8 has been proposed for a magmatic intrusion (Torbat-e-Jam Granite) into the deformed terrigenous sequences of the Miankuhi Formation at about 50km east of the Aghdarband, in the north of Torbat-e-Jam, (Zanchetta et al., 2013), suggesting a minimum age of Norian for the timing of the inversion and deformation of the Aghdarband basin (Zanchi et al., 2016). The dinoflagellate cyst assemblage (*Hebecysta, Heibergella, Rhaetogonyaulax, Sverdrupiella*) reported from this formation considered of Norian age are largely corroded with no good preservation and the species-level identifications are tentative (Ghasemi-Nejad et al., 2008). In addition, the described dinoflagellate cysts are not exclusively restricted to the Norian but reach down far into the Carnian (e.g., Wiggins 1973; Bujak & Fisher 1976; Bucefalo Palliani & Buratti 2006; Riding et al., 2010; Mangerud et al., 2019; Mantle et al., 2020). The *Hebecysta Balmei* Zone typical of the Middle Norian reported in the lowermost part of the studied succession (Ghasemi-Nejad et al., 2008) could be you
Appearance of Balme found in lowermost succession which is typical in Norian

On combining these important remarks, we propose a new position for the Eo-Cimmerian event in the studied area before the middle-Norian. The deformation of Miankuhi beds during an intense compressional event caused a significant uplift (Zanchi et al., 2016), forming the upper unconformable boundary of this formation covered by Jurassic strata, Kashaf-Rud Formation, recording a new geodynamic cycle (Zanchi et al., 2016). The recorded unconformity at the base of the Ghal'eh Qabri Shales, Bajocian in age (Seyed-Emami, 2003), may therefore indicate the occurrence of Mid-Cimmerian Orogeny.
The Mid-Cimmerian tectonic event occurred across the Iran Plate (Central Iran and Alborz Mountains of northern Iran) and Turan Plate when these plates were already attached. Hence, it remains plausible that the unconformity between the Sina and the Miankuhi formations could have a tectonic origin or could be related to simple sedimentary dynamics and/or the climatic driver, which is the main candidate for this scenario.

The fluvial sediments govern the depositional pattern of the sediments in the lowermost Miankuhi Formation with plant-bearing marls and histosol horizons that likely developed under humid ecological conditions. The prevalence of a relative humid and rainy paleoclimate

could also be deduced from the variation of the plant community (including sphenophytes, ginkgophytes, conifers, and *incertis sedis*) at this site and the surrounding areas (Boersma & Van Konijnenburg–van Cittert 1991; Mazaheri-Johari et al., 2021). The morphospecies groups determined by quantitative analyses reflect a clear shift towards hygrophytic elements in the lowermost Miankuhi Formation suggesting the expansion of wet habitats on the continent and the sporomorph assemblages point to a latest early Carnian to late Carnian age for this interval. The observed sedimentological and palynological patterns as well as plant fossil assemblages, show a close resemblance to those observed during the humid phases that mark the Carnian Pluvial Episode in many stratigraphical sections worldwide. This episode of global climate change dated from the Julian 2 (early Carnian) to the Tuvalian 2 (late Carnian) and is comprised of several humid pulses (Breda et al., 2009; Kozur and Bachmann, 2010; Stefani et al., 2010; Dal Corso et al., 2018; Baranyi et al., 2019) coupled to substantial changes in marine and terrestrial ecosystems (e.g., Dal Corso et al., 2020). In marine sedimentary basins, particularly in the Tethyan realm, interruption of carbonate sedimentation, sudden input of huge amounts of terrigenous materials, and the establishment of local anoxic conditions mark the onset of the CPE (Simms and Ruffell 1989; Hornung et al., 2007a,b; Rigo et al., 2007; Preto et al., 2010; Dal Corso et al., 2015; Gattolin et al., 2015; Mueller et al., 2016; Sun et al., 2016; Shi et al., 2017; Jin et al., 2020). On land, paleobotanical and palynological investigations from different latitudes revealed a shift of floral associations towards the elements with a high preference for humid conditions (e.g., Roghi et al., 2010; Preto et al., 2010; Mueller et al., 2016b; Baranyi et al., 2019; Fijałkowska-Mader et al., 2020).

The CPE has indeed been detected in the adjacent area, NE Iraq in the Arabian Plate, where abundant siliciclastics took place as a result of oscillation between arid and humid settings manifested by lower Baluti clastic unit (shale B1 from Member B of Kurra Chine Formation: see discussion in Lunn, 2020) (Hanna, 2007; Lunn et al., 2019; Davies and Simmons, 2020, Lunn, 2020) (Fig. 9). In the Eurasian Plate, along the northern foothills of the Turkestan-Alai Range (SW Kyrgyzstan), a thick succession of clastic sediments, Madygen Formation, accumulated in a lush vegetated basin under humid to semi-humid climatic conditions (Brener et al., 2009; Moisan et al., 2012, 2021). The flora of the Madygen Formation (Pteridosperms, conifers, ginkgophytes, ferns, horsetails, lycopsids, and several types of bryophytes) is quite similar to those reported from the CPE. Although this formation seems to be early Carnian in age (the base of the unit gives a ~237+/- 2-Ma) (Moisan et al., 2021), there is no precise age dating for this formation. No records of CPE have been reported from other parts of the Iran

region (Iran plate) due to the Late Carnian to Early (?) Norian sedimentary gap, and in some places even younger, in response to the Cimmerian collision and subsequent uplift and erosion (Seyed-Emami, 2003; Fürsich & Hautmann, 2005; Fürsich et al., 2009; Zanchi et al., 2009; Krystyn et al., 2019) (Fig. 9).

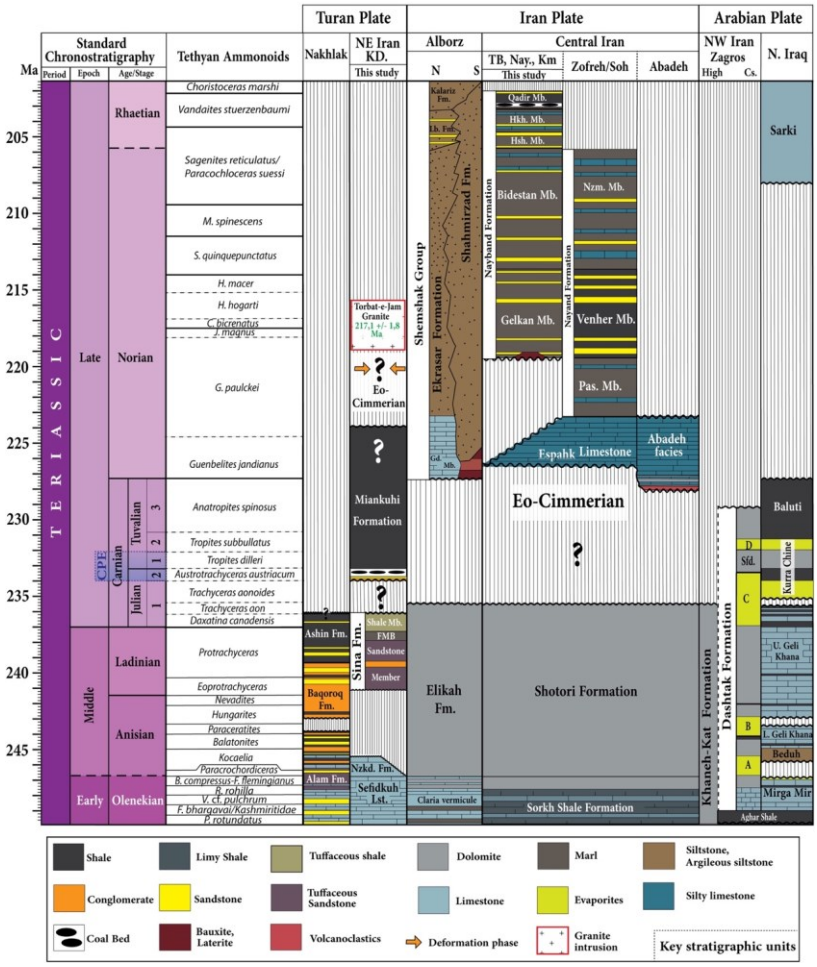

Figure 9: Lithostratigraphy of Triassic rock units from Iran region (Turan Plate, Iran Plate, and Zagros basin) and NE Iraq as part of the Arabian Plate (modified after Seyed-Emami, 2003, 2009; Fürsich et al., 2005, 2009; Balini et al., 2009; Zanchetta et al., 2013; Krystyn et al., 2019; Liaghat et al., 2021; Lunn et al., 2019; Zanchi et al., 2016). Ammonoid zones: *P. rotundatus: Prionolobus rotundatus*, *F. bhargavai/Kashmiritidae: Flemingites bhargavai/Kashmiritidae*, *V.* cf. *pulchrum*: *Vercherites* cf. *pulchrum*, *R. rohilla*: *Rohillites rohilla*, *B. compressus*: *Brayardites compressus*, F. flemingianus: *Flemingites flemingianus*. Abbreviations: Std. Standard; KD: Kopeh-Dagh; TB: Tabas Block; Nay: Nayband area; Km: Kerman region; Cs: Coastal; Nzkd. Fm.: Nazar-Kardeh Formation; Shale Mb.: Shale Member; Gd. Mb.: Galanderud Member; Lb. Fm.: Laleband Formation; Hsh. Mb.: Howz-e-Sheikh Member; Hkh. Mb.: Howz-e-Khan Member; Pas. Mb.: Parsefid Member; Nzm. Mb.: Niazmargh Member; Sfd: Sefidar limestone; L. Geli Khana: Lower Geli Khana; U. Geli Khana: Upper Geli Khana.

During Late Triassic, the Turan Plate as part of the southern margin of Eurasia was located in a relatively stable position at about ~35°N (Muttoni et al., 2015; Garzanti and Gaetani, 2002) and therefore, the observed change towards humidity (from Xerophytic assemblages to Hygrophytic ones) could not be related to a change in paleolatitudinal position.

The short duration of CPE (lasted for 1.2–1.6 Myrs) (e.g., Zhang et al., 2015; Miller et al., 2017; Bernardi et al., 2018), its global records in many different stratigraphic successions, and the global carbon cycle disruption marked by sharp negative carbon-isotope excursions in terrestrial and marine organic matter, and in marine carbonate carbon (Dal Corso et al., 2012, 2015; Mueller et al., 2016a, 2016b; Sun et al., 2016; Miller et al., 2017) during Carnian, bring into question the interpretation of the CPE as a consequence of Cimmerian Orogeny proposed by some researchers (e.g., Chu et al., 2021) when they are combined with the diachronous collision patterns of the Cimmerian event.

7. Conclusions

Iran Plate as part of the Cimmerian terranes collided with the Turan Plate (southern margin of Eurasia) in Late Triassic time and resulted in the Eo-Cimmerian orogeny (e.g., Stöcklin 1974; Sengör 1979, 1984, 1990; Ricou 1994; Stampfli & Borel 2002; Wilmsen et al. 2009; Zanchi et al. 2009a, 2009b). The deformation of surrounding arc-related basins well records this compressional event, but the exact timing of this collision has long been debated. The Aghdarband Basin, Northeast Iran, preserves a record of the Eo-Cimmerian orogenic event reflected in the severe deformation structures of its Triassic units. The Upper Triassic shale-dominated Miankuhi beds of the Aghdarband basin are the youngest rock units that convey the intense deformations they have endured, where strong folding, faulting, and deformational phases have been observed on these rocks (Ruttner, 1991; Zanchi et al., 2009, 2016). An erosional unconformity defines the lower boundary of the Miankuhi Formation, where it meets the underlying volcanoclastic-turbiditic sequences of the Middle to Upper Triassic (early Carnian) Sina Formation. This unconformity is manifested by a conglomeratic nature for the base of the Miankuhi Formation continued by continental sediments deposited in a wet alluvial plain environment (Mazaheri-Johari et al., 2021). Three main pollen assemblages have been detected based on the distribution of palynological elements. The composition of the assemblages found in the lowermost Miankuhi Formation is dominated by the occurrence of *Aulisporites astigmosus*, *A. circulus*, *Spiritisporites spirabilis*, *Cycadopites* sp., *Kyrtomisporis*

laevigatus, *Equisetosporites* sp. and *Annulispora* sp. giving an age of latest early Carnian to late Carnian to the strata. The discovered assemblages are also characterized by the lack of circumpollens and cavatomonolete Aratrisporites typical of this age at lower latitudes. The quantitative palynological analysis revealed increases in abundances of hygrophytic elements, pointing to a climatic shift towards more humid conditions at that time. The increase in the hygrophytic vegetation elements is consistent with humid signals inferred from sedimentological analyses. The prevalence of humid conditions in the Carnian of the Aghdarband Basin, accompanied by the abundant presence of the typical *Aulisporites* forms, strongly reminds the Carnian Pluvial Episode (CPE), a time of global climate change in the latest Julian to early Tuvalian (~234–232 Ma). The occurrence of Carnian Pluvial Episode in the basal continental interval of the Miankuhi Formation of Carnian age justifies assigning these clastic materials, resting unconformably on the Sina Formation, to high weathering rates within a humid climatic context rather than solely tectonic factors, Cimmerian collision, sedimentary dynamics, and changes in paleolatitude. These results have provided new insights into the Eo-Cimmerian orogeny, older than Middle Norian but younger than Late Carnian, at least in the case of our finding. However, the precise timing of this orogenic event is still a matter of debate.

Acknowledgments

We thank the cooperation of colleagues from the Geological Survey of Iran, the Mashhad branch, particularly Jafar Taheri, Abradat Maafi, and Maryam Hosseiniyoon, and the University of Tehran for assistance in fieldwork. Thanks also to Mine Engineer Hajiyan (from Maadan Khavar) for providing hospitality at the Aghdarband Coal mine during our fieldwork.

References

Alavi, M. (1991) - Sedimentary and structural characteristics of the Paleo-Tethys remnants in northeastern Iran. *Geological Society of America Bulletin*, 103, 983–992.

Alavi, M., Vaziri, H., Seyed-Emami, K. & Lasemi, Y. (1997) - The Triassic and associated rocks of the Nakhlak and Aghdarband areas in central and northeastern Iran as remnants of the southern Turanian active continental margin. *Bulletin of the Geological Society of America*, 109(12): 1563–1575.

Allen, M., Jackson, J., & Walker, R. (2004) - Late Cenozoic reorganization of the Arabia-Eurasia collision and the comparison of short-term and long-term deformation rates. *Tectonics*, 23(2).

Allen, M. B., Kheirkhah, M., Emami, M. H., & Jones, S. J. (2011). Right-lateral shear across Iran and kinematic change in the Arabia—Eurasia collision zone. *Geophysical Journal International*, 184(2), 555-574.

Arche, A., Lopez-Gomez, J. (2014) - The Carnian Humid Event in Western Europe: New data from Iberia and correlation with the Western Neotethys and Eastern North America–NW Africa regions. *Earth Science Reviews*, 128, 196-231.

Balini, M., Nicora, A., Berra, F., Garzanti, E., Levera, M., Mattei, M., Muttoni, G., Zanchi, A., Bollati I., Larghi, C., Zanchetta, S., Salamati, R. & Mossavvari, F. (2009) - The Triassic stratigraphic succession of Nakhlak (central Iran) a record from an active margin. *Geological Society Special Publication*, 312(1): 287–321.

Balini, M., Lucas, S.G., Jenks, J.F., & Spielmann, J.A. (2010) - Triassic ammonoid biostratigraphy: an overview. *Geological Society Special Publication*. 334, 221–262.

Balini, M., Nicora, A., Zanchetta, S., Zanchi, A., Marchesi, R., Vuolo, I., Hosseiniyoon, M., Norouzi, M. & Soleimani, S. (2019) - Olenekian to Early Ladinian stratigraphy of the western part of the Aghdarband window (Kopeh-Dag, NE Iran). Riv. It. Palaeontol. Strat., 125(1): 283–315.

Balme, B.E. (1995). Fossil in situ spores and pollen grains. An annotated catalogue. *Review of Palaeobotany and Palynology*, 87, 81–323.

Baranyi, V., Miller, C. S., Ruffell, A., Hounslow, M. W., & Kürschner, W. M. (2019) - A continental record of the Carnian Pluvial Episode (CPE) from the Mercia Mudstone Group (UK): palynology and climatic implications. *Journal of the Geological Society*, 176(1), 149-166.

Baranyi, V., Rostási, Á., Raucsik, B., & Kürschner, W. M. (2019) - Palynology and weathering proxies reveal climatic fluctuations during the Carnian Pluvial Episode (CPE)(Late Triassic) from marine successions in the Transdanubian Range (western Hungary). *Global and Planetary Change*, 177, 157-172.

Barrenechea, J. F., López-Gómez, J., & De La Horra, R. (2018) - Sedimentology, clay mineralogy and palaeosols of the Mid-Carnian Pluvial Episode in eastern Spain: insights into humidity and sea-level variations. *Journal of the Geological Society*, 175(6), 993-1003.

Barrier, E., Vrielynck, B., Brouillet J.-F., Brunet M.-F. (2018) - Palaeotectonic reconstruction of the Central Tethysan Realm, Atlas of 20 Maps. CGMW/CCGM, Paris, France.

Baud A., Brandner R. & Donofrio D.A. (1991a) - The Sefid Kuh Limestone-A late Lower Triassic Carbonate Ramp (Aghdarband, NE-Iran). In: Ruttner A.W. (Ed.) - The Triassic of Aghdarband (AqDarband), NE-Iran, and its Pre-Triassic Frame. *Abhandlungen der Geologischen Bundes-Anstalt*, 38: 111–123.

Baud A., Stampfli G. & Stephen D. (1991b) - The Triassic Aghdarband Group: Volcanism and geological evolution. In: Ruttner A.W. (Ed.) - The Triassic of Aghdarband (AqDarband), NE-Iran, and its Pre-Triassic Frame. *Abhandlungen der Geologischen Bundes-Anstalt*, 38: 125-137.

Berberian M. & King G.C.P. (1981) - Towards a Paleogeography and Tectonic Evolution of Iran. *Canadian Journal of Earth Sciences*, 18(2): 210–265.

Berner, U., Scheeder, G., Kus, J., Voigt, S., Schneider, J.W. (2009) - Organic geochemical characterization of terrestrial source rocks of the Triassic Madygen Formation (Southern Tien Shan, Kyrgyzstan). Oil, Gas 35, 135–139.

Bittner, A. (1895) - Lamellibranchiaten der Alpinen Trias. Abh. geol. Reich- sanst., Bd. 18, Heft 1, Wien.

Boersma, M. & Van Konijnenburg-van Cittert, J.H.A. (1991) - Late Triassic plant megafossils from Aghdarband (NE-Iran). In: A.W. Ruttner (Ed.) - The Triassic of Aghdarband (AqDarband), NE-Iran, and its pre-Triassic frame. *Abhandlungen der Geologischen Bundes-Anstalt*, 38: 223–252.

Boulin, J. (1988) - Hercynian and Eocimmerian events in Afghanistan and adjoining regions. *Tectonophysics*, 148, 253– 278.

Brayard, A., Escarguel, G., Bucher, H., Monnet, C., Brühwiler, T., Goudemand, N., …. (2009) - Good genes and good luck: Ammonoid diversity and the end-permian mass extinction. *Science*, 325: 1118-1121.

Breda, A., Roghi, G., Furin, S., Meneguolo, R., Ragazzi, E., Fedele, P., Gianolla, P., (2009) - The Carnian Pluvial Event in the Tofane area (Cortina d'Ampezzo, Dolomites, Italy). Geo. Alp. 6, 80–115.

Bujak, J.P. & Fisher, M.J. (1976) - Dinoflagellate cysts from the Upper Triassic of arctic Canada. *Micropaleontology,* 22(1): 44–70.

Buryakovsky, L.A., Chilinger, G.v., and Aminzadeh, F., (2001) - Petroleum geology of the South Caspian Basin. *Gulf Professional Publishing USA*, 442pp.

Calzolari, G., Rossetti, F., Della Seta, M., Nozaem, R., Olivetti, V., Balestrieri, M. L., ... & Vignaroli, G. (2016) - Spatio-temporal evolution of intraplate strike-slip faulting: The Neogene–Quaternary Kuh-e-Faghan Fault, central Iran. *Bulletin*, 128(3-4), 374-396.

Wenchao, c., Zahirovic, S., Flament, N., Williams, S., Golonka, J., & Müller, R. D. (2017) "Improving global paleogeography since the late Paleozoic using paleobiology." *Biogeosciences* 14, no. 23: 5425-5439.

Chen, Y., Krystyn, L., Orchard, M.J., Lai, X.-L., Richoz, S. (2016) - A review of the evolution, biostratigraphy, provincialism, and diversity of Middle and early late Triassic conodonts Pap. Palaeontol, pp. 235-263, 10.5061/dryad.34r55.

Chu, Y., Wan, B., Allen, M. B., Chen, L., Lin, W., & Talebian, M. (2021) - Tectonic evolution of Paleo-Tethys in NE Iran (No. EGU21-3557). Copernicus Meetings.

Dal Corso, J., Mietto, P., Newton, R.J., Pancost, R.D., Preto, N., Roghi, G., Wignall, P.B. (2012) - Discovery of a major negative $\delta^{13}C$ spike in the Carnian (Late Triassic) linked to the eruption of Wrangellia flood basalts. *Geology* 40, 79–82.

Dal Corso, J., Gianolla, P., Newton, R.J., Franceschi, M., Roghi, G., Caggiati, M., Raucsik, B., Budai, T., Haas, J., Preto, N. (2015) - Carbon isotope records reveal synchronicity between carbon cycle perturbation and the “Carnian Pluvial Event” in the Tethys realm (Late Triassic). Glob. Planet. Change 127, 79–90.

Dal Corso, J., Gianolla, P., Rigo, M., Franceschi, M., Roghi, G., Mietto, P., Manfrin, S., Raucsik, B., Budai, T., Jenkyns, H.C., Reymond, C.E., Caggiati, M., Gattolin, G., Breda, A., Merico, A., Preto, N. (2018) - Multiple negative carbon-isotope excursions during the Carnian Pluvial Episode (late Triassic). Earth Sci. Rev. 185, 732–750.

Dal Corso, J., Mills, B. J., Chu, D., Newton, R. J., Mather, T. A., Shu, W., ... & Wignall, P. B. (2020) - Permo–Triassic boundary carbon and mercury cycling linked to terrestrial ecosystem collapse. *Nature Communications*, 11(1), 1-9.

Davies, R. B., & Simmons, M. D. (2020) - Dating and correlation of the Baluti Formation, Kurdistan, Iraq: Implications for the regional recognition of a Carnian “marker dolomite”, and a review of the

Triassic to Early Jurassic sequence stratigraphy of the Arabian Plate. *Journal of Petroleum Geology*, 43(1), 95-108.

Davoudzadeh, M. & Schmidt, K. (1985) - Contribution to the paleogeography, stratigraphy and tectonics of the Cretaceous and Paleocene of Iran. *Neues Jahrbuch für Geologie und Paläontologie. Abhandlungen*, 169(3): 284–306.

Donofrio, D.A. (1991) - Radiolaria and Porifera (spicula) from the Upper Triassic of Aghdarband (NE-Iran). *Abhandlungen der Geologischen Bundes-Anstalt*, 38: 205–222.

Dunhill, A. M., Foster, W. J., Sciberras, J., & Twitchett, R. J. (2018) - Impact of the Late Triassic mass extinction on functional diversity and composition of marine ecosystems. *Palaeontology*, *61*(1), 133-148.

Eftekharnezhad, J. & Behroozi, A. (1991) - Geodynamic significance of recent discoveries of ophiolites and late Paleozoic rocks in NE-Iran (including Kopet Dagh). *Abhandlungen der Geologischen Bundes-Anstalt*, 38: 89–100.

Fijałkowska Mader, A. (1999) - Palynostratigraphy, palaecology, and palaeoclimatology of the Triassic in South-Eastern Poland. Zentralblatt für Geologie und Paläontologie, Teil I, 7–8, 601–627.

Fijałkowska-Mader, A., Jewuła, K., Bodor, E. (2020) - Record of the Carnian Pluvial Episode in the Polish microflora. *Palaeoworld* 30, 106–1025.

Franz, M., Kaiser, S. I., Fischer, J., Heunisch, C., Kustatscher, E., Luppold, F. W., Berner, U., & Röhling, H. G. (2015) - Eustatic and climatic control on the Upper Muschelkalk Sea (late Anisian/Ladinian) in the Central European Basin. *Global and Planetary Change*, *135*, 1-27.

Fu, X., Wang, J., Wen, H., Wang, Z., Zeng, S., Song, C., ... & Wan, Y. (2020) - A possible link between the Carnian Pluvial Event, global carbon-cycle perturbation, and volcanism: New data from the Qinghai-Tibet Plateau. Global and Planetary Change, 194, 103300.

Fürsich, F. T., & Hautmann, M. (2005) - Bivalve reefs from the Upper Triassic of Iran. *Sezione di Museologia Scientifica e Naturalistica*, *1*, 13-24.

Fürsich, F.T., Wilmsen, M., Seyed-Emami, K. and Majidifard, M.R. (2009a) - Lithostratigraphy of the Upper Triassic-Middle Jurassic Shemshak Group of northern Iran. In: *South Caspian to Central Iran Basins* (M.-F. Brunet, M. Wilmsen and J. Granath, eds), Geol. Soc. Lond. Spec. Publ., 312, 129– 160.

Gaetani, M. (1997) - The Nonh Karakoram in the framework of the Cimmerian blocks. *Him. Geol*, *18*, 33-48.

Garzanti, E., & Gaetani, M. (2002) - Unroofing history of Late Paleozoic magmatic arcs within the "Turan plate"(Tuarkyr, Turkmenistan). *Sedimentary Geology*, *151*(1-2), 67-87.

Gattolin, G., Preto, N., Breda, A., Franceschi, M., Isotton, M. & Gianolla, P. (2015) - Sequence stratigraphy after the demise of a high-relief carbonate platform (Carnian of the Dolomites): Sea-level and climate disentangled. Palaeogeography, Palaeoclimatology, Palaeoecology, 423:1–17.

Ghasemi-Nejad, E., Head, M.J. & Zamani, M. (2008) - Dinoflagellate cysts from the Upper Triassic (Norian) of northeastern Iran. *Journal of Micropalaeontology*, 27(2): 125–134.

Gianolla, P., Ragazzi, E., & Roghi, G. (1998) - Upper Triassic amber from the Dolomites (Northern Italy). A paleoclimatic indicator?. *Rivista Italiana di Paleontologia e Stratigrafia*, 104(3).

Gianolla, P., Caggiati, M., & Riva, A. (2021) - The interplay of carbonate systems and volcanics: Cues from the 3D model of the Middle Triassic Sciliar/Schlern platform (Dolomites, Southern Alps). *Marine and Petroleum Geology*, 124, 104794.

Hanna,M.T. (2007) - PalynologyoftheupperpartoftheBaluti formation (Upper Triassic) and the nature of its contact with the Sarki formation at Amadiya district, northern Iraq. Ph.D Thesis, University of Mosul, Iraq, 219p.

Hardenbol, J. A. N., Thierry, J., Farley, M. B., Jacquin, T., De Graciansky, P. C., & Vail, P. R. (1998) - Mesozoic and Cenozoic sequence chronostratigraphic framework of European basins.

Haq, B. U. (2018) - Triassic eustatic variations reexamined. *Gsa Today*, *28*(12), 4-9.

Hornung, T., Krystyn, L. & Brandner, R. (2007a) - A Tethys-wide mid-Carnian (Upper Triassic) carbonate productivity crisis: Evidence for the Alpine Reingraben Event from Spiti (Indian Himalaya)? Journal of Asian Earth Sciences, 30:285–302.

Hornung, T., Brandner, R., Krystyn, L., Joachimski, M.M. & Keim, L. (2007b) - Multistratigraphic constraints on the NW Tethyan "Carnian Crisis". New Mexico Museum of Natural History Bulletins, 4:9–67.

Horton, B.K., Hassanzadeh, J., Stockli, D.F., Axen, G.J., Gillis, R.J., Guest, B., Amini, A., Fakhari, M.D., Zamanzadeh, S.M. and Grove, M. (2008) - Detrital zircon provenance of Neoproterozoic to Cenozoic deposits in Iran: implications for chronostratigraphy and collisional tectonics. *Tectonophysics*, 451, 97– 122.

Jelen B. Kusej J. (1982) - Quantitative palynological analysis of Julian clastic rocks from the lead-zinc deposit of Mezica. Geologija, v. 25, pp. 2L3-227, Ljubljana.

Jin, X., Gianolla, P., Shi, Z., Franceschi, M., Caggiati, M., Du, Y., & Preto, N. (2020) - Synchronized changes in shallow water carbonate production during the Carnian Pluvial Episode (Late Triassic) throughout Tethys. *Global and Planetary Change*, *184*, 103035.

Kavary E. (1966) - A palynological study of the subdivision of the Cardita Shales (Upper Triassic) of Bleiberg, Austrra. Wrh. Geol. Bundesanst., 1966/1-2, pp. 178-1,89, Wien.

Keim, L., Brandner, R., Krystyn, L., & Mette, W. (2001) - Termination of carbonate slope progradation: an example from the Carnian of the Dolomites, Northern Italy. *Sedimentary Geology*, *143*(3-4), 303-323.

Kozur, H.W. & Bachmann, G.H. (2010) - The Middle Carnian Wet Intermezzo of the Stuttgart formation (Schilfsandstein), Germanic Basin. Palaeogeography, Palaeoclimatology, Palaeoecology, 290:107–119.

Kräusel, R., Schaarschmidt, F. (1966) - Die Keuperflora von Neuewelt bei Basel. IV. Pterophyllen und Taeniopteriden. Schweizerische Paläontologische Abhandlungen 84, 1–64.

Kristan-Tollmann, E., Haas, J., and Kovács, S. (1991) - Karnische Ostracoden und Conodonten der Bohrung Zsámbék–14 im Transdanubischen Mittelgebirge (Ungarn). *Jubiläumsschrift 20 Jahre Geologische Zusammenarbeit Österreich–Ungarn*, 193–220.

Krystyn L. & Tatzreiter F. (1991) - Middle Triassic ammonoids from Aghdarband (NE-Iran) and their paleobiogeographical significance. *Abhandlungen der Geologischen Bundes-Anstalt*, 38: 139–165.

Krystyn, L., Balini, M., Aghababalou, B. S., & Hairapetian, V. (2019) - Norian ammonoids from the Nayband Formation (Iran) and their bearing on Late Triassic sedimentary and geodynamic history of the Iran Plate. *Rivista Italiana di Paleontologia e Stratigrafia*, 125(1).

Liaghat, M., Adabi, M. H., Swennen, R., Mohammadi, Z., & Alijani, H. (2021) - An integrated facies, diagenesis and geochemical analysis along with sequence stratigraphy of the Lower Triassic Aghe-Darband basin (north-east Iran). *Journal of African Earth Sciences*, *173*, 103952.

Lunn, G. A., Miller, S., & Samarrai, A. (2019) - Dating and correlation of the Baluti Formation, Kurdistan, Iraq: Implications for the regional recognition of a Carnian "marker dolomite", and a review of the Triassic to Early Jurassic sequence stratigraphy of the Arabian Plate. *Journal of Petroleum Geology*, *42*(1), 5-36.

Lunn, G. A. (2020) - Dating and correlation of the Baluti Formation, Kurdistan, Iraq: Implications for the regional recognition of a Carnian "marker dolomite", and a review of the Triassic to Early Jurassic sequence stratigraphy of the Arabian Plate. *Journal of Petroleum Geology*, *43*(1), 109-125.

Mancuso, A. C., Benavente, C. A., Irmis, R. B., & Mundil, R. (2020) - Evidence for the Carnian pluvial episode in Gondwana: new multiproxy climate records and their bearing on early dinosaur diversification. *Gondwana Research*, *86*, 104-125.

Mangerud, G., Paterson, N. W., & Riding, J. B., (2019) - The temporal and spatial distribution of Triassic dinoflagellate cysts. Review of palaeobotany and palynology, 261, 53-66.

Mantle, D. J., Riding, J. B., & Hannaford, C., (2020) - Late Triassic dinoflagellate cysts from the Northern Carnarvon Basin, Western Australia. *Review of Palaeobotany and Palynology* 104254.

Mattei M., Muttoni G. & Cifelli F. (2014) - A record of the Jurassic massive plate shift from the Garedu Formation of central Iran. *Geology*, 42(6): 555–558.

Matthews, K. J., Maloney, K. T., Zahirovic, S., Williams, S. E., Seton, M., & Mueller, R. D. (2016) - Global plate boundary evolution and kinematics since the late Paleozoic. *Global and Planetary Change*, *146*, 226-250.

Mazaheri-Johari, Mina., Kustatscher, E., Roghi, G., Ghasemi-Nejad, E., & Gianolla, P. (2021) - A monotypic stand of Neocalamites iranensis n. sp. from the Carnian Pluvial Episode (Late Triassic) of the Aghdarband area, NE Iran (Turan Plate). *Rivista Italiana di Paleontologia e Stratigrafia*, *127*(2).

Mietto, P., Manfrin, S., Preto, N., Rigo, M., Roghi, G., Furin, S., ... & Buratti, N. (2012) - The global boundary stratotype section and point (GSSP) of the Carnian stage (Late Triassic) at Prati di

Stuores/Stuores Wiesen section (Southern Alps, NE Italy). *Episodes-Newsmagazine of the InternationalUnion of Geological Sciences*, *35*(3), 414.

Miller, C.S., Peterse, F., da Silva, A.-C., Baranyi, V., Reichart, G.J. & Kürschner, W. (2017) - Astronomical age constraints and extinction mechanisms of the Late Triassic Carnian crisis. Scientific Reports, 2557.

Moisan, P., Voigt, S., Schneider, J.W., Kerp, H. (2012) - New fossil bryophytes from the Triassic Madygen Lagerstätte (SW Kyrgyzstan). Rev. Palaeobot. Palynol. 187, 29–37.

Moisan, P., Krings, M., Voigt, S., & Kerp, H. (2021) - Fossil roots with root nodules from the Madygen Formation (Ladinian–Carnian; Triassic) of Kyrgyzstan. *Geobios*, *64*, 65-75.

Morley, C.K., Kongwung, B., Julapour, A.A., Abdolghafourian, M., Hajian, M., Waples, D., Warren, J., Otterdoom, H., Srisuriyon, K. and Kazemi, H. (2009) - Structural development of a major late Cenozoic basin and transpressional belt in central Iran: The Central Basin in the Qom-Saveh area. *Geosphere*, 5(4), pp.325-362.

Mueller, S., Krystyn, L. & Kürschner, W.M. (2016a) - Climate variability during the Carnian Pluvial Phase – a quantitative palynological study of the Carnian sedimentary succession at Lunz am See, Northern Calcareous Alps, Austria. Palaeogeography, Palaeoclimatology, Palaeoecology, 441:198–211.

Muttoni G., Tartarotti P., Chiari M., Marieni C., Rodelli D., Dallanave E. & Kirscher U. (2015) - Paleolatitudes of Late Triassic radiolarian cherts from Argolis, Greece: Insights on the paleogeography of the western Tethys. *Palaeogeography, Palaeoclimatology, Palaeoecology*, 417: 476–490.

Natal'in, B.A., Sengör, A.M.C., (2005) - Late Palaeozoic to Triasic evolution of the Turan and Scythian platforms: The pre-history of the Palaeo-Tethyan closure. Tectonophysics 404, 175–202.

Nozaem, R., Mohajjel, M., Rossetti, F., Della Seta, M., Vignaroli, G., Yassaghi, A., ... & Eliassi, M. (2013) - Post-Neogene right-lateral strike–slip tectonics at the north-western edge of the Lut Block (Kuh-e–Sarhangi Fault), Central Iran. *Tectonophysics*, *589*, 220-233.

Oberhauser, R. (1991) - Triassic foraminifera from the Faqir Marl Bed of the Sina Formation (Aghdarband Group, NE-Iran). *Abhandlungen der Geologischen Bundesanstalt*, 38: 201–204.

Palliani, R. B., & Buratti, N. (2006) - High diversity dinoflagellate cyst assemblages from the Late Triassic of southern England: new information on early dinoflagellate evolution and palaeogeography. *Lethaia*, *39*(4), 305-312.

Poursoltani, M.R., Moussavi-Harami, R., Gibling, M.R. (2007) - Jurassic deep-water fans in the Neo-Tethys Ocean: The Kashafrud Formation of the Kopet-Dagh Basin, Iran. Sedimentary Geology, 198, pp. 53-74.

Praehauser-Enzenberg, M. (1970) - Beitragzur mikroflora derobertrias von Heiligkreuz (Gadertal, Dolor.r.iten). Festb.Geol. Inst. 300-Jabr-Feier. Unia. Innsbr., pp. 321-337, Innsbruck.

Preto, N., Kustatscher, E., Wignall, P.B. (2010) - Triassic climates—state of the art and perspectives. Palaeogeogr. Palaeoclimatol. Palaeoecol. 290, 1–10.

Ricou, L. E. (1994) - Tethys reconstructed: plates, continental fragments and their Boundaries since 260 Ma from Central America to South-eastern Asia. *Geodinamica acta*, *7*(4), 169-218.

Riding, J.B., Mantle, D.J., Backhouse, J. (2010) - A review of the chronostratigraphical ages of Middle Triassic to Late Jurassic dinoflagellate cyst biozones of the North West Shelf of Australia. Review of Palaeobotany and Palynology, 162(4): 543-575.

Rigo, M., Preto, N., Roghi, G., Tateo, F., Mietto, P. (2007) - A rise in the Carbonate Compensation Depth of western Tethys in the Carnian (Late Triassic): deep-water evidence for the Carnian Pluvial Event. Palaeogeogr. Palaeoclimatol. Palaeoecol. 246, 188–205.

Robert A.M.M., Letouzey J., Kavoosi M.A., Sherkati S., Müller C., Vergés J. & Aghababaei A. (2014) - Structural evolution of the Kopeh Dagh fold-and-thrust belt (NE Iran) and interactions with the South Caspian Sea Basin and Amu Darya Basin. *Marine and Petroleum Geology,* 57: 68-87.

Robinson, A.C., Ducea, M. and Lapen, T.J., (2012) - Detrital zircon and isotopic constraints on the crustal architecture and tectonic evolution of the northeastern Pamir. *Tectonics*, 31, doi:10.1029/2011TC003013.

Roghi, G., (2004) - Palynological investigations in the Carnian of Cave del Predil area (once Raibl, Julian Alps). Rev. Palaeobot. Palynol. 132, 1–35. https://doi.org/10.1016/j. revpalbo.2004.03.001.

Roghi, G., Gianolla, P., Minarelli, L., Pilati, C., Preto, N. (2010) - Palynological correlation of Carnian humid pulses throughout western Tethys. Palaeogeogr. Palaeoclimatol. Palaeoecol. 290, 89–106.

Ruffell, A., Simms, M.J. & Wignall, P.B. (2015) - The Carnian Humid Episode of the late Triassic: a review. Geological Magazine, 153:271–284.

Ruttner, A.W. (1984) - The pre-Liassic basement of the eastern Kopet Dagh Range. *Neues Jahrbuch für Geologie und Paläontologie-Abhandlungen*, 168: 256–268.

Ruttner A.W. (1991) - Geology of the Aghdarband Area (Kopet Dag, NE-Iran). In: Ruttner A.W. (Ed) – The Triassic of Aghdarband (AqDarband), NE-Iran and its pre-Triassic frame. *Abhandlungen der Geologischen Bundes-Anstalt,* 38: 7–79.

Saidi, A., Brunet, M.-F. and Ricou, L.-E. (1997) - Continental accretion of the Iran Block to Eurasia as seen from Late Paleozoic to Early Cretaceous subsidence curves. *Geodin. Acta*, 10, 189– 208.

Şengör, A.M.C. (1979) - Mid-Mesozoic closure of Permo–Triassic Tethys and its implications. *Nature*, 279: 590–593.

Şengör, A.M.C. (1984) - The Cimmeride orogenic system and the tectonics of Eurasia. *Geological Society of America Special Paper*, 195: 82.

Şengör A.M.C. (1990) - A new model for the late Palaeozoic-Mesozoic tectonic evolution of Iran and implications for Oman. *Geological Society Special Publication*, 49(1): 797–831.

Seyed-Emami, K. (2003) - Triassic in Iran. *Facies*, *48*(1), 91-106.

Sheikholeslami M.R. & Kouhpeyma M. (2012) - Structural analysis and tectonic evolution of the eastern Binalud Mountains, NE Iran. *Journal of Geodynamics*, 61: 23–46.

Shi, Z., Preto, N., Jiang, H., Krystyn, L., Zhang, Y., Ogg, J. G., Jin, X., Yuan, J., Yang, X., and Du, Y. (2017) - Demise of Late Triassic sponge mounds along the northwestern margin of the Yangtze Block, South China: Related to the Carnian Pluvial Phase?. *Palaeogeography, Palaeoclimatology, Palaeoecology*, *474*, 247-263.

Siblik, M. (1991) - Triassic brachiopods from Aghdarband (NE-Iran). *Abhandlungen der geologischen Bundesanstalt*, *38*, 165-175.

Simms, M.J., and Ruffell, A.H. (1989) - Synchroneity of climatic change and extinctions in the Late Triassic: Geology v. 17, p. 265–268, https://doi.org/10.1130/0091-7613(1989)017<0265:SOCCAE>2.3.CO;2

Simms, M.J., Ruffell, A.H. (1990) - Climatic and biotic change in the late Triassic. J. Geol. Soc. Lond. 147, 321–327.

Stampfli G.M. & Borel G.D. (2002) - A plate tectonic model for the Paleozoic and Mesozoic constrained by dynamic plate boundaries and restored synthetic oceanic isochrons. *Earth and Planetary Science Letters*, 196(1-2): 17–33.

Stefani, M., Furin, S. & Gianolla, P. (2010) - The changing climate framework and depositional dynamics of the Triassic carbonate platforms from the Dolomites. Palaeogeography, Palaeoclimatology, Palaeoecology, 290:43–57.

Stöcklin J. (1974) - Possible Ancient Continental Margins in Iran In: Chreighton, A.B & Drake, C.L. (Eds.), The Geology of Continental Margins:873–887. Springer Berlin Heidelberg.

Sun, Y.D., Wignall, P.B., Joachimski, M.M., Bond, D.P.G., Grasby, S.E., Lai, X.L., Wang, L.N., Zhang, Z.T., Sun, S. (2016) - Climate warming, euxinia and carbon isotope per- turbations during the Carnian (Triassic) Crisis in South China. Earth Planet. Sci. Lett. 444, 88–100.

Taheri, J., Fürsich, F.T., Wilmsen, M. (2009) - Stratigraphy, depositional environments and geodynamic significance of the Upper Bajocian-Bathonian Kashaf Rud Formation, NE Iran. Geological Society, London, Special Publications, 312 (2009), pp. 175-188.

Tozer, E.T. (1967) - A standard for Triassic time. Geological Survey of Canada Bulletin, 156, 104 pp.

Vigran, J.O., Mangerud, G., Mørk, A., Worsley, D., Hochuli, P.A. (2014) - Palynology and geology of the Triassic succession of Svalbard and the Barents Sea Geol. Surv. Norway Spec. Publ., 14 (2014), pp. 1-247.

Visscher, H., and Van der Zwan, C. J. (1981) - "Palynology of the circum-Mediterranean Triassic: phytogeographical and palaeoclimatological implications." *Geologische Rundschau*70, no. 2: 625-634.

Visscher, H., Van Houte, M., Brugman, W.A., Poort, R.J. (1994) - Rejection of Carnian (Late Triassic) “pluvial event” in Europe. Revew of Palaeobotany and Palynology 83, 217–226.

Wiggins, V.D., (1973) - Upper Triassic dinoflagellates from arctic Alaska. Micropaleontology 19, 1–17.

Wilmsen, M., Fürsich, F.T. and Taheri, J. (2009a) - The Shemshak Group (Lower–Middle Jurassic) of the Binalud Mountains, NE Iran: stratigraphy, facies and geodynamic implications. In: *South Caspian to Central Iran Basins* (M.-F. Brunet, M. Wilmsen and J. Granath, eds), Geol. Soc. London, Spec. Publ., 312, 175– 188.

Wilmsen, M., Fürsich, F. T., Seyed-Emami, K., Majidifard, M. R., & Taheri, J. (2009b) - The Cimmerian Orogeny in northern Iran: Tectono-stratigraphic evidence from the foreland. *Terra Nova*, *21*(3), 211-218.

Wöhrmann, S. (1889) - Die Fauna der sogenannten Cardita- und Rai- bler-Schichten in den Nordtiroler und bayerischen Alpen. - Jb. Geol. R.-A., 39, 181-258, pls. 5-10, Wien 1889.

Zanchetta, S., Berra F., Zanchi, A., Bergomi, M., Caridroit, M., Nicora, A. & Heidarzadeh, G. (2013) - The record of the Late Palaeozoic active margin of the Palaeotethys in NE Iran: Constraints on the Cimmerian orogeny. *Gondwana Research*, 24(3-4): 1237–1266.

Zanchi A., Zanchetta S., Berra F., Mattei M., Garzanti E., Molyneux S., Nawab A. & Sabouri J. (2009a) - The Eo- Cimmerian (Late? Triassic) orogeny in North Iran. In M.-F. Brunet, M. Wilmsen & J.W. Granath (Eds) - South Caspian, northern and central Iran sedimentary basins. *Geological Society Special Publication*, 312 (1): 31–55.

Zanchi, A., Zanchetta, S., Balini, M. & Ghassemi, M.R. (2016) - Oblique convergence during the Cimmerian collision: Evidence from the Triassic Aghdarband Basin, NE Iran. *Gondwana Research*, 38: 149–170.

Zhang, Y., Li, M., Ogg, J., Montgomery, P., Huang, C., Chen, Z.-Q., Shi, Z., Enos, P., Lehrmann, D.J., (2015) - Cycle-calibrated Magnetostratigraphy of middle Carnian from South China: Implications for Late Triassic Time Scale and Termination of the Yangtze Platform. Palaeogeogr. Palaeoclimatol. Palaeoecol. 436, 135–166. https:// doi.org/10.1016/j.palaeo.2015.05.033.

Chapter 4

Upper Triassic (Norian-Rhaetian) dinoflagellate cyst zonation of Nayband Formation, Tabas Block, East - Central Iran

First major revision received from the Journal of Palynology
on 10th February 2021

Upper Triassic (Norian-Rhaetian) dinoflagellate cyst zonation of Nayband Formation, Tabas Block, East - Central Iran

Mina Mazaheri-Johari[a]*, Mohsen Allameh[b], Ebrahim Ghasemi-Nejad[c], Piero Gianolla[d]

[a] *Department of Physics and Earth Sciences, University of Ferrara, Italy*. e-mail: mzhmni@unife.it

[b] *Department of Geology, Islamic Azad University, Mashhad Branch, Mashhad, Iran*. e-mail: *allameh0277@mshdiau.ac.ir*

[c] *Department of Geology, Faculty of Science, University of Tehran, Iran.* e-mail: *eghasemi@khayam.ut.ac.ir*

[d]*Department of Physics and Earth Sciences, University of Ferrara, Italy.* e-mail: *glr@unife.it*

*Corresponding author e-mail: mzhmni@unife.it

Abstract

The Upper Triassic Nayband Formation is a marine mixed carbonate-siliciclastic unit deposited in the Central East Iranian Microcontinent (CEIM) and records the infilling of peripheral foreland basins after the Eo-Cimmerian event. In the type section, the Nayband Formation comprises five members (Gelkan, Bidestan, Howz-e-Sheikh, Howz-e-Khan, and Qadir) which have relied heavily on terrestrial palynology to provide biostratigraphical control. This study analyses the occurrence of dinoflagellate cysts in the middle-upper Nayband Formation (the shale-dominant Bidestan Member and the overlying Howz-e-Sheikh Member) from a section of the Tabas Block, one of three structural units forming the CEIM. The studied section attains a thickness of 800 meters consists of shales, sandstones and some interbedded limestones. Palynological assessments of 174 slides derived from 58 rock samples deduced moderately diverse dinoflagellate cyst assemblages which lead to the identification of *Rhaetogonyaulax rhaetica* Zone and led to an age of ?late Norian-Rhaetian for the rock units. The recovered dinoflagellate cysts exhibit close resemblances with those recorded in Australia, Northwest Europe, Arctic Canada, and Northern Iran.

Keywords: Marine Palynology, Late Triassic, Central Iran, Nayband.

1.1.Introduction

In the fossil record and among marine palynomorphs, dinoflagellate cysts are widely considered as one of the most important associations for relative age dating and correlation, as well as proxies for some palaeoclimatology and palaeoecological aspects (Stover et al. 1996). During Late Triassic, marine deposition took place along the margins of Pangea supercontinent (Mangerud et al. 2019) and by the development of rifting episodes at this time, the spread of seafloor started and Pangea began to break up (Ziegler et al. 1983, 2003; Golonka 2004, 2007; Golonka et al. 2018). As a consequence, marine deposition occurred along some of these rifts and led to the enhancement of the areal development of marine borderlands. Surrounding the Late Triassic continents, the first dinoflagellates cysts appeared, evolved with moderately low diversities, and spread into these relatively shallow marine environments (MacRae et al. 1996; Mangerud et al. 2019).

On a global scale, Late Triassic palynological studies have mainly focused on terrestrially-derived palynomorphs while the marine palynomorph contents are not highly studied (Mangerud et al. 2019). Upper Triassic successions of Central Iran (Iran Plate) suffers from insufficient marine palynological studies, as well, and despite the early pioneer work, relatively little work has been conducted in this region since. The remoteness of the region could be the reason for comparatively few studies conducted on the Late Triassic palynology of this region. Paleogeographicaly, Triassic witnessed the collision of the Iran Plate (as part of the Cimmerian continent) with Eurasia (Eurasia: Turan Plate) (e.g., Sengör 1990; Wilmsen et al. 2009), due to the opening of the Neotethys sea and its subduction at the southern margin of the Iran Plate (Arvin et al. 2007). The exact collision timing is still controversial, although recent studies suggested later Early Carnian as the time of this collision concurrent to the onset of the Carnian Humid Episode (Krystyn et al. 2019). The subduction process, however, is thought to have developed extensional basins on the interior parts of Iran Plate in which prevalently siliciclastic sediments known as the Shemshak Group have been deposited (Fürsich et al. 2005; Mannani & Yazdi 2009; Wilmsen et al. 2009; Nützel et al. 2010) (Fig., 1 A, B). The oldest rock unit of the Shemshak Group of Central Iran is represented by the Upper Triassic Nayband Formation with a maximum thickness of approximately 3,000 m in the western part of the Lut desert where its type section was defined (Stocklin et al. 1965). An extensive outcrop of the formation has been mapped by Stocklin et al. (1965) in the southwestern part of the Shotori Mountains in the Tabas block while outcrops also occur around Ferdows, northern Lut Block (Eftekhar-Nezhhad et al. 1975).

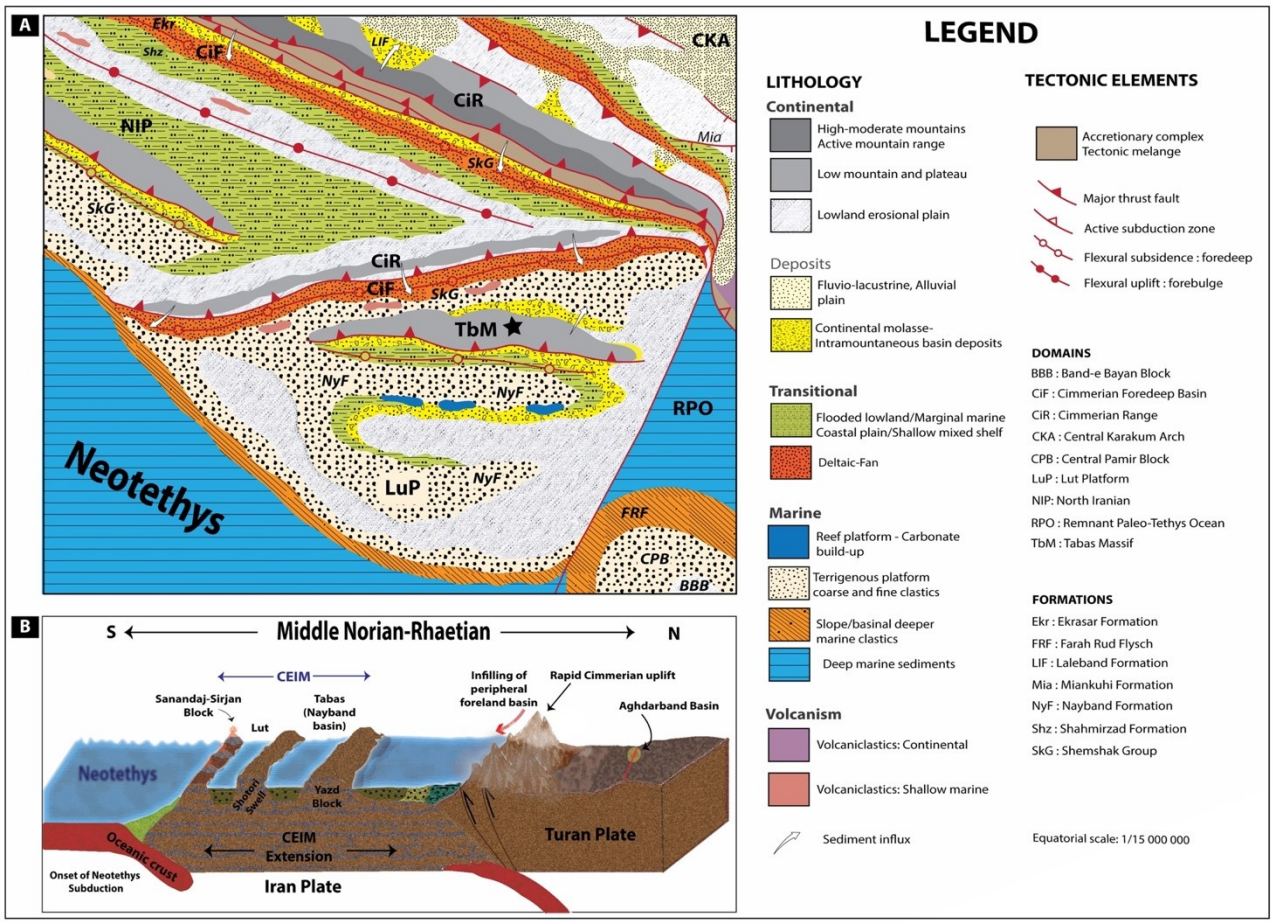

Fig. 1. A: Paleogeographic and Paleotectonic reconstruction of the Middle East in Upper Triassic (Late Norian). The studied area (Tabas Block in east-central Iran) is indicated by black star (modified from Barrier *et al*. 2018). Abbreviations: RPO: Remnant Paleo-Tethys Ocean, TbM: Tabas Massif, LuP: Lut Platform, BBB: Band-e-Bayan Block, CPB: Central Pamir Block, CiF: Cimmerian Foredeep Basin, CiR: Cimmerian Range, NIP: North Iranian Platform, CKA: Central Karakum Arch, NyF: Nayband Formation, FRF: Farah Rud Flysch, LIF: Laleband Formation, Mia: Miankuhi Formation, Shz: Shahmirzad Formation, SkG: Shemshak Group, Ekr: Ekrasar Formation. **B:** Geodynamic model of Iran, not to scale, during the Middle Norian-Rhaetian (modified from Wilmsen *et al*. 2009b).

Based on the investigations of Steel National Company (SNC) in the type section, the southern flank of Nayband Mountain, five members form the Nayband Formation, which are in ascending stratigraphic order, the Gelkan, Bidestan, Howz-e-Sheikh, Howz-e-Khan, and Qadir. The lithological members have distributed in four different areas in the Tabas Block including the Parvade area, Nayband area, Kuhbanan-Buhabad area, and Kerman area (Fig., 2). However, rapid lateral facies changes and strongly varying thicknesses of these members at the type

section make it difficult to trace them inter-regionally (Fursich et al. 2005). Late Triassic palynological study of Central Iran, can be dated back to the 1970s. Arjang (1975) first reported the spore-pollen fossils from the Late Triassic (upper Rhaetian) coal-bearing deposits of Kerman area, Central Iran (Iran Plate). Since then, several palynologists investigated the palynomorph contents, particularly terrestrial ones, in different localities of this basin (e.g. Kimyai 1977; Achilles et al. 1984; Bharadwaj & Kumar 1986; Cirilli et al. 2005; Sajjadi et al. 2015; Sabbaghiyan et al. 2015).

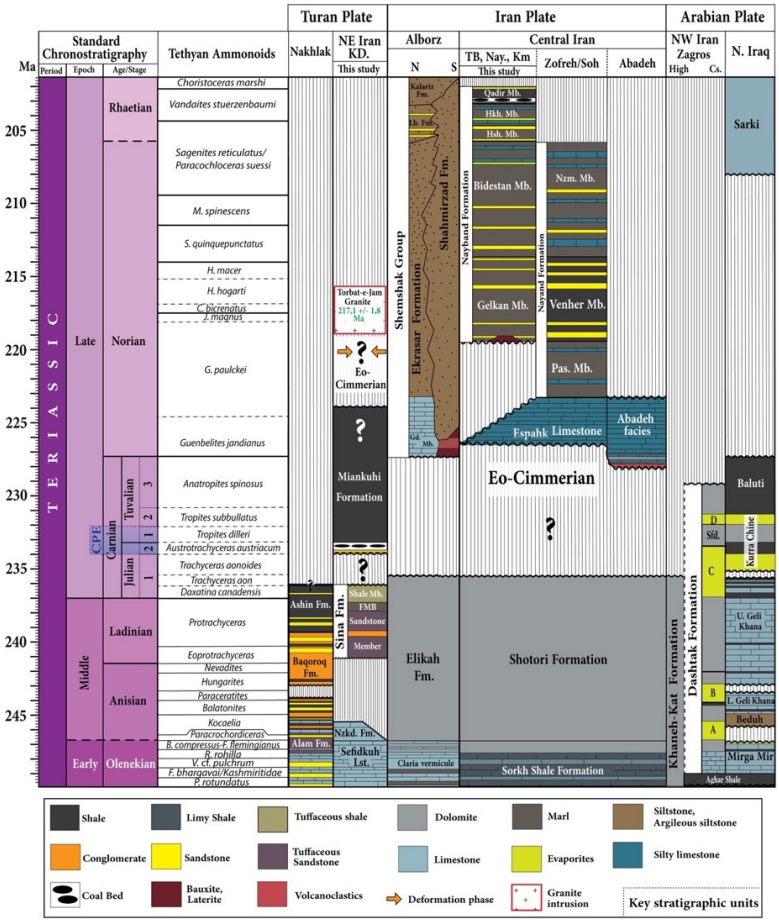

Figure 2: Lithostratigraphy of Triassic rock units from Iran region (Turan Plate, Iran Plate, and Zagros basin) and NE Iraq as part of the Arabian Plate (modified after Seyed-Emami, 2003, 2009; Fürsich et al., 2005, 2009; Balini et al., 2009; Krystyn et al., 2019; Liaghat et al., 2021; Lunn et al., 2019). Ammonoid zones: *P. rotundatus: Prionolobus rotundatus*, *F. bhargavai/Kashmiritidae: Flemingites bhargavai/Kashmiritidae*, *V.* cf. *pulchrum*: *Vercherites* cf. *pulchrum*, *R. rohilla*: *Rohillites rohilla*, *B. compressus*: *Brayardites compressus*, F. flemingianus: *Flemingites flemingianus*. Abbreviations: Std. Standard; KD: Kopeh-Dagh; TB: Tabas Block; Nay: Nayband area; Km: Kerman region; Cs: Coastal; Nzkd. Fm.: Nazar-Kardeh Formation; Shale Mb.: Shale Member; Gd. Mb.: Galanderud Member; Lb. Fm.: Laleband Formation; Hsh. Mb.: Howz-e-Sheikh Member; Hkh. Mb.: Howz-e-Khan Member; Pas. Mb.: Parsefid Member; Nzm. Mb.: Niazmargh Member; Sfd: Sefidar limestone; L. Geli Khana: Lower Geli Khana; U. Geli Khana: Upper Geli Khana.

Based on some preliminary work carried out from the 1920s, different ages have been attributed to the Nayband Formation as early Triassic to Rhaetian (Douglas 1929), Ladinian to Rhaetian (Seyed-Emami 1971) and Late Triassic (Bronniman et al. 1971; Senowbari-Daryan et al. 1997). The basal part of the Nayband Formation in the Zefreh/Soh facies (Isfahan, Central Iran) is assigned to the late Middle Norian based on ammonoid fauna (Krystyn et al. 2019) while in the Nayband area, where this fauna is not present, age of Early Norian is detected based on terrestrial-palynomorphs (Cirilli et al. 2005). The overlying Niazmargh (Zefreh/Soh facies, Isfahan) and Bidestan (Nayband and Parvasdeh areas) members have been dated as late Norian on the basis of the occurrence of the bivalve *Monotis salinaria* and *Heterastridium* (Krystyn et al. 2019). The occurrence of *Rhaetavicula contorta* (Portlock 1843) and the absence of *Heterastridium* in Howz-e-Sheikh and Howz-e-khan members led to an age of Rhaetian for these rock units (Krystyn et al. 2019). A Triassic-type bivalve fauna with the presence of the genus *Indopecten* from the last unit of this succession, Qadir Member, recorded an early Rhaetian age for the top of the Nayband Formation (Hautmann 2001; Krystyn et al. 2019).

Since 2000, age dating of the Nayband Formation using palynological investigations has received much more attention and different outcrops of the formation and its correlative successions throughout the Iran plate examined with the purpose of age determination and revealing the corresponding paleoenvironmental circumstances. Cirilli et al. (2005) assigned an early Norian age to the Gelkan Member and most of the Bidestan Member in a section close to the type section (Nayband section) while the upper part of the Bidestan Member is dated as Middle to Late Norian, and the lower part of the Howz-e-Sheikh Member is thought to correspond to the Rhaetian. A recent palynological study on the Nayband Formation revealed reasonably diverse and relatively preserved palynofloras of exclusively terrestrial derivation in the Kamar Macheh Kuh, southeastern Tabas, east-central Iran (Sajjadi et al. 2015). The palynofloras comprise radially symmetrical and monolete spores and pollen and based on the key misopore species an age of Norian-Rhaetian has been allocated to the host strata (Sajjadi et al. 2015). Indeed, the predominance of ferns and coniferophytes in the parent flora of the palynofloras studied by Sajjadi et al. (2015) led to the discovery of a moist warm climate at the time of the deposition of Nayband Formation which proceeds by decreasing temperature during late Late Triassic. However, these conclusions derived from terrestrial palynomorphs and no marine palynomorphs encountered in the examined samples. Association of marine palynomorphs (dinoflagellate cysts) studied by Sabbaghiyan et al. (2015) indicate a Late

Triassic (Rhaetian) age for the Qadir Member of the Nayband Formation in the Parvadeh area of the Tabas block.

Paleozoic and Mesozoic rock units of the Central Iran Basin are similar to those of Alborz Basin, north of Iran, and therefore similar facies representing similar depositional conditions can be detected in lithostratigraphic units of two basins (Agha-Nabati 1977). Unpublished preliminary work was performed on the palynological contents of the lower sandstone up to the upper carbonaceous units in the northern Alborz Mountains and the age of Rhaetian to Jurassic was concluded based on spore and pollen grains (NISCO: National Iranian Steel Company 1998). A similar section in this basin, southwest of Zirab city, was described by Dabiri (2002) and dated as Norian–Rhaetian based on palynomorphs. Ghasemi-Nejad et al. (2004) investigated the Triassic part of the Shemshak Group in the Galandrud area, north of the Alborz Mountains, palynologicaly. Their investigations yielded a relatively rich assemblage of dinoflagellates that are comparable to the well-known biozones discovered in the Triassic successions of Australia. Based on the dinoflagellate associations and the ammonites found by Ghasemi-Nejad et al. (2004), an age of early Norian has been determined for the base of the Shemshak group. Furthermore, another palynological study of the Upper Triassic rocks of Iran was done on the basement of the Koppeh-Dagh Range, Aghdarband Group (Ghasemi-Nejad et al. 2008) and revealed close similarity between the Upper Triassic dinoflagellate cyst associations of Aghdarband Group, Miankuhi Formation, with assemblages reported from Australia, New Zealand, Indonesia, Northwest Europe, arctic Canada, and Alaska while the age of early Late Norian was implied for this formation based on the association recorded (Ghasemi-Nejad et al. 2008).

As discussed above, previous works on the Upper Triassic sequences of Iran, particularly Central Iran, are mainly focused on terrestrial palynology while there is still a need for exploring the marine palynological contents of these successions which are not widely understood. Palynological analysis of the Nayband Formation of the Tabas Block, part of the Central East Iranian Microcontinent (CEIM; Takin 1972), therefore, is undertaken to refine the stratigraphic distribution of the dinoflagellate cyst assemblages and improve our knowledge of the cyst zonation of this succession to evaluate precise age of the rock unit. Subsequently, a comparison between identified cyst zonation and zonal assemblages reported worldwide will also be pursued.

1.2.Geological setting

In the late Triassic, Central Iran (CI) as an extensive land located between Paleothetys and Neothetys suture zones (Stocklin 1968), was consisting of several normal faults due to tectonic movements and extensional regime while, it was a stable platform throughout Paleozoic (Davoudzadeh 1997). As a significant sector of CI, the Central-East-Iran microplate (CEIM; Takin 1972) occupied the northeast of the Urumieh–Dokhtar magmatic Belt (UDMB) and is surrounded by Sistan, Naein and Baft ophiolitic suture zones, Doroone fault and Kashmar-Sabzevar ophiolites. This microplate encompasses different structural components that are not similar in lithostratigraphic aspects and they are separated by major faults (Soffel et al. 1996). These blocks are including Lut Block, Yazd Block, Anarak-Khur Block, and the Kerman-Tabas Block, (See Berberian & King 1981; Berberian et al. 1982; Davoudzadeh 1997; Soffel et al. 1996 for geological overviews) (Fig., 3 A). This study is conducted on the Tabas Block, where Mesozoic and Paleozoic sedimentary strata are well-developed (Soffel et al. 1996). The Nayband Formation of the Nayband area is composed of various siliciclastic rocks and mixed carbonate-siliciclastic deposits. The lower contact of the Nayband Formation leads to Middle Triassic ancient karst called Shotori Formation and the upper contact ambiguously ends up with the Lower Jurassic Ab-e Haji Formation due to the high facies similarity between the Upper Triassic (Nayband Formation) and Lower Jurassic succession (Ab-e Haji Formation) (Kluyver et al. 1983).

The chief reason for opting the Tabas Block as our study area was relatively well-development of Nayband Formation in this block in the CEIM and based on earlier literature (e.g. Hautmann 2001), the fauna of Nayband Formation (ammonoides, bivalves, sponges, corals, brachiopods) demonstrates moderately high diversity in this block, as well (e.g. Fürsich et al. 2005; Krystyn et al. 2019). The present research has been carried out on a section (we have called Sar-Chelenoh) close to the type section of the formation, 8 km west of Naybandan village and in the vicinity of Sar-Chelenoh village in the middle part of the Tabas block near its eastern border (Nayabandan fault) (Fig., 3B).

1.3.Upper Triassic Marine Palynology

According to MacRae et al. (1996), during the Norian stage, the diversity of dinoflagellate cysts is limited to a small number of about 24 species worldwide and they continued to expand throughout the Jurassic and reached the peak of diversity in the Cretaceous (Mangerud et al. 2019). A few studies, therefore, are present on the dinoflagellate cysts recorded in the Late Triassic marine sequences. These include the present Arctic (The Norwegian Arctic, The

Sverdrup Basin, Alaska, and Arctic Russia), Europe, Iran, Australia, and Africa (Mangerud et al. 2019 and references therein). Northwest Europe, where the standard Triassic GSSPs are located, consists of most of the studies on this issue for the Northern Hemisphere and the oldest dinoflagellate cysts founded in this region are assigned to the *Rhaetogonyaulax rhaetica* Zone of Rhaetian age. The base of this zone was placed at the base of the Rhaetian Stage (Morbey 1978), although the international definition of the Rhaetian Stage and the position of its base is still a controversial issue (Ogg 2005; Kuerschner et al. 2007). The temporal and spatial distribution of Triassic dinoflagellate cysts is discussed by Mangerud et al. (2019).

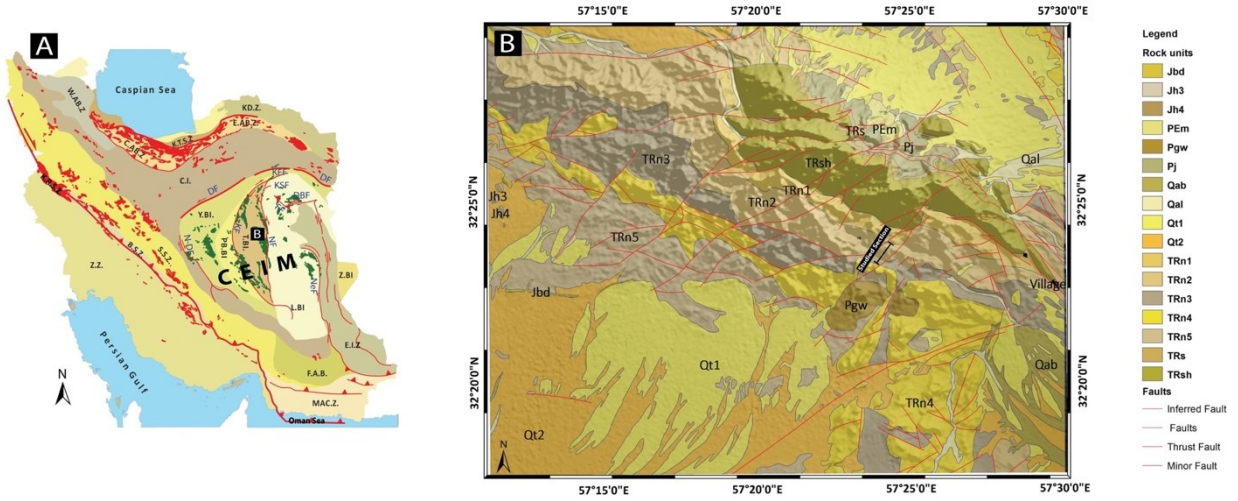

Fig. 3. A: Distribution of Triassic deposits in Iran. Triassic deposits of East-Central Iran and the other zones have been shown in green and orange, respectively. Its base map illustrates the main structural zones of Iran plateau and major faults of CEIM block (after Allen *et al*. 2004, 2011; Berberian, 1983; Berberian & King, 1981; Calzolari, Della Seta, *et al*. 2016; Morley *et al*. 2009; Nozaem *et al*. 2013; Stöcklin & Nabavi, 1973): B.S.Z: Bisutun sub-zone; C.AB.Z: Central Alborz zone; E.AB.Z: Eastern Alborz zone; W.AB.Z: Western Alborz zone; C.I: Central Iran; E.I.Z: Eastern Iran zone; Z.Z: Zagros zone; S.S.Z: Sanandaj-Sirjan zone; F.A.B: Forearc basin; K.R.S.Z: Kermanshah Radiolarite sub-zone; K.T.S.Z: Khazar-Talesh sub-zone; KD.Z: Koppeh-Dagh zone; L.BI: Lut Block; T.BI: Tabas Block; PB.BI: Posht-e-Badam Block; Y.BI: Yazd Block; MAC.Z: Makran zone; Z.BI: Zabol Block; DBF: Dasht-e-Bayaz Fault; DF: Doruneh Fault; FF: Ferdows Fault; KF: Kuhbanan Fault; KFF: Kuh-e-Faghan fault; KSF: Kuh-e-Sarhangi fault; NF: Naybandan Fault; N-DF: Nain-Dehshir Fault; NeF: Neh Fault. **B:** Simplified geological map of the studied area (Modified from Naybandan geology map (scale: 1:100000), Provided by the Geological Survey of Iran, 1981); Its base map is Digital Elevation Model (DEM). Rock unit description: PEm: Phyllitic, sandy siltstone, shale; Pj: Conglomerate, sandstone, and shale; TRn1: Recessive dark grey-green shale, arkose laterite at base Gelkan Member; TRn2: Shale, sandstone, thin orange weathering limestone fossiliferous Bidestan Member; TRn3: Recessive shale and sandstone, grey-green Howz-e-Sheikh Member; TRn4: Cliff-forming, grey, fossiliferous, reefal limestone Howz-e-Khan Member; TRn5: Silty

sandstone, shale shaly siltstone, thin limestone, coal seams; TRs: Orthoquartzite and laterite at base, oolitic limestone, yellow and red shaly limestone; TRsh: Massive dolostone, light coloured, thin grey; Jbd: Shale and thin limestone, thick oolitic limestone at top; Jh3: Sandstone, shale, (intercalated), thin coal seams; Jh4: Shale, siltstone, recessive, minor sandstone; Pgw: Rhyolitic-dacitic (welded) tuff; Qab: Alluvium in braided channels and flood plains; Qal: Alluvium in major stream channels or immediately adjacent; Qt1: Alluvium in older terraces; Qt2: Alluvium in young terraces; (PE: Pre Cambrian; Pj: Permian; TR: Triassic; J: Jurassic; Pg: Paleogene; Q: Quaternary).

1.4.Materials and methods

Fifty-eight rock samples were collected from the Bidestan and Howz-e-Sheikh members of the Nayband Formation at Sar-Chelenoh section, near the eastern border of Tabas block and prepared in the palynology laboratory of the Department of Geology of the University of Tehran using the Traverse (2007) preparation method.

The lower member (the Bidestan Member) is dominantly made up of shale while the upper one (the Howz-e-Sheikh Member) encompasses a lithology of shale with a high number of sandstone thin interbeds (Fig., 4). Lithologically, soft to rough shale layers of the Bidestan Member, with a thickness of 520m, mostly show a gray to green color that are included some interbedded limestones on scales from centimeters to several meters. The interbedded fossiliferous limestones are comprised of ripple mark traces in some intervals. The Bidestan Member is overlain by the Howz-e-Sheikh Member that reaches a thickness of 280m. It consists mainly of shales with red sandstone interbeds including ripple mark traces in some layers. The collected samples were crushed into tiny pieces (about 2 mm) and dried after the passing washing process. To dissolve carbonates, the crushed samples were soaked in Cold hydrochloric acid (HCL, 10%), neutralized with distilled water, and afterward the hydrofluoric acid (HF, 50%) was used to dissolve silicates. The residue was neutralized again and boiled in HCL (10%) and then centrifuged in $ZnCl_2$ (specific gravity 1.9) to segregate heavy minerals. Eventually, a 15 μm nylon mesh was used to sieve the residues, and then they mounted onto microscope slides using liquid Canada balsam as the mounting medium.

The microscope slides were investigated under a Leica DM750 light microscope, and the index species were photographed using the Leica ICC50 W digital camera and have been presented in Plate I. Indeed, the stratigraphic distribution of the identified taxa is drawn and presented as Figure 4. The slides are housed in the Department of marine and earth sciences, University of Ferrara.

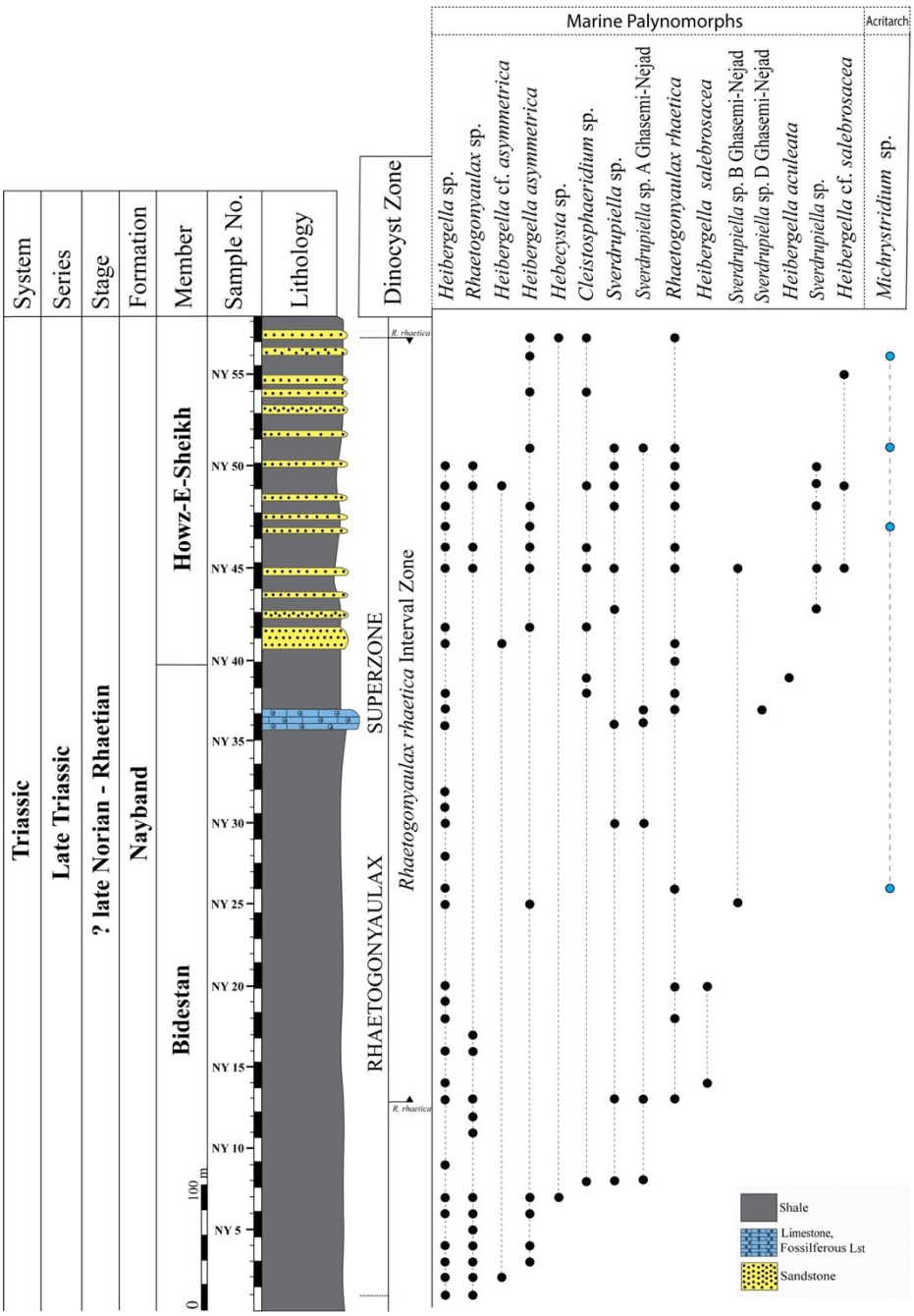

Fig. 4. Biozonation and stratigraphic distribution of dinoflagellate cysts throughout the Bidestan and Howz-e-Sheikh Members of the Nayband Formation in the Tabas Block, Central Iran.

1.5.Results

1.5.1. Palynology of Nayband Formation

The dominant components of the studied slides are the dark brown to black and mostly degraded biostructured woody tissues, including tracheidal phytoclasts, with subordinate angular black particles (Pl. 1, Fig., 27). A rare number of fungal spores is also present while amorphous organic matter (AOM) is not recorded, or only rarely present in a couple of slides. Spores and pollen grains are recorded relatively frequent (more than 40% of the total number

of particles) and dinoflagellate cysts are present sporadically (up to 5–10% of the total number of particles). *Heibergella*, *Hebecysta*, *Sverdrupiella*, *Cleistosphaeridium,* and *Rhaetogonyaulax* form the dominant floras of the studied successions. The marine palynomorphs, however, are poorly-preserved and many specimens have undergone strong thermal alteration as the finer morphological features are usually not preserved. Although the specimens suffered from severe corrosion, it is possible to identify some of them to generic and even tentatively specific levels based on their distinctive overall morphology as usually happens in marginal palynology (Traverse 1972). The poor preservation of specimens, however, makes it difficult to obtain reliable counts of specimens (from one to three specimens were recorded on each slide). Figure 4 illustrates the spatial distribution of detected taxa and the better-preserved specimens are presented on Plate I.

1.5.2. Dinoflagellate cyst assemblages

Records of dinoflagellate cysts from the Bidestan and Howz-e-Sheikh members of the Nayband Formation can be assigned to a single association comprised of specimens assigned to five previously described genera. The Genus *Heibergella* is represented by *Heibergella* sp. cf. *H. asymmetrica* Bujak & Fisher, 1976 (Pl. 1, Figs. 1-3); *Heibergella* sp. cf. *H. aculeata* Bujak and Fisher, 1976 (Pl. 1, Fig. 4); *Heibergella* sp. (Pl. 1, Figs. 5-7); *Heibergella* sp. cf. *H. salebrosacea* Bujak & Fisher, 1976 (Pl. I, Figs. 8, 9). The Genus *Hebecysta* is recorded by *Hebecysta* sp. Bujak & Fisher, 1976 (Pl. I, Fig. 10). The Genus *Rhaetogonyaulax* is represented by *Rhaetogonyaulax* sp. (Pl. I, Fig. 11) and *Rhaetogonyaulax rhaetica* Woollam & Riding, 1983 (Pl. I, Figs. 12-15). The Genus *Sverdrupiella* is represented by an unidentified species as *Sverdrupiella* sp. Bujak & Fisher, 1976 (Pl. I, Fig. 16), and the informally designated *Sverdrupiella* sp. A Ghasemi-Nejad et al. 2008 (Pl. I, Figs. 17-20), *Sverdrupiella* sp. B Ghasemi-Nejad et al. 2008 (Pl. I, Figs. 21, 22), and *Sverdrupiella* sp. D Ghasemi-Nejad et al., 2008 (Pl. I, Fig. 23). The Genus *Cleistosphaeridium* is represented by *Cleistosphaeridium* sp. Davey et al. 1966 (Pl. I, Figs. 24, 25).

Plate I

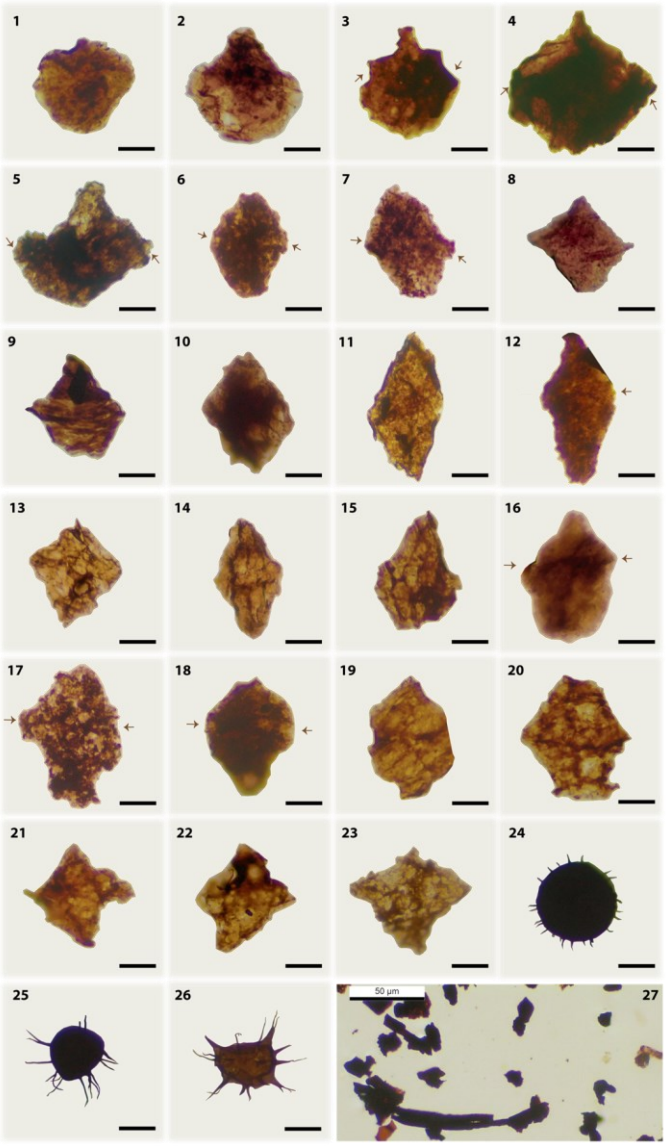

Plate I. Dinoflagellate cysts recorded from the Bidestan and Howz-e-Sheikh members of the Nayband Formation (Rhaetian) East-Central Iran. The scale bar represents 10 µm and the light brown arrows representing the cingulum of dinocysts. **1-3.** *Heibergella asymmetrica* Bujak and Fisher, 1976. 1: sample NY - 42, slide 42c, 2: sample NY - 46, slide 46b, 3: sample NY - 45, slide 45a. **4.** *Heibergella aculeata* Bujak and Fisher, 1976. sample NY - 39, slide 39a. **5-7.** *Heibergella* sp., 5:sample NY - 26, slide 26c, 6: sample NY - 32, slide 32c, 7: sample NY - 45, slide 45a. **8-9.** *Heibergella salebrosacea* Bujak and Fisher, 1976. 8: sample NY - 14, slide 14a, 9: sample NY-20, slide 20b. **10.** *Hebecysta* sp. sample NY - 57, slide 57c. **11.** *Rhaetogonyaulax* sp. sample NY - 46, slide 46b. **12-15.** *Rhaetogonyaulax rhaetica* (Sarjeant, 1963) Loeblich and Loeblich, 1968. 12: sample NY - 45, slide 45a, 13: sample NY - 26, slide 26c, 14: sample NY - 40, slide 40a, 15: sample NY - 51, slide 51a. **16.** *Sverdrupiella* sp. sample NY - 50, slide 50b. **17-20.** *Sverdrupiella* sp. A (Ghasemi-Nejad et al., 2008). 17: sample NY - 8, slide 8b, 18: sample NY - 13, slide 13c, 19: sample NY - 36, slide 36b, 20: sample NY - 37, slide 37b. **21-22.** *Sverdrupiella* sp. B (Ghasemi-Nejad et al., 2008). 21: sample NY - 45, slide 45c, 22: sample NY - 25, slide 25a. **23.** *Sverdrupiella* sp. D (Ghasemi-Nejad et al., 2008). 23: sample NY - 37, slide 37c. **24-25.** *Cleistosphaeridiurn* sp., 24: sample NY – 49, slide 49a, 25: sample NY – 45, slide 45b. **26.** *Michrystridium* sp. sample NY - 56, slide 56b. **27.** sample NY - 30, slide 30a.

1.6.Discussion and Comparison

In the present study, the recorded assemblages yielded some confined taxa with those recorded in the present Arctic (Canadian Arctic and Barents Sea/Svalbard), Northwest Europe (United Kingdom), Iran (Alborz Mountains, Koppeh-Dagh Basin, and Central Iran), and Oceanica (Australia and New Zealand). These include *Heibergella asymmetrica, Heibergella aculeata, Heibergella salebrosacea, Heibergella* sp., *Hebecysta* sp., *Sverdrupiella* sp., *Rhaetogonyaulax* sp.*, Rhaetogonyaulax rhaetica*, and *Cleistosphaeridium* sp. (Plate. I).

The genus *Heibergella* has been reported from Carnian to Rhaetian in the northern hemisphere and from Norian to Rhaetian in the southern hemisphere (e.g., Baranyi et al. 2019; Bucefalo Palliani & Buratti 2006). This taxon was limited to higher palaeolatitudes throughout Carnian and Norian (Australia, Seram, Arctic Canada, and New Zealand) (e.g., Bujak & Fisher 1976; Felix & Burbridge, 1978; O'Sullivan et al. 1985; Helby et al. 1987b; Helby & Wilson 1988; Martini et al. 2004; Mantle et al. 2020) while, they occupied the middle palaeolatitudes of the Northern Hemisphere during the Rhaetian (England and Austria: Morbey 1975; Morbey & Dunay 1978; Gaunt et al. 1992). The Genus *Sverdrupiella*, which occurs intermittently through the studied section, has been reported from Norian strata of Arctic Canada, Alaska, New Zealand, Indonesia and Australia (e.g., Bujak & Fisher 1976; Witmer et al. 1981; Helby et al. 1987b; Helby & Wilson 1988; Martini et al. 2004; Riding et al. 2010; Mangerud et al. 2019; Mantle et al. 2020), Norian to Rhaetian strata of Iran (Ghasemi-Nejad et al. 2004, 2008; Sabaghian et al. 2015), and Rhaetian strata of United Kingdom (e.g., Warrington 1974; Below 1987a; Bucefalo Palliani & Buratti 2006).

In the Barents Sea, the records of *Sverdrupiella mutabilis*, *Heibergella asymmetrica*, and *Heibergella salebrosacea* co-occurring with *Rhaetogonyaulax arctica* have been reported in the Assemblage C which they assigned an early Norian age (Hochuli et al. 1989). On Spitsbergen, *Rhaetogonyaulax rhaetica* is the dominant species throughout the Knorringfjellet Formation (Norian) but *Heibergella* and *Sverdrupiella* are also present (Vigran et al. 2014). This association was observed at Wilhelmøya Island in eastern Svalbard, as well (Vigran *et al.* 2014). In the Central Barents Sea, Flatsalen Formation, a rich assemblage of *Rhaetogonyaulax*, including *Rhaetogonyaulax rhaetica*, along with *Sverdrupiella* was also described by Vigran et al. (2014) and Paterson et al. (2018). In the southern Barents Sea, low numbers of *Rhaetogonyaulax rhaetica* were found in the Norian strata from exploration wells (Vigran et al. 2014; Paterson & Mangerud 2017) while a few species of *Noricysta* and *Sverdrupiella* were reported from an offshore well in strata of presumed Norian age (Vigran et al. 2014).

In the western Sverdrup Basin, lower Heiberg Formation, *Sverdrupiella*, *Heibergella*, *Noricysta*, and *Hebecysta* were found in a relatively high number while *Rhaetogonyaulax* was reported as being extremely sporadic and rare but persistently present (Bujak & Fisher 1976; Fisher & Bujak 1975). However, the representatives of the genus *Rhaetogonyaulax* is often abundant in Late Triassic sediments from the Arctic Island with a close resemblance to *Rhaetogonyaulax rhaetica* from the Rhaetian of England (Fisher & van Helden 1979). The same assemblage including *Sverdrupiella usitata*, *Hebecysta brevicornuta*, *Heibergella asymmetrica*, *Noricysta fimbriata*, *Rhaetogonyaulax arctica*, and *Rhaetogonyaulax rhaetica* was reported from offshore exploration wells (Felix & Burbridge 1977, 1978). On Ellesmere Island from the eastern Sverdrup Basin, rich assemblages of terrestrial palynomorphs and dinoflagellate cysts were described by Suneby & Hills (1988) who erected four palynozones for the Heiberg Formation and the uppermost Barrow Formation. The youngest of these palynozones was characterized by the first occurrence of the dinoflagellate cysts *Hebecysta brevicornuta*, *Noricysta fimbriata, Noricysta pannucea*, *Heibergella aculeata*, *Heibergella asymmetrica*, *Sverdrupiella mutabilis*, *Sverdrupiella sabinensis* and *Sverdrupiella usitata* and a Norian age was detected based on an ammonite and bivalves (Norford et al. 1973; Embry 1982).

In the European Basins, *Rhaetogonyaulax rhaetica* and *Dapcodinium priscum* were reported from the Rhaetian successions of western Switzerland (Mettraux & Mohr 1989) and theses species together with *Valvaeodinium* spp. were described by Schneebeli-Hermann et al. (2018) in the Rhaetian rock units of northern Switzerland. *Rhaetogonyaulax rhaetica* has been also recorded from the upper Rhaetian mergel-facies in the Calcareous Austrian Alps (Karle, 1984) while it was reported by Morbey & Neves (1974) and Morbey (1975) from the lowermost Rhaetian of Kendelbachgraben in Austria. Indeed, Hoelstein (2004) and Kürschner et al. (2007) recorded this species from the Kössen beds and Tiefengraben of Austria, respectively. Slovakia, Tatra Mountains, is another region where rare to common occurrences of *Rhaetogonyaulax rhaetica* have been reported from a Triassic–Jurassic boundary section (Ruckwied & Götz 2009; Michalík et al. 2010). This species was indeed described by Paterson & Mangerud (2015) from the Early Norian successions at Hopen, Norway. The Genus *Rhaetogonyaulax* was recognized from the Rhaetian successions of England, as well (e.g., Warrington 1974; Below 1987a). Furthermore, a rich dinoflagellate cyst assemblage dominated by *Rhaetogonyaulax rhaetica* with rare records of *Heibergella asymmetrica*, *Heibergella* sp. cf. *H. salebrosacea*, *Suessia swabiana*, *Noricysta pannucea*, and *Sverdrupiella mutabilis* was

recorded in the Rhaetian of St Audrie's Bay and Manor Farm in southwest England (Bucefalo Palliani & Buratti 2006). The sporadic occurrences of *Rhaetogonyaulax rhaetica* and *Rhaetogonyaulax* sp. have been reported from the Rhaetian Höganäs Formation of southern Sweden (Lindström 2002) while the species *Rhaetogonyaulax rhaetica* found dominantly in the Rhaetian successions near Lyon, France (Courtinat et al. 1998). *Rhaetogonyaulax rhaetica* together with *Dapcodinium priscum* were also observed in the Rhaetian of the Massif-Central, south of Lyon (Courtinat et al. 2002).

Helby et al. (1987a) defined the Shublikodinium (now Rhaetogonyaulax) Superzone with an age of Anisian–Pliensbachian in the North West Shelf of Australia. The oldest zone was based on the lowest occurrence of *Hebecysta balmei*, *Rhaetogonyaulax wigginsii*, *Suessia listeria* (now *Wanneria listeri*), and *Rhaetogonyaulax rhaetica*. Later, a palynological revision was performed by Riding et al. (2010) and they detected an age of Late Ladinian, probably Carnian, for the zones of the *Rhaetogonyaulax* Superzone of Australia. Riding *et al.* (2010) have indeed considered the uppermost occurrence of *Rhaetogonyaulax rhaetica* within the latest Triassic. A recent palynological study from the Upper Triassic successions of the Northern Carnarvon Basin, Western Australia, has indeed documented a diverse assemblage of dinocysts including Hebecysta, Heibergella, Noricysta, Sverdrupiella, Rhaetogonyaulax, Wanneria, Suessia, Dapcodinium, Beaumontella, and Goodwynia as a new genus (Mantle et al., 2020). In New Zealand, the occurrence of *Sverdrupiella* as the dominant dinoflagellate genus was recorded in association with only one single specimen of *Rhaetogonyaulax* in beds with Monotis shell beds, which correlates to the Cordillaranus Zone of late Norian age (Helby & Wilson 1988). An assemblage of *Beaumontella delicata*, *Beaumontella caminuspina*, *Heibergella asymmetrica*, *Heibergella aculeata*, and *Rhaetogonyaulax rhaetica* was recorded from Indonesia and correlated to the middle-upper Norian *Heibergella* (now *Hebecysta*) *balmei* Interval Zone of Helby *et al.* (1987a) (Martini *et al.* 2004). *Heibergella* spp. and *Rhaetogonyaulax rhaetica* were also reported from the Andaman Islands, India (Sharma & Sarjeant 1987). One specimen of Rhaetogonyaulax was found in the Flagstone Benc Formation of East Antarctica by Foster *et al.* (1994) which is concurrent with the Onslow Microflora of Norian age.

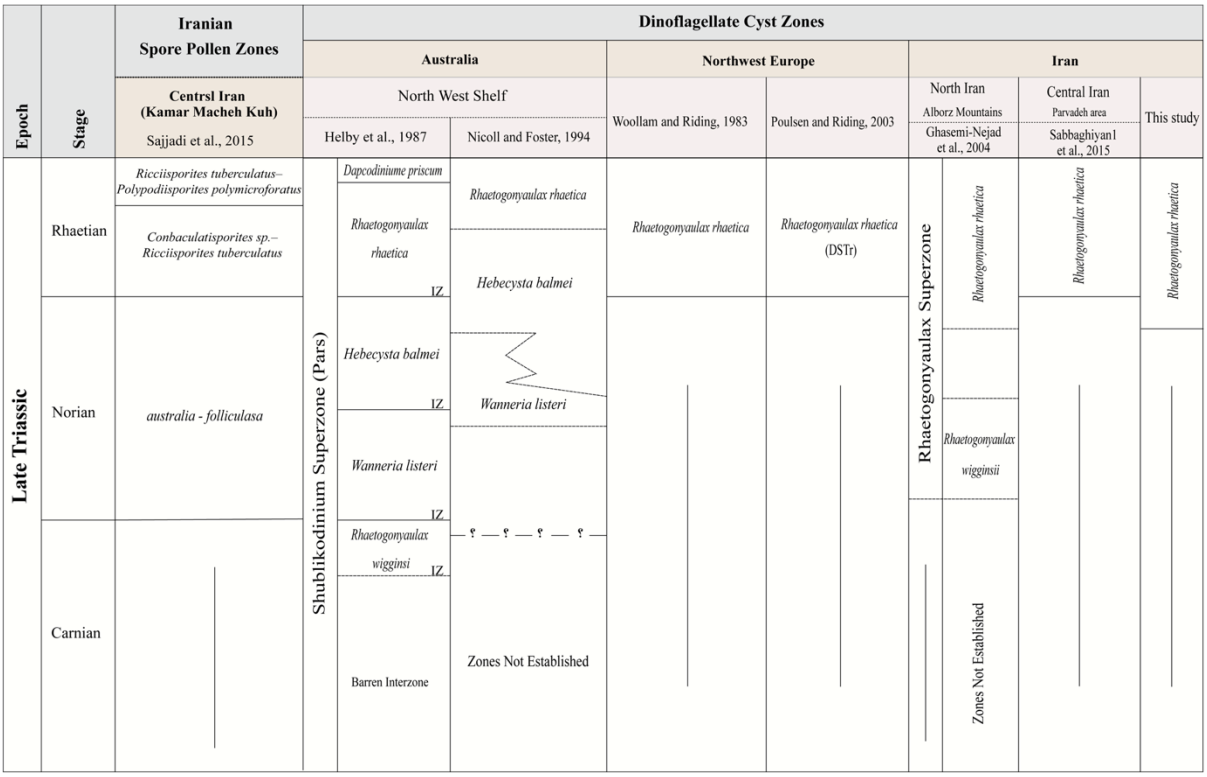

Table 1. Comparison and correlation of the dinoflagellate cyst zonation erected for the studied strata (Bidestan and Howz-e-Sheikh Mbrs of the Nayband Formation), with those of Northwest Europe (Poulsen and Riding, 2003; Woollam and Riding, 1983), Australia (Nicoll and Foster, 1994; Helby et al., 1987), North Iran (Ghasemi- Nejad et al*.,* 2004) and Central Iran (Sabbaghiyan et al., 2015).

Some palynological studies have reported dinoflagellate cysts from the Upper Triassic successions in different parts of Iran. Ghasemi-Nejad *et al.* (2004) recognized the *Rhaetogonyaulax wigginsii* and *Rhaetogonyaulax rhaetica* zones of the *Rhaetogonyaulax* Superzone. *Rhaetogonyaulax wigginsii* zone is comprised of abundant *Heibergella aculeata*, *Heibergella asymmetrica,* and *Heibergella salebrosacea* with an age of lower-middle Norian based on the ammonite contents. From northeastern Iran, Koppeh-Dagh Basin, diverse and poor-preserved Norian dinoflagellate cyst assemblages recorded by Ghasemi-Nejad *et al.* (2008) from the Miankuhi Formation. The assemblages included various species of *Heibergella*, *Hebecysta, Sverdrupiella*, *Rhaetogonyaulax*, and to two indeterminate genera with an age of Upper Norian based on the *Heibergella balmei* zone of Australia. Recent work on the Qadir Member of Nayband Formation in east-central Iran (Sabbaghiyan *et al.* 2015) reported a relatively rich dinoflagellate cyst assemblage. *Rhaetogonyaulax rhaetica* in association with *Dapcodinium priscum*, *Hebecysta brevicornuta*, *Heibergella asymmetrica*,

Heibergella kendelbachia, *Heibergella salebrosacea*, *Noricysta pannucea,* and *Sverdrupiella* cf. *mutabilis* are present throughout the interval studied. The age of this unit is Rhaetian based on plant macrofossils.

1.6.1. Dinoflagellate cyst Zonation and age attribution

Considering the maximum abundance of dinoflagellate cyst species and based on their first and last appearances throughout the studied section, the *Rhaetogonyaulax* Superzone was recognized. This superzone, which is equivalent to the late Triassic *Shublikodinium* Superzone (Shublikodinium is a junior synonym for Rhaetogonyaulax based on Stover & Evitt (1978) and Helby *et al.* (1987)), encompasses here only the *Rhaetogonyaulax rhaetica* Zone (Fig., 4).

This zone is characterized by the first common occurrence and the last appearance of *Rhaetogonyaulax rhaetica* and is assigned to Upper Triassic (Rhaetian) according to the Woollam and Riding, 1983, who erected this biozone for the first time from Rhaetian strata in Britain. This dinocyst zone encompasses an extensive range of our studied section (approximately 712m out of 800m). The index species was recorded in some samples collected from both Bidestan and Howz-e-Sheikh members (from 165m to 782m).

The range of the prominent *Rhaetogonyaulax rhaetica* clearly defines this zone, although this can be controlled by provincialism and environmental conditions as it is prominent in open marine settings and rare in some shallower marine environments (Riding *et al.* 2010).
The zone is comparable to the *Rhaetogonyaulax rhaetica* Zone of Woollam & Riding (1983) for Great Britain. They defined the base of the Rhaetian stage by *Rhaetogonyaulax rhaetica* first appearance along with *Dapcodinium priscum*. Morbey (1978) assigned a Rhaetian age for the *Rhaetogonyaulax rhaetica* Zone of late Triassic and early Jurassic subsurface successions in northwestern Europe. Indeed, investigations on the Lower Rhaetian strata in Australia led to the recognition of *Rhaetogonyaulax raetica* Zone for these deposits (Helby *et al.* 1987). This zone can also be equal to the *Rhaetogonyaulax rhaetica* Zone of Ainsworth *et al.* (1989) from the upper Triassic of North Celtic Sea. Bralower *et al.* (1992) and Brenner *et al.* (1992) detected Rhaetian calcareous nannofossils and ostracods from the lower and upper parts of the *Rhaetogonyaulax rhaetica* Zone from the Wombat Plateau, offshore Western Australia. Nicoll & Foster (1994) dated this zone as Early to Late Rhaetian based on conodont evidence while they have also reported this zone from the Triassic sediments of Western and Northwestern Australia and Timor with an age of early Rhaetian. Batten *et al.* (1994) recorded this zone in

Uppermost Triassic to Middle Jurassic strata of the Danish Basin and dated it as Rhaetian. Besides, this zone has been used by Poulsen & Riding (2003) as DSTr for Subboreal Northwest Europe. Ghasemi-Nejad *et al.* (2004) determined this zone in the Alborz Mountains (North Iran) and dated it as Late Norian? to Rhaetian. Reviewing the chronostratigraphical ages of Middle Triassic to Late Jurassic dinoflagellate cyst biozones of the North West Shelf of Australia by Riding *et al.* (2010), confirmed the *Rhaetogonyaulax rhaetica* Zone for the Rhaetian of relevant deposits. At last, in a more recent publication on the Late Triassic of Central Iran (Nayband Formation, Qadir Member), Sabbaghiyan *et al.* (2015) dated this rock unit as Rhaetian based on the presence of *Rhaetogonyaulax rhaetica* index species. Table 1 illustrates the global correlation of the identified dinocyst zones in this study with the well-known established biozonations for the Triassic deposits of Australia, Subboreal Northwest Europe, North Iran, and Central Iran.

The species *Rhaetogonyaulax rhaetica* and *Rhaetogonyaulax* sp. are the only forms found through this zone suggesting an age of late Norian? to Rhaetian based on the recorded dinoflagellate cysts and stratigraphic position of the surrounding strata. The proposed relative age can be confirmed by other palynomorph groups which have already been reported from theses members in the various case studies such as Buratti *et al.* (2001), Cirilli *et al.* (2005), Sajjadi *et al.* (2007, 2015) and Ghavidel-Syooki *et al.* (2015). Foraminiferal association of the Nayband Formation in the northeast of Esfahan, CI, has also pointed to a mixed fauna of Triassic–Jurassic age and the occurrence of the genus *Aulotortus* with the species *A. tumidus*, *A. tenuis*, and *A. friedli* confirming most probably a Rhaetian age for this section (Senowbari-Daryan *et al.* 2010). Elsewhere in CI, ammonoids, yielding a Middle Norian age (Seyed-Emami 1975, 2003; Repin 1987), have been retrieved from the lower part of the Nayband Formation.

1.7.Conclusion

Palynological content of 58 rock samples from the Nayband Formation at the Tabas block, East-Central Iran were examined. The host strata contain moderately diverse and poorly preserved dinoflagellate cysts. These palynomorphs collectively denote an age of ?late Norian-Rhaetian (Late Triassic) for the Formation. A *Rhaetogonyaulax rhaetica* dinocyst zone has been established as well. The oldest occurrences of *Rhaetogonyaulax rhaetica* in the upper Triassic appear to have widespread correlative (in Great Britain, northwestern Europe, Australia, and North Iran). The detected dinoflagellate cyst associations including *Heibergella*

asymmetrica, Heibergella. sp., *Heibergella. aculeata, Heibergella. salebrosacea, Hebecysta* sp., *Sverdrupiella* sp., *Rhaetogonyaulax* sp., *Rhaetogonyaulax rhaetica*, and *Cleistosphaeridium* sp. indicate close similarity with those recorded in Northwest Europe, Arctic Canada, Australia, and Northern Iran. *Heibergella* and *Sverdrupiella* species have also been reported in the northern hemisphere from Carnian to Rhaetian and in the southern hemisphere from Norian to Rhaetian.

Acknowledgments

The authors would like to thank the University of Tehran and also the University of Ferrara for providing the required equipment for this research.

References

- Aghanabati, S.A., 1977: Etude geologique de la region de Kalmard (W Tabas). Geol. Surv. Iran, 1–230 (Report 35).
- Aghanabati, S.A., 2007: Geology of Iran: Geological Survey of Iran, 586. [in Persian]
- Achilles, H., Kaiser, H., Schweitzer, H.J., Hushmand-Zadeh, A., 1984: Die rato - jurassischen Floren des Iran und Afghanistans. 7. Die Mikroflora der obertriadisch-jurassischen Ablagerungen des Alborz-Gebirges (Nord-Iran). Palaeontographica, Abteilung, 194(1–4): 14–95.
- Ainsworth, N.R., O'Neill, M.O., Rutherford, M.M., 1989: Jurassic and upper Triassic biostratigraphy of the North Celtic Sea and Fastnet basins. In: Batten, D.J., Keen, M.C. (Eds.), Northwest European Micropalaeontology and Palynology. Ellis Horwood, 1(4): 4.
- Arjang, B., 1975: Mikroflora der rato-jurassischen Ablagerungen des Kermaner Beckens (Zentral-Iran). Palaeontographica Abteilung, 152: 85–148.
- Baranyi, V., Rostási, Á., Raucsik, B., & Kürschner, W. M., 2019: Palynological and X-ray fluorescence (XRF) data of Carnian (Late Triassic) formations from western Hungary. Data in brief, 23, 103858.
- Batten, D.J., Koppelhus, E.B., Nielsen, L.H., 1994: Uppermost Triassic to middle Jurassic palynofacies and palynomiscellanea in the Danish Basin and Fennoscandian Border Zone. Cah. Micropaleontol. Nouv. Ser, 9: 21– 45.
- Below, R., 1987: Evolution und Systematik von Dinoflagellaten-Zysten aus der Ordnung Peridiniales. I. Allgemeine Grundlagen und Subfamilie Rhaetogonyaulacoideae (Familie Peridiniaceae). Palaeontogr. Abt. B 205, 1–6), 1–164.
- Berberian, M., King, G.C.P., 1981: Towards a paleogeography and tectonic evolution of Iran. Canadian Journal of Earth Sciences, 18(2): 210–265.
- Berberian, F., Muir, I.D., Pankhurst, R.J., Berberian, M., 1982: Late Cretaceous and early Miocene Andean-type plutonic activity in northern Makran and Central Iran. Journal of the Geological Society, 139(5): 605-614.
- Besse, J., Torcq, F., Gallet, Y., Ricou, L.E., Krystyn, L., Saidi, A., 1998: Late Permian to Late Triassic palaeomagnetic data from Iran: constraints on the migration of the Iranian block through the Tethyan Ocean and initial destruction of Pangaea. Geophys. J. Int, 135: 77–92.

- Bharadwaj, D.C., Kumar, P., 1986: Palynology of Jurassic sediments from Iran: 1, Kerman area. Biol. Mem, 12(2): 46–172.
- Bragin, N., Jahanbakhsh, F., Golubev, S.A., Badovnikov, G., 1976: Stratigraphy of the Triassic-Jurassic coal-bearing deposits of Alborz. Unpublished technical report, National Iranian Steel corporation, 1-51.
- Bralower, T.J., Bown, P.R., Siesser, W.G., 1992: Upper Triassic calcareous nannoplankton biostratigraphy, Wombat Plateau, northwestern Australia. Proceedings of the Ocean Drilling Program, Scientific Results, 122: 437–451.
- Brenner, W., Bown, P.R., Bralower, T.J., Crasquin-Soleau, S., Dèpêche, F., Dumont, T., Martini, R., Siesser, W.G., Zaninetti, L., 1992: Correlation of Carnian to Rhaetian palynological, foraminiferal, calcareous nannofossil, and ostracode biostratigraphy, Wombat Plateau. Proceedings of the Ocean Drilling Program, Scientific Results, 122: 487–495.
- Bronnimann, P., Zaninetii, L., Bozorgna, F., Dashti, G.R., Moshtaghian, A., 1971: Lithostratigraphy and foraminifera of the Upper Triassic Naiband Formation, lran. Revue de Micropaleontologie, 14: 7–16.
- Bucefalo Palliani, R., Buratti, N., 2006: High diversity dinoflagellate cyst assemblages from the Late Triassic of southern England: new information on early dinoflagellate evolution and palaeogeography. Lethaia, 39: 305–312.
- Bujak, J.P., Fisher, M.J., 1976: Dinoflagellate cysts from the upper Triassic of Arctic Canada. Micropaleontology, 22(1): 44-70.
- Buratti, N., Cirilli, S., Senowbari-Daryan, B., 2001: Stratigraphy and palaeogeography in Central Iran (Nayband Formation, Upper Triassic): A mixed Asiatic-Gondwanian microflora. IGCP Congress, England.
- Cirilli, S., Buratti, N., Senowbari-Daryan, B., Fursich, F.T., 2005: Stratigraphy of the Upper Triassic Nayband Formation of East-Central Iran and paleoclimatological implications. Riv. Ital. Paleontol. Stratigr, 111: 259–270.
- Corsin, P., Stampfli, G., 1977: La formation de Shemshak dans l'Elburz Oriental (Iran). Flore Stratigraphie Paleogeographie. Geobios, 10: 509–571.
- Couper, R.A., 1953: Upper Mesozoic and Cenozoic spores and pollen grains from New Zealand. New Zealand Dept. Sci. Ind. Res., Geol. Surv. Palaeontol. Bull., 22: 1-77.
- Couper, R.A., 1958: British Mesozoic microspores and pollen grains. Palaeontographica, 103: 75-179.
- Courtinat, B., Piriou, S., 2002: Palaeoenvironmental distribution of the Rhaetian dinoflagellate cysts Dapcodinium priscum EVITT, 1961, emend. Below, 1987 and Rhaetogonyaulax rhaetica (SARJEANT) LOEBLICH and LOEBLICH, 1976, emend. Harland et al., 1975, emend. Below, 1987. Geobios 35 (4), 429–439.
- Courtinat, B., Malartre, F., Giraud, F., 1998: Le Rhétien en région lyonnaise: analyse palynologique Géologie de la France, No. 1. pp. 3–19.
- Dabiri, O., 2002: Palynozonation and paleoenvironmental study of upper Triassic sediments (basal parts of Shemshak Group) in north of Alborz Mountains, Iran. Research Institute for Earth Sciences of the Geological Survey and Mineral Exploration of Iran. Unpublished thesis (in Persian), 160 pp.
- Davoudzadeh, M., 1997: Iran. In: Moores, E.M., Fairbridge, R.W. (Eds.), Encyclopedia of European and Asian regional geology. Chapman and Hall, London, 384–405.
- Davoudzadeh, M., Schmidt, K., 1982: Zur Trias des Iran. Geol. Rundsch, 71: 1021–1039.

- Davoudzadeh, M., Schmidt, K., 1984: A review of the Mesozoic paleogeography and paleotectonic evolution of Iran. Neues Jahrbuch für Geologie und Paläontologie, Abhandlungen, 168 (2/3): 182-207.
- Davoudzadeh, M., Soffel, H., Schmidt, K., 1981: On the rotation of the Central-East Iran microplate: Neues Jahrbuch fur Geologie und Palaontologie, Monatshefte, 3: 180-192.
- DE Jersey, N. J., 1959: Jurassic spores and pollen grains from the Rosewood Coalfield. Qld Govt Min. II, 60: 344-66 (Also PubIs Geol Surv. Qld, 294: 1-14. 1960).
- Douglas, J.A., 1929: A marine Triassic fauna from eastern Persia. Q. J. Geol. Soc. Lond, 85: 625–650.
- Eftekhar-Nezhad , J., 1975: Brief history and structural development of Azarbaijan. Geo. Surv. Iran. Internal report 8p.
- Felix, C.J. Burbridge, P.P., 1978: Status of Triassic Palynology in the Canadian Arctic Islands. Palinologia, 1: 225-231.
- Foster, C.B., Balme, B.E., Helby, R., 1994: First record of Tethyan palynomorphs from the late Triassic of East Antarctica. AGSO J. Aust. Geol. Geophys. 15 (2), 239–246.
- Fursich, T.F., Hautmann, M., Senowbari-Daryan, B., Seyed-Emami, K., 2005: The Upper Triassic Nayband and Darkuh formation of east-central Iran: Stratigraphy, facies pattern, and biota of extensional basins on an accreted terrain. Beringeria, 35: 53–134.
- Fursich, F.T., Wilmsen, M., Seyed-Emami, K., Majidifard, M.R., 2009: Lithostratigraphy of the Upper Triassic–Middle Jurassic Shemshak Group of Northern Iran, vol. 312. The Geological Society, London, Special Publications, 312 (1): 129–160.
- Gaunt G.D., Fletcher, T.P., Wood, C. J., 1992: Geology of the country around Kingston upon Hull and Brigg. Memoir for 1:50000 Geological sheets 80 and 89 (England and Wales), New Series. Geological Survey of Great Britain, 80: 172.
- Ghasemi-Nejad, E., Agha-Nabati, A., Dabiri, O., 2004: Late Triassic dinoflagellate cysts from the base of the Shemshak 26 Sabbaghiyan et al. Geopersia, 5(1), 2015 Group in north of Alborz Mountains, Iran. Review of Palaeobotany and Palynology, 132: 207-217.
- Ghasemi-Nejad, E., Head, M.J., Zamani, M., 2008: Dinoflagellate cysts from the Upper Triassic (Norian) of northeastern Iran. Journal of Micropalaeontology, 27(2): 125-134.
- Ghavidel-Syooki, M., Yousefi, M., Mohnhoff, D., 2015: Palynostratigraphy, Palaeogeography, and Source Rock Evaluation of the Nayband Formation at the Parvadeh area, Central Iran, Iran. Journal of Sciences, Islamic Republic of Iran, 26(3): 241-263.
- Golonka, J., 2004: Plate tectonic evolution of the southern margin of Eurasia in the Meso- zoic and Cenozoic. Tectonophysics 381, 235–273.
- Golonka, J., 2007: Late Triassic and Early Jurassic palaeogeography of the world. Palaeogeogr. Palaeoclimatol. Palaeoecol. 244, 297–307.
- Golonka, J., Embry, A.F., Krobicki, M., 2018: Late Triassic Global Plate Tectonics. In: Tanner, L.H. (Ed.), The Late Triassic World, Top. Geobiol. 46. Springer Verlag.
- Hautmann, M., 2001: Taxonomy and phylogeny of cementing Triassic bivalves (families Prospondylidae, Plicatulidae, Dimyidae, and Ostreidae). Palaeontology, 44(2): 339–373.
- Helby, R., Wilson, G.J., 1988: A new species of Sverdrupiella Bujak & Fisher (Dinophyceae) from the Late Triassic of New Zealand. New Zealand Journal of Botany, 26: 117-122.
- Helby, R., Morgan, R., Partridge, A.D., 1987a: A palynological zonation of the Australian Mesozoic. Association of Australasian Palaeontologists, Memoir, 4: 1–94.
- Helby, R., Wiggins, V.D., Wilson, G.J., 1987b: The circum-Pacific occurrence of the Late Triassic dinoflagellate Sverdrupiella. Australian Journal of Earth Sciences, 34: 151–152.

- Kimyai, A., 1968: Jurassic plant microfossils from the Kerman region. Bull. Iranian Pet. Inst, 33: 91–111.
- Kimyai, A., 1974: Jurassic Plant Microfossils from Iran, vol. 3. Birbal Sahni Institute of Palaeobotany, Special Publication, 1–8.
- Kimyai, A., 1977: Further information on the palynological stratigraphy of the Mesozoic coaly sediments from Kerman, Iran. In: Proceeding of the 2nd Geological Symposium of Iran, Iranian Petroleum Institute, Tehran, 191–217. [in Persian]
- Kluyver, H.M., Tirrul, R., Chance, P.N., Johns, G.W., Meixner, H.M., 1983: Explanatory text of the Naybandan quadrangle map 1:250,000. Geol. Surv Iran. Geol. Quadrangle J8, 143.
- Krystyn, L., Balini, M., Aghababalou, B. S., & Hairapetian, V., 2019. Norian ammonoids from the Nayband Formation (Iran) and their bearing on Late Triassic Sedimentary and Geodynamic history of the Iran Plate. *RIVISTA ITALIANA DI PALEONTOLOGIA E STRATIGRAFIA*, *125*(1).
- Lindström, S., 2002: Lunnomidinium scaniense Lindström, gen. et sp. nov., a new suessiacean dinoflagellate cyst from the Rhaetian of Scania, southern Sweden. Rev. Palaeobot. Palynol. 120, 247–261.
- Loeblich Jr, A.R., Loeblich III, A.R., 1968: Index to the genera, subgenera, and sections of the Pyrrhophyta, II. Journal of Paleontology, 42: 210-213.
- MacRae, R.A., Fensome, R.A., Williams, G.L., 1996: Fossil dinoflagellate diversity, originations, and extinctions and their significance. Can. J. Bot. 74 (11), 1687–1694.
- Mangerud, G., Paterson, N. W., & Riding, J. B., 2019: The temporal and spatial distribution of Triassic dinoflagellate cysts. Review of palaeobotany and palynology, 261, 53-66.
- Mantle, D. J., Riding, J. B., & Hannaford, C., 2020. Late Triassic dinoflagellate cysts from the Northern Carnarvon Basin, Western Australia. *Review of Palaeobotany and Palynology*, 104254.
- Martini, R., Zaninetti, L., Lathuilliere, B., Cirilli, S., Cornée, J.J., Villeneuve, M., 2004: Upper Triassic carbonate deposits of Seram (Indonesia): palaeogeographic and geodynamic implications. Palaeogeography, Palaeoclimatology, Palaeoecology, 206(1): 75-102.
- Moix, P., Beccaletto, L., Kozur, H.W., Hochard, C., Rosselet, F., Stampfli, G.M., 2008: A new classification of the Turkish terranes and sutures and its implication for the paleotectonic history of the region. Tectonophysics, 451: 7–39.
- Morbey, S.J., 1975: The palynostratigraphy of the Rhaetian Stage, Upper Triassic in the Kendelbachgraben, Austria. Paleontographica, 152: 1-75.
- Morbey, S.J., 1978: Late Triassic and Early Jurassic subsurface palynostratigraphy in northwestern Europe. Palinologia Número Extraordinario, 1: 355–365.
- Morbey, S.J., Dunay, R.E., 1978: Early Jurassic to Late Triassic dinoflagellate cysts and miospores. In Thusu, B. (ed.): Distribution of biostratigraphically diagnostic dinoflagellate cysts and miospores from the Northwest European continental shelf and adjacent areas. Continental Shelf Institute Publication, 100: 47-59.
- Muttoni, G., Kent, D.V., Channell, J.E.T., 1996: Evolution of Pangaea: paleomagnetic constrains from the Southern Alps, Italy. Earth Planet. Sci. Lett, 140: 97–112.
- Muttoni, G., Garzanti, E., Alfonsi, L., Cirilli, S., Germani, D., Lowrie, W., 2001: Motion of Africa and Adria since the Permian: paleomagnetic and paleoclimatic constraints from northern Libya. Earth Planet. Sci. Lett, 192: 159–174.
- Nicoll, R.S., Foster, C.B., 1994: Late Triassic conodont and palynomorph biostratigraphy and conodont thermal maturation, North West Shelf, Australia. AGSO Journal of Geology and Geophysics, 15: 101–118.

- Nutzel, A., Senowbari-Daryan, B., 1999: Gastropods from the Late Triassic (Norian–Rhaetian) Nayband Formation of central Iran. Beringeria, 23: 93–132.
- Nutzel, A., Hamedani, A., Senowbari-Daryan, B., 2003: Some Late Triassic Gastropods from the Nayband Formationin Central Iran. Facies, 48: 127–134.
- Nutzel, A., Hamedani, A., Senowbari-Daryan, B., Yazdi, M., 2010: Gastropods from the Late Triassic Nayband Formation (Iran), their relationships to other Tethyan fauna sandremarks on the Triassic gastropod body size problem. Neues Jb. Geol. Palaontol. Abh, 256(2): 213–228.
- Nutzel, A., Aghababalou, B., Senowbari-Daryan, B., 2012: Gastropods from the Norian (Late Triassic) Nayband Formation near Natanz (Iran). Bull. Geosci, 87(1): 53–65.
- O'Sullivan, T., Pegum, D., Tarigan, J., 1985: Seram oil research, past discoveries, and future potential. Indonesian Petroleum Association, Proceedings of the 14th Annual Congress, Jakarta, October 1985.
- Paterson, N.W., Mangerud, G., 2015: Late Triassic (Carnian–Rhaetian) palynology of Hopen, Svalbard. Review of Palaeobotany and Palynology, 220: 98-119.
- Playford, G. and Dettmann, M.E., 1965: Rhaeto-Lassie plant microfossils from the Leigh Creek Coal Measures, South Australia. Senckenbergiana Lethaea, 46: 127-181.
- Poulsen, N.E., Riding, J.B., 2003: The Jurassic dinoflagellate cyst zonation of Subboreal Northwest Europe. In: Ineson, J.R., Surlyk, F. (Eds.), The Jurassic of Denmark and Greenland: Geological Survey of Denmark and Greenland Bulletin, 1: 115–144.
- Powell, A.J., 1992: Dinoflagellate cysts of the Triassic System. In Powell, A.J. (ed.): A stratigraphic index of dinoflagellate cysts. British Micropaleontological Society Publication Series, 1-7.
- Rashidi, K., Senowbari-Daryan, B. 2011: Sponges from a section of the Upper Triassic Nayband Formation, northeast of Esfahan, central Iran. Annalen des Naturhistorischen Museums in Wien. Serie A für Mineralogie und Petrographie, Geologie und Paläontologie, Anthropologie und Prähistorie, 113: 309-371.
- Repin Y.S., 1987: Stratigraphy and palaeogeography of coal-bearing sediments of Iran. Unpublished Report, National Iranian Steel Company, 1: 326. [in Persian]
- Repin Y.S., 1996: Novye pozdnetriasovye dvustvorchatye mollyuski Irana I taksonomiya nadsemejstva Spondylacea. Paleontologicheskiy Zhurnal, 3-8. [in Russian]
- Riding, J.B., Mantle, D.J., Backhouse, J., 2010: A review of the chronostratigraphical ages of Middle Triassic to Late Jurassic dinoflagellate cyst biozones of the North West Shelf of Australia. Review of Palaeobotany and Palynology, 162(4): 543-575.
- Sabbaghiyan, H., Ghasemi-Nejad, E., Aria-Nasab, M., 2015: Dinoflagellate cysts from the Upper Triassic (Rhaetian) strata of the Tabas Block, East-Central Iran. Geopersia, 5(1): 19-26.
- Saidi, A., Brunet, M.F., Ricou, I.E., 1997: Continental accretion of the Iran Block to Eurasia as seen from Late Paleozoic to Early Cretaceous subsidence curves. Geodin. Acta, 10(5): 189–208.
- Sajjadi, F., Hashemi, H., Dehbozorgi, A., 2007: Middle Jurassic palynomorphs of the Kashafrud Formation, Koppeh Dagh Basin, northeastern Iran. Micropaleontology, 53(5): 391–408.
- Sajjadi, F., Hashemi, H., Borzuee, E., 2015: Palynostratigraphy of the Nayband Formation, Tabas, Central Iran Basin: Paleogeographical and paleoecological implications. Journal of Asian Earth Sciences, 111: 553-567.
- Sarjeant, W.A.S., 1963: Fossil dinoflagellates from Upper Triassic sediments. Nature, 199(4891): 353-54.

- Sengor, A.M.C., 1984: The Cimmeride orogenic system and the tectonics of Eurasia. Geol. Soc. Am. Spec. Pap, 195: 1–82.
- Sengor, A.M.C., 1990: A new model for the late Palaeo-zoic–Mesozoic tectonic evolution of Iran and its implications for Oman. In: Robertson, A.H.F., Ries, M.P., Searle, A.C. (Eds.), The Geology and Tectonics of the Oman Region, vol. 49. Geological Society, London, Special Publications, 49(1): 797–831.
- Sengor, A.M.C., 1998: Die Tethys: Vor hundert Jahren und heute. Mitt. Osterreich. Geol. Ges, 89: 5–178.
- Senowbari- Daryan, B., 1996: Upper Triassic reefs and reef communities of Iran.In: Reitner, J., Neuweiler, F., Gunkel, F. (Eds.), Global and Regional Controls on Biogenic Sedimentation. Gottinger Arbeiten Geologie und Paläontologie Sb2, 299-304.
- Senowbari-Daryan, B., 2005: Hypercalcified Sphinctozoan Sponges from Upper Triassic (Norian–Rhaetian) Reefs of the Nayband Formation (Central and Northeast Iran). Jahrbuch der Geologischen Bundesanstalt, Wien, 145(2): 171–277.
- Senowbari-Daryan, B., Flugel, E., 1996: A "Problematic Fossil" Revealed: Pycnoporidium? eomesozoicum Flugel, 1972 (Late Triassic, Tethys). Not an Enigmatic Alga but a Strophomenid Brachiopod (Gosaukammerella n. g.). Facies, 34: 83–100.
- Senowbari-Daryan, B., Kube, B., 2003: The ichnogenous Palaxius (crustacean coprolite) and description of P. hydranensis n. sp. from the Upper Triassic (Norian part of "Pantokrator" limestone) of Hydra (Greece). Paläontologische Zeitschrift, 77(1): 115-122.
- Senowbari-Daryan, B.A.B.A., Seyed-Emami, K.A.Z.E.M., Aghanabati, A., 1997: Some inozoid sponges from Upper Triassic (Norian-Rhaetian) Nayband Formation of Central Iran. Rivista Italiana di Paleontologia e Stratigrafia (Research in Paleontology and Stratigraphy), 103(3).
- Senowbari-Daryan, B., Torabi, H., Rashidi, K., 2008: New solenoporaceans from Upper Triassic (? Norian–Rhaetian) reef limestone in central Iran. Geologia Croatica, 61(2–3): 135–157.
- Senowbari-Daryan, B., Rashidi, K., Torabi, H., 2010: Foraminifera and their associations of a possibly Rhaetian section of the Nayband Formation in central Iran, northeast of Esfahan. Facies, 56(4): 567-596.
- Seyed-Emami, K., 1971: A summary of the Triassic in Iran. Geol. Surv. Iran, 41–53. [Report 20]
- Seyed-Emami, K., 1975: A new species of Distichites (Ammonoidea) from the Upper Triassic Nayband Formation of the Zefreh area (Central Iran). Neues Jahrbuch fuer Geologie und Palaeontologie Monatshefte, 12: 734–744.
- Seyed-Emami, K., 2003: Triassic in Iran. Facies, 48: 91–106.
- Shadan, M., Hosseini-Barzi, M., 2013: Petrography and geochemistry of the Ab-e-Haji Formation in CI: implications for provenance and tectonic setting in the southern part of the Tabas block. Rev Mex Cien Geol, 30: 80-95.
- Shariatnia, H., 1994: Geological characteristics of the Parvadeh region of the Tabas coal-bearing basin, Central Iran. In: Embry, A.F., Beauchamp, B., Glass, D.J. (Eds.), Pangea Global Environments and Resources, vol. 17. Canadian Society of Petroleum Geologists, Memoir, 497–509.
- Sharma, J., Sarjeant, W.A.S., 1987: Late Triassic dinoflagellate cysts and acritarchs from the Andaman Islands, India. Mod. Geol. 11, 255–264.
- Skarby, A., 1964: Revision of Gleicheniidites senonicus Ross. Distributor, Almqvist & Wiksell.

- Soffel, H.C., Davoudzadeh, M., Rolf, C., Schmidt, S., 1996: New paleomagnetic data from Central Iran and a Triassic paleoreconstruction. Geol. Rundsch, 85: 293–302.
- Stampfli, G., Marcoux, J., Baud, A., 1991: Tethyan margins in space and time. Palaeogeogr. Palaeoclimat. Palaeoecol, 87: 373–409.
- Stöcklin, J., 1961: Lagunäre Formationen und Salzdome in Ostiran. Eclogae Geological Helvetiae, 54: 1-27.
- Stocklin, J., 1968: Structural history and tectonics of Iran: a review. AAPG Bulletin, 52(7): 1229-1258.
- Stocklin, J., Eftekhar-Nezhad, J., Hushmand-Zadeh, A. 1965: Geology of Shotori Range (Tabas area, East Iran). Geol. Surv. Iran, 3: 68. [Report 3].
- Stover, L.E., Evitt, W.R., 1978: Analyses of pre-Pleistocene organic-walled dinoflagellates. Geological Sciences, 15. Stanford University Publications, 15: 300.
- Stover, L.E., Brinkhuis, H., Damassa, S.P., de Verteuil, L., Helby, R.J., Monteil, E., Partridge, A.D., Powell, A.J., Riding, J.B., Smelror, M., Williams, G.L., 1996: Chapter 19. Mesozoic-Tertiary dinoflagellates, acritarchs and prasinophytes. In: Jansonius, J., McGregor, D.C. (Eds.), Palynology: principles and applications. American Association of Stratigraphic Palynologists Foundation, 2, pp. 641–750.
- Takin, M., 1972: Iranian geology and continental drift in the Middle East. Nature, 235: 147–150.
- Traverse, A., 1972: A case of marginal palynology: a study of the Franciscan mélanges. Geoscience and Man, 4: 87-90.
- Traverse, A., 2007: Paleopalynology. Topics in Geobiology, second ed. Springer, Dordrecht, The Netherlands, 813 pp Wiggins, V.D., 1973. Upper Triassic dinoflagellates from Arctic Alaska. Micropaleontology, 19: 1–17.
- Warrington, G., 1974: Studies in the palynological biostratigraphy of the British Trias. I. Reference sections in West Lancashire and North Somerset. Rev. Palaeobot. Palynol. 17, 133–147.
- Wiggins, V.D., 1976: Upper Triassic–Lower Jurassic dinoflagellates. Paper was given to the 9thAnnual Meeting of the American Association of Stratigraphic Palynologists. [unpublished]
- Wilmsen, M., Fursich, F.T. and Taheri, J., 2009a: The Shemshak Group (Lower-Middle Jurassic) of the Binalud Mountains, NE Iran: stratigraphy, facies, and geodynamic implications. In: South Caspian to Central Iran Basins (M.-F. Brunet, M. Wilmsen and J. Granath, eds), Geol. Soc. London, Spec. Publ, 312: 175–188.
- Woollam, R., Riding, J.B., 1983: Dinoflagellate cyst zonation of the English Jurassic. Institute of Geological Sciences Report, 83(2): 42.
- Ziegler, A.M., Scotese, C.R., Barrett, S.F., 1983: Mesozoic and Cenozoic paleogeographic maps. In: Broesche, P., Sündermann, J. (Eds.), Tidal Friction and The Earth's Rotation II. Springer-Verlag, Berlin, pp. 240–252.

Conclusion

The Carnian Pluvial Episode (CPE) was a time of global environmental change and biotic crisis that occurred during the Carnian (Late Triassic). The enhancement of hydrological cycling marked by four episodes of extreme rainfall in low-mid latitudes is the most obvious feature of CPE. Humid pulses of CPE are accompanied with substantial changes in both marine and terrestrial ecosystems possibly caused by a global carbon cycle perturbation and an interval of overall global warming (e.g., Dal Corso et al., 2012, 2020, Sun et al., 2016). Multiple negative carbon isotope excursions (NCIE) both in the marine and terrestrial realms suggest the injection of a significant amount of ^{13}C-depleted CO_2 into the ocean-atmosphere-soil system during the CPE. Volcanism and associated feedbacks are the most likely triggers for the injection of ^{13}C-depleted CO_2. The emplacement of the Wrangellia Large Igneous Province could have been one of the main volcanic sources. Although the onset of the CPE is very well constrained in many stratigraphic sections from Tethys domain to Panthalassa or, inside Pangea, from western Eurasia to South America, there are several areas where this event has not been clearly documented as along the southern margin of the Eurasia. Moreover, the possible connection between the CPE and eruption of the Wrangellia Large Igneous Province (as the prime candidate) is still a controversial issue.

In order to explore the occurrence of CPE in Iran region (Turan Plate and Iran Plate) and to elucidate the probable sources of CPE environmental changes, this PhD project undertook a high-resolution geochemical, paleobotanical, palynological, sedimentological, and stratigraphical study of the Upper Triassic (Carnian) stratigraphical successions in Central and Northeast Iran (Iran plate and Turan plate) and Western Tethys regions (Northern Calcareous Alps, Transdanubian Range, and Southern Alps). Main conclusions are as follows.

- The new data show pulses of increased Hg loading in the Western Tethys during the early Late Triassic CPE. The pulses occur in correspondence to NCIEs, but the Hg/TOC record is different in different basins. A rise of Hg/TOC is recorded in the more distal, open, and complete basin successions of the Northern Calcareous Alps (Austria) and the Transdanubian Range (Hungary) at the onset of the first NCIE of the CPE, but the same spike is not recorded during the same interval in the more proximal, and closed, basins of the Southern Alps (Italy), where the successions might not be complete

(Dolomites) or the sampling resolution is lower (Julian Alps). Further increases of Hg/TOC are recorded at the second and third NCIEs also in the Southern Alps. Major between-basins differences in Hg concentrations and Hg/TOC are recorded during other Mesozoic events linked to emplacements of oceanic plateaux, and are explained by the less efficient dispersal of Hg from submarine volcanism. Overall, data support the hypothesis that pulses of Wrangellia activity triggered multiple injections of isotopically light Carbon into the atmosphere-ocean system and associated environmental perturbations.

- The paleobotanical assessments of the upper Triassic successions of Turan Plate, Aghdarband Basin in the Kopeh-Dagh Range (NE Iran), resulted in the identification of a plant fossil assemblage coming from the basal marginal marine and continental facies of the Miankuhi Formation dominated by roots and vegetative organs of *Neocalamites iranensis* n. sp., with few seeds and plant fossils of undefined botanical affinity. The basal part of this formation yielded relatively diverse and well-preserved assemblages of terrestrial palynomorphs, as well, confirming a latest early Carnian to late Carnian age for this interval and reveal, for the first time, a clear link between this plant-bearing continental wet interval, and a time of global environmental changes, the Carnian Pluvial Episode. This is the first report of the Carnian Pluvial Episode in the Turan plate (southern margin of Eurasia) and Iran.

- The qualitative and quantitative palynological analysis on the Upper Triassic succession of Turan Plate (NE Iran) document a shift from xerophytic associations in the Upper Ladinian (Upper Sina Formation) to hygrophytic elements in the Carnian (Lower Miankuhi Formation). The increase in the hygrophytic vegetation elements in the studied area is coincident with the one found in the Tethyan same latitude belt suggesting more humid climate in the lower part of the Minakuhi Formation, corresponding to the Carnian Pluvial Episode. The sedimentological and stratigraphical analyses showing an interval of fluvial deposits with histosol levels at the basal Miankuhi Fm. support the humid climate in the studied area by that time. The defined unconformable boundary between the formations is, therefore, interpreted as a result of a climatic change to more humid conditions, decoupling the impact of Eo-Cimmerian collision as the origin of this unconformity in our studied area. The results suggests that

this orogenic event is younger than Carnian and positioned somewhere before the Middle-Norian (217.1 ± 1.8 Ma). However, the exact timing of this event and how it evolved remains controversial.

- Palynological investigations of the middle-upper Nayband Formation from a section of the Tabas Block (Central Iran), revealed moderately diverse dinoflagellate cyst assemblages which lead to the identification of *Rhaetogonyaulax rhaetica* Zone and confirmed the middle Norian-Rhaetian age for the studied interval in Iran Plate.

Outlook

The research around the CPE is still relatively "young". Our understanding of the phenomena that occurred during this time interval is still fragmentary and very limited. Many fundamental questions remain open and need to be addressed.

Despite the remarkable studies on the possible implications of volcanism and climate change for mercury concentrations during intervals of mass extinction and global environmental change, the current knowledge on the other factors controlling Hg deposition in terrestrial and marine settings is still primitive. A deeper knowledge of the temporal links between volcanism, climate change, and biotic turnover will permit to develop global biogeochemical models to understand the causal relationships and the long-term effects of the climate perturbation on the environments and biota.

It is necessary to pursue new records of this important, but yet poorly understood, phase of global climate change (CPE) in different stratigraphical sections worldwide and investigate the effects of the CPE on continents, shallow marine environments, and oceans. There are signals of major environmental changes in Upper Triassic strata from Iran block and adjacent areas suffering from precise age determinations many of which indicating a possible Carnian age (?Carnian) and need to be further investigated in terms of age dating, paleoenvironmental conditions and basin evolution.

Increasing precision in dating and improved knowledge of fossil records will also improve our understanding of the long-lasting impact of this major perturbation on the rebuilding of new ecosystems in the sea and on land.

SUPPLEMENTAY INFORMATION

Mercury deposition in Western Tethys during the Carnian Pluvial Episode (Late Triassic)

Mina Mazaheri-Johari[1]*, Piero Gianolla[1], Tamsin Mather[2], Joost Frieling[2], Daoliang Chu[3], and Jacopo Dal Corso[3]*

[1]Dipartimento di Fisica e Scienze della Terra, University of Ferrara, Ferrara, Italy.

[2]Department of Earth Sciences, University of Oxford, South Parks Road, Oxford, UK

[3]State Key Laboratory of Biogeology and Environmental Geology, School of Earth Sciences, China University of Geosciences, Wuhan, China.

*emails: mzhmni@unife.it; j.dalcorso@cug.edu.cn

EXTENDED GEOLOGICAL SETTING

1. Southern Alps (Italy)

1.1. Dolomites

The Dolomites region, located in the northcentral part of Southern Alps (Bosellini et al., 2003), displays an impressive and outstanding exposure of Triassic rocks of the Alps (Fig. 1c). During the Middle–Late Triassic, the area occupied a northern equatorial position in the western margin of the Tethys Ocean (Fig. 1a, b) (Muttoni et al., 2015). In the Early Carnian (Julian), the paleotopography was characterized by an emerged land (Adriatic foreland) towards the present South, then attached and isolated rimmed microbial carbonate platforms (Cassian Dolomite) and relatively deep basins, characterized by mixed carbonate-siliciclastic sedimentation (San Cassiano Formation) (Masetti et al., 1991; De Zanche et al., 1993; Gianolla et al., 1998a; Keim et al., 2006; Stefani et al., 2010; Mietto et al., 2012). Near the end of the Early Carnian, a consistent siliciclastic input to marginal basins associated with the general demise of high relief carbonate platforms (Keim et al., 2001; Dal Corso et al., 2012; Gattolin et al., 2015) caused the infilling of the intraplatform basins by the Heiligkreuz Formation and the flattening of Early Carnian topography (Pisa et al., 1980; De Zanche et al., 1993; Gianolla et al., 1998a,b, 2018; Preto and Hinnov, 2003; Keim et al., 2006; Neri et al., 2007; Breda et al., 2009; Stefani et al., 2010; Dal Corso et al., 2015, 2018; Gattolin et al., 2015). The Heiligkreuz Formation is thus characterized by a complex lithostratigraphic architecture with different members recording mainly the interplay between climatic forcing and relative sea level

oscillations (Preto and Hinnov, 2003; Neri et al., 2007; Breda et al., 2009; Stefani et al., 2010; Gattolin et al., 2015; Gianolla et al., 2018). The Borca Member documents the onset of local anoxia, a change from microbial to skeletal carbonate factory, and the basin infilling phase by skeletal carbonates and/or siliciclastics. The Dibona Member documents an overall transgressive phase and is marked by terrigenous pulses in the lower and uppermost parts. The last members of the unit are the Lagazuoi Member and the Falzarego Sandstone, documenting a regressive phase with progradation of mixed carbonate-terrigenous shallow water depositional systems.

Above the Heiligkreuz Formation, continental to shallow-marine siliciclastic-carbonates of Travenanzes Formation (Tuvalian) were deposited in a marginal marine dryland coastal system (Breda and Preto, 2011) (Fig. 2). Several studies such as those carried out by Breda et al. (2009), Dal Corso et al. (2018), and Maron et al. (2017) performed a high-resolution biostratigraphic framework of this succession in the Dolomites area. The base of Heiligkreuz Formation (Borca member) is assigned to the Julian 1 - 2 boundary (T. aonoides/A. austriacum ammonoid zones) while the upper part (upper Dibona Member and Falzarego/Lagazuoi members) belongs to the Tuvalian 1 (T. dilleri ammonoid zone). In this study we have analysed two stratigraphic sections that together form a composite section of the entire Heiligkreuz Formation.

The Milieres section (Dal Corso et al., 2012, 2018), placed just below the Dibona section (De Zanche et al, 1993; Gianolla et al., 1998a; Preto and Hinnov, 2003; Neri et al., 2007; Breda et al., 2009; Gattolin et al., 2015), is a succession of marls and limestones deposited in a relatively deep basin, recording the boundary between San Cassian Formation and the lowermost part of the Borca Member of Heiligkreuz Formation, the age is within the A. austriacum ammonoid zone (Julian 2) (see discussion in Dal Corso et al., 2018). The Heiligkreuz section (Dal Corso et al., 2018), also known as Peraguda section (Koken, 1913), Santa Croce/Heiligkreuz section (Gianolla et al., 1998b) or Kreuzkofel section (Keim et al., 2001, 2006) encompasses the uppermost Borca, Dibona, and Lagazuoi members of the Heiligkreuz Formation, the age is within the A. austriacum ammonoid zone (Julian 2) for the Borca and part of the Dibona members while the uppermost Dibona and Lagazuoi members belong to the T. dilleri ammonoid zone (Tuvalian 1) (Gianolla et al., 1998b; De Zanche et al., 2000; Dal Corso et al., 2018).

A total number of fifty samples analysed in this study come from this composite section: 20 samples come from the Milieres section and 30 samples come from the Heiligkreuz section.

1.2. Julian Alps

The studied sequence in the Julian Alps is located in the Cave del Predil area (formerly Raibl), near Tarvisio, where the historical type-area of the Carnian stage has been defined (Mojsisovics, 1869; Wörhmann, 1894; Assereto et al., 1968; Lieberman, 1980) (Fig. 1c). In this area, a well-preserved carbonate platform-basin depositional system records microbial platform demise, basin infilling by siliciclastics, transition to mixed terrigenous-skeletal carbonate ramp system, and finally microbial carbonate platform recovery (Schulz, 1970; De Zanche et al., 2000; Gianolla et al., 2003; Caggiati et al., 2018; Dal Corso et al., 2018).

The carbonate platform (Schlern Dolomite or "Dolomia Metallifera" Auctorum) is a high-relief microbial buildup and is interfingered the Predil Limestone, a dysoxic-anoxic unit made up of laminated limestones, marly limestones, marls, and thin to coarse calcarenites. The latter unit is sharply overlain by the Rio del Lago Formation, which consists at the base by a silty interval ("Barren beds" Auctorum), then by subtidal marly shales, with marly and calcareous intercalations in the upper part. The unit is lapping on the slope of the demise carbonate platform (De Zanche et al., 2000). According to Dal Corso et al. (2018), the Rio del Lago Formation represents the onset of CPE by the infilling of a relatively deep basin, which had almost been completed by the deposition of overlying Conzen Formation (De Zanche et al., 2000). Above, a deepening upward succession of marls, siltstone, and marly limestone, the Tor Formation, comprises the Julian – Tuvalian boundary (Lieberman, 1980; De Zanche et al., 2000) and the rest of Tuvalian is represented by the Portella Dolomite, the conformably overlying basinal Carnitza Formation (*Subbullatus* to *Anatropites* Ammonoid zones), and the interfingered Dolomia Principale carbonate platform (De Zanche et al., 2000; Gianolla et al., 2003; Caggiati et al., 2018).

In the Cave del Predil area, the Rio Conzen and neighboring Rio delle Cascate sections (De Zanche et al., 2000; Roghi, 2004) have been sampled. The sections are very close to each other and a good correlation between them can be achieved with marker beds. They encompass the Predile Dolomite (Julian 1 = *Trachyceras* zone), the Rio del Lago, the Conzen, and part of the Tor formations (Julian 2 = *A. austriacum* zone). Fifty-eight samples analysed in this study come from this composite section which was previously studied for stratigraphy, palynology and carbon-isotope records by De Zanche et al. (2000), Roghi (2004), and Dal Corso et al. (2018).

2. Transdanubian Range (Hungary)

The Transdanubian Range (TDR) is a NE-SW trending chain of moderately elevated mountains located in the north-western part of Hungary, developed in a length of about 200 km (Fig. 1c).

It is made up predominantly of Middle and Late Triassic shallow-marine carbonates and coeval relatively deep basinal sediments representing a large segment of the Neotethys passive margin (Haas et al., 1995; Gawlick, 2000; Mandl, 2000; Haas et al., 2012). During Early Carnian a significant change in the lithofacies occurred in the Balaton Highland in the TDR as pelagic limestones (Füred Limestone) passes into a thick marl succession (Veszprém Marl Formation (VMF)) with a marked siliciclastic input (Fig. 2) (Budai and Haas, 1997; Rostási et al., 2011; Dal Corso et al., 2018; Baranyi et al., 2019). This major change in the sedimentation is associated with the CPE climatic shift from arid to more humid conditions as documented by clay mineralogy (Rostási et al., 2011) and by palynomorph assemblages (Baranyi et al., 2019). In the Balaton Highland, the VMF with a variety of thickness (from 100 to 600 m) is comprised of four members: Mencshely Marl Member, Nosztor Limestone Member, Buhimvolgy Breccia Member and Csicso Marl Member (Góczán et al., 1991, Góczán and Oravecz-Scheffer, 1996a,b; Budai et al., 1999; Haas and Budai, 1999). The basal part of the Veszprém Marl (Mencshely Marl Member), included of a relatively thick marl-dominated succession with some intercalations of sandstone, is separated from the pelagic marls of the upper part (Csicso Marl Member) by a 20 m-thick pelagic limestone member (Nosztor Limestone) (Góczán et al., 1991; Budai et al., 1999). Above, the Sàndhoregy Formation (Góczán and Oravecs-Scheffer,1996; Nagy, 1999) is a succession of shallow-water shales and carbonates, which represent the final stage of the infilling of the intraplatform basins during late Carnian (Tuvalian). On top of this unit the Main Dolomite deposited from late Tuvalian to the Norian (Budai and Haas, 1997). The Carnian successions of the TDR are also biostratigraphically well constrained with ammonoids, sporomorphs, and conodonts (Budai et al., 1999; Dal Corso et al., 2018; Baranyi et al., 2019). A total number of seventy-three samples analyed in this study come from two core materials (Rostási et al., 2011). 34 samples come from the Met-1 core which encompasses the Veszprém Marl Formation and 39 samples are from the Bfü-1 borehole included of Füred Limestones and the base of Mencshely Marl Member of Veszprém Marl Formation.

3. Northern Calcareous Alps (Austria)

The Lunz area, located in the eastern Northern Calcareous Alps (Fig. 1c), is well-known for containing coal seams with numerous remnants of Late Triassic plant fossils and reptiles (Verloop, 1908; Tollmann, 1976; Dobruskina, 1998; Pott et al., 2008). The Early Carnian stratigraphy of the Lunz nappe (Austria), represents a succession of carbonate–siliciclastic sedimentary rocks from deep water to delta and carbonate shelf basins (Rüffer and Bechstädt,

1998; Roghi et al., 2010; Dal Corso et al., 2015; Mueller et al., 2016). The Upper Ladinian–Lower Julian sequence is characterized by deep-water nodular limestones of the Reifling Formation (greyish-coloured filament wackestones), which is overlain by the Göstling Member (Mueller et al., 2016). The laminated dark mudstones and grainstones of the Göstling Member deposited in a deep and low-energy setting represent the demise of microbial platform and the temporary replacement of a skeletal carbonate factory (Mueller et al., 2016), nutrient excess, oxygen depletion in the basin that mark the onset of CPE (Hornung and Brandner, 2005; Hornung et al., 2007a,b; Dal Corso et al., 2015). The sequence continues with the Reingraben Formation, overlain by the coarse terrigenous Lunz Formation. The deep-marine deltaic sandstones and siltstones of Lunz Formation with a turbiditic origin change to deltaic sediments through basin fill and the infilling process of basins was completed by the shale and coal member of the Lunz Formation (Köppen, 1997; Hornung and Brandner, 2005; Wessely, 2006; Pott et al., 2008; Roghi et al., 2010; Mueller et al., 2016). Above, the succession continues with Opponitz Formation and Hauptdolomit (Tollmann, 1976, Roghi et al., 2010). The age of the studied succession is assigned to Carnian using ammonoid and sporomorph biostratigraphy (Roghi et al., 2010; Dal Corso et al., 2015; Mueller et al., 2016). Sixty-two samples analysed in this study come from two stratigraphic sections in this area: Steinbach section and Polzberg section. The Steinbach section encompasses the Reifling Fm. and part of the Göstling Mb. (Julian 1 = *Trachyceras* zone, Julian 2 = *A. austriacum* zone) while in the Polzberg section the uppermost part of the Göstling Mb. and the lower part of the Reingraben Fm. are exposed (Julian 2 = *A. austriacum* zone).

4. Location of the studied sections and cores

Milieres section, Dolomites, Italy: 46°31’41.60″N, 12°4′7.34″E

Heiligkreuz section, Dolomites, Italy: 46°35′50.56″N, 11°56′46.22″E

Rio Conzen section, Cave del Predil, Julian Alps, Italy: 46°26′38.43″N; 11°56′46.22″E

Rio delle Cascate section, Cave del Predil, Julian Alps, Italy: 46°26′10.9″N; 13°35′3.54″E

Steinbach section (= Göstling section in Dal Corso et al., 2015), Northern Calcareous Alps, Austria: 47°48′22.6″N, 14°57′3.44″E

Polzberg section, Northern Calcareous Alps, Austria: 47°53′4.09″N; 15°4′28.17″E

BFÜ-1 and MET-2 cores are stored at Szépvízér (repository of the Hungarian Office for Mining and Geology) in Hungary.

For more information on how to find and reach the studied sections, please contact P. Gianolla (piero.gianolla@unife.it) or J. Dal Corso (j.dalcorso@cug.edu.cn).

SUPPLEMENTARY TABLES (Hg is ppb, TOC in wt%)

Table S1 Hg, TOC, and Hg/TOC data from the Dolomites (Milieres and Heiligkreuz sections), Southern Alps, Italy.

SAMPLE	Meter	Hg ppb	TOC wt%
MILIERES			
MI 20/1	0.22	6.8	0.40
MI 20/2	0.62	9.3	0.56
MI 20/3	1.52	6.4	0.45
MI 20/4	2.62	7.1	0.43
MI 20/4B	2.9	7.8	0.35
MI 20/5	3.56	10.7	0.44
MI 20/6	7.6	4.4	0.51
MI 20/7	14.3	2.9	0.29
MI 20/8	14.62	10	0.64
MI 20/9	16.96	8.4	0.67
MI 20/10	17.84	8.9	0.84
MI 20/11	19.74	10	0.59
MI 20/12	21.12	10	0.55
MI 20/13	23.12	10.3	0.58
MI 20/14	26.44	3.9	0.65
MI 20/15	29.34	5.9	0.58
MI 20/16	34.02	9	0.65
MI 20/17	36.3	12	0.63
MI 20/17B	40.2	15.7	1.18
MI 20/18	42.2	27.7	1.17
HEILIGKREUZ			
SSC 1	0.4	0.2	
SSC 2	0.92	0.9	0.11
SSC 3	1.32	2.5	0.11
SSC 4	1.9	0.5	0.08
SSC 6	2.45	0.9	0.11
SSC 7A	2.65	0.4	0.18
SSC 9	3.29	3	0.18
SSC 10	3.73	2	0.11
SSC 14	4.9	0.9	0.21

SSC 22	8.86	5.7	
SSC 26	9.77	5.3	0.22
SSC 30	14.2	0.6	0.32
SSC 31	16.24	4.4	1.02
SSC 31C	19.24	3.6	0.07
SSC 31 F	22.53	11	0.39
SSC 32	22.93	13	9.30
SSC 34	29.32	6.7	20.47
SSC 39	32.59	17	0.50
SSC 42	39.72	27	0.40
SSC 45	42.22	12	0.64
SSC 46	42.77	33	0.64
SSC 47	43.34	6.7	0.30
SSC 48	43.6	1.2	0.27
SSC 49	47.31	32	0.41
SSC 50	53.1	11	0.45
SSC 52	59.66	23	0.14

Table S2. Hg, TOC, and Hg/TOC data from the Julian Alps (Cave del Predil), Italy.

Sample	Meter	Hg ppb	TOC wt%
PRSC2	16	11	0.52
PRSC3	18.6	15	0.82
PRSC4	24.8	9	0.41
PRSC7	49.7	21	0.61
PRSC11	68.7	13	0.73
PRSC14	119.8	4.9	0.25
PRSC15	128.4	1.8	0.31
PRSC16	148.3	3.3	0.21
PRSC17	156.8	2.6	0.29
PRSC18A	162	3	0.12
RLSR29	166.8	9.5	0.64
RLSR30	178.3	13	0.53
RLSR31	188.4	4.3	0.47
RLSR32	200.4	14	0.71
RLSR34	217	4.2	0.31
RLSR35	246	8.3	0.25
RLSR36	261.8	6.1	0.46

RLSR40	344.3	4.3	0.31
LG1Ca	405.5	5	0.36
LG1Cb	405.5	17	0.47
LG5	411.2	5.4	0.23
LG6	411.9	1.8	0.53
LG7	413.3	0	0.14
LG8	414.4	6	0.14
LG10	420	0.8	0.11
LG11	422.8	2.9	0.41
LG12	423.2	2	0.29
LG13	424.8	2.1	
LG23	428.3	1.8	0.19
LG15	428.3	3.6	0.35
LG24	429	0.3	
LG26	431.5	0.4	
LG27	431.7	6.8	0.26
LG37	432.6	0	0.10
LG28	432.8	1.9	
LG30	434.6	8.2	0.45
LG17	435.2	26	0.70
LG31A	435.3	19	0.48
LG31B	435.3	13	0.71
LG38	435.3	27	0.61
LG32	436.1	4.1	0.60
LG39	436.2	4.2	0.16
LG40	436.7	0.8	
LG41	437.2	27	0.55
LG42	438.4	24	0.69
LG18	439.4	3.9	0.41
LG43	439.6	17	0.81
LG19	439.8	16	0.53
LG45	440.1	16	0.55
LG20	440.2	22	0.51
LG46	440.3	20	0.62
LG21	441.5	2.6	

LG49	441.7	7.4	0.29
LG52	468.2	17	0.48
LG58	471.3	13	0.42
LG66	478.5	17	0.46
LG68	479.9	11	0.45

Table S3. Hg, TOC, and Hg/TOC from the TDR (Balaton Highland) boreholes (Bfü-1, Met-1), Hungary.

SAMPLE	Meter	Hg ppb	TOC wt%
BFU-1			
SZBF 2	6	35	0.80
BFU 1	10.5	34	0.67
BFU 2	16	38	0.50
BFU 4	22.5	31	0.43
BFU 6	27.4	33	0.60
SZBF 22	31.2	17	0.65
BFU 7	32.5	28	0.56
BFU 9	36.5	8.9	0.39
BFU 11	40.3	7.9	0.40
BFU 12	45.2	6.3	0.32
BFU 13	46.5	29	0.71
SZBF 29	47	24	0.47
BFU 14	50.5	12	0.46
BFU 15	51.5	31	0.52
BFU 16	52.5	39	0.74
SZBF 35	54	22	0.57
BFU 17	56.5	20	0.57
BFU 18	57.5	34	0.60
BFU 19	59.2	25	0.46
SZBF 41	59.5	32	0.50
BFU 20	61	28	0.38
SZBF-45	62	32	0.68
BFU 21	63	38	0.34
BFU 22	65	29	0.57
BFU 23	66	43	0.64
SZBF 53	67.8	35	0.87
SZBF 54	68.5	23	0.22
BFU 24	71.5	12	1.25
SZBF 56	73.2	5.7	0.71
SZBF 57	74.7	11	2.27

SZBF 59	76.8	6.5	0.03
SZBF 61	79.5	9.5	0.13
SZBF 68	85.3	14	0.07
SZBF 71	88	1.3	0.03
SZBF 77	93	6.8	3.36
SZBF 85	105.2	34	0.06
SZBF 88	112.5	5.6	0.18
SZBF 96	126.5	9.5	0.28
MET-1			
Met-1 1	33.8	61	0.65
Met-1 4	49.4	28	0.21
Met-1 7	61	22	0.56
Met-1 10	72	25	0.62
Met-1 13	85	31	0.85
Met-1 16	98	34	0.83
Met-1 19	114.5	32	0.61
Met-1 21	122.9	38	0.62
Met-1 22	135.1	13	0.89
Met-1 23	147.03	13	0.66
Met-1 24	150	41	0.55
Met-1 25	155.8	27	0.66
Met-1 26	162	31	0.62
Met-1 27	177.4	3.2	0.34
Met-1 28	184	9.3	0.38
Met-1 31	192.9	16	0.56
Met-1 33	202	23	0.59
Met-1 36	215.1	14	0.49
Met-1 40	228.4	27	0.56
Met-1 43	242.7	12	0.34
Met-1 46	255.4	9.3	0.40
Met-1 48	267.2	29	0.56
Met- 1 51	273.5	17	0.52
Met-1 54	299.5	22	0.52
Met-1 55	309	40	0.55
Met-1 56	312.3	38	0.57
Met-1 57	325.9	44	0.70
Met-1 58	331	19	0.49
Met-1 59	337.5	59	0.67
Met-1 60	343.2	55	0.53
Met-1 61	359.5	38	0.59
Met-1 62	361.7	61	0.54
Met-1 63	370	17	0.73
Met-1 64	373.9	35	0.67

Table S4. Hg, TOC, and Hg/TOC data from the NCA (Steinbach and Polzberg sections), Austria.

SAMPLE	Meter	Hg ppb	TOC wt%
STI 2	0.71	4.5	0.04
STI 6	2.1	6.7	0.08
STI 10	3.52	7	0.11
STI 16	5.1	78	0.36
STI 17	5.25	5.9	0.13
STI 18	5.4	96	3.38
STI 19	5.67	81	0.31
STI 21	6.2	8.5	0.12
STI 22	6.25	38	1.13
STI 23	6.48	109	0.78
STI 24	6.6	33	0.22
STI 25	6.87	83	0.51
STI 27	7.05	72	0.43
STI 28	7.25	526	0.13
STI 29	7.86	59	0.89
STI 30	8	24	
STI 31	8.08	6.5	0.11
STI 33	9.24	2.3	0.08
STI 34	9.63	274	3.49
STI 35	9.95	25	0.51
STI 36	10.1	23	0.17
STI 37	10.48	4.3	0.16
STI 38	10.84	127	
STI 39	11.06	10	0.14
STI 40	12.21	4.8	0.34
STI 41	12.4	3.8	0.16
STI 42	12.67	5.6	0.11
STI 43	13.26	36	3.49
STI 43a	13.3	70	9.30
STI 46	15.35	8.2	0.23
STI 47	15.65	99	
STI 49	15.85	358	
STI 51	16.42	331	
STI 52	16.5	324	
STI 53	16.54	11	0.15
STI 54	16.85	68	
STI 55	17.03	137	6.42
STI 56	17.18	240	7.32

STI 57A	17.35	134	5.32
POZ 2	17.48	13	0.20
POZ 3	17.52	15	0.42
POZ 4	17.54	13	0.59
POZ 5	17.62	6.9	0.25
POZ 6	17.67	42	2.20
POZ 7	17.73	8.9	0.37
POZ 10	17.93	14	1.01
POZ 11	18	4.5	0.29
POZ 12	18.07	28	0.61
POZ 14	18.29	6.6	0.89
POZ 15	18.37	2	0.63
POZ 16	18.43	14	0.31
POZ 17	18.5	6.4	0.50
POZ 18	20.56	49	0.90
POZ 19	20.71	11	1.16
POZ 20	20.86	56	1.32
POZ 21	21.01	70	1.03
POZ 22	21.15	37	1.38
POZ 23	21.15	34	0.74
POZ 24	21.44	28	1.36
POZ 26	21.73	46	1.31

SUPPLEMENTARY FIGURES

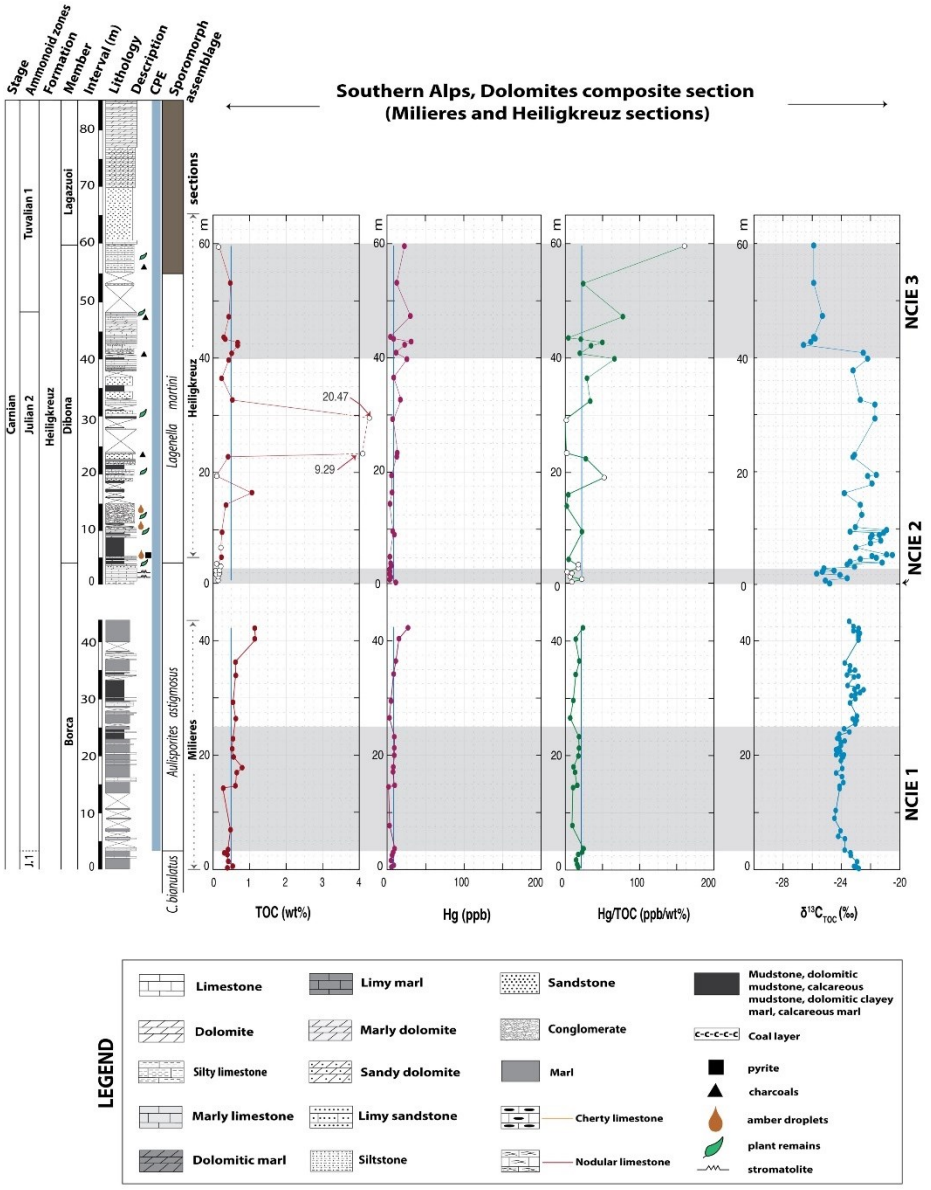

Fig. S1. Mercury geochemistry of the Southern Alps, Dolomites composie section. The TOC chemostratigraphy, Hg enrichments and Hg/TOC ratios produced in this study. Milieres section: Lithostratigraphy modified from Dal Corso et. al., (2018); Biostratigraphy and organic carbon-isotope curves from Dal Corso et al. (2012, 2018). The grey bar shows the negative carbon isotope excursion (NCIE-1) detected by Dal Corso et al. (2018). J. 1 = Julian 1 = *Trachyceras* zone, Julian 2 = *Austrotrachyceras austriacum* zone. Heiligkreuz section: Lithostratigraphy modified from Dal Corso et al., (2018). Biostratigraphy and organic carbon-isotope curves from Dal Corso et al. (2018). Grey bars show the two negative carbon isotope excursions (NCIE-2 and NCIE-3) detected by Dal Corso et al. (2018). The dark brown area in the palynostratigraphical zonations represent intervals of uncertain palynostratigraphic attribution. White circles represent TOC values below 0.2 wt% and their corresponding Hg/TOC ratios. The two outlier points in TOC (9.2 and 20.4) are from wood-rich samples. Vertical blue lines represent the average values of each dataset (only TOCs>0.2 are included in average). J-1 = Julian 1= *Trachyceras* zone, Julian 2 = *Austrotrachyceras austriacum* zone; Tuvalian 1 = *Tropites dilleri* zone.

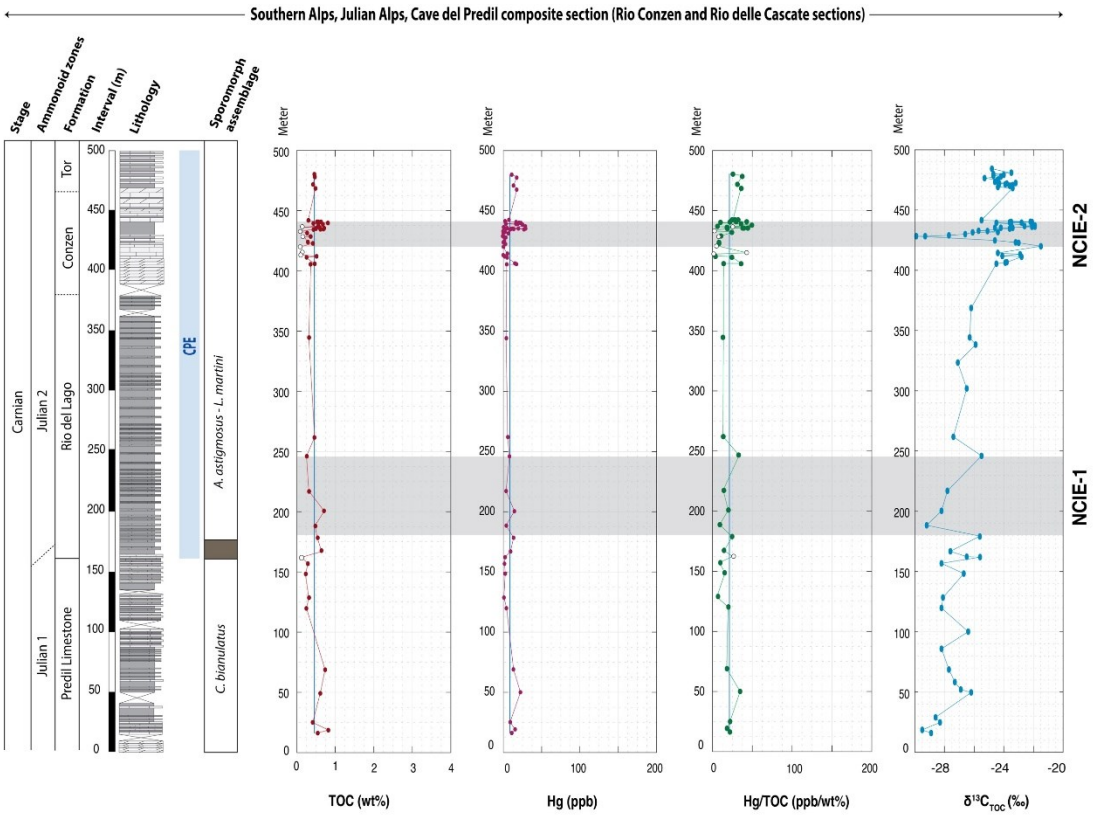

Fig. S2. Mercury geochemistry of the Julian Alps, Cave del Predil composite section (Rio Conzen and Rio delle Cascate sections). The TOC chemostratigraphy, Hg enrichments and Hg/TOC ratios produced in this study. Lithostratigraphy modified from De Zanche et al. (2000), Roghi (2004), and Dal Corso et al., (2015, 2018); Biostratigraphy and carbon-isotope curves from Dal Corso et al. (2018). Grey bars show the two negative carbon isotope excursions (NCIE) detected by Dal Corso et al. (2018). The dark brown area in the palynostratigraphical zonations represent intervals of uncertain palynostratigraphic attribution. White circles represent TOC values below 0.2 wt% and their corresponding Hg/TOC ratios. Vertical blue lines represent the average values of each dataset (only TOCs>0.2 are included in average). Julian 1 = *Trachyceras* zone, Julian 2 = *Austrotrachyceras austriacum* zone. The legend of the lithostratigraphic units is the same as in Figure 3.

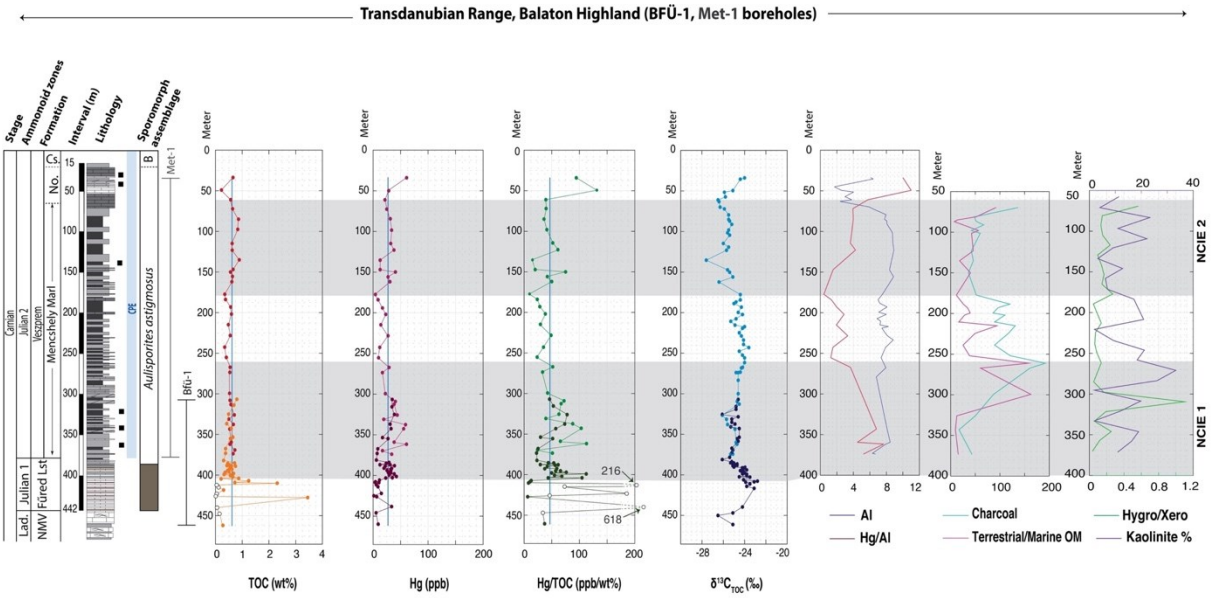

Fig. S3. Mercury geochemistry of the Transdanubian Range, Met-1 (light colours) and Balatonfüred-1 (Bfü-1, darker colours) boreholes. The TOC chemostratigraphy, Hg enrichments and Hg/TOC ratios produced in this study. Lithostratigraphy from Rostási et al. (2011), Dal Corso et al. (2018) and Baranyi et al. (2019); palynostratigraphy from Roghi et al. (2010), Dal Corso et al. (2018), Baranyi et al. (2019) and organic carbon-isotope curves from Dal Corso et al. (2015, 2018). The charcoal abundances, terrestrial/marine organic matter distribution, hygrophytic/xerophytic ratios, aluminum, and kaolinite contents are from Baranyi et al. (2019). Grey bars show the two negative carbon isotope excursions (NCIE) detected by Dal Corso et al. (2015, 2018). The dark brown area in the palynological zonation represent intervals of uncertain palynostratigraphic attribution. White circles represent TOC values below 0.2 wt% and their corresponding Hg/TOC ratios. Vertical blue lines represent the average values of two datasets (only TOCs>0.2 are included in average). Julian 1 = *Trachyceras* zone, Julian 2 = *Austrotrachyceras austriacum* zone. Abbreviations: No = Nosztor Limestone, Cs = Csicsó Marl, Hygro/Xero = Hygrophytic/Xerophytic, Al = Aluminium content, B = *Lagenella martini* palynozone, Lad. = Ladinian (*Protrachyceras* zone). The legend of the stratigraphic units is the same as in Figure 3.

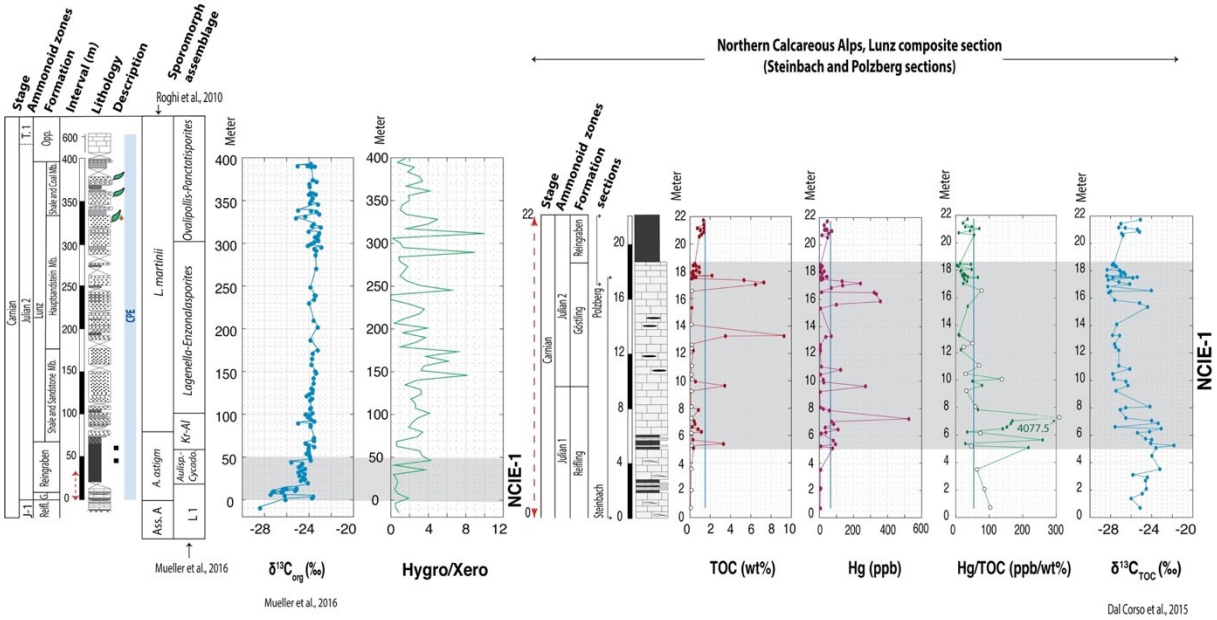

Fig. S4. Mercury geochemistry of the Northern Calcareous Alps, Lunz composite section. The TOC chemostratigraphy, Hg enrichments and Hg/TOC ratios produced in this study. Lithostratigraphy modified from Dal Corso et al. (2015) and Mueller et al. (2016); Organic carbon isotope curves from Dal Corso et al. (2015) and Mueller et al. (2016). Biostratigraphy from Roghi et al. (2010) and Mueller et al. (2016). The Hygrophytic/Xerophytic ratios from Mueller et al. (2016). Grey bars show the negative carbon isotope excursion detected by Dal Corso et al. (2015) and Mueller et al. (2016). White circles represent TOC values below 0.2 wt% and their corresponding Hg/TOC ratios. Vertical blue lines represent the average values of each dataset (only TOCs>0.2 are included in average). Abbreviations: Reifl. = Reifling Formation, G. = Göstling Member, Opp. = Opponitz Formation, J-1 = Julian-1 = *Trachyceras* zone, Julian 2 = *Austrotrachyceras austriacum* zone, T. 1: Tuvalian 1 = *Tropites dilleri* zone. The legend of the stratigraphic units is the same as in Figure 3.

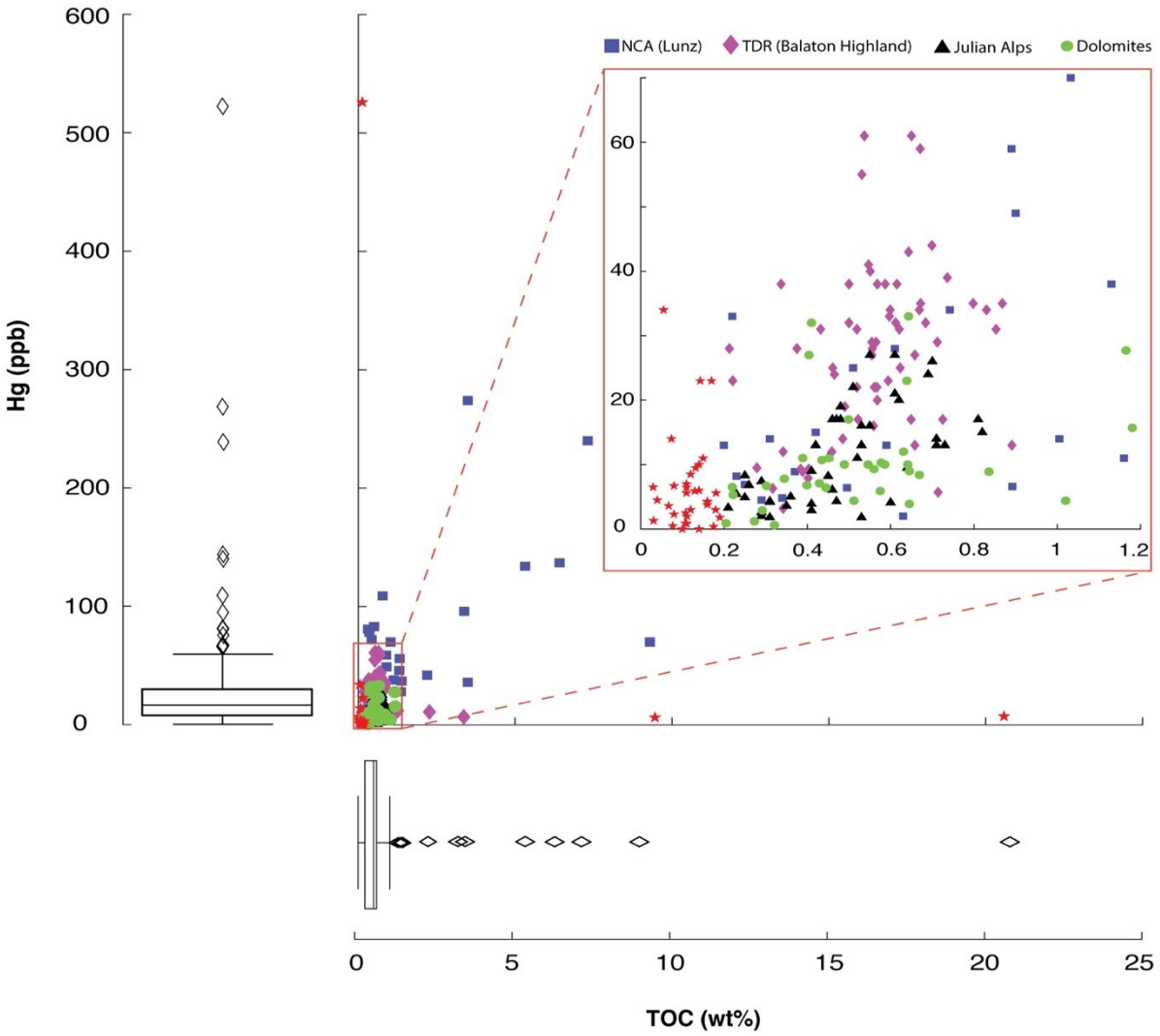

Figure (A). All Hg *vs* TOC values from the studied successions of the Western Tethys. Most of the data are concentrated in a narrow range (Hg < 70 ppb and TOC < 1.2 wt%). Red stars indicate TOC values below 0.2 wt%.

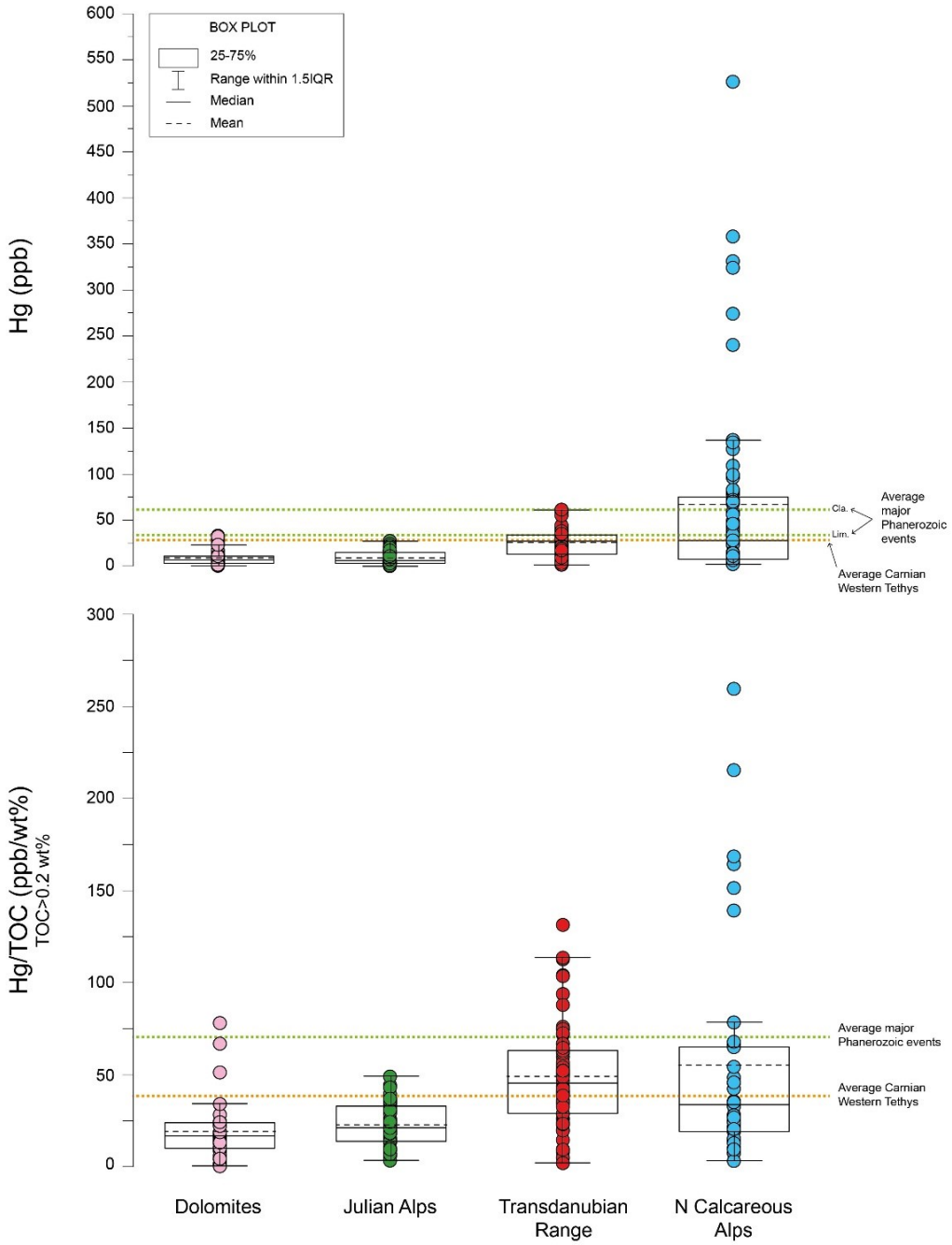

Figure (B). Box plots showing Hg and Hg/TOC data from the different analysed localities of the Western Tethys. Hg concentrations and Hg/TOC are in general lower than the average values of other Phanerozoic events (Grasby et al., 2019), especially in the basins of the Southern Alps (Dolomites and Julian Alps). Cla. = Clastic; Lim. = Limestone.

SUPPLEMENTARY REFERENCES

1. Assereto, R., Desio, A., di Colbertaldo, D., and Passeri, L.D., 1968, Note illustrative della Carta Geologica d'Italia: Foglio 14 A Tarvisio. Servizion Geologico Italiano, Roma, p. 70.
2. Baranyi, V., Rostási, Á., Raucsik, B., and Kürschner, W.M., 2019b, Palynology and weathering proxies reveal climatic fluctuations during the Carnian Pluvial Episode (CPE) (Late Triassic) from marine successions in the Transdanubian Range (western Hungary): Global and Planetary Change, v. 177, p. 157-172, https://doi.org/10.1016/j.gloplacha.2019.01.018.
3. Bin, C., Xiaoru, W., and Lee, F.S.C., 2001, Pyrolysis coupled with atomic absorption spectrometry for the determination of mercury in Chinese medicinal materials: Analytica Chimica Acta, v. 447, p. 161-169, https://doi.org/10.1016/S0003-2670(01)01218-1.
4. Bosellini, A., Gianolla, P., and Stefani, M., 2003, Geology of the Dolomites: Episodes, v. 26, p. 181-185, https://doi.org/10.18814/epiiugs/2003/v26i3/005.
5. Breda, A., and Preto, N., 2011, Anatomy of an Upper Triassic continental to marginal-marine system: The mixed siliciclastic-carbonate Travenanzes Formation (Dolomites, Northern Italy): Sedimentology, v. 58, p. 1613–1647, https://doi.org/10.1111/j.1365-3091.2011.01227.x.
6. Breda, A., Roghi, G., Furin, S., Meneguolo, R., Ragazzi, E., Fedele, P., and Gianolla, P., 2009, The Carnian Pluvial Event in the Tofane area (Cortina d'Ampezzo, Dolomites, Italy): Geo.Alp, v. 6, p. 80–115.
7. Budai, T., and Haas, J., 1997, Triassic sequence stratigraphy of the Balaton Highland, Hungary: Acta Geologia Hungarica, v. 40, p. 307–335.
8. Budai, T., Császár, G., Csillag, G., Dudko, A., Koloszár, L., and Majoros, Gy, 1999, Geology of the Balaton Highland (Explanation to the Geological Map of the Balaton Highland, 1:50000): Budapest: Geological Institute of Hungary, Special Publication 197, p. 171–257.
9. Caggiati, M., Gianolla, P., Breda, A., Celarc, B., and Preto, N., 2018, The start-up of the Dolomia Principale/Hauptdolomit carbonate platform (Upper Triassic) in the eastern Southern Alps: Sedimentology, v. 65, p. 1097-1131, https://doi.org/10.1111/sed.12416.
10. Dal Corso, J., et al., 2018, Multiple negative carbon-isotope excursions during the Carnian Pluvial Episode (late Triassic): Earth-Science Reviews, v. 185, p. 732–750, https://doi.org/10.1016/j.earscirev.2018.07.004.
11. Dal Corso, J., Gianolla, P., Newton, R.J., Franceschi, M., Roghi, G., Caggiati, M., Raucsik, B., Budai, T., Haas, J., and Preto, N., 2015, Carbon isotope records reveal synchronicity between carbon cycle perturbation and the "Carnian Pluvial Event" in the Tethys realm (Late Triassic): Global and Planetary Change, v. 127, p. 79–90, https://doi.org/10.1016/j.gloplacha.2015.01.013.
12. Dal Corso, J., Mietto, P., Newton, R.J., Pancost, R.D., Preto, N., Roghi, G., and Wignall, P.B., 2012, Discovery of a major negative $\delta^{13}C$ spike in the Carnian (Late Triassic) linked to the eruption of Wrangellia flood basalts, Geology, v. 40, p. 79–82, https://doi.org/10.1130/G32473.1.
13. De Zanche V., Gianolla P., Mietto P., Siorpaes C., and Vail P.R., 1993, Triassic sequence stratigraphy in the Dolomites (Italy): Memorie Scienze Geologiche, v. 45, pp. 1-27.
14. De Zanche, V., Gianolla, P., and Roghi, G., 2000, Carnian stratigraphy in the Raibl/Cave del Predil area (Julian Alps, Italy): Ecologae Geologicae Helvetiae, v. 93, p. 331-347.

15. Dobruskina, I.A., 1998, Lunz flora in the Austrian Alps-a standard for Carnian floras: Palaeogeography, Palaeoclimatology, Palaeoecology, v. 143, p. 307–345, https://doi.org/10.1016/S0031-0182(98)00116-3.
16. Gattolin, G., Preto, N., Breda, A., Franceschi, M., Isotton, M., and Gianolla, P., 2015, Sequence stratigraphy after the demise of a high-relief carbonate platform (Carnian of the Dolomites): Sea-level and climate disentangled: Palaeogeography, Palaeoclimatology, Palaeoecology, v. 423, p. 1–17, https://doi.org/10.1016/j.palaeo.2015.01.017.
17. Gawlick, H. J., 2000, Paläogeographie der Ober-Trias Karbonatplattform in den Nördlichen Kalkalpen: Mitteilungen der Österreichischen Geologischen Gesellschaft, v. 44, p. 45-95.
18. Gianolla, P., De Zanche, V., and Mietto, P., 1998a. Triassic Sequence Stratigraphy in the Southern Alps (Northern Italy): Definition of Sequences and Basin Evolution, in: de Graciansky, P.-C, Hardenbol, J., Jacquin, T., Vail, P.R. (Eds.), Mesozoic and Cenozoic Sequence Stratigraphy of European Basins. SEPM Special Publications, pp. 719–747. https://doi.org/10.2110/pec.98.02.0719.
19. Gianolla, P., De Zanche, V., and Roghi, G., 2003, An Upper Tuvalian (Triassic) Platform-Basin System in the Julian Alps: the start-up of the Dolomia Principale (Southern Alps, Italy): Facies, v. 49, p. 135 – 150, https://doi.org/10.1007/s10347-003-0029-7.
20. Gianolla, P., Morelli, C., Cucato, M., and Siorpaes, C., 2018. Note Illustrative - Foglio 016 Dobbiaco, in: Carta Geologica d'Italia alla Scala 1:50000. ISPRA, Roma.
21. Gianolla, P., Ragazzi, E., and Roghi, G., 1998b, Upper Triassic amber from the Dolomites (Northern Italy). A paleoclimatic indicator?: Rivista Italiana di Paleontologia e Stratigrafia, v. 104, p. 381-390, https://doi.org/10.13130/2039-4942/5340.
22. Góczán, F., and Oravecz-Scheffer A., 1996a, Tuvalian Sequence of the Balaton Highland and the Zsámbér Basin. Part I: Litho-bio and chronostratigraphic subdivision: Acta Geologica Hungarica, v. 39/1, pp. 1-31.
23. Góczán, F., and Oravecz-Scheffer A., 1996b, Tuvalian Sequence of the Balaton Highland and the Zsámbér Basin. Part II: Characterization of sporomorph and foraminifer assemblages, biostratigraphic, palaeogeographic, and geohistoric conclusion: Acta Geologica Hungarica., v. 39/1, pp. 33-101.
24. Góczán, F., Oravecz-Scheffer, A., and Csillag, G., 1991, Balatoncsicsó, CsukrétiÁrok cordevolei és juli képződményeinek biosztratigráfiai jellemzése (The stratigraphic characterization of the Cordevolian and Julian formations of Csukrét ravine, Balatoncsicsó). Ann. Rep. Hung. Geol. Inst. on. 1989, pp. 241-323.
25. Grasby, S. E., Sanei, H., Beauchamp, B., and Chen, Z., 2013, Mercury deposition through the Permo–Triassic biotic crisis: Chemical Geology, v. 351, p. 209-216, https://doi.org/10.1016/j.chemgeo.2013.05.022.
26. Grasby, S.E., Beauchamp, B., Bond, D.P.G., Wignall, P.B., Talavera, C., Galloway, J.M., Piepjohn, K., Reinhardt, L., and Blomeier, D., 2015, Progressive environmental deterioration in northwest- ern Pangea leading to the latest Permian extinction: Geological Society of America Bulletin, v. 127, p. 1331–1347, https://doi.org/10.1130/ B31197.1.

27. Haas, J., Budai, T., and Raucsik, B., 2012, Climatic controls on sedimentary environments in the Triassic of the Transdanubian Range (Western Hungary): Palaeogeography, Palaeoclimatology, Palaeoecology, v. 353–355, p. 31–44, https://doi.org/10.1016/j.palaeo.2012.06.031.
28. Haas, J., Kovács, S., Krystyn, L., and Lein, R., 1995, Significance of late Permian–Triassic facies zones in terrane reconstructions in the Alpine–North Pannonian domain: Tectonophysics, v. 242, p. 19–40, https://doi.org/10.1016/0040-1951(94)00157-5.
29. Hornung, T., and Brandner, R., 2005, Biochronostratigraphy of the Reingraben Turnover (Hallstatt Facies Belt): local black shale events controlled by regional tectonics, climatic change and plate tectonics: Facies, v. 51, p. 460-479, https://doi.org/10.1007/s10347-005-0061-x.
30. Hornung, T., Brandner, R., Krystyn, L., Joachimski, M.M. and Keim, L., 2007b, Multistratigraphic constraints on the NW Tethyan "Carnian Crisis": The Global Triassic, New Mexico Museum of Natural History Bulletins, v. 4, p. 9–67.
31. Hornung, T., Krystyn, L., and Brandner, R., 2007a, A Tethys-wide mid-Carnian (Upper Triassic) carbonate productivity decline: evidence for the Alpine Reingraben Event from Spiti (Indian Himalaya): Journal Asian Earth Science, v. 30, p. 285–302, http://dx.doi.org/10.1016/j.jseaes.2006.10.001.
32. Keim, L., Brandner, R., Krystyn, L., and Mette, W., 2001, Termination of carbonate slope progradation: an example from the Carnian of the Dolomites, Northern Italy: Sedimentary Geology, v. 143, p. 303-323, https://doi.org/10.1016/S0037-0738(01)00106-3.
33. Keim, L., Spöti, C., and Brandner, R., 2006, The aftermath of the Carnian carbonate platform demise: a basinal perspective (Dolomites, Southern Alps): Sedimentology, v. 53, p. 361-386, https://doi.org/10.1111/j.1365-3091.2006.00768.x.
34. Koken, E., 1913, Kenntnis der Schichten von Heiligenkreuz (Abteil. Südtirol), Abhandlungen der Kaiserlich−Koniglichen Geologischen Reichsanstalt, v. 16, p. 1-44.
35. **Köppen, A., 1997, Faziesentwicklung in der frühen Obertrias Mitteleuropas – ein sequenzstratigraphischer Vergleich** [Ph.D. thesis]: Gaea Heidelbergensis, v. 2, p. 1-233.
36. Lieberman, H.M., 1980, The suitability of the Raibl sequence as a stratotype for the Carnian Stage and the Julian Substage of the Triassic: Newsletters on Stratigraphy, v. 9, p. 35–42, http://doi.org/10.1127/nos/9/1980/35.
37. Mandl, G.W., (2000), The Alpine sector of the Tethyan shelf–examples of Triassic to Jurassic sedimentation and deformation from the Northern Calcareous Alps: Mitteilungen der Österreichischen Geologischen Gesellschaft, v. 92, p. 61-77.
38. Maron, M., Muttoni, G., Dekkers, M. J., Mazza, M., Roghi, G., Breda, A., Krijgsman W., and Rigo, M., 2017, Contribution to the magnetostratigraphy of the Carnian: new magneto-biostratigraphic constraints from Pignola-2 and Dibona marine sections, Italy: Newsletters on Stratigraphy, v. 50, p. 187-203, https://doi.org/10.1127/nos/2017/0291.
39. Masetti, D., Neri, C., and Bosellini, A., 1991, Deep-water asymmetric cycles and progradation of carbonate platforms governed by high-frequency eustatic oscillations (Triassic of the Dolomites, Italy): Geology, v. 19, p. 336-339, https://doi.org/10.1130/0091-7613(1991)019<0336:DWACAP>2.3.CO;2.

40. Mietto, P., et al., 2012, The global boundary stratotype section and point (GSSP) of the Carnian stage (Late Triassic) at Prati di Stuores/Stuores Wiesen section (Southern Alps, NE Italy): Episodes, v. 35, 414-430, https://doi.org/10.18814/epiiugs/2012/v35i3/003.
41. Mojsisovics, E.M., von, 1869, Über die Gliederung der oberen Triasbildungen der östlichen Alpen: Jahrbuch der Geologischen Bundesanstalt, v. 19, p. 91-150.
42. Mueller, S., Krystyn, L., and Kürschner, W.M., 2016, Climate variability during the Carnian Pluvial Phase-a quantitative palynological study of the Carnian sedimentary succession at Lunz am See, Northern Calcareous Alps, Austria: Palaeogeography, Palaeoclimatology, Palaeoecology, v. 441, p. 198–211, https://doi.org/10.1016/j.palaeo.2015.06.008.
43. Muttoni, G., Tartarotti, P., Chiari, M., Marieni, C., Rodelli, D., Dallanave, E., and Kirscher, U., 2015, Paleolatitudes of Late Triassic radiolarian cherts from Argolis, Greece: Insights on the paleogeography of the western Tethys: Palaeogeography, Palaeoclimatology, Palaeoecology, v. 417, p. 476-490, https://doi.org/10.1016/j.palaeo.2014.10.010.
44. Nagy, Z.R.,1999, Platform-basin transition and depositional models for the Upper Triassic (Carnian) Sándorhegy Limestone, Balaton Highland, Hungary: Acta Geologica Hungarica, v. 42/3, p. 267-299.
45. Natali, C., Bianchini, G., and Carlino, P., 2020, Thermal stability of soil carbon pools: Inferences on soil nature and evolution: Thermochimica Acta, v. 683, 178478, https://doi.org/10.1016/j.tca.2019.178478.
46. Neri C., Gianolla P., Furlanis S., Caputo R., and Bosellini A., 2007 - Note illustrative della Carta Geologica d'Italia. Foglio Cortina d'Ampezzo 029. Scala 1:50.000. Servizio Geologico d'Italia, 200 pp.
47. Pisa, G., Marinelli, M., and Viel, G., 1980, Infraraibl Group: a proposal (Southern Calcareous Alps, Italy): Rivista Italiana di Paleontologia e Stratigrafia, v. 85, p. 983-1002.Pott, C., Krings, M., and Kerp, H., 2008, The Carnian (Late Triassic) flora from Lunz in Lower Austria: Paleoecological considerations: Palaeoworld, v. 17, p. 172-182, https://doi.org/10.1016/j.palwor.2008.03.001.
48. Preto, N., and Hinnov, L.A., 2003, Unraveling the origin of carbonate platform cyclothems in the Upper Triassic Dürrenstein Formation (Dolomites, Italy): Journal of Sedimentary Research, v. 73, p. 774-789, https://doi.org/10.1306/030503730774.
49. Roghi, G., 2004, Palynological investigations in the Carnian of Cave del Predil area (once Raibl, Julian Alps): Review of Palaeobotany and Palynology, v. 132, p. 1–35, https://doi.org/10.1016/j.revpalbo.2004.03.001.
50. Roghi, G., Gianolla, P., Minarelli, L., Pilati, C., and Preto, N., 2010, Palynological correlation of Carnian humid pulses throughout western Tethys: Palaeogeography, Palaeoclimatology, Palaeoecology, v. 290, p. 89–106, https://doi.org/10.1016/j.palaeo.2009.11.006.
51. Rostási, Á., Raucsik, B., and Varga, A., 2011, Palaeoenvironmental controls on the clay mineralogy of Carnian sections from the Transdanubian Range (Hungary): Palaeogeography, Palaeoclimatology, Palaeoecology, v. 300, p. 101–112. https://doi.org/10.1016/j.palaeo.2010.12.013.
52. Rüffer, T., and Bechstädt, T., 1998, Triassic sequence stratigraphy in the western part of the Northern Calcareous Alps (Austria): in: de Graciansky, P.-C, Hardenbol, J., Jacquin, T., Vail, P.R. (Eds.),

Mesozoic and Cenozoic Sequence Stratigraphy of European Basins. SEPM Special Publications, v. 60, p., https://doi.org/10.2110/pec.98.02.0751.

53. Schulz, O., 1970, Vergleichende petrographische Untersuchungen an Karnischen Sedimenten der Julischen Alpen, Gailtaler Alpen und des Karwendels: Verh. Geol. B.-A., v. 1970, p. 165-229.
54. Stefani, M., Furin, S., and Gianolla, P., 2010, The changing climate framework and deposi- tional dynamics of the Triassic carbonate platforms from the Dolomites: Palaeogeography, Palaeoclimatology, Palaeoecology, v. 290, p. 43–57, https://doi.org/10.1016/j.palaeo.2010.02.018.
55. Tollmann, A., 1976, Analyse des klassischen nordalpinen Mesozoikums: Stratigraphie, Fauna und Fazies der Nördlichen Kalkalpen XV: Deuticke Wien, 580 p., Springer, Berlin, Heidelberg New York.
56. Verloop, J.H., 1908, Profil der Lunzer Schichten in der Umgebung von Lunz: Zeitschrift deutscher geologischer Gesellschaft, Monatsberichte, v. 60, p. 81-89.
57. Wessely, G., 2006, Niederösterreich-Geologie der Österreichischen Bundesländer: Vienna, Austria, Verlag der Geologische Bundesanstalt, 416 p.
58. Wörhmann, S.F. von, 1894. Die Raibler Schichten nebst kritischer Zusammenstellung ihrer Fauna: Jahrbuch der Kaiserlich-Koniglichen Geologischen Reichsanstalt, v. 43 (1893), p. 617-768.